UNIVERSITAT DE BARCELONA

# Molecular mechanisms involved in the cerebral cortex development and their implications in neurodevelopmental disorders

Isabel Pijuán Jiménez

# Molecular mechanisms involved in the cerebral cortex development and their implications in neurodevelopmental disorders

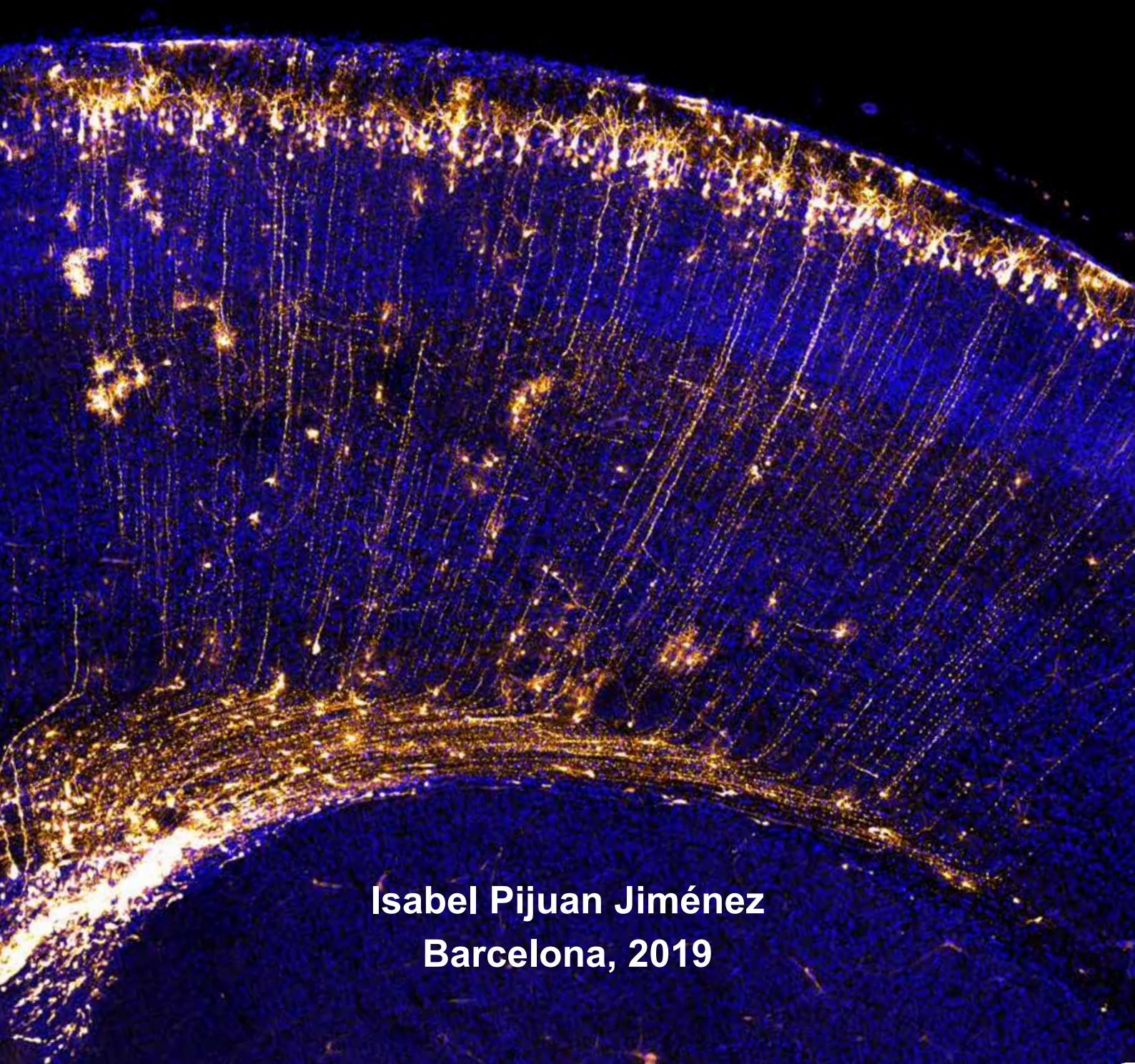

Isabel Pijuan Jiménez

Barcelona, 2019

PROGRAMA DE DOCTORADO EN BIOMEDICINA
FACULTAD DE BIOLOGÍA
2019

# MOLECULAR MECHANISMS INVOLVED IN THE CEREBRAL CORTEX DEVELOPMENT AND THEIR IMPLICATIONS IN NEURODEVELOPMENTAL DISORDERS

Memoria presentada por Isabel Pijuan Jiménez para optar al Grado de Doctor por la Universidad de Barcelona.

Trabajo realizado bajo la dirección de la Dra. Mª Lourdes Arbonés de Rafael y la Dra. Mª José Barallobre Filgueira en el Instituto de Biología Molecular de Barcelona (IBMB-CSIC).

DIRECTOR

Mª Lourdes Arbonés de Rafael

CO-DIRECTOR

Mª José Barallobre Filgueira

TUTOR

Marta Pascual Sánchez

DOCTORANDO

Isabel Pijuan Jiménez

Isabel Pijuan was supported by a predoctoral fellowship of the Spanish Ministry of Education and Science (Ayudas para contratos predoctorales para la formación de doctores 2014; BES-2014-069217). This work was supported by grants of the Spanish Ministry of Education and Science (SAF2013-46676-P and SAF2016-77971-R).

# ACKNOWLEDGEMENTS

Pensando en cómo empezar estos agradecimientos, me ha venido a la cabeza la primera vez que fui al laboratorio de Mariona, hace casi 7 años, para hacer unas prácticas de verano. Desde el principio la cosa prometía, recuerdo llegar a casa emocionada diciendo "¡He cortado un cerebro!", "¡He visto una neurona en el micro!". Creo que mantuve ese nivel de emoción todo el verano. Me ilusionaba hacer cualquier cosa que me enseñaran. Claro que con el tiempo algunas de esas cosas dejaron de ser tan excitantes, pero no miento si digo que me sigue emocionando igual conseguir buenos cortes o mirar en el micro una tinción bonita. Me siento muy, muy afortunada de haber podido hacer este trabajo y a la primera persona a quién se lo tengo que agradecer es a Mariona: moltíssimes gràcies per confiar en mi i donar-me aquesta oportunitat. En concret, et vull agrair que sempre m'hagis fet saber allò que faig bé, perquè m'ha fet sentir valorada i útil; però sobretot, que m'hagis fet saber allò que faig malament i hagis dedicat hores i hores a seure amb mi per treballar-ho. He aprés molt de tu i espero que estiguis tan contenta i satisfeta com jo d'aquests anys de feina (no tinguis en compte la redacció d'aquests agraïments, please!!). Y luego, por supuesto, a todos mis compañeros de laboratorio. ¡Qué suerte he tenido con vosotros! He aprendido muchísimo de todos, no sólo los pasos a seguir de un protocolo, también la necesidad de entender el porqué de cada paso, y a interpretar el resultado con honestidad. Sois un gran ejemplo. Mariajo, contigo tengo una mentora, una profesora, una amiga, una psicóloga y, con tu optimismo innato, una *cheerleader*. A estas alturas me pareces imprescindible. Me encantan tu manera de ver la vida y la practicidad con la que te enfrentas a cualquier cosa, y me gustaría pensar que, a fuerza de pasar tanto tiempo juntas, se me han enganchado un poquito. Este espacio se me queda corto para agradecerte la generosidad que has tenido conmigo durante estos años y el apoyo que supones para mí, tanto dentro como fuera del lab. Espero devolvértelo con muchas risas, vino y buenos momentos. Sònia, com he enyorat tenir-te al lab aquest últim tram!! Admiro molt la teva manera d'emocionar-te amb la ciència i t'agraeixo que sempre hagis estat disposada a ensenyar-me i a donar voltes als meus resultats, quan sovint m'he desesperat perquè eren el contrari del que esperava. Amb el temps t'has convertit en una persona essencial per mi i m'alegra saber que, malgrat la distància, continues disposada a contestar els meus àudios infumables jajaj. Ai Juan, a ti también te he echado mucho de menos en el laboratorio estos últimos años... Gracias por haber sido tan buen compañero, estar siempre dispuesto a ayudar y por enseñarme a hacer los bloques de agarosa con tanto mimo. Parece que si no te digo que lo que más echo de menos de ti son tus carcajadas, no me quedo tranquila, siempre han sido terapéuticas, sobre todo después de un mal resultado. Me alegra un montón tenerte por Barcelona otra vez y seguir oyéndolas a menudo. Álex, qué guay tu llegada al lab cuando estábamos Mariajo y yo más solas que la una. ¡Me encanta tu sentido del humor! Que las cres odiosas que no salen y las inmunos de BrdU no te lo quiten nunca. Estoy segura de que vas a acabar con un buen proyecto y mucha confianza en ti mismo, ¡disfruta todo lo que puedas de esta aventura! Elisa, gracias infinitas por aquél verano de prácticas. Me hiciste partícipe desde el día 1 de tu proyecto, siendo súper generosa con las explicaciones y depositando un montón de confianza en mí (que no había tocado una pipeta en la vida). Gracias por ser tan clara conmigo con los pros y contras de hacer un doctorado cuando se presentó la oportunidad, aunque tengo que confesarte que para entonces ya me habías contagiado de tu entusiasmo por los oligodendrocitos. Cris Cruji, me declaro tu fan número 1, ¡qué apañada eres, madre! Gracias por aquél año de risas, complicidad y comidas ricas. Juan Martínez, ¡¿qué dolores de cabeza nos han dado los ratones, eh?! Espero que guardes un buen recuerdo de nosotros al menos jajaj Muchas gracias por tu ayuda y por ser tan buena persona. Mari, moltes gràcies per la teva ajuda i per les estones de xerrades amb els ratolinets.

También quiero dar las gracias a todos los colaboradores. Eduardo Fernández, Cristina Soto y Gema Martínez, por los análisis de microscopía electrónica y enseñarme el procedimiento de

cirugía estereotáxica, pero sobre todo gracias por acogerme en vuestro laboratorio unos días y hacerme sentir como en casa. A Ricky Joshi, por ayudarme con el análisis bioinformático y enseñarme un montón de trucos para manejar datos. A Susana de la Luna y Chiara Di Vona, por los análisis de transcriptómica y dedicar horas a darle vueltas a los datos.

Esta tesis también ha sido posible gracias a la ayuda de toda la gente que se encarga de las *facilities* del centro. Tengo que agradecer a Elena Rebollo enseñarme a usar los microscopios, por intentar no sólo que supiera usarlos, sino que también los entendiera, y por hacer magia cuando alguna preparación se ha puesto imposible. A Jaume Boix, gràcies per l'ajuda als microscopis, i un milió de gràcies més per implicar-te en els projectes com ho fas. Perquè el dia que vas arribar amb una macro pensada per al comptatge dels nòduls em vas fer recuperar la fe en la humanitat! (i em vas estalviar setmanes de comptatges feixucs!). A Eva Prats, por hacer siempre lo posible por facilitarnos el trabajo en el estabulario.

Me siento también muy afortunada por haber coincidido con gente genial en el IBMB. Gracias a Elisa y a todo su grupo, que con sus preguntas e ideas han contribuido a dar forma a mi proyecto. Gwen, Lucía, Elena, Murielle, Jose, Irene, Susana, René, gracias por escuchar 20 mil veces la historia de los oligos y no dormiros (casi nunca, o hacerlo con disimulo) y por ser mi lugar favorito para desconectar un rato. En especial, gracias a Gwen, por dejarme participar en tu proyecto y darme confianza plena. A Sebastián y a Toni os agradezco mucho el *feedback* en los seminarios y vuestra colaboración en el proyecto de los colágenos, estoy segura que, de una manera u otra, sacaremos algo bonito!! También a Jari, por la de veces que te has cruzado el Parc para acercarme alguna alícuota y la sonrisa con la que lo haces. Y a Andrea, que, aunque nos veamos poquito, siempre tenemos algo que contarnos. A las chicas de Marian, que son las vecinas ideales porque siempre tienen café y dulces. Raquel, gracias por creer en mí como científica, por hacerme compañía en el laboratorio a horas intempestivas y por escuchar el discurso sobre mi póster aquella noche en Alicante jajajaj Stella, mi compi de council, gracias por tantas confidencias. Simona, Marta, me encanta teneros cerca para sacar la nariz de vez en cuando y hablar un ratito con vosotras. No me puedo olvidar de Raúl, el chico más famoso del IBMB de esta generación jajaj gracias por tantos buenos ratos. Adrián, gracias por esas charlas sobre sueños y anhelos, ya las echo de menos. També vull donar les gràcies a la Leonor Calopa per l'eficàcia a l'hora de resoldre qualsevol tràmit administratiu, i a l'Irma, perquè sempre rep amb un somriure i em sap llegir la cara i donar-me ànims quan els necessito.

A mis amigos tengo que agradecerles el mantenerme cuerda. Andreu, quina sort tenir-te tant a prop, gràcies per creure en mi més que jo mateixa. Marta Reus, mi vecina eterna, qué hagués fet jo sense els nostres vinets en tornar a casa… Elena y David, mis amiguis del alma, me arrepiento un montón de haberos dado la lata con la tesis durante nuestro último viaje, prometo que os compensaré visitando tantos castillos y sitios fríos como queráis. Álvaro, gracias por estar siempre ahí de forma incondicional. Juls, no vull ser bleda que sé que no t'agrada, però *namaste* súper profund. Vane, que vinieras a Barcelona con tu energía y positivismo ha sido de lo mejorcito que me podía pasar. Vane, Juls y "los chicos del vermú", por hacer del domingo mediodía mi momento favorito de la semana, no sois conscientes pero me habéis salvado la tesis. Euge, mi compita de pis.. m'ha encantat compartir aquests anys amb tu, moltes gràcies per les nostres nits de dilluns i, sobretot, per donar-me tant suport aquests últims mesos d'escriure.. sentir la clau a la porta quan arribaves al vespre era el moment que més esperava del dia.

A mi familia tengo que agradecerles tanto que no sé ni por dónde empezar. Tengo la gran suerte de contar con unos abuelos (porque os tengo presentes más que nunca) y unos padres que me quieren con locura y que me han dado todo lo que han podido y más, aunque eso signifique sacrificar muchas cosas. Por vosotros estoy donde estoy, haciendo algo que me gusta, sin preocuparme de otra cosa más que ser feliz. Lo mucho que creéis en mi, la seguridad que me dais, es el motor que me impulsa siempre. Deciros tan sólo "gracias" me parece tan ridículo...

(patético que diríamos nosotras, ¿no, mama?). Edu, yo pensé que mi papel era protegerte y darte ejemplo y resulta que hace tiempo que se han cambiado las tornas. Admiro todo de ti y eres mi mayor apoyo. Me siento infinitamente orgullosa de vosotros. Os prometo que, ahora que seré doctora, no vamos a discutir más en la mesa, porque voy a tener razón yo en todo por defecto. Esta nueva etapa que estamos empezando, con Alex's incluidos, promete, ¡qué ganas de vivirla juntos!

Y para acabar, si alguien ha sufrido esta tesis ha sido mi compañero de vida. Álex, gracias por tu paciencia infinita, por adaptarte en lo que ha hecho falta y por ser el principal responsable de mi felicidad. Te quejabas de que dijera que nuestra relación es para mi como hacer una tesis. Espero que, después todo, cuando tengas ésta en las manos te des cuenta que justamente de eso se trata. Que quiero dedicarme a entenderlo todo y a mimar hasta el último detalle de lo nuestro y que, al final del día, el único resultado que me importa son las risas contigo en el sofá de casa.

Las enfermedades *de novo*, que surgen sin avisar, forman parte de la lógica molecular de la vida, que no es otra que la generación de diversidad y variabilidad. Por eso, estas patologías van a acompañar siempre a nuestra especie y contínuamente seguirán apareciendo nuevas afecciones provocadas por nuevas mutaciones en genes en los que hasta ahora no se habían detectado mutaciones causantes de enfermedades. Dado que las enfermedades *de novo* van a ser fieles compañeras de la vida humana, su estudio debe ser objeto de atención prioritaria y continua, pues solo mediante la investigación se encontrarán las claves de su comprensión y de su eventual curación.

Carlos López-Otín, La vida en cuatro letras (2019)

# ABSTRACT

During the process of corticogenesis, cortical radial glial cells (RGs) generate sequentially most of the distinct types of neurons and glial cells that will populate the neocortex. The generation of these cells at the proper time and adequate numbers is key for the establishment of fully functional cerebral circuits. During the phase of neuronal production, RGs experience important changes in morphology, division mode and fate of their neuronal progeny.

To provide evidence of the genetic networks underlying these changes, in the first part of this work we have compared the expression of protein-coding genes at the onset of neurogenesis (embryonic day (E)11.5) and during middle-late neurogenesis (E15.5). We found that the expression levels of 25% of these genes are regulated during neurogenesis, and a quarter of them are targets of developmentally regulated miRNAs. Down-regulated genes at E15.5 are mainly associated to cell cycle regulation, while most of the up-regulated genes encode for ion-transport proteins that may be involved in modulating the membrane potential of RGs. Moreover, we found significant up-regulation of synapse-related genes, supporting published reports that claim for the existence of a transcriptional “pre-patterning” in RGs. Among the regulated genes, we found significant enrichment in TEAD2 targets. YAP-TEAD transcriptional activity is regulated by mechanical cues and we found that a great number of differentially expressed genes in RGs encode for structural extracellular matrix (ECM) proteins, suggesting a dynamic remodelling of the ECM along neurogenesis. This remodelling likely varies the physical properties of the ECM, and thereby YAP-TEAD transcriptional activity in RGs. The integrated analysis of the developmental regulated mRNAs and miRNAs suggests that let-7 miRNAs are involved in the regulation of collagen and other structural ECM genes. Lastly, our RNA-seq data shows that alternative splicing (AS) is also developmentally regulated in RGs and affects the expression of splicing events in 19% of the expressed protein-coding genes. Functional enrichment analysis of these genes indicates that AS in RGs may be involved in silencing synapse-related genes and the regulation of RG critical cellular functions such as the biogenesis of the cilium.

In the second part of this work, we addressed the effects of *DYRK1A* haploinsufficiency in the generation and differentiation of cortical glial cells. DYRK1A is a kinase that has a conserved role in brain growth through evolution and regulates the generation, survival and differentiation of different neuron types. Mutations in *DYRK1A* cause a syndrome, named *DYRK1A*-haploinsufficiency syndrome, that is characterized by the presence of microcephaly and other clinical features including intellectual disability, autistic traits and

epilepsy. Gliosis and hypomyelination have also been reported in affected children. Previous work of the laboratory has shown that the *Dyrk1a*$^{+/-}$ mouse mimics several of the phenotypic traits of the syndrome, including an increased number of astrocytes and hypomyelination of the corpus callosum (CC). Here, we show that the augmented number of astrocytes in *Dyrk1a*$^{+/-}$ neocortices results from an enhanced developmental astrogliogenesis. Moreover, we have observed a decreased generation of oligodendrocyte precursor cells (OPCs) in *Dyrk1a*$^{+/-}$ embryos that correlates with a delay in the appearance of oligodendrocytes in the CC. Focal demyelination experiments in the adult CC indicate that *Dyrk1a*$^{+/-}$ OPCs differentiate properly, suggesting that the oligodendroglial phenotype in *Dyrk1a*$^{+/-}$ mutants results from alterations in the generation of OPCs during development. In addition to hypomyelination, the CC of adult *Dyrk1a*$^{+/-}$ mice shows altered proportion of the myelin proteins PLP and MBP, shorter nodes of Ranvier and a deficit in the expression of the nodal sodium channel NAV1.6. Collectively, these results show that deficits in the generation and differentiation of glial cells may contribute to the neurological defects reported in individuals with *DYRK1A*-haploinsufficiency syndrome.

# RESUMEN

La mayoría de las neuronas y células gliales de la corteza cerebral se generan secuencialmente durante el desarrollo a partir de progenitores pluripotentes denominados glía radial (GR). La correcta generación y diferenciación de estas células es crítica para el establecimiento de circuitos funcionales.

En la primera parte de esta Tesis, hemos estudiado los cambios de expresión génica que tienen lugar en la GR durante la neurogénesis. Los resultados obtenidos muestran cambios de expresión en el 25% de los genes codificantes e indican que la expresión de una cuarta parte de éstos está regulada por micro-ARNs. Entre los genes expresados diferencialmente encontramos un enriquecimiento en targets del complejo YAP-TEAD, cuya actividad transcripcional responde a estímulos mecánicos. Además, encontramos enriquecimiento en genes que codifican componentes de la matriz extracelular (MEC), sugiriendo que cambios en las propiedades físicas de ésta podrían modular la actividad YAP-TEAD en la GR. Por último, nuestros resultados indican que la regulación por *splicing* alternativo durante la neurogénesis es muy extensa (afectando al 19% de los genes codificantes) y podría estar implicada en silenciar genes neuronales en la GR y en otras funciones como la biogénesis del cilio.

En la segunda parte, hemos estudiado los efectos de la haploinsuficiencia de *DYRK1A* en la generación y diferenciación de células gliales. *DYRK1A* codifica una quinasa con funciones clave en el desarrollo cerebral. Mutaciones *de novo* en *DYRK1A* causan un síndrome de discapacidad intelectual y autismo. Los cerebros de niños afectados presentan gliosis e hipomielinización. El ratón *Dyrk1a*$^{+/-}$ recapitula varios de los fenotipos del síndrome, incluyendo un incremento de astrocitos cerebrales e hipomielinización del cuerpo calloso (CC). Nuestros estudios en este modelo indican que la generación de células gliales está alterada durante el desarrollo y correlaciona con un retraso en la aparición de oligodendrocitos en el CC. La corteza adulta del ratón *Dyrk1a*$^{+/-}$ muestra alteraciones en los nodos de Ranvier y en la composición de proteínas de la mielina. Este fenotipo glial podría contribuir a los problemas neurológicos observados en el modelo *Dyrk1a*$^{+/-}$ y abrir nuevas vías de terapia para los individuos con mutaciones en el gen *DYRK1A*.

# TABLE OF CONTENTS

# LIST OF FIGURES

# Abbreviations

**Adj.:** adjusted
**AEP:** anterior entopeduncular area
**AS:** alternative splicing
**ASD:** autism spectrum disorders
**a.u.:** arbitrary units
**BrdU:** 5-bromo-2'-deoxyuridine
**BSA:** bovine serum albumin
**Bp:** base pairs
**CC:** corpus callosum
**CNS:** central nervous system
**CRG:** Centre de Regulació Genòmica
**DM:** dissociation media
**DPL**: days post-lesion
**ΔPSI:** absolute PSI change
***DYRK1A*-related syndrome:** *DYRK1A*-related intellectual disability syndrome
**E:** embryonic day
**ESC:** embryonic stem cell
**FACS:** fluorescence-activated cell sorting
**FC:** fold change
**GO:** Gene Ontology
**HDAC:** histone deacetylases
**INM:** interkinetic nuclear migration
**IP:** intermediate progenitor
**ITR:** transposon-specific inverted terminal repeat
**LGE:** lateral ganglionic eminence
**L.I.:** labelling index
**LPC:** lysolecithin
**MGE:** medial ganglionic eminence
**miRNA:** microRNA
**NE:** neuroepithelial stem cell
**NMD:** nonsense mediated decay
**NSC:** neural stem cell
**ON:** overnight
**OPC:** oligodendrocyte precursor cell
**oRG:** outer radial glia
**oSVZ:** outer subventricular zone
**P:** postnatal day
**PBS:** phosphate buffer saline
**PCB:** Parc Científic de Barcelona
**PCR:** polymerase-chain-reaction
**PFA:** paraformaldehyde
**PSI:** percentage of alternative sequence inclusion
**qPCR:** quantitative PCR
**RBP:** RNA-binding protein
**RG:** radial glial cell
**RT:** reverse transcription
**rT:** room temperature
**S.D.:** standard deviation
**S.E.M.**: standard deviation of the mean
**SVZ:** subventricular zone
**TF:** transcription factor
**UTR:** untranslated region
**VZ:** ventricular zone

# INTRODUCTION

# 1. The mammalian neocortex

## 1.1. Cytoarchitecture and function

The neocortex is the most evolved region of the mammalian brain and it is responsible for higher cognitive functions such as consciousness, sensory perception and processing information. Alterations in the development or physiology of this region underlie several neurological diseases, such as epilepsy, autism, schizophrenia and intellectual disability (Rubenstein, 2010; Hu et al., 2014; Sloan and Barres, 2014).

The neocortex allocates in the most outer part of the cerebral hemispheres and consists in a mantle of grey matter covering the underlying white matter. Tangentially, it is compartmentalized into functional areas that are specialized in the processing of different inputs: the primary visual cortex (V1) processes information from the retina; the somatosensory cortex (S1) from the body; the auditory cortex (A1) from the inner ear; and the motor cortex (M1) controls voluntary movement of the body parts (O'Leary et al., 2007; **Fig I.1**). Radially, the neocortex is organized in functional columns (Mountcastle, 1997) in which neurons are stereotypically interconnected in the vertical dimension (Rakic, 2000). In addition, neurons in the columns are organized into six histological layers, which contain developmentally and functionally distinct neuron types (Greig et al., 2013; Lodato and Arlotta, 2015).

The organization of the neocortex in areas, columns and layers is preserved in all mammalian species (Mountcastle, 1997). However, shape, size and neuron number vary dramatically between species, presumably explaining the differences in cognitive ability. The human brain has expanded dramatically relative to body size in comparison with other species such as the mouse and its surface is not smooth (lissencephalic) but presents multiple gyrus (gyrencephalic; Florio and Huttner, 2014).

The majority of neurons in the neocortex (70-80%) are excitatory glutamatergic neurons (Parnavelas, 2000; Molyneaux et al., 2007). These neurons are stereotypically distributed within the cortical layers. Glutamatergic neurons located in layer IV receive inputs from the sensory thalamic nuclei and project their axons locally to target upper and deeper layers (Jabaudon, 2017; see **Fig I.1**). The neurons located in the deeper cortical layers (VI, V) project their axons outside the cortex, mainly to target subcortical (thalamus) and subcerebral structures (brainstem and spinal cord) (**Fig I.1**). Neurons in the upper layers (II/III) project their axons both ipsilaterally (intrahemispheric) and

contralaterally (interhemispheric) to reach layers II/III and V (**Fig I.1**). These neurons, also named callosal neurons, integrate information between the two cerebral hemispheres and their contralaterally-projecting axons form the corpus callosum (CC), which represents the major cortical white matter tract (Fame et al., 2011). The remaining neocortical neurons (20-30%) are GABAergic inhibitory interneurons, which make local connections within the cortex. These neurons show remarkable diversity with up to 50 different populations identified so far (Lim et al., 2018). Traditionally, they have been classified into three "major" classes based on the expression of the following markers: parvalbumin (~50%), somatostatin (~30%) and calretinin (~15%) (Wonders and Anderson, 2006).

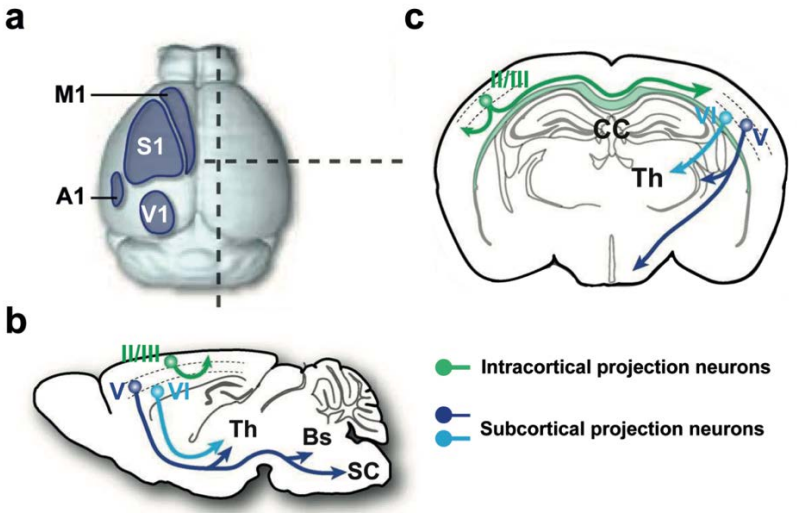


**Figure I.1. Primary functional areas and laminar organization of the neocortex. (a)** Schematic representation of the four primary areas in the mouse adult neocortex. **(b,c)** Sagittal (b) and coronal (c) views of the adult brain in which layer-specific connectivity is indicated. A1, auditory cortex; Bs, Brainstem; CC, corpus callosum; M1, motor cortex, S1, somatosensory cortex; SC, spinal cord; Th, thalamus; V1, visual cortex. Adapted from Jabaudon (2017).

Like in other brain regions, approximately half of the cells populating the neocortex are glial cells (Bandeira et al., 2009). Glial cells in the adult are astrocytes and oligodendrocytes -macroglial cells- and microglial cells (Rowitch and Kriegstein, 2010). For long considered passive supporting cells, it is now clear that these cells reciprocally interact with neurons to modulate neocortical formation and function (Allen and Lyons, 2018). Astrocytes are in intimate contact with synapses and are potent regulators of synapse formation, plasticity and maintenance. Besides, astrocytes provide structural and metabolic support to neurons, maintain the blood-brain barrier, regulate the cerebral blood flood and participate in the inflammatory response after injury (Freeman and Rowitch, 2013). Evolutionary, the ratio of astrocytes to neurons has increased with the

acquisition of complex brain functions (Oberheim et al., 2009; Pereira and Furlan, 2010). Oligodendrocytes enwrap neuronal axons with myelin to allow saltatory conduction of nerve impulses. Increasing evidence supports that dynamic regulation of myelin in the adult brain permits fine-tuning of the neuronal circuits in response to life experience. The human brain has proportionally more myelin than other species, including primates, especially in the neocortex (Schoenemann et al., 2005). In addition, oligodendrocytes provide support to axon integrity and they are also known to regulate the cerebral blood flood (Freeman and Rowitch, 2013).

Neocortical neurons and macroglial cells are generated during development in a time-regulated manner in distinct proliferative regions (see Sections 1.2.2. and 1.2.5).

## 1.2. Development

The neocortex emerges from the most rostral part of the neural tube. Around embryonic day (E) 9 in the mouse, the neural tube closes to form the telencephalic vesicles that will later develop into the cerebral cortices (Chen et al., 2017).

### 1.2.1. Neural progenitors

All neocortical cells, except microglial cells, ultimately derive from the early neural stem cells (NSCs), named neuroepithelial stem cells (NEs), that form the pseudostratified epitelium of the early neural tube (Gotz and Huttner, 2005). These cells present apico-basal polarity and expand the entire width of the neuroepithelium, touching the basal lamina with their basal plasma membrane and facing the lumen with the apical membrane, where a primary cilium that protrudes into the ventricle senses signals from the cerebrospinal fluid. Neighboring NEs are highly connected by tight and adherent junctions (Aaku-Saraste et al., 1996; Chenn et al., 1998). NEs undergo rounds of symmetric proliferative divisions to expand the stem cell pool before differentiation (McConnell, 1995; Rakic, 1995). As NEs progress through the cell cycle, their nuclei move along the apico-basal axis of the cell in a process named interkinetic nuclear migration (INM), with mitosis taking place in the apical side (Miyata, 2008; Sauer, 1935). INM has been proposed to allow for increased number of cells proliferating in the limited ventricular surface (Taverna and Huttner, 2010).

NEs transform into **radial glial cells** (RGs; see **Fig I.2**) when they start to undergo asymmetric divisions, which in the mouse occurs around E11.5 (Gotz and Huttner, 2005; Huttner and Kosodo, 2005). RGs are also NSCs because they are pluripotent but, in

contrast to NEs, they show astroglial characteristics and lose the tight junctions in the apical domain. However, they retain INM, apico-basal polarity (by maintaining adherent junctions), the primary cilium facing the ventricular lumen, and the basal process that gets more elongated than in NEs (Gadisseux and Evrard, 1985; Aaku-Saraste et al., 1996; Huttner and Brand, 1997).

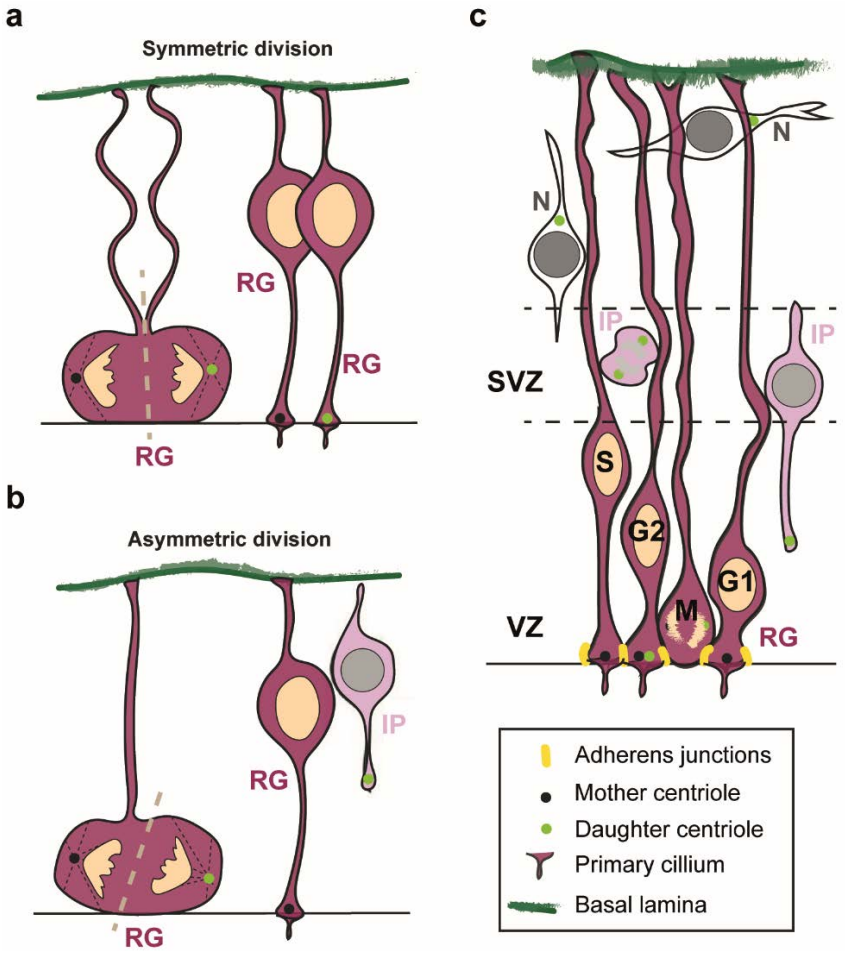


**Figure I.2. Radial glia apico-basal polarity, division modes and interkinetic nuclear migration. (a)** Symmetric divisions yield two radial glial cells (RGs). The basal process is equally distributed between daughters. **(b)** Asymmetric divisions yield one RG daughter and either an intermediate progenitor (IP) or a neuron (N). The basal process and the mother centriole are inherited preferentially by the RG daughter. **(c)** Interkinetic nuclear migration (INM). The RG nucleus occupies different positions along the apical-basal axis depending on the phase of the cell cycle. Mitosis (M) occurs at the apical surface, whereas S phase takes place at a more basal location. Nuclei migrate from apical to basal during G1 and inversely during G2. During neurogenesis, INM is confined to the ventricular zone (VZ). SVZ, subventricular zone. Adapted from Mukhtar and Taylor (2018) and Taverna and Huttner (2010).

RGs of the dorso-lateral telencephalon (pallium) generate glutamatergic neocortical neurons and macroglial cells (**Fig I.3**) in distinct temporal phases: the neurogenic phase that takes place in the embryo and the gliogenic phase that starts around birth (Malatesta et al., 2000; Noctor et al., 2001; see **Fig I.4**). As described in next section, time is an important factor in dorsal neuron production. RGs of the ventral telencephalon (subpallium) produce GABAergic interneurons and cells of the glial lineage in overlapping temporal windows (**Fig I.3**). Virtually all the parvalbumin and somatostanin interneurons are generated in the medial ganglionic eminence (MGE; Lim et al., 2018). Oligodendroglial cells are generated in the MGE, the anterior entopeduncular area (AEP) and the lateral ganglionic eminence (LGE; Kessaris et al., 2006). Part of these interneurons and ventral-generated oligodendroglial cells migrate tangentially to reach their final position in the neocortex at postnatal stages (**Fig I.3**; Marin and Rubenstein, 2003).

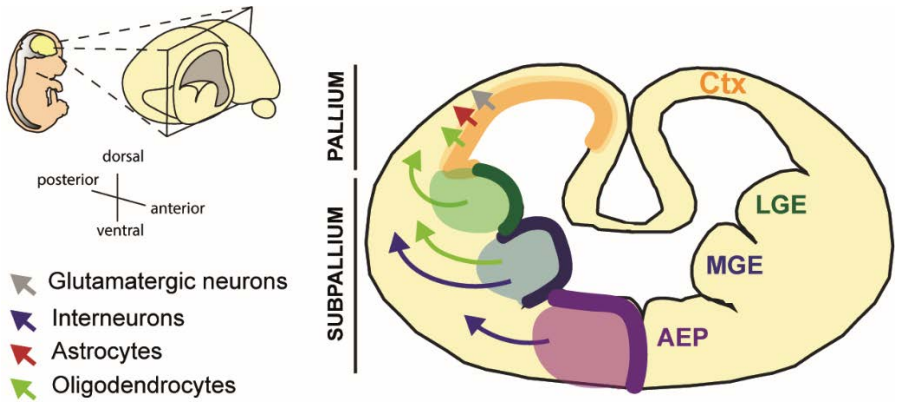


**Figure I.3. Domains of generation of cortical cells**. Schematic representation of the developing brain and spatial orientation of the coronal view (upper left) and a coronal section showing the ventricular zone domains where the different populations of cortical cells are generated. Glutamatergic neurons, astrocytes and some oligodendroglial cells are generated in the cortex (Ctx in orange). Other oligodendrocytes are generated in the lateral ganglionic eminence (LGE in green) and medial ganglionic eminence (MGE in blue), where most cortical interneurons are produced. Color arrows indicate the migration routes of these cells to their final position in the neocortex. AEP, anterior entopeduncular area. Adapted from Rowitch and Kriegstein (2010).

There are two different models to explain how dorsal RGs generate the vast amount of cortical cell types: the multipotent progenitor model and the fate-restricted progenitor model. The first one considers that each RG has the potential to generate orderly all the different subtypes of excitatory neurons and macroglial cells. By contrast, the fate-restricted model claims that distinct subtypes of RGs coexist and are pre-specified to generate different type of neurons and glial cells. Therefore, in this model the fate of the

postmitotic cell is specified by the progenitor type rather than by the time of birth (Franco and Muller, 2013). The multipotent progenitor model was firstly proposed based on transplantation experiments performed in the ferret two decades ago showing that early-stage cortical progenitors are able to produce all types of cortical neurons when transplanted in an older cortex, and that old-stage progenitors transplanted in a younger cortex are only able to produce late-fate neurons (Frantz and McConnell, 1996; Desai and McConnell, 2000). More recently, a clonal analysis, through labeling single progenitors and tracing their progeny in the developing mouse neocortex *in* vivo, revealed that each RG orderly produce eight-to-nine neurons spanning all the cortical layers and that about one in six RG continues to produce glial cells (Gao et al., 2014). Although the study supports the multipotent progenitor model, it does not exclude the possibility that fate-restricted progenitors also exist. In fact, lineage-tracing experiments from Müller's group showed that RG progenitors expressing the transcription factor (TF) CUX2, which is also a marker for upper layer neurons, are specified early in development to produce upper- but not lower-layer neurons (Franco et al., 2012). Thus, these fate-restricted progenitors may coexist with multipotent progenitors.

An additional assumption from the multipotent progenitor model is that the fate potential of the progenitors is progressively restricted with time (Frantz and McConnell, 1996; Desai and McConnell, 2000). Recently, Jabaudon's group has shared breaking results regarding this issue. They showed that single RGs isolated from older cortices are able to generate neurons of a younger-fate when transplanted into younger cortices (Oberst et al., 2018), indicating that RGs remain multipotent along neurogenesis. These results and others bring to light the importance of environmental factors in regulating and re-specifying the potency of RGs.

### 1.2.2. Neurogenesis in the dorsal telencephalon

The process of neurogenesis in the dorsal and the ventral telencephalon shares some important similarities; although this process has been historically more studied in the dorsal part. For this reason, in the next sections I will only refer to dorsal neurogenesis.

At the onset of neurogenesis RGs begin to divide asymmetrically producing one RG and either a neuron (neurogenic division) or a more neurogenic-restricted progenitor known as intermediate progenitor (IP, proliferative division). RG-derived IPs delaminate from the apical ventricular zone (VZ), losing the cell apico-basal polarity, and migrate radially to a more basal proliferative region, the subventricular zone (SVZ), where they undergo symmetric divisions producing neurons directly or, less frequently, after 1 to 3 rounds of

symmetric proliferative divisions (Haubensak et al., 2004; Noctor et al., 2004; Sessa et al., 2008).

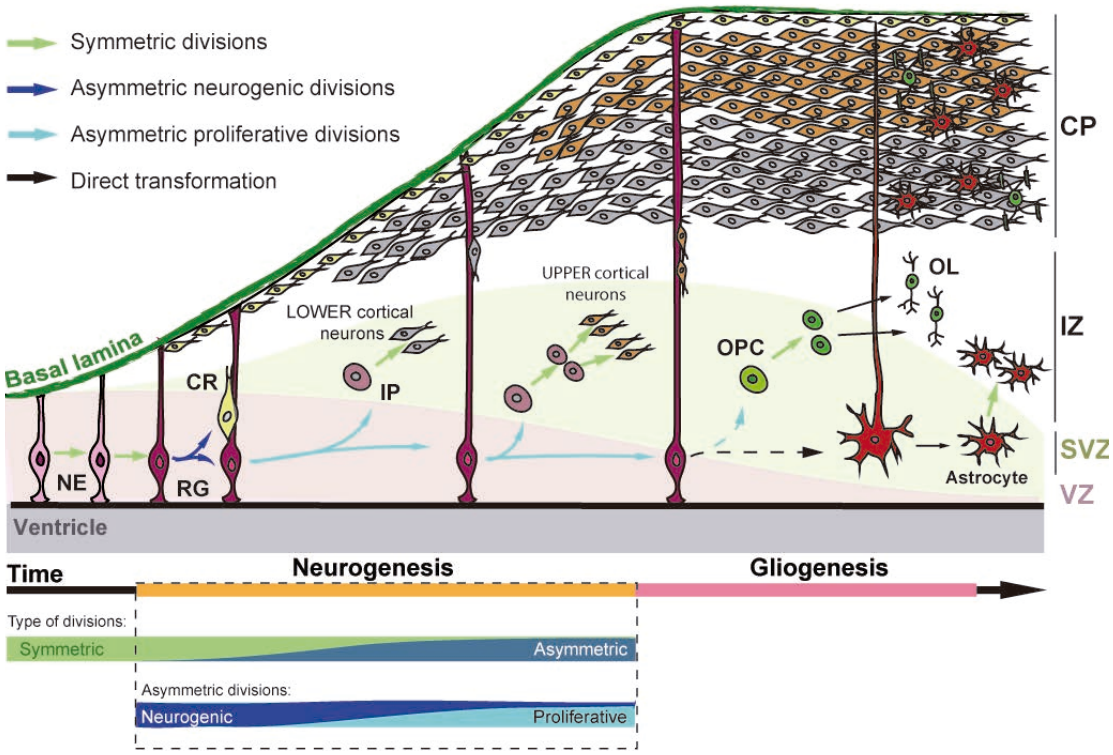


**Figure I.4. Development of the mammalian neocortex.** Glutamatergic neurons and cortical glial cells are generated sequentially from pluripotent neural progenitors of the dorsal telencephalon. During early stages of neocortical development, neuroepithelial cells (NEs) undergo symmetric divisions to expand the progenitor pool. Then, they transform into radial glial cells (RGs) capable of dividing asymmetrically. During neurogenesis, asymmetric RG divisions produce either a neuron (neurogenic divisions) or an intermediate progenitor (IP, proliferative divisions). RG- and IP-derived neurons are generated in an inside-out fashion (first grey neurons and then orange neurons). During gliogenesis, RGs produce oligodendrocyte precursor cells (OPCs) and astrocytes directly or trough asymmetric divisions (blue and black discontinuous lines). The abundance of symmetric and asymmetric divisions of the NEs and RGs along development is indicated bellow the scheme. CR, Cajal-Retzius neurons; CP, cortical plate; IZ, intermediate zone; SVZ, subventricular zone; VZ, ventricular zone.

In humans and other gyrencephalic species, the SVZ is thicker due to the appearance of an additional proliferative region, the outer SVZ (oSVZ; Smart et al., 2002; Zecevic et al., 2005), which contains outer radial glial progenitors (oRGs). These progenitors originate from basal RG divisions and lack the apical domain (Fietz et al., 2010; Hansen et al., 2010; Reillo et al., 2011; see also **Fig I.5)**. Fifty to 75% of SVZ cells in humans are oRGs while in the mouse these progenitors represent only 10% of SVZ cells (Hansen et al., 2010; Shitamukai et al., 2011; Wang et al., 2011b; Betizeau et al., 2013). oRGs can undergo multiple rounds of self-amplification before generating neurons or IPs, being the

major contributor of neuronal production in the human cortex (Hansen et al., 2010; Betizeau et al., 2013). In fact, different works have shown a positive correlation between oRG-self amplification and cortical expansion and folding, even in lisencephalic mice (Nonaka-Kinoshita et al., 2013; Stahl et al., 2013). Overall, these observations indicate that evolutionary expansion of the neocortex is explained by differences in the proliferative behaviour of the neural progenitors.

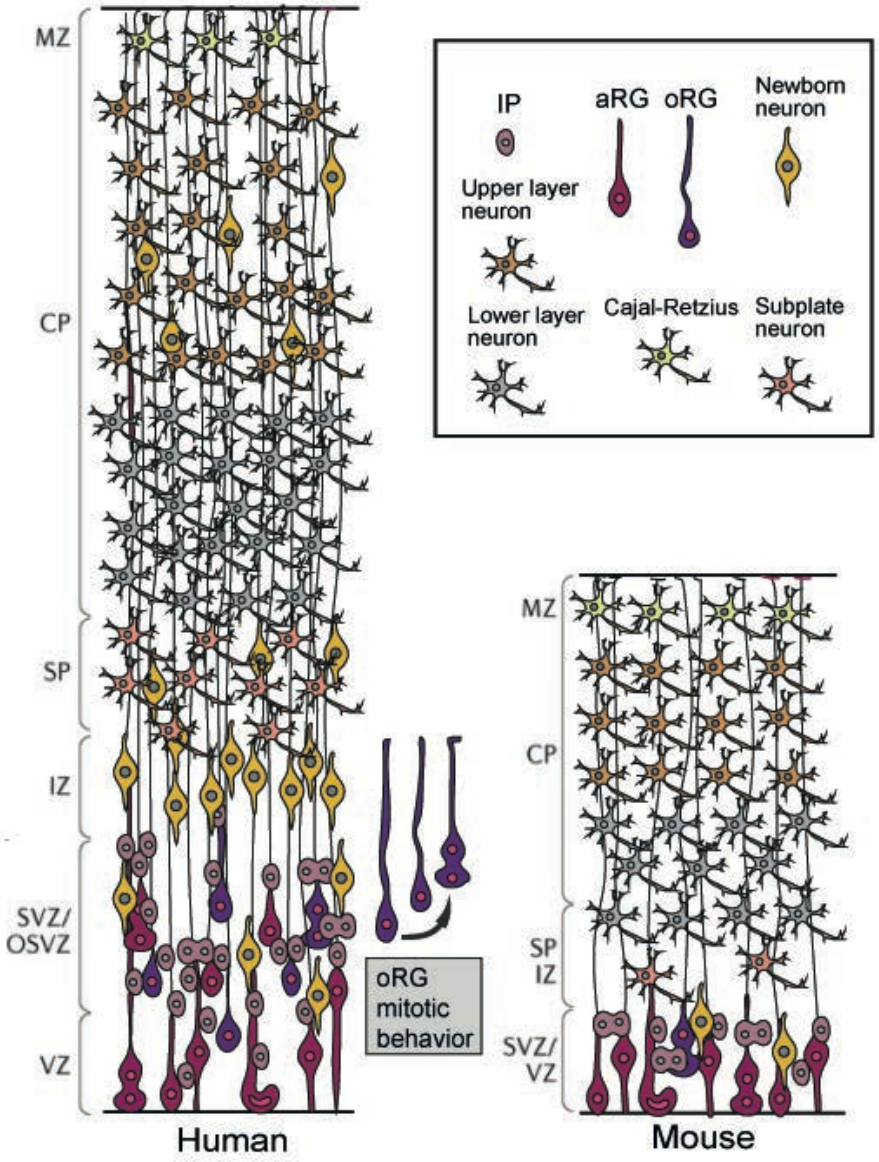


**Figure I.5. Cellular composition and laminar organization of the developing human and mouse neocortex.** Human and mouse developing neocortex differentiate in the subventricular region (SVZ). In the human neocortex, SVZ is expanded in comparison to the mouse and outer radial glial progenitors (oRGs) are abundant. oRGs undergo extensive proliferation before they differentiate. In the mouse SVZ, oRGs are scarce and the most abundant cells are intermediate progenitors (IPs). Adapted from Di Lullo and Kriegstein (2017).

According to the multipotent progenitor model described above, the distinct types of dorsal neurons are produced in a time-regulated manner. The first generated neurons are Cajal-Retzius and subplate neurons (see **Fig I.4**). These neurons form a transient layer called preplate (Angevine and Sidman, 1961; Luskin and Shatz, 1985) that later splits and forms the superficial marginal zone (layer I, made by Cajal-Retzius neurons) and the subplate. The cortical plate develops in between these two layers in an "inside-out manner": early-born neurons stay close to the place where they are generated and form the deepest layers (layer VI and V) of the neocortex while late-born neurons migrate radially surpassing these layers and forming the external layers IV to II (see **Fig I.4**).

### 1.2.3. Distribution of cell components in radial glial cell divisions

The accomplishment of an asymmetric division, generating a RG and a neuron or a RG and an IP, is likely the result from unequal distribution of cellular components and cell fate determinants (Paridaen and Huttner, 2014). Experiments in *Drosophila* neuroblasts showed that orientation of the cleavage plane during cell division determines the mode of division and, therefore, the fate of cell daughters. In this animal model, the cleavage plane of an asymmetric division is horizontal (parallel to the ventricle) and cell fate determinants such as Numb, Pros (PROX1 in vertebrates) and Brat segregate asymmetrically promoting cell cycle exit (differentiation) in one of the two daughters (Homem and Knoblich, 2012).

The link between orientation of progenitor division and the fate of the daughter cells is less clear in mammals. During neurogenesis, the cleavage plane of most RG divisions is perpendicular or oblique to the ventricular surface (**see Fig I.2a**), while horizontal cleavages are very rare and appear at late neurogenesis (Paridaen and Huttner, 2014). There is evidence that asymmetric inheritance of the apical domain is critical for daughter cell identity (Huttner and Kosodo, 2005). However, the fraction of RG divisions in which the apical domain is entirely inherited by one of the two daughters seems to be small; indeed, it has been reported that in most asymmetric divisions the apical domain is split between the two daughter cells (**Fig I.2b**; Konno et al., 2008; Shitamukai et al., 2011). On the contrary, the basal process in asymmetric divisions segregates to one of the daughter cells (Miyata et al., 2004; Shitamukai et al., 2011) and, in most cases, the cell that failed to inherit this process is the one that differentiates (**Fig I.2b**). Consistently, during symmetric divisions the basal process splits in between the two daughter cells (Kosodo et al., 2008), or even re-extends in case of not inheritance (Miyata et al., 2004), so that the two daughters maintain a polarized morphology. There is evidence that

integrin signaling mediated through the basal process is important for the proliferation of the oRG population (retaining basal but not apical process) in the ferret (Fietz et al., 2010), suggesting that contact to the basal lamina could provide important signals for the self-renewal of this RG subtype.

In addition to the epithelial structure, centrosomes also play a role in determining the daughter cell fate during asymmetric divisions. Centrosomes are cellular organelles formed by two centrioles that function as microtubule-organizing center. In cycling cells, one new centriole is formed next to the pre-existing ones in every cell cycle (Nigg and Holland, 2018). There is evidence that the daughter cell that inherits the “old mother” centriole remains as RG, whereas the cell inheriting the new centriole differentiates (see **Fig I.2;** Wang et al., 2009). The “old mother” centriole acts as a basal body to dock the primary cilium, which is reabsorbed during mitosis. Interestingly, it has been demonstrated that ciliary membrane remnants remain attached to the mother centriole during cell division and apparently this allows the inheriting cell to reassembly faster the cilium and get exposed to the cerebrospinal fluid signals (Paridaen et al., 2013).

### 1.2.4. Regulation of gene expression during neurogenesis

Generation of the distinct types of neurons at the correct time and appropriate numbers relies on an exquisite control of gene expression, which is achieved by transcriptional and post-transcriptional regulation.

Mechanisms involved in transcriptional regulation are influenced by both endogenous and exogenous factors, which ultimately affect the activity of TFs. Herein, I explain the role of morphogens in establishing regional patterning by the induction of specific TFs and how molecular interactions among TFs guide temporal specification. Then, I briefly summarize the external cues and signaling pathways that are known to be relevant for the progression of neurogenesis. And finally, I shortly explain the relevance of two well-known post-transcriptional mechanisms, alternative splicing (AS) and microRNAs (miRNAs), which add complexity to gene expression regulation. It is important to note that epigenetic modifications of chromatin also play a critical role along this process since they define the active or repressive state of the genes, allowing or inhibiting their transcription. Since the role of epigenetic regulation in cortical RGs has been studied mostly in the context of the neurogenic-gliogenic switch, I will review this aspect of transcriptional regulation in Section 1.2.5.

#### 1.2.4.1. Transcription factors

Early in development, the telencephalon is divided in different areas due to the gradients of morphogens such as Wingless/Integrated (WNT), Sonic Hedgehog (SHH), Fibroblast Growth Factors (FGFs) and Bone Morphogenetic Proteins (BMPs) along the dorso-ventral and the medio-lateral axes (Hoch et al., 2009). This patterning results in the activation of different TFs in the progenitors and constitutes the first level of transcriptional regulation. Dorsal identity is established by WNT and BMP gradients, whereas ventral identity relies on SHH (see **Fig I.6a**). FGF signaling influences patterning along the anterio-posterior axis by inducing the expression of the transcription factor *Pax6* (Bertrand et al., 2000), which is a key regulator for cerebral cortex development expressed in progenitors before the onset of neurogenesis. PAX6 exerts a dual role during neurogenesis. Around the onset of neurogenesis PAX6 promotes stemness maintenance and proliferation by modulating the expression of cell cycle regulators like *Cdk4 and Cdk6*, transcriptional regulators like *Hmga2*, and *Fabp7*, a gene encoding a fatty acid binding protein essential for NEs maintenance (Arai et al., 2005; Sansom et al., 2009; Mi et al., 2013). At later stages, PAX6 promotes neuronal differentiation by inducing the expression of pro-neural TFs such as *Neurog2* and *Sox4* (Scardigli et al., 2003; Sansom et al., 2009). Apparently, PAX6 can accomplish these two roles (promoting stemness and differentiation) because: (1) PAX6 expression in RGc changes during neurogenesis allowing the activation of different dosage-sensitive targets (Osumi et al., 2008; Sansom et al., 2009); and (2) alternative splicing of *Pax6* pre-mRNA produces different protein isoforms that differ in their DNA-binding domain (Walcher et al., 2013).

The bHLH TFs NEUROG1 and NEUROG2 are the main transcriptional activators of neurogenesis in cortical progenitors (Nieto et al., 2001; Schuurmans et al., 2004). These factors, which are induced by dorsal WNTs, turn-on the expression of a cascade of genes that promotes differentiation into glutamatergic neurons and represses ventral identity (Schuurmans et al., 2004). Conversely, the bHLH transcription factor ASCL1 promotes neuronal differentiation into GABAergic neurons and represses dorsal identity (Castro et al., 2011).

In addition to the regional patterning just described, there is a temporal patterning that assures the sequential generation of the different neuronal subtypes in the dorsal and ventral domains (see **Fig I.6b**). For example, FOXG1, which expression is induced by FGF8 gradient (Shimamura and Rubenstein, 1997), marks the transition between the generation of Cajal-Retzius neurons and deep-layer neurons by suppressing the

competence of RGs to generate Cajal-Retzius neurons (Kumamoto et al., 2013). The switch from deep- to upper-layer neurons seems more complex as it involves multiple regulatory cascades (Toma and Hanashima, 2015). Briefly, CTIP2, a transcription factor necessary for the specification of layer V neurons, has to be repressed for the specification of both early- and late-born neurons. Post-mitotically, TBR1 represses CTIP2 for the specification of layer VI neurons, while CTIP2 is repressed by SATB2 promoting the specification of layer II/III neurons. During layer V neuron specification, FEZF2 induces CTIP2 and represses precocious expression of SATB2 (see **Fig I.6b**; Britanova et al., 2008; Chen et al., 2008b; McKenna et al., 2011).

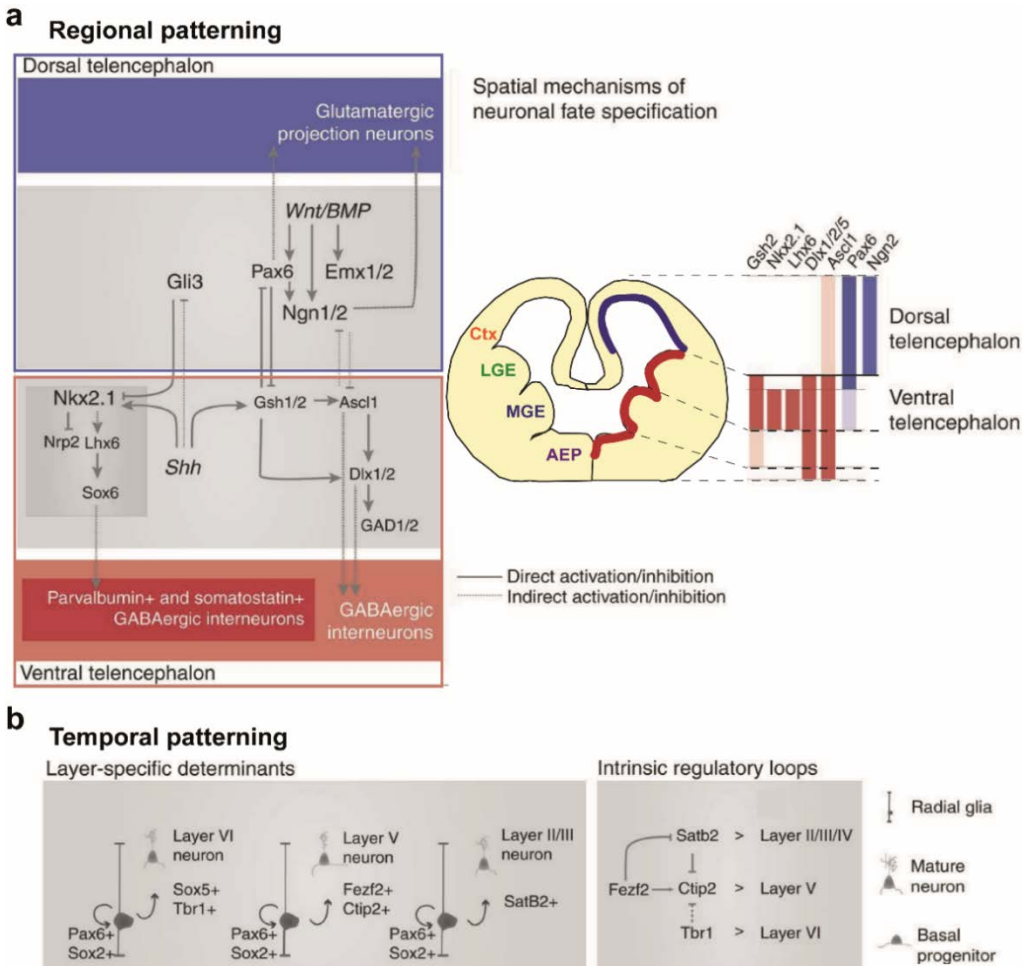


**Figure I.6. Mechanisms of regional and temporal patterning in the embryo mouse brain.** **(a)** Transcriptional mechanisms for the regulation of regional patterning include BMP and WNT signals, diffusing from the dorsal midline of the telencephalon and inducing the dorsal fate, and SHH signaling form the ventral midline and inducing the ventral fate (left panel). The expression of the transcriptional regional regulators is shown in the right panel. **(b)** The distinct classes of cortical glutamatergic neurons are specified by combinations of transcription factors (left), which are involved in cross-repressive interactions (right). AEP, anterior entopeduncular area; Ctx, cortex; LGE, lateral ganglionic eminence; MGE, medial ganglionic eminence. Adapted from Martynoga et al. (2012).

### 1.2.4.2. Signalling pathways

The onset and progression of neurogenesis are regulated by distinct signaling pathways. Moreover, there is extensive crosstalk among them, so that they can cooperate or modulate each other to trigger cellular responses in adaptation to external stimulus.

One of the signaling pathways that play an important role in RG maintenance along neurogenesis is NOTCH (Gaiano et al., 2000; Lutolf et al., 2002; Hatakeyama et al., 2004; Mason et al., 2006). NOTCH pathway acts through lateral signaling between neighboring cells and it is activated by NOTCH binding to the ligands DLL1 and JAG1. NOTCH activation induces the expression of the bHLH transcription factors HES1 and HES5. These TFs repress the expression of pro-neural genes such as *Ascl1*, *Neurog1* and *Neurog2*, thus inhibiting neuronal differentiation and maintaining a RG fate (Gaiano et al., 2000; Lutolf et al., 2002; Hatakeyama et al., 2004). Accordingly, mice deficient in Notch receptor 1 (*Notch1*) showed advanced neuronal production (Lutolf et al., 2002; Mason et al., 2006). Interestingly, signaling components of the NOTCH pathway are asymmetrically inherited by the daughters of RG asymmetric divisions: the cell showing higher NOTCH signaling is the one that remains as a RG, while the other differentiates (Shimojo et al., 2008; Ochiai et al., 2009; Dong et al., 2012). FGF signaling synergizes with NOTCH activity up-regulating *Hes1* transcription (Rash et al., 2011).

The other relevant signaling pathway is the WNT pathway. Canonical WNT signaling senses external cues and works through β-catenin, which in the presence of external WNT ligands translocates to the nucleus and mediates transcriptional regulation (Wrobel et al., 2007; Nusse and Clevers, 2017). At the onset of neurogenesis, WNT activity promotes symmetric proliferative divisions of RGs (Chenn and Walsh, 2003; Machon et al., 2003; Woodhead et al., 2006; Zhou et al., 2006; Wrobel et al., 2007). At later stages, WNT signaling promotes the generation of neurons by up-regulating *N-myc*, *Neurog1* and *NeuroD1* in the IPs (Hirabayashi et al., 2004; Kuwahara et al., 2010; Munji et al., 2011). Apart from its role in patterning, **SHH** also regulates neurogenesis (Shikata et al., 2011; Wang et al., 2011a; Willaredt et al., 2013; Saade et al., 2017). SHH activity is sensed by the primary cilium, where SHH binds to the Patched receptor triggering the activation of GLI TFs by relieving Smoothened (SMO) inhibition. In the absence of SHH activity, GLI3 acts as a repressor. GLI3 activity is important for the production of IPs and neuronal differentiation in the mouse dorsal telencephalon (Wang et al., 2011a). In the chick spinal cord SHH activity promotes symmetric proliferative divisions (Saade et al., 2017). Thus, in these two models changes in SHH levels seem to be important for regulating the division mode of RGs along neurogenesis.

The RG basal end-feet are in contact with the meninges, which are the source of retinoic acid. Retinoic acid signaling promotes the switch from symmetric to asymmetric divisions during the early phase of neurogenesis (Siegenthaler et al., 2009).

Another pathway that is lately attracting attention regarding its role in neurogenesis is the Hippo pathway. This pathway regulates size in many organs and tissues by balancing cell proliferation and apoptosis in response to different upstream signals, including cell adhesion, mechanical stress or signaling through G-protein coupled receptors (Kim and Jho, 2018). Activation of the pathway results in the phosphorylation and subsequent degradation of the transcriptional regulators YAP and TAZ. When the pathway is inactive, dephosphorylated YAP/TAZ translocates to the nucleus and regulates transcription of multiple genes (Totaro et al., 2018). Interestingly, the mechanical deformation of the nucleus also regulates YAP translocation into the nucleus in a phosphorylation-independent manner (Elosegui-Artola et al., 2017). In fact, YAP has emerged as an important mechano-transducer of cell environment independent of Hippo signaling activation (Dobrokhotov et al., 2018). There is evidence that transcriptional regulation by YAP/TAZ in the telencephalon promotes the expansion of RGs and reduces differentiation (Cappello et al., 2013; Lavado et al., 2013; 2014). In other cellular contexts cytoplasmic YAP/TAZ participates in the formation of the β-catenin destruction complex, thus promoting β-catenin degradation and inhibiting WNT-β-catenin signaling (Heallen et al., 2011; Azzolin et al., 2014).

#### 1.2.4.3. Alternative splicing

AS is a powerful mechanism to amplify molecular diversity from the genome. It consists in the inclusion or exclusion of exonic and intronic sequences of pre-mRNA resulting in the generation of distinct mature transcripts from a unique gene. Alteration of the transcript sequence can lead to the generation of distinct proteins (with related or different functions) that may have different stability and subcellular location (Vuong et al., 2016). In addition, AS can introduce premature termination codons into the mature mRNA resulting in the down-regulation of the mRNA via nonsense mediated decay (NMD; Yan et al., 2015). It has been reported that over 90% of the multi-exonic human genes undergo AS (Pan et al., 2008; Wang et al., 2008a). Interestingly, splicing forms are regulated in a tissue-, cell-, and developmental stage-specific manner (Raj and Blencowe, 2015).

The mammalian brain is the tissue expressing the greatest number of alternative mRNA isoforms (Licatalosi and Darnell, 2010). Several studies performed in the human and

mouse cerebral cortex have shown that splicing patterns change among cell populations (Ayoub et al., 2011; Zhang et al., 2014; 2016a) and along development (Dillman et al., 2013; Irimia et al., 2014; Molyneaux et al., 2015; Weyn-Vanhentenryck et al., 2018). For example, by doing RNA-seq in different micro-dissected regions of E14.5 mouse cerebral cortices, Ayoub et al. (2011) demonstrated that the splicing patterns in the VZ (progenitors) and the cortical plate (neurons) are different. The list of differentially expressed AS forms between progenitors and neurons has been enlarged by other studies (Zhang et al., 2016a; Liu et al., 2018) and reveals that differential AS affect genes related to proliferation, differentiation, neuronal migration and neuronal maturation, reinforcing the importance of AS in cortical development.

AS events are largely controlled by particular RNA-binding proteins (RBPs). RBPs recognize and bind specific regulatory sequences within the pre-mRNA and influence the choice of splice sites (Vuong et al., 2016). Some of these RBPs are enriched in the brain (Zhang et al., 2010; Charizanis et al., 2012; Licatalosi et al., 2012; Li et al., 2014; Weyn-Vanhentenryck et al., 2014) and their dysregulation in humans has been linked to several neurodevelopmental disorders including autism, schizophrenia and epilepsy (Irimia et al., 2014; Scotti and Swanson, 2016; Conboy, 2017).

The role of RBPs in the nervous system has been extensively studied in the context of synaptic function. For example, it is known that the RBPs SAM68 and PTBP2 are involved in the splicing regulation of *Neurexin*, a gene encoding a presynaptic protein that is translated by AS into more than 3,000 protein isoforms (Tabuchi and Sudhof, 2002). This protein diversification is thought to define synapse specificity (Vuong et al., 2016). Neurotransmitter receptor pre-mRNAs, such as the GABA receptor subunits, are also known for undergoing large AS regulation (Vuong et al., 2016).

The knowledge about RBPs generating neuronal diversity is still limited. One of the RBP proteins involved in AS with a known role in neural progenitors is PTBP1 (Boutz et al., 2007). The conditional deletion of *Ptbp1* in the mouse cerebral cortex causes premature differentiation resulting in lethal hydrocephaly (Shibasaki et al., 2013). More recently, Christopher Walsh's group (Zhang et al., 2016a) reported that PTBP1 regulates the splicing of *Flna* (Filamin A), which encodes an actin-binding protein that serves as a scaffold for proteins in the membranes. When PTBP1 is present in the cell, it avoids the inclusion of an exon coding for a premature stop codon in the mature *Flna* mRNA, thus allowing *Flna* to be translated, thereby preserving the polarity of neural progenitors. These results support a role for PTBP1 in maintaining the progenitor pool. Interestingly, it has been shown that the switch between PTBP1 and PTBP2 expression is important

for neuronal differentiation (Boutz et al., 2007). Both PTBP1 and PTBP2 present similar RNA-binding properties but while the former is restricted to neural progenitors the latest is predominantly expressed in neurons. PTBP1 represses PTBP2 expression by inhibiting the inclusion of exon 10 in the mature *PTBP2* transcript, which leads to degradation of the transcript by NMD (Boutz et al., 2007; Makeyev et al., 2007). During neuronal differentiation, *Ptbp1* expression is down-regulated and PTBP2 protein levels increase. Interestingly, *Ptbp2* expression is critical in a restricted time-window in differentiating neurons, when it prevents the expression of adult protein isoforms involved in neurite growth and synapsis (Vuong et al., 2016).

Other RBPs with function in neural progenitors are RBFOX (RBFOX1, RBFOX2 and RBFOX3, also known as NEUN), where they promote differentiation. Interestingly, one of the identified RBFOX1/2/3 targets is *Ninein*, which encodes a microtubule-anchoring protein. The NINEIN isoform expressed in progenitors is associated with the mother centriole. When the progenitor differentiates, RBFOX promotes the expression of another NINEIN isoform that delocalizes from the centrosome (Zhang et al., 2016a).

Another RBP involved in neural differentiation is SRRM4. Although this protein lacks a canonical RNA-binding domain it can bind exons near PTBP binding elements, suggesting that it may antagonize PTBP activity (Vuong et al., 2016). The phenotype of the *Srrm4* knockout mice suggests a role for this protein in neural progenitor specification and differentiation (Raj et al., 2011; Quesnel-Vallieres et al., 2015). One of its reported targets is REST, a key repressor of neuronal genes expression in neural progenitors (Tang, 2009). It has been reported that SRRM4 promotes the expression of a REST isoform with less transcriptional repression activity (Raj et al., 2011), thus modulating indirectly the expression of neuronal genes. Interestingly, SRRM4 is an essential factor for the inclusion of microexons, which are exons ranging from 3 to 30 nucleotides (Volfovsky et al., 2003).

#### 1.2.4.4. MicroRNAs

miRNAs are small RNA molecules that inhibit the expression of their mRNA targets by inducing mRNA degradation and/or repressing translation (Bartel, 2004). miRNAs are grouped into families according to the similarity of their seed sequences, which is the sequence that pairs to the mRNA targets. Usually, miRNAs act convergently on regulating one target or related mRNAs in order to achieve a cellular effect (Barca-Mayo and De Pietri Tonelli, 2014).

The process of miRNA biogenesis is complex and has been extensively studied (**Fig I.7**; Ha and Kim, 2014). Briefly, genes encoding miRNAs are transcribed by RNA polymerase II as long primary transcripts (*pri-miRNA*) that contain a stem-loop structure with the miRNAs sequences embedded. The *pri-miRNA* can encode a single miRNA or a cluster of often related miRNAs (Lau et al., 2001; Wang et al., 2016). The nuclear RNase III Drosha together with its cofactor DGCR8 crop the *pri-miRNA*. This reaction results in a smaller hairpin-shaped RNA, the *pre-miRNA*. The *pre-miRNA* is then exported to the cytoplasm where it is further processed by the RNAse III Dicer to obtain a small RNA duplex that contains two complementary miRNA sequences. The duplex is loaded onto an AGO protein to form the RNA-induced silencing complex (RISC). Then, one of the strands is removed and the one staying acts as a mature miRNA. Both strands can act as a mature miRNA, but in general one of the strands prevails over the other. Once in the RISC, the miRNA is able to recognize and bind to specific sequences in the 3' untranslated regions (UTR) of mRNA targets.

miRNAs are abundant in the cerebral cortex and some of them display a dynamic expression pattern along development, suggesting a role in specific developmental phases (Krichevsky et al., 2003; Sempere et al., 2004).

Fist evidences about the role of miRNAs in cortical development arose from the analysis of different conditional Dicer mutant lines (Bernstein et al., 2003). The *Emx1*-Cre; *Dicer*$^{lox/lox}$ conditional mutant mouse, in which *Dicer* is deleted from the onset of neurogenesis (E10.5) in progenitors of the dorso-lateral telencephalon, presents a microcephalic brain with impaired cortical stratification (De Pietri Tonelli et al., 2008; Kawase-Koga et al., 2009). Similar phenotypes were observed in *Nestin*-Cre; *Dicer*$^{lox/lox}$ and *Foxg1*-Cre; *Dicer*$^{lox/lox}$ mice, in which Dicer is depleted from E9.5-E10.5 in most telencephalic cells (Makeyev et al., 2007; Kawase-Koga et al., 2009; Nowakowski et al., 2011). Microcephaly in these conditional mutants is in part due to an augmented apoptotic cell death, especially in progenitors. These mutants also display defects in proliferation, differentiation and neuronal migration. Interestingly, the acute deletion of Dicer in E13.5 RGs by expressing Cre-recombinase in *Dicer*$^{lox/lox}$ embryo brains via *in utero* electroporation resulted in an enlarged neurogenic phase that lasted until postnatal stages (Nowakowski et al., 2013). This experiment suggested that miRNAs determines the duration of neurogenesis. miRNAs are also important for the maturation of the neurons, since the depletion of Dicer in cortical post-mitotic neurons (*CamK2*-Cre; *Dicer*$^{lox/lox}$ mouse) affected neuronal polarity and dendritic branching (Davis et al., 2008). Collectively, these results show that miRNAs play an important role in the formation of

cortical circuits. Despite of this, the number of miRNAs with a known function in brain development is still limited. Next, I explain the role of few of these miRNAs in cortical proliferation/differentiation.

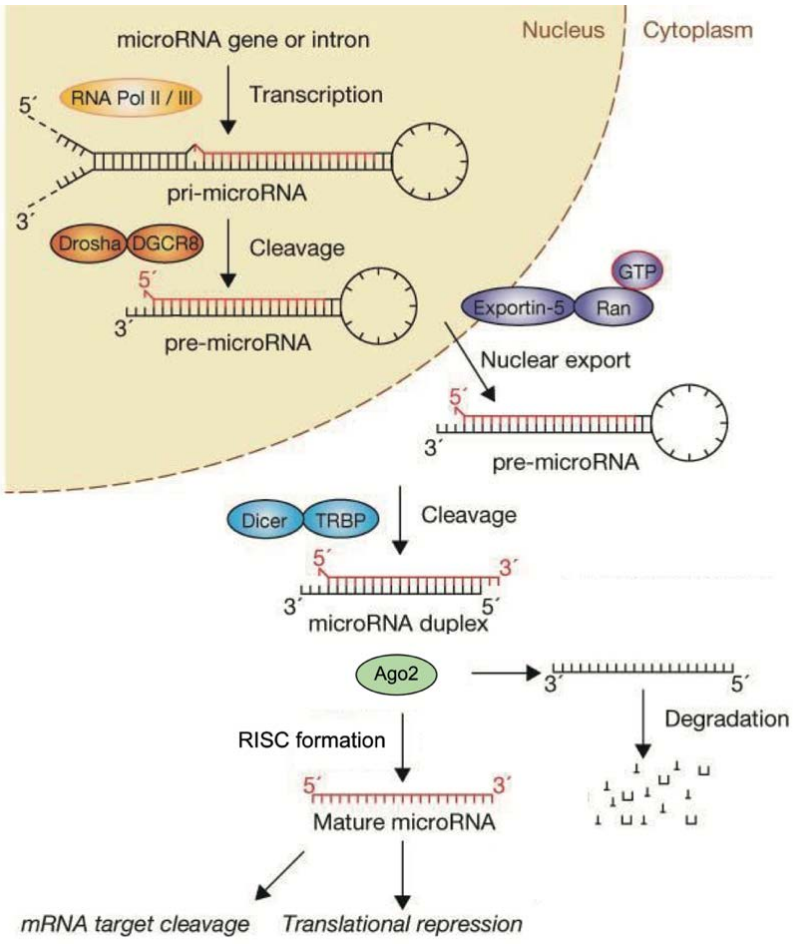


**Figure I.7. MicroRNA biogenesis.** RNA polymerase II or III transcribe the *miRNA* gene generating a *pri-miRNA* that is cleaved by the microprocessor complex Drosha–DGCR8 in the nucleus. The resulting precursor hairpin, the *pre-miRNA*, is exported from the nucleus by Exportin-5–Ran-GTP. In the cytoplasm, the RNase Dicer in complex with the RNA-binding protein TRBP cleaves the *pre-miRNA* to its mature length. The functional strand of the mature miRNA is loaded together with Argonaute (Ago2) proteins into the RNA-induced silencing complex (RISC), where it guides RISC to silence target mRNAs through mRNA cleavage or translational repression, whereas the passenger strand (black) is degraded. From Winter et al. (2009).

miRNAs of the lethal-7 (let-7) family were one of the first mammalian miRNAs studied in brain development because their orthologous in *Caenorhabditis elegans* were found to control timing of stem-cell division and differentiation (Reinhart et al., 2000). During early development, members of the let-7 family are involved in the suppression of pluripotency and commitment into the neuronal lineage. One of the best-known let-7 targets is the RBP LIN28, an inducer of pluripotency (Yu et al., 2007). In fact, the expression of let-7

and LIN28 are mutually regulated in a feedback loop since LIN28 inhibits let-7 biogenesis. Later in development, let-7 members reduce proliferation and accelerate neuronal differentiation in the developing neocortex targeting the cell cycle regulator Cyclin D1 and the nuclear receptor *Tlx,* involved in stem cell renewal (Zhao et al., 2010; Zhao et al., 2013).

Other miRNAs that have been studied in the context of cortical development are miR-9 and miR-124. MiR-9 is expressed in neural progenitors since the onset of neurogenesis where it regulates proliferation by repressing *Meis2*, a known transcriptional repressor of *Pax6* (Shibata et al., 2011). In addition, miR-9 participates together with let-7 in the repression of *Tlx* (Zhao et al., 2013) and regulates the generation of Cajal-Retzius neurons by repressing *Foxg1* (Shibata et al., 2011). In post-mitotic cells, mir-9 together with mir-124 represses *Rest*, thereby promoting the expression of neuronal genes (Barca-Mayo and De Pietri Tonelli, 2014). miR-9 also regulates neuronal migration by targeting *Foxp2* and axonal growth and branching by targeting *Map1b* and *Elavl1*, respectively (Kosik and Nowakowski, 2018). miR-*124* targets *Ptbp1* leading to the accumulation of PTBP2, therefore inducing pro-neuronal splicing patterns (Makeyev et al., 2007).

The conditional deletion of the miRNA cluster *mir-17-92* (*mir-17, mir-18, mir-19* and *mir-92*) in the dorsal mouse telencephalon before neurogenesis suppresses RG expansion and enhances IP production. These effects are mediated by the increased expression of the *mir-92* target *Tbr2*, a TF with a role on the specification of IPs, and the *mir-19* target *Pten*, a tumor suppressor factor that inhibits RG production (Bian et al., 2013; Nowakowski et al., 2013). In addition, miR-17 participates in IP production by controlling the expression of the cell cycle regulator *p21* (Chen et al., 2014b).

### 1.2.5. Gliogenesis

At the end of embryonic development RGs of the dorsal telencephalon stop producing neurons and start to generate OPCs (oligodendrocyte precursor cells, expressing the cell marker OLIG2) and astrocytes (**Fig I.4**). At birth, glial cells only comprise ~3% of the cells in the rodent cerebral cortex. This cell population increases up to 50-fold from P0 to P21 and in the adult represent ~50% of the cells, a percentage that remains stable along adulthood (Bandeira et al., 2009).

As I will detail in the following sections, generation and differentiation of glial cells is highly influenced by neuronal signals. In turn, glial cells are crucial for the establishment

of neuronal connections. Therefore, timely appearance of the right type and number of glial cells depends on the neuronal population and is essential to accomplish a successful maturation of the cerebral circuits.

#### 1.2.5.1. Types and sources of cortical astrocytes

Astrocytes are a heterogeneous population. Traditionally, two classes of astrocytes have been recognized: protoplasmatic and fibrous (see **Fig I.8;** Miller and Raff, 1984). Protoplasmatic astrocytes populate the grey matter and possess highly branched "bushy" processes. The end-feet of these cells contact to neuronal synapses and participate in synaptic communication (Henneberger et al., 2010; Reichenbach et al., 2010; Uwechue et al., 2012). The processes of the protoplasmatic astrocytes occupy non-overlapping domains that can cover ~20,000-120,000 synapses per unit in mice and up to 2 million synapses in human (Bushong et al., 2002). This subtype of astrocytes also enwraps blood vessels. Fibrous astrocytes populate mainly the white matter and have a "star-like" appearance. These cells are associated to the myelinated axonal tracts and are in contact with the nodes of Ranvier. Moreover, they also contact the blood vessels. In contrast to the protoplasmatic astrocytes, fibrous astrocytes maintain high GFAP (glial fibrillary acidic protein) expression in the adult brain. Besides these two astrocyte types, the cortical layer-I is populated by astrocytes that show "bushy" morphology like the protoplasmatic astrocytes but express high levels of GFAP like fibrous ones (Garcia-Marques and Lopez-Mascaraque, 2013; Martin-Lopez et al., 2013). The processes from layer-I astrocytes locate just under the pia matter and form the glial limiting membrane. In the human neocortex, two additional subtypes of astrocytes have been identified: interlaminar and varicose projection (**Fig I.8**). The interlaminar astrocytes show a spheroid cell body located in cortical layer-I and several processes that point to the pial surface, where they contribute to the glia limitants, and a long radial process that extend to the layer III/IV. The varicose projection astrocytes are located in the deep cortical layers and extend one or two thick long processes to the upper layers (Oberheim et al., 2006). In addition, other regions of the nervous system present specialized astrocytes, such as the Bergmann glia in the cerebellum and the Muller glial in the retina.

More recent studies have reported that the astrocyte molecular profile within subtypes varies across different brain regions and along development. For example, the expression levels of synaptogenic factors and the capacity to induce synapse formation vary among astrocytes from different brain regions (Bachoo et al., 2004). In agreement with this regional heterogeneity, it has been shown that astrocytes induce more

functional synapses when cultured with neurons from the same brain region (Morel et al., 2017).

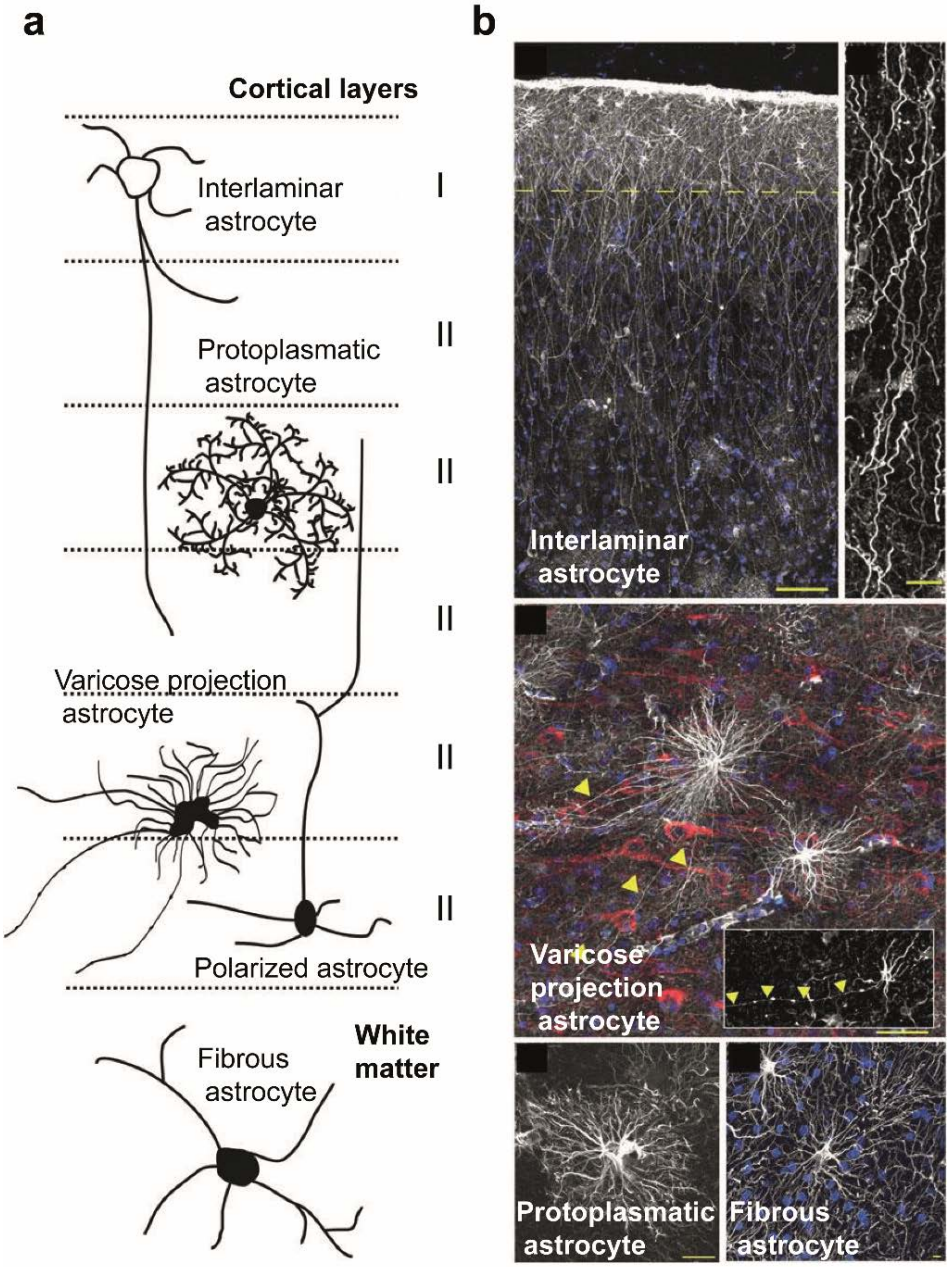


**Figure I.8. Types of astrocytes in the human neocortex**. **(a,b)** The distinct types of astrocytes are located within different neocortical layers. **(b)** Representative immunostainings of the different types of astrocytes in the human neocortex: interlaminar astrocytes (scale bar: 10 mm), variscose projection astrocytes (scale bar: 50mm), protoplasmatic astrocytes (scale bar: 20 mm) and fibrous astrocytes (scale bar: 10 mm). Adapted from Oberheim et al. (2012).

Already in 1911, Santiago Ramón y Cajal proposed that RGs likely transform into astrocytes in the cortex because of the morphological similarities between the two types of cells that he observed using the Golgi impregnation (Ramón y Cajal, 1899). Subsequently, others have confirmed Cajal's theory showing that at the end of neurogenesis most RGs detach from the ventricle, loss their radial orientation and extend multiple stellate processes in the course to become individual astrocytes (**Fig I.4**; Schmechel and Rakic, 1979; Voigt, 1989; Gressens et al., 1992). Later, the group of Arnold Kriegstein filmed this transformation by live imaging in cultured rat brain slices and showed that differentiated cells present astroglial electrophysiological properties (Noctor et al., 2004). The RG-derived astrocytes migrate radially from their ventricular source domain to the cortical grey matter, where they transform into protoplasmatic astrocytes, or to the white matter and become fibrous astrocytes (**Fig I.9;** Magavi et al., 2012; Tsai et al., 2012). Once in their final location, astrocytes undergo extensive proliferation during the first two postnatal weeks (Burns et al., 2009; Ge et al., 2012). Fate mapping experiments revealed that local proliferation of astrocytes in the cortex contributes for the major portion of astrocytes (almost 50%) in the postnatal mouse cortex (Ge et al., 2012). The direct contribution of RGs to the postnatal population is believed to be small (around 30%; Magavi et al., 2012; Ge and Jia, 2016). Moreover, lineage tracing experiments have demonstrated that the clones of astrocytes generated from an individual RG are either protoplasmatic or fibrous astrocytes (Price and Thurlow, 1988; Garcia-Marques and Lopez-Mascaraque, 2013), suggesting that these two cell populations arise from different progenitors.

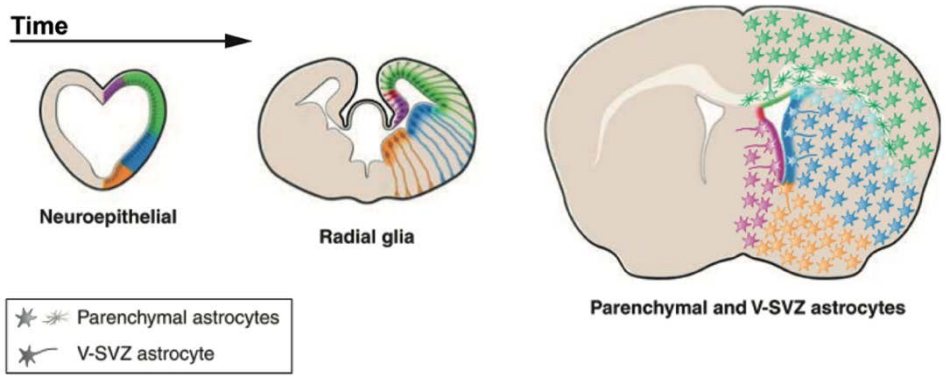


**Fig I.9. Regional specification of neural progenitors and astrocytes throughout development.** Scheme of a coronal view of the telencephalon at different developmental times. Note that in postnatal sections (right), parenchymal and ventricular and subventrivular (V-SVZ) astrocytes are distributed in a region-restricted manner according to their domains of origin. From Bayraktar et al. (2014).

Several evidences show that glial progenitors in the postnatal SVZ also contribute to the cortical astrocyte population (Tabata, 2015; Ge and Jia, 2016). The postnatal SVZ is in the wedge-shaped structure between the pallium and the subpallium and it is composed by cells derived from subpallial RGs (Marshall and Goldman, 2002). Retroviral injections show that in early postnatal days SVZ cells migrate dorsally and differentiate both into astrocytes and oligodendrocytes (Tabata, 2015; Ge and Jia, 2016). However, the contribution of these cells to the pool of cortical astrocytes is still not clear (Ge and Jia, 2016).

There is evidence that OPCs can differentiate into protoplasmatic astrocytes. Firsts evidences about the astroglial potential of these progenitors came from *in vitro* studies showing that OPCs derived from the optic nerve differentiate into cells with a characteristic astroglial morphology (called type 2 astrocytes) when cultured in the presence of fetal calf serum (Raff et al., 1983). Nonetheless, lineage tracing experiments using transgenic mice that express Cre-recombinase in OPCs show that the contribution of these progenitor type to the astrocyte population during normal development is minor and restricted to the pyriform cortex and other ventral brain regions such as the amygdala and the hypothalamus (Zhu et al., 2008; Guo et al., 2009; Huang et al., 2019).

Layer-I astrocytes are already present in the cortex during early embryonic development. This particular population of astrocytes seems to arise from VZ-derived cells that move to the basal lamina during the formation of the preplate (Marin-Padilla, 1995). At later stages, the population of layer-I astrocytes increases probably by cells produced by SVZ glial progenitors (Tabata, 2015).

In the adult cortex, astrocytes continue to proliferate at a very low rate (Ge et al., 2012). In case of injury or disease, these cells can become reactive and proliferate extensively. Reactive state is characterized by increased GFAP expression and extensive hypertrophy (Sofroniew, 2009).

#### 1.2.5.2. Molecular mechanisms involved in astrogliogenesis

The timing of astrocyte generation relies on a complex interplay between epigenetic mechanisms, extracellular cues and signaling pathways.

**Epigenetic mechanisms: the gliogenic switch**

For years it had been considered that astrocytes were the first glial cell type generated in the cortex. Nowadays it is known that cells from the oligodendroglial lineage differentiate from the RGs as soon as neurogenesis finishes. However, research on the

neurogenic to gliogenic switch had traditionally focused on the factors promoting the transition between neuron to astrocyte production.

During neurogenesis, the astroglial genes are silenced. Multiple evidences support that the potential to generate astrocytes is acquired by epigenetic changes that derepress astroglial genes transcription in RGs. DNA methylation and histone modifications represent the main epigenetic mechanisms involved in this process (MuhChyi et al., 2013).

DNA methylation is associated to transcriptional repression, especially at gene promoters where it impedes sterically the binding of TFs to the DNA (Watt and Molloy, 1988). During early neurogenesis, the promoter of the glial-specific gene glial fibrillary acidic protein (*Gfap*) is hypermethylated (Takizawa et al., 2001; Fan et al., 2005) and it is demethylated during gliogenesis. Indeed, the conditional deletion in RGs of *Dnmt1*, coding for the methyltransferase responsible for methylation maintenance, results in accelerated demethylation of the glial promoters and precocious generation of astrocytes (Fan et al., 2005). NOTCH signaling promotes the demethylation of the *Gfap* promoter through the induction of the nuclear factor I A (NFIA), which dissociates DNMT1 from the glial promoters and allows *Gfap* expression (Namihira et al., 2009; Sparmann et al., 2013).

In addition, proteins of the Polycomb group (PcG) have been demonstrated to set the timing of the gliogenic switch through histone methylation. The depletion of PcG components results in prolonged neurogenesis and delayed onset of astrogliogenesis (Hirabayashi et al., 2009; Sparmann et al., 2013). Some components of the PcG complex catalyze histone H3 trimethylation at lysine 27 (H3K27me3), which leads to transcriptional silencing. During corticogenesis, the levels of H3K27me3 gradually increase at the promoter of the neuronal gene *Neurog1* until being completely repressed (Hirabayashi et al., 2009). This event has been proposed as an intrinsic timer that defines the end of the neurogenic period. NEUROG1 is a known activator of the expression of other neuronal genes (see Section 1.2.4.1). Moreover, it sequesters p300/CBP, a co-activator of the pro-astroglial Janus kinase (JAK)-STAT pathway (Sun et al., 2001). Therefore, NEUROG1 repression allows the activation of JAK-STAT pathway and weakens the expression of other neuronal genes.

**Pro-astroglial signaling pathways**

The JAK-STAT signaling pathway is key for the differentiation of astrocytes. The activation of JAK-STAT is induced by cytokines of the interleukin-6 family secreted by

newborn neurons such as LIF (leukemia inhibitory factor), CNTF (ciliary neurotrophic factor) and CT-1 (cardiotrophin-1). Upon activation of JAK receptors there is a cascade of molecular events that ends with the translocation of the TF STAT3 to the nucleus, where it activates the transcription of astroglial genes, such as *Gfap* (Barnabe-Heider et al., 2005). Nevertheless, the presence of external glial cues is not sufficient to induce astrocyte differentiation. *In vitro* evidence indicates that demethylation of astroglial promoters by the activation of NOTCH signaling is a requisite for the onset of astrogliogenesis and is induced by NOTCH ligands expressed by newborn neurons and IPs during mid-neurogenesis (Campos et al., 2001; Namihira et al., 2009). NOTCH also promotes astrogliogenesis by repressing neuronal and oligodendroglial genes, presumably thought the repressor activity of HES1 and HES5 (Louvi and Artavanis-Tsakonas, 2006), and by potentiating the phosphorylation of STAT3 by recruiting the kinase JAK2 (Kamakura et al., 2004).

BMP signaling has also shown to promote astrocyte differentiation. During neurogenesis, BMP activity promotes progenitor fate (see Section 1.2.4.1) and later in development it acts in synergy with the JAK-STAT pathway to promote astrocyte differentiation (Gross et al., 1996; Nakashima et al., 1999). SMAD1, an effector of the BMP pathway, is able to bind STAT3 to form a transcriptional activator complex, SMAD1/STAT3/p300, that induces astroglial genes (Nakashima et al., 1999). Moreover, BMP signaling inhibits oligodendroglial fate *in vitro* and in the spinal cord (Mekki-Dauriac et al., 2002; Samanta and Kessler, 2004).

#### 1.2.5.3. The oligodendroglial lineage

Myelinating oligodendrocytes are the result of a complex and precise process of proliferation and differentiation of OPCs. Different stages of the lineage progression can be distinguished by using the different markers showed in **Fig I.10**. The analysis of the expression profile of the oligodendroglial lineage from OPC to mature oligodendrocyte revealed a progression through a strict program of six developmental stages. In addition, mature oligodendrocytess can be clustered in six different groups, indicating that they form a heterogeneous population (Marques et al., 2016).

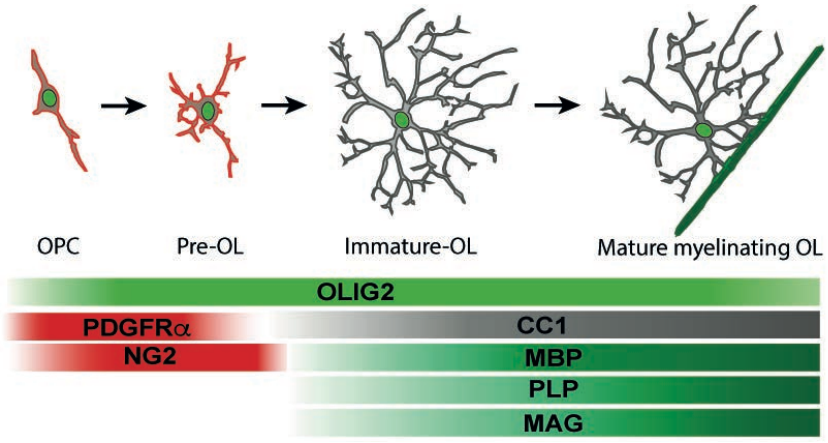


**Fig I.10. The oligodendroglial lineage.** Schematic representation of the oligodendroglial lineage progression from an oligodendrocyte precursor cell (OPC) to a myelinating oligodendrocyte (OL) and the stage-specific markers (indicated by colored gradients). Notice that OLIG2 is expressed throughout all stages of the oligodendroglial lineage. The list of markers is limited to the markers used in the present study.

In the embryonic telencephalon, OPCs are generated in three sequential waves from RGs of different regions of the germinal VZ (**Fig I.11**; (Kessaris et al., 2006). The first wave of OPC generation in the mouse starts around E12.5 in the MGE and the AEP, in the ventral telencephalon. Second wave of OPCs arises from the LGE around E15.5. Ventral-originated OPCs migrate laterally and dorsally while they proliferate to populate the entire telencephalon. Perinatally, RGs of the dorsal VZ also start to produce OPCs that proliferate and spread along the cortex. After birth, OPCs from the first wave disappear (Kessaris et al., 2006; Tripathi et al., 2011). In the adult mouse neocortex ~80% of oligodendrocytes derive from OPCs of the dorsal VZ and ~20% from the LGE (Tripathi et al., 2011). In addition, there is evidence that the adult SVZ generate OPCs (Nait-Oumesmar et al., 1999; Menn et al., 2006). The generation of OPCs in a ventral-to-dorsal fashion seems to be conserved in humans (Jakovcevski et al., 2009).

During development, OPCs from different origins express different markers (Kessaris et al., 2006) and they behave different in front of stimuli, such as growth factors or injury (Ortega et al., 2012; Crawford et al., 2016). Interestingly, the ablation of ventral or dorsal OPCs by means of the targeted expression of a toxin gene (DTA) results in the spread of OPCs from neighboring populations to restore normal oligodendrocyte density and distribution and normal myelination (Kessaris et al., 2006). Furthermore, the ablation of practically all telencephalic OPCs results in the forward migration and proliferation from diencephalic OPCs (Bergles and Richardson, 2015). These observations indicate that OPCs are highly homeostatic and suggest that OPCs from different origins might be functionally equivalent.

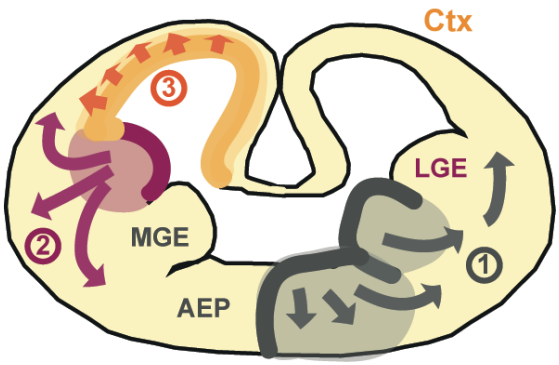


**Fig I.11. Waves of oligodendroglial production in the mouse developing telencephalon.** Scheme representing the origins of the three sequential waves of oligodendrocyte precursor cell (OPC) production. First wave starting around E12.5, second wave starting around E15.5; and, third wave starting at perinatal stages. Arrows indicate the migration routes of the OPCs. AEP, anterior entopeduncular area; Ctx, cortex; LGE, lateral ganglionic eminence; MGE, medial ganglionic eminence. Adapted from Richardson et al. (2007).

The final location of the oligodendrocytes may also reflect a functional diversity (Dimou et al., 2008; Schulz et al., 2011). Beyond of intrinsic differences, there is evidence that oligodendrocyte diversity is the results of their adaptation to neuronal needs (Marques et al., 2018; van Tilborg et al., 2018).

OPCs remain abundant in the adult brain, where they comprise around 5% of the cells (Dawson et al., 2003). Adult OPCs are responsible for the generation of new oligodendrocytes to maintain and remodel myelin in response to learning experiences or environmental stimuli (Birey et al., 2017). In case of demyelinating lesion, OPCs are recruited to the lesion and proliferate and generate new oligodendrocytes to drive remyelination (Franklin and Goldman, 2015).

#### 1.2.5.4. OPC specification and differentiation

OPC specification in the ventral telencephalon is induced by SHH from the MGE and LGE neural progenitors (Nery et al., 2001; Tekki-Kessaris et al., 2001). In these domains, progenitors express OLIG2 and give rise to both neurons and OPCs. OLIG2 is a key TF for OPC generation; its expression is down-regulated in neuron-committed cells but remains high throughout all the oligodendroglial lineage (**Fig I.10;** Lu et al., 2002; Ligon et al., 2006). The molecular mechanisms that regulate the neuron-to-OPC switch in the ventral telencephalon are not well understood. It is known that OLIG2+ progenitors in the pMN progenitor domain of the spinal cord generate first motoneurons and later oligodendrocytes. This cell fate switch relies on the phosphorylation of a particular residue (serine 147) in OLIG2 that likely alters its transcriptional activity (Li et al., 2011). FGF signaling also plays a role in ventral OPC specification since conditional knockout

of the FGF receptors *Fgfr1* or *Fgfr2* in the mouse ventral telencephalon results in reduced number of OPCs (Furusho et al., 2011).

Although the mechanisms involved in the specification in dorsal OPCs are poorly understood, there is evidence that dorsal BMP and WNT signaling repress the generation of OPCs during early development (Gomes et al., 2003; Langseth et al., 2010). At later stages dorsal RG cells can generate OPCs independently of SHH by a FGF-dependent mechanism (Chandran et al., 2003; Cai et al., 2005). However, more recently, Winkler et al. (2018) elegantly demonstrates that SHH signaling is necessary for normal OPCs generation in the dorsal telencephalon. Interestingly, they identify migrating interneurons as the source of SHH ligand for dorsal progenitors. Consistently, two recent reports claim the existence of a SHH-dependent domain in the dorsal postnatal SVZ that accounts for the production of a large number of OPCs (Tong et al., 2015; Sanchez and Armstrong, 2018).

OPCs generated in the germinal VZ migrate following chemo-attractive signals, such as the spatial gradients of SHH, BMP and WNT and other local cues (growth factors, ECM proteins, axon guidance molecules), until they reach their final destination (van Tilborg et al., 2018). Neurons, through the activation of AMPA and glutamate receptors, and blood vessels also contribute to OPC migration (Gudz et al., 2006; Tsai et al., 2016).

Once in their final destination, OPCs proliferate in response to PDGF-A, which is secreted by astrocytes and neurons (Noble et al., 1988; Raff et al., 1988; Fruttiger et al., 1999) and other extracellular signals such as NOTCH, WNTs and BMPs that act together to inhibit differentiation (Emery and Lu, 2015). The balance between proliferation and differentiation is tightly regulated and it relies in the coordinated action of intrinsic and extrinsic regulators. A large number of TFs, including NKX2.2, OLIG1, ASCL1, YY1, SOX10 and MYRF, are known as positive regulators of OPC differentiation (Emery and Lu, 2015). As a prevailing mechanism, most of these TFs promote the expression of myelin-associated proteins, such as MBP (Myelin basic protein) and PLP (Myelin proteolipid protein).

Transcriptional regulatory networks in differentiating oligodendrocytes are highly influenced by epigenetic modifications. Deacetylation of histones causes chromatin compaction, which is associated to gene silencing. Several studies showed that histone deacetylases (HDACs) HDAC1 and HDAC2 function by repressing genes that inhibit oligodendrocyte differentiation (He et al., 2007; Shen et al., 2005; Ye et al., 2009). Additionally, it has been shown that they hijack the WNT effector TCF7L2 to prevent its

association with β-catenin and the subsequent transcription of WNT signaling target genes (Ye et al., 2009). Moreover, there is evidence that the ATP-dependent chromatin remodeling enzyme Smarca4 (BRG1) increases accessibility of promoters of genes required for myelination, presumably by cooperation with OLIG2 (Yu et al., 2013). More recently, Marie et al. (2018) claimed a similar function for the remodeling factors CDH7 and CDH8.

#### 1.2.5.5 Myelination

In the mouse brain, myelination starts postnatally and its extension is heterogeneous among the distinct fiber tracts (Sturrock, 1980). In the CC, the major fiber tract formed by axons from callosal neurons (see Section 1.1), oligodendrocytes generate myelin at a high rate during approximately the first 10 postnatal weeks. After, they continue to form myelin at an ever-decreasing rate (Sturrock, 1980). In humans, the prolonged period of myelination is extended through the firsts 20 years of life (Fields, 2008) and particularly in the neocortex there is significant increase in white matter volume until the third decade (Shaw et al., 2008; Bartzokis et al., 2010; Miller et al., 2012).

In the process of differentiation, post-mitotic oligodendrocytes extend a complex network of processes to contact adjacent axons. The diameter of the axon dictates the temporal order of myelination: larger axons are myelinated first and axons smaller than 0.2 μm are never myelinated (Almeida et al., 2011; Lee et al., 2012). The mechanism by which oligodendrocytes sense axonal size remains unknown. However, there is evidence that oligodendrocytes respond to some molecules secreted by the axon and that the secretion of these molecules correlates with the axonal caliber (Goebbels et al., 2017). Moreover, electrical activity (Ishibashi et al., 2006; Gibson et al., 2014; Wake et al., 2015; Mitew et al., 2018), factors released by astrocytes such as the leukemia inhibitory factor (LIF; Ishibashi et al., 2006) and the density of OPCs (Rosenberg et al., 2008) also contribute to the axonal selection.

When the oligodendrocyte starts to myelinate an axon, the process in contact with the axon expands laterally and wraps the axon in concentric layers of myelin membrane. The wrapping mechanism has been long studied. The prevailing mechanism is the “carpet-crawler” in which wrapping is led by an inner tongue of uncompacted myelin in contact with the axon (Bauer et al., 2009; Snaidero et al., 2014). Then, myelin compaction starts from the outermost layers to the inners as the system develops (see **Fig I.12**; Snaidero et al., 2014). MBP plays a major role in myelin compaction. In the

*shiverer* mutants, which lack MBP, there is no compacted myelin and, consequently, the myelin membrane is instable and cannot grow (Inoue et al., 1981; Roach et al., 1983).

Lateral expansion of the myelin sheaths defines the length of the internodes (myelin units). These myelin units electrically insulate the axons and limit the influx of ions to the nodes of Ranvier, the unmyelinated spaces between internodes (**Fig I.13**). This configuration permits the saltatory conduction of the action potential, thus allowing for rapid and efficient transmission of the signal through large distances (Hartline and Colman, 2007). Voltage-gated sodium and potassium channels are clustered at nodes and the regions of axo-oligodendroglial interactions flanking the nodes, the paranodes, are enriched in scaffolding and cell adhesion proteins. Correct paranodal organization is crucial for the assembly and maintenance of the nodes of Ranvier (see **Fig I.13**; Eshed-Eisenbach and Peles, 2013; Rasband and Peles, 2015).

Axon diameter, myelin thickness, internode length, and the structure and composition of the nodes of Ranvier are critical determinants of the conduction speed of myelinated axons (Fields, 2008). Interestingly, the group of Douglas Fields has recently reported that molecules secreted by perinodal astrocytes, which cover some nodes, influence nodal gap length and myelin thickness (Dutta et al., 2018).

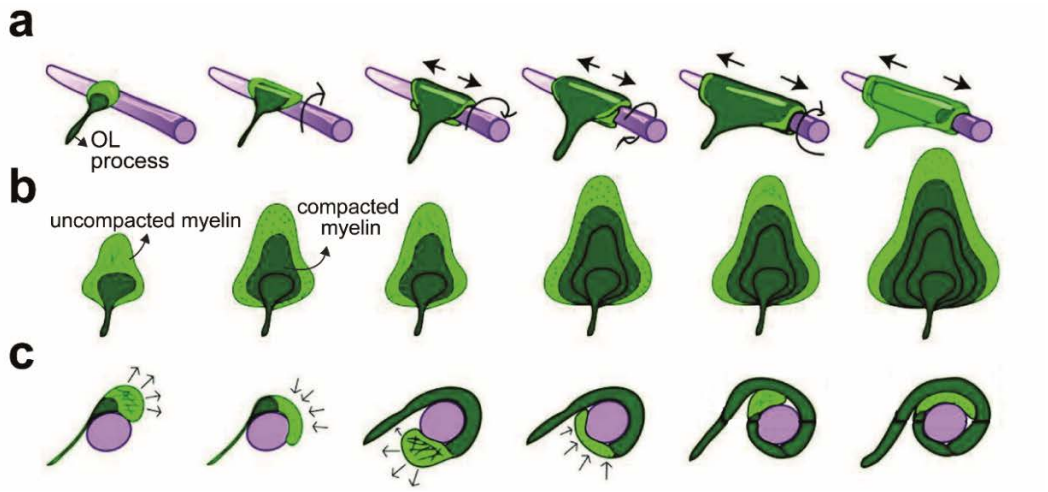


**Fig I.12. Model of myelin biogenesis in the central nervous system. (a)** An oligodendrocyte (OL) process contacts the axon (in pink) with the leading edge tip (in light green) and wraps it in concentric layers while the myelin sheaths expand laterally. **(b)** Flattened view of the myelinating process as it growths to show how it spreads and compacts. **(c)** Growth of the myelinating process as seen in a cross section showing that the uncompacted inner tongue advances in contact with the axon and displaces the myelin layers synthesized previously. From Klingseisen and Lyons (2018).

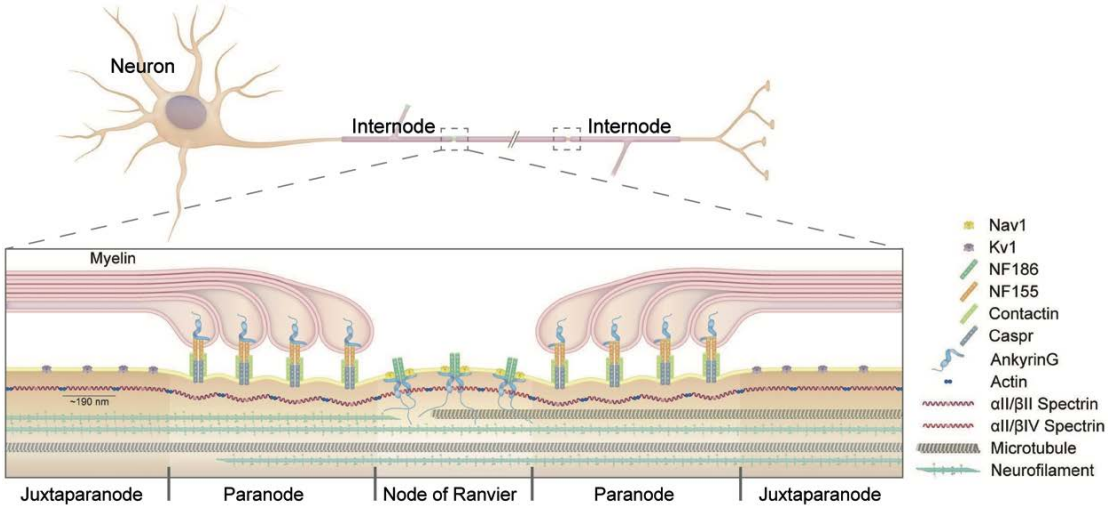


**Fig I.13. Domains of the myelinated axon and nodal architecture.** Representation of the different domains of a myelinated neuron. The unmyelinated spaces between internodes form the nodes of Ranvier, enriched in voltage-gated $Na^+$ channels. The paranode is the region where the myelin is attached to the axon through cellular adhesion proteins, including neuronal CASPR and oligodendroglial ligand NF155, and other scaffolding proteins. The juxtaparanode is the region under the myelin that concentrates $K^+$ channels. Key molecules expressed in each domain are depicted. Adapted from Pan and Chan (2017).

## 1.3. Neurodevelopmental disorders

Connectivity defects are thought to underlie autism, intellectual disability and neuropsychiatric disorders (Hu et al., 2014). As the understanding of the glial functions in development and maintenance of brain circuitry evolves, the number of studies dealing with the pathological role of these cells in developmental disorders is increasing.

### Autism

Autism spectrum disorders (ASDs) have been related to defects in synapse formation, synapse function and plasticity (Parikshak et al., 2013). Consistent with the role of astrocytes in synapse regulation, astrocyte alterations have been reported in ASD syndromes, such as Rett syndrome and Fragile X syndrome. Rett syndrome is caused by mutations in the transcriptional repressor MECP2. *Mecp2* mutant astrocytes fail to promote synapse development in wild-type neurons (Ballas et al., 2009; Williams et al., 2014). Moreover, the conditional reactivation of MECP2 in the GFAP+ astrocytes of a mouse model of Rett syndrome restores normal dendritic morphology and ameliorates the locomotor and behavioral deficits (Lioy et al., 2011). Similarly, astrocytes with mutations in the RBP FMR1 that cause Fragile X syndrome, induce defective synapse development in wild-type neurons (Jacobs et al., 2010), and the dendritic abnormalities

of *Fmr1*-deficient neurons are significantly recovered when cultured with wild-type astrocytes (Jacobs and Doering, 2010). Defective astroglial function has been associated to excessive secretion of Neurotrophin 3, which inhibits dendritic outgrowth, and reduced secretion of Thrombospondin 1 (TSP1; Allen and Eroglu, 2017), which is involved in the structural assembly of glutamatergic synapses.

Finally, neuroimaging studies utilizing diffusion tensor imaging and magnetic resonance imaging show that white matter disruption occurs in brain regions of children with ASD (Carmody and Lewis, 2010). Moreover, molecular genetic studies also reveal alterations in the expression level and epigenetic regulation of myelin-related genes in the brain of ASD patients (Richetto et al., 2017).

**Down syndrome**

Several abnormalities have been reported in Down syndrome brains, including defects in neurogenesis, neuronal differentiation and reduced synaptic plasticity (Siarey et al., 1999; Chakrabarti et al., 2007; Cramer et al., 2015). Additionally, syndromic brains exhibit alterations in the neuron-glia associations. Wild-type neurons cultured with Down syndrome astrocytes show abnormal spine development and reduced synaptic density and activity (Garcia et al., 2010). As in the Fragile X syndrome, the impairment of astroglial function has been associated to reduced secretion of TSP1. In fact, addition of TSP1 to the co-cultures of wild-type neurons and Down syndrome astrocytes rescue the spine and synaptic alterations in these neurons (Garcia et al., 2010). In addition, genome-wide analysis in syndromic brains shows disregulation in the expression of genes involved in oligodendrocyte differentiation and myelination. Consistently, morphological analyses revealed hypomyelination and impaired formation of the nodes of Ranvier in mice that model the syndrome (Olmos-Serrano et al., 2016).

**Myelin disorders**

Inherited myelin disorders characterized by abnormal myelin development or maintenance (dysmyelination or demyelination, respectively) are considered leukodystrophies. Symptoms depend on the onset of the disease: in general, those beginning during early childhood are characterized by severe motor and cognitive development. Axonal degeneration and lost are common at advanced stages of the disease. Leukodystrophy genes are very heterogeneous and do not only affect oligodendrocytes (Nave, 2010). Astrocyte dysfunction is the primary cause of Alexander disease, a leukodystrophy that results from gain-of-function mutations in the *GFAP* gene (Olabarria and Goldman, 2017). This disease is characterized by enlargement of

astrocytes accompanied by white matter degeneration. Recently, Li et al. (2018) reported that *GFAP* mutant astrocytes reduce the proliferation of healthy OPCs and impair myelination.

**Psychiatric disorders**

White matter alterations have been reported in a wide range of psychiatric disorders, including schizophrenia, bipolar disorder and obsessive-compulsive disorder (Fields, 2008). Evidences for the implication of oligodendrocytes and myelin in the pathogenesis of schizophrenia are very robust. Schizophrenia can be influenced by a high amount of genes (polygenic risk) and environmental factors, and it is characterized by disabling symptoms as hallucinations, disordered thoughts and delusions. Postmortem brain analyses of schizophrenic subjects have shown diminished number of oligodendrocytes in different regions including the neocortex (Flynn et al., 2003; Uranova et al., 2007). In addition, genetic studies revealed abnormal expression of genes associated to oligodendrocyte development and myelination (Hakak et al., 2001; Iwamoto et al., 2005; Wan et al., 2005; Zai et al., 2005), including genes related to the formation of the nodes of Ranvier such as *Scna8* (coding for the sodium channel NAV1.6) and Ankyrin 3 (*Ank3*; (Davis et al., 2003; Nazeri et al., 2013; Arancibia-Carcamo and Attwell, 2014).

# 2. DYRK1A

## 2.1. Protein structure and regulation

Human DYRK1A (Dual-specificity tyrosine (Y) phosphorylation - Regulated Kinase 1A) is a 90 KDa protein kinase encoded on human chromosome 21 (HSA21; Guimera et al., 1999; Song et al., 1996) whose dysregulation leads to disease. DYRK1A belongs to the evolutionary conserved family of DYRKs, which is present in all eukaryotes (Aranda et al., 2011). All DYRK members have been associated cell homeostasis and differentiation processes. The mammalian DYRK family comprises 5 members further classified in two subfamilies according to their homology: class I, comprising the paralogs DYRK1A and DYRK1B; and class II, comprising DYRK2, DYRK3 and DYRK4. At the protein level, all mammalian DYRKs share the kinase domain and a sequence upstream of this domain known as DYRK homology (DH)-box, which is involved in the stabilization of the protein in a catalytically active conformation (Becker et al., 1998; Soundararajan et al., 2013). The paralogues DYRK1A and DYRK1B share two additional homologies: a nuclear location signal (NLS) in the N-terminal domain that targets those proteins to the nucleus,

and a PEST motif in the C-terminal domain that seems to be involved in protein stability. As shown in **Fig I.14** DYRK1A presents the following distinctive traits: (1) a second NLS inside the catalytic domain (Aranda et al., 2011); (2) a poly-histidine (His) stretch in the C-domain, which seems to be responsible for the accumulation of the protein in the splicing factor compartment (Alvarez et al., 2003); and (3) a region rich in serine/threonine (S/T) residues of unknown function that is also located in the C-domain (Aranda et al., 2011).

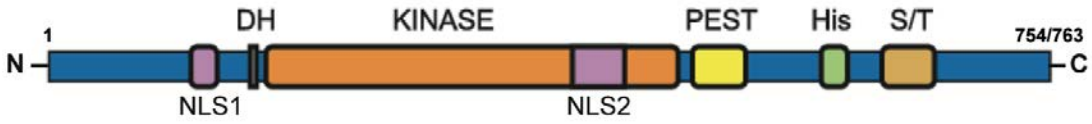


**Fig I.14. DYRK1A protein motifs.** Schematic representation of DYRK1A showing the different protein motifs from the N-terminus to the carboxy (C)-terminus domain. NLS, nuclear localization signal; DH, DYRK homology box; KINASE, kinase domain; HIS, polyhistidine domain; S/T, motif rich in serine and threonine residues. From Aranda et al. (2011).

Most kinases can adopt distinct active and inactive conformations. Usually, fluctuation between these states depends on the reversible phosphorylation of a residue in the so-called “activation loop”. In the case of DYRK proteins, they adopt an active conformation by an autophosphorylation in the second tyrosine residue of the motif Tyr-X-Tyr within the catalytic domain (Himpel et al., 2001). Remarkably, this autophosphorylation takes place during translation independently of regulatory signals (Lochhead et al., 2005) and is irreversible; in consequence, DYRKs are constitutively active kinases. The mature DYRK proteins are only able to phosphorylate substrates at serine and threonine residues (Becker and Sippl, 2011). Initially, DYRKs were classified as proline-directed kinases because of the regular presence of a proline residue at the P+1 position in the phosphorylated sequences. Using a peptide library, (Himpel et al., 2000) identified the optimal substrate sequence for DYRK1A phosphorylation: RPx(S/T)P, where x is any aminoacid and S/T are the phosphorylable residues.

Given that DYRK1A is constitutively active, mechanism to modulate expression and activity levels must be of utmost importance. However, only few regulatory mechanisms have been described to date. At the transcriptional level, *DYRK1A* gene, which consists of 17 exons, can be presumably transcribed from 3 distinct promoter regions (pA, pB and pM) that generate transcripts differing in their 5’UTR (Guimera et al., 1997). Each promoter seems to have particular activity, pA is reported to induce 10-fold higher reporter gene activity than pB (Maenz et al., 2008), and also particular regulation

because they respond different to the TF E2F1; and only pA shows a binding site for CRE binding protein (CREB; Impey et al., 2004). The TF Activator protein 4 (AP4) and its co-repressor, Geminin, repress DYRK1A transcription in non-neuronal cells by recruiting HDAC3 to pB and pM (Kim et al., 2006). In addition, alternative splicing of exon 4 gives rise to 2 protein isoforms differing in the inclusion/exclusion 9 aminoacids in the N-terminal (Aranda et al., 2011). The fact that some of the transcript variants show tissue-specific patterns suggests that the different encoded isoforms might play different roles; however, no functional differences among them have been reported to date. Other transcriptional activators of *DYRK1A* are: p44, an isoform of p53 (Pehar et al., 2014); OLIG2, which is also encoded in HSA21 (Liu et al., 2015); REST, which up-regulates DYRK1A specifically in neural cells (Lu et al., 2011a) and, MEF2D, a TF involved in neuronal differentiation (Wang et al., 2017).

Expression of *DYRK1A* is also regulated by miRNAs: miR-199b is under the control of Calcineurin/NFAT signalling and down-regulates *DYRK1A* expression in mouse models of cardiac hypertrophy (da Costa Martins et al., 2010). Also, let-7b and miR-1246, induced by p53, target *DYRK1A* in cell cultures (Buratti et al., 2010; Zhang et al., 2011). Interestingly, CREB, NFAT, p53 and REST, are indeed substrates of DYRK1A (Tejedor, 2018), suggesting that *DYRK1A* expression is regulated by feedback and feedforward mechanisms.

A ribonucleoprotein complex that includes the actin-regulatory protein MENA, the RBPs PCBP1 and HNRNPK, and SATB2, regulates local translation of *Dyrk1a* in the developing axons, both under steady-state conditions and upon potentiation of protein synthesis using brain derived neurotrophic factor (BDNF) stimulation (Vidaki et al., 2017). Moreover, the RBP CPEB4, whose expression is altered in the brain of autistic individuals, shortens the poli(A) tail of *Dyrk1a* mRNA hampering its translation in the cytosol (Parras et al., 2018).

The interaction of DYRK1A with other regulatory proteins modulates its kinase activity. For instance, the autophosphorylation of DYRK1A on Ser520 (outside the catalytic domain) triggers the interaction with the regulatory protein 14-3-3β that results in increased DYRK1A activity (Alvarez et al., 2007). On the contrary, the interaction of DYRK1A with SPRED1/2 (Sprouty-related protein with a EVH1 domain) seems to compete for the same binding with other substrates and inhibit DYRK1A activity (Li et al., 2010). It has also been shown that the phosphorylation of DYRK1A by the Hippo effector kinase LAST2 enhances DYRK1A phosphorylation of LIN52, a subunit of the DREAM complex (Tschop et al., 2011) involved in cell cycle-regulated gene expression

(Sadasivam and DeCaprio, 2013).

Despite showing two nuclear location signals, DYRK1A protein has been found both in the nucleus and the cytoplasm of different cell types (Marti et al., 2003; Kaczmarski et al., 2014). Indeed, DYRK1A targets are proteins that act in the nucleus and in the cytoplasm. Thus, the control of the subcellular location of DYRK1A provides an additional mechanism to modulate the different DYRK1A activities/functions. In accordance with this notion, a switch from nuclear to cytoplasmatic expression has been described during differentiation of chicken Purkinje cells *in vivo* (Hammerle et al., 2002). Little is known about the mechanisms regulating DYRK1A location.

According to the assorted type of putative DYRK1A regulators and substrates, this kinase seems to participate in a plethora of cell functions. Due to the neural phenotype of the *DYRK1A* mutants (see Section 2.3), one of the studied functions regulated by DYRK1A is cell cycle progression. Several of the known DYRK1A substrates are cell cycle regulators such as Cyclin D1 (Soppa et al., 2014; Najas et al., 2015), the cyclin-dependent kinase inhibitor p27Kip1 (Soppa et al., 2014) or LIN52 (Tschop et al., 2011). Another known cellular function regulated by DYRK1A is cell survival. DYRK1A is an anti-apoptotic kinase that acts as a negative regulator of well-known cell death effectors as Caspase-9 (Laguna et al., 2008), p53 (Guo et al., 2010b) and ASK1 (Choi and Chung, 2011). Moreover, the nuclear DYRK1A interactome has recently revealed that DYRK1A binds to central regulators of DNA damage response, including the E3 ubiquitin-protein ligase RNF169 and members of the BRCA1-A complex (Guard et al., 2019; Roewenstrunk et al., 2019). DYRK1A has been proposed to regulate splicing due to its accumulation in the splicing compartment (Alvarez et al., 2003), where it targets splicing factors and members of the spliceosoma machinery (de Graaf et al., 2006; Yin et al., 2012). DYRK1A also regulates gene expression. It phosphorylates several TFs such as CREB (Yang et al., 2001), NFAT (Arron et al., 2006), FOXO1 (von Groote-Bidlingmaier et al., 2003), GLI1 (Mao et al., 2002), REST (Lu et al., 2011a) and STAT3 (Matsuo et al., 2001); chromatin regulators such as Histone H3 (Himpel et al., 2000); and RNA polymerase II (Di Vona et al., 2015). In addition, DYRK1A and its homologue in *Drosophila* Minibrain (MNB) phosphorylates a great number of actin (ABLIM1, N-WASP) and microtubule (MAP1B, TAU, β-tubulin) proteins, indicating a role for DYRK1A in cytoskeletal regulation (Tejedor and Hammerle, 2011).

The phenotypes of *Dyrk1a* loss- and gain- of function mouse models demonstrate that DYRK1A is key for neurodevelopment and aging processes. DYRK1A regulates different signalling pathway. For the purpose of this thesis, I will briefly cite some of the signalling

pathways that have a well-known role in the central nervous system (CNS). Mammalian DYRK1A and *Drosophila* MNB have been shown to negatively regulate NOTCH pathway by reducing the transcriptional activity of the NOTCH intracellular domain (NCID) and, consequently, counteracting its anti-differentiative role during neurogenesis (Fernandez-Martinez et al., 2009; Hammerle et al., 2011). In contrast, in the adult, DYRK1A sustain self-renewal promoting Epidermal Growth Factor (EGF) signalling by preventing the degradation of EGF receptor through a mechanism that involves the phosphorylation of Sprouty proteins (Ferron et al., 2010). DYRK1A promotes FGF signalling phosphorylating Sprouty2, which is a negative regulator of FGF signalling pathway (Aranda et al., 2008). The regulation of SHH signalling by DYRK1A seems to be cell context specific since it has been reported that DYRK1A promotes the transcriptional activity of GLI1 by nuclear retention (Mao et al., 2002) and may have the opposite effect triggering a cascade that results in the destabilization of GLI1 (Schneider et al., 2015). Moreover, DYRK1A phosphorylates STAT3 enhancing the activity of the JAK-STAT signalling pathway in neural progenitors (Kurabayashi et al., 2015).

## 2.2. Brain expression

*DYRK1A* transcripts are ubiquitously detected in both developing and adult mammalian tissues, being the brain one of the tissues that show highest expression levels (Guimera et al., 1999; Okui et al., 1999). In the developing CNS, *Dyrk1a* mRNA is detected from early embryonic stages in both rodent and chick, and shows dynamic patterns in most areas (Song et al., 1996; Fotaki et al., 2002; Hammerle et al., 2002; 2008). Persistent expression is found in the telencephalon, particularly in the outer layers where neurons are located, the olfactory bulb and the spinal cord. Immunohistochemical analyses revealed similar protein expression patterns with some local differences in relative intensity levels. Remarkably, DYRK1A protein levels are temporally-regulated in distinct areas of the rat brain: peaking around birth and decreasing during postnatal development (Okui et al., 1999). In addition, during neurogenesis the expression of DYRK1A is high in progenitors, down-regulated in migrating neurons and again high in late differentiating neurons (Hammerle et al., 2008; 2011). This tightly regulation suggest a relevant role of DYRK1A in brain development.

In the mouse brain and retina, *Dyrk1a* is expressed in the proliferating NEs before the onset of neurogenesis and is maintained in pluripotent progenitors, in progenitors with a more restricted fate like OPCs, and in postmitotic cells (Hammerle et al., 2008; Laguna et al., 2008; Najas et al., 2015 and unpublished results). Interestingly, *Dyrk1a* mRNA in

NEs cells is asymmetrically distributed during mitosis between the two daughter cells of a NE before the first neurogenic division, suggesting that DYRK1A may have a role in the transition from proliferative to neurogenic divisions (Hammerle et al., 2002). In addition, asymmetric distribution of DYRK1A protein has been observed in dividing NSCs of the adult SVZ resulting in a daughter cell with high levels of EGFR that remains stem cell and a daughter with low levels of EGFR that differentiates (Ferron et al., 2010).

DYRK1A expression is maintained in adult neurons and astrocytes in both human and mouse brains (Marti et al., 2003; Wegiel et al., 2004). In adult neurons, DYRK1A is detected both in the nucleus and the cytoplasm, including the neuronal processes and synapses (Marti et al., 2003; Wegiel et al., 2004). In astrocytes, DYRK1A concentrates in cytoplasmatic granules. However, nuclear localization of DYRK1A in astrocytes seems to be specie-specific because it is excluded from the nucleus of human astrocytes (Wegiel et al., 2004), while it is detected in this compartment in mouse primary cultured astrocytes (Marti et al., 2003).

Remarkably, it has been reported that brain DYRK1A immunoreactivity increases in neurodegenerative diseases in both neurons and astrocytes (Ferrer et al., 2005; Kimura et al., 2007; Wegiel et al., 2008). In this regard, several data indicate that reducing DYRK1A activity might be a valid therapeutic strategy to treat Alzheimer's like pathology associated to Down syndrome (Branca et al., 2017; Garcia-Cerro et al., 2017).

## 2.3. DYRK1A and neurodevelopmental disorders

Alterations in the *DYRK1A* gene dosage, both overexpression and haploinsufficiency, lead to neurodevelopmental disorders in humans. *DYRK1A* overexpression contributes to some of the neurodevelopmental alterations associated to Down Syndrome (Altafaj et al., 2013; Garcia-Cerro et al., 2014; Jiang et al., 2015; Najas et al., 2015). Also, *DYRK1A* haploinsufficiency is the leading cause of another intellectual disability syndrome, named *DYRK1A*-related intellectual disability syndrome (Courcet et al., 2012; Ji et al., 2015; van Bon et al., 2016).

The use of transgenic mouse models has been instrumental to study the consequences of *DYRK1A* dosage imbalance in these neurodevelopmental disorders. For the purpose of this thesis, in the following sections I will focus on *DYRK1A*-related intellectual disability syndrome and the *Dyrk1a* mutant mouse that models this condition, the *Dyrk1a*$^{+/-}$ mouse. However, it is worthy to mention that several mice overexpressing *Dyrk1a*, either alone or in conjunction with other genes, have been used in the context

of Down Syndrome. Some of the most relevant models are **Ts65Dn** and **mBACTg*Dyrk1a*** (Tg*Dyrk1a*). The first one carries an additional chromosome containing approximately 100 genes orthologous to HSA21 genes, including DYRK1A (Davisson et al., 1990; Reinholdt et al., 2011). The Tg*Dyrk1a* mice have an additional copy of the *Dyrk1a* gene together with its own regulatory regions integrated in a BAC (Bacterial Artificial Cromosome; Guedj et al., 2012). Remarkably, both models mimic some of the phenotypes observed in the Down Syndrome, such as developmental delay, learning and memory deficits, motor deficits, etc. (Reeves et al., 1995; Holtzman et al., 1996; Costa et al., 1999; Souchet et al., 2014).

### 2.3.1. *DYRK1A*-related intellectual disability

Human *DYRK1A* was first associated to developmental delay, microcephaly and mental retardation in genotype-phenotype correlation studies performed in rare cases of individuals with HSA21 monosomies (Chettouh et al., 1995; Matsumoto et al., 1997). Later, *DYRK1A* contribution to these phenotypes was strongly indicated by the work of Moller et al. (2008) in which they described two unrelated patients with a balanced translocation truncating *DYRK1A* that presented microcephaly, intrauterine growth retardation, developmental delay, feeding problems, large ears and febrile seizures. Subsequently, several reports describing cases of *de novo DYRK1A* mutations in patients with similar phenotypic features were published. Remarkably, high-throughput sequencing studies applied to cohort of patients with developmental disorders revealed that DYRK1A is one of the most frequent *de novo*-mutated genes in autism spectrum disorders (0.1-0.5% of the affected population; Iossifov et al., 2012; De Rubeis et al., 2014; Stessman et al., 2017) and that accounts for approximately 0.5-1% of syndromic intellectual disability cases (Deciphering Developmental Disorders, 2015; Evers et al., 2017).

Phenotypic comparisons among distinct cases of patients with *DYRK1A* mutations led to the proposal that the heterozygous disruption of *DYRK1A* causes a recognizable syndrome (Courcet et al., 2012; Ji et al., 2015; van Bon et al., 2015), named *DYRK1A*-related intellectual disability syndrome, also known as *DYRK1A*-haploinsufficiency syndrome, associated to the MRD7 locus (OMIM #614104) or *DYRK1A* syndrome for short (http://www.dyrk1a.org). The core clinical manifestations of patients with *DYRK1A*-related syndrome include microcephaly, developmental delay, intrauterine growth retardation, moderate to severe mental retardation, autism spectrum disorder-related deficits, seizures, speech problems, motor gait disturbances, feeding problems,

hypertonia, and characteristic dysmorphic facies (Bronicki et al., 2015; Ji et al., 2015; van Bon et al., 2015; Li et al., 2015; Luco et al., 2016; Earl et al., 2017).

In addition to microcephaly, magnetic resonance imaging performed in some patients with *DYRK1A* syndrome revealed prevalence of small brain stem, enlarged ventricles, thin optic chiasm, brain atrophy, gliosis, hypoplasia of the CC and hypomyelination (Ji et al., 2015; van Bon et al., 2015; Kim et al., 2017).

To date, the causative mutations in all the recognized affected individuals with the syndrome are *de novo* (not inherited) and comprise missense mutations (changing an aminoacid), nonsense mutations (resulting in a premature stop codon) and small insertions or deletions in the *DYRK1A* gene as well as chromosomal re-arrangements affecting the gene (Moller et al., 2008; Oegema et al., 2010; van Bon et al., 2011; Courcet et al., 2012; O'Roak et al., 2012; Ji et al., 2015; Bronicki et al., 2015; Ruaud et al., 2015; Stessman et al., 2017; Dang et al., 2018). Most of the reported *DYRK1A* mutations are truncating mutations that affect the kinase domain or the N-terminal region of the DYRK1A protein. The reported missense mutations are also concentrated in the kinase domain and recent functional studies have shown that most of them result in DYRK1A protein that has not enzymatic activity (Widowati et al., 2018; Arranz et al., 2019). Therefore, most of the mutations causing the *DYRK1A*-related phenotypes are loss-of-function mutations.

Supporting the high functional conservation of *DYRK1A* among species, flies and mice models carrying loss-of function mutations in the orthologous genes, *minibrain (mnb)* and *Dyrk1a* respectively, mimic several phenotypes displayed by the individuals with the syndrome.

### 2.3.2. *Dyrk1a*$^{+/-}$ model

A *Dyrk1a* loss-of-function mouse model carrying one disrupted *Dyrk1a* allele (*Dyrk1a*$^{+/-}$) was generated in our laboratory by gene targeting (Fotaki et al., 2002). *Dyrk1a*$^{+/-}$ mice display some of the core traits of the *DYRK1A*-related syndrome, including developmental delay, microcephaly, gait disturbances, learning problems, autism-related traits (defective social interactions and stereotypic behaviours), epileptic activity and impaired communicative ultrasonic vocalizations (Fotaki et al., 2002; Fotaki et al., 2004; Arque et al., 2008; Arranz et al., 2019). More recently a new *Dyrk1a*$^{+/-}$ mouse carrying a truncating mutation has been generated using CRISPR/Cas9-medited mutagenesis. Confirming our previous findings, this mouse also presents developmental delay,

microcephaly, learning problems and altered social behaviours (Raveau et al., 2018).

*Dyrk1a*$^{+/-}$ mice show general growth delay and a 30% body size reduction compared to wild-type littermates that is maintained life-time. Their brains maintain normal cytoarchitecture but are microcephalic and show a weight reduction that is proportional to the body size. However, the reduction in size is not uniform across the distinct brain regions. In the adult *Dyrk1a*$^{+/-}$ brain, hindbrain and midbrain regions, particularly the mesencephalic tectum, are more severely reduced than forebrain regions such as the olfactory bulbs and the neocortex. Similarly, cellularity is altered in a structure-specific manner. In particular, cellular density is increased by 30% in certain areas of the somatosensory and pyriform *Dyrk1a*$^{+/-}$ cortices, while other nuclei or laminated structures, such as the superior *colliculum* contained in the mesencephalic tectum, present normal cell densities (Fotaki et al., 2002; Guedj et al., 2012). In addition to an increased cellularity, *Dyrk1a*$^{+/-}$ neocortices exhibit altered proportion of excitatory and inhibitory neurons (Arranz et al., 2019), which likely entails an imbalance in excitatory/inhibitory activity. Interestingly, disturbance of the excitatory/inhibitory activity has been proposed as a pathogenic mechanism in autism spectrum disorders and epilepsy (Rubenstein, 2010; Bozzi et al., 2012). In addition, *Dyrk1a*$^{+/-}$ brains exhibit a deficit in *sustancia nigra* dopaminergic neurons, which might underlie the motor disorders observed in these mutants (Fotaki et al., 2004; Martinez de Lagran et al., 2007).

The study of the microstructure of cortical neurons in the adult *Dyrk1a*$^{+/-}$ brain revealed that these cells are considerably smaller, less branched and with less dendritic spines per branch than neurons from wild-type littermates (Benavides-Piccione et al., 2005). In addition, *Dyrk1a*$^{+/-}$ callosal neurons show reduced axonal diameters (Balducci, 2012). The alterations in neuron numbers and neuron morphology reported in the *Dyrk1a*$^{+/-}$ brain are likely to contribute to the neurological alterations associated to *DYRK1A* syndrome.

Glial populations also seem to be affected in *Dyrk1a*$^{+/-}$ brains. Excessive number of astrocytes has been detected in distinct regions of the postnatal and adult *Dyrk1a*$^{+/-}$ brain, including the cerebral cortex and the hippocampus (Balducci, 2012; Fotaki et al., 2002; Guedj et al., 2012). Interestingly, the number of astrocytes is diminished in the Tg*Dyrk1a* hippocampus and these observations are in striking contradiction with the role of DYRK1A in the promotion of the pro-astrogliogenic JAK-STAT activity (Kurabayashi et al., 2015). Further research is necessary to understand the role of DYRK1A in astrogliogenesis during normal development. Moreover, in the adult *Dyrk1a*$^{+/-}$ CC there is an increase in the density of unmyelinated axons in comparison to the CC in wild-type

animals and, consequently, altered ratio of myelinated/unmyelinated axons. In addition, the, myelin sheaths in other axonal tracts of the adult *Dyrk1a*$^{+/-}$ mouse, such as the optic nerve and the sciatic nerve, are thinner than the wild-types but in these tracts the axonal diameter in the mutant condition is normal (Laguna et al., 2008; Balducci, 2012). These alterations are consistent with the gliosis and hypomyelination observed in the brain of individuals with *DYRK1A* syndrome. Overall, these data suggest that an imbalanced dosage of *DYRK1A* may affect the generation and differentiation of the glial cells. Supporting this hypothesis, recent transcriptome data showed alterations in the expression of glial genes (*Gfap*, *Mbp*, *Cnp*, *Aqp4*, *S100β*) and genes involved in gliogenesis (*Nfib*, *Notch2*, *Sox4*, *Sox11*) in the cortex of early postnatal *Dyrk1a*$^{+/-}$ mice (Arranz et al., 2019).

## 2.4. DYRK1A in neurogenesis and mammalian cortical development

Firsts evidences involving DYRK1A in neurogenesis and brain growth were provided by the phenotype of flies carrying a loss-of-function mutation in *mnb*. These flies exhibit a prominent size reduction of the optic lobes and central brain hemispheres that is in partly due to the failure in generating neurons in the larva stage (Tejedor et al., 1995). Loss-of-function mutations in the *DYRK1A* loci also cause microcephaly in zebrafish (Kim et al., 2017) indicating that the function of DYRK1A/MNB in brain growth is conserved across evolution. Interestingly, the Tg*Dyrk1a* mouse, carrying 3 *Dyrk1a* alleles, shows the opposite brain size alterations than the haploinsufficient *Dyrk1a*$^{+/-}$ mouse (Guedj et al., 2012; see also **Fig I.15)**, indicating that the role of *DYRK1A* in brain growth is dosage dependent.

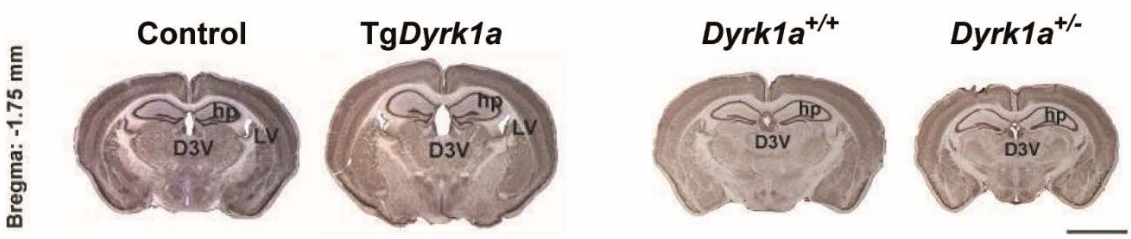


**Fig I.15. Morphometric variations in the brain of Tg*Dyrk1a* and *Dyrk1a*$^{+/-}$ mutant mice.** Coronal slices from the adult brain of Tg*Dyrk1a*, *Dyrk1a*$^{+/-}$ and their respective control littermates at Bregma -1.75 mm stained with the neuron marker NeuN. Notice that the size of the Tg*Dyrk1a* brain is increased while the size of the *Dyrk1a*$^{+/-}$ brain is decreased in comparison to their respective controls. D3V, dorsal third ventricle; hp, hippocampus; LV, lateral ventricle. Scale bar: 2 mm. Adapted from Najas (2014).

Different studies have converged in the conclusion that DYRK1A/MNB inhibits cell cycle progression in neural progenitors by controlling the expression of cell cycle regulatory proteins. In the RGs of the developing mouse neocortex, DYRK1A protein levels negatively correlate to Cyclin D1 nuclear levels (Najas et al., 2015). This negative correlation is due to the capacity of DYRK1A to phosphorylate Cyclin D1 in a particular residue, which leads to Cyclin D1 nuclear export and its degradation through the ubiquitin proteasome pathway (Chen et al., 2013; Najas et al., 2015). In line, studies from our group demonstrated that at the onset of neurogenesis, Tg*Dyrk1a* dorsal RGs show longer cell cycles and longer G1 phases. Consistent with the well-accepted idea that the G1 length of a RG division determines the fate of its daughter cells (Salomoni and Calegari, 2010), Tg*Dyrk1a* RGs undergo less asymmetric neurogenic divisions and more asymmetric proliferative divisions, which leads to a deficit of RG-derived neurons and an excess of IPs (Najas et al., 2015). Conversely, at the onset of neurogenesis *Dyrk1a*$^{+/-}$ dorsal RGs produce more RG-derived neurons at the expense of IPs (Najas et al., 2015).

DYRK1A overexpression also affects neurogenesis in the ventral telencephalon, although this effect may not be caused by the action of DYRK1A on Cyclin D1 turnover since the levels of Cyclin D1 in ventral Tg*Dyrk1a* progenitors are normal (Najas, 2014). As we have explained earlier (see section 1.2.1), ventral progenitors give rise to cortical interneurons. In the Tg*Dyrk1a* MGE the number and subtype of progenitors (apical and basal) is altered during neurogenesis, suggesting that the overexpression of DYRK1A also impacts on the mode of division of MGE progenitors (Najas, 2014). In consistency with this developmental defect, adult Tg*Dyrk1a* neocortices show an altered proportion of parvalbumin and somatostatin interneurons (Najas, 2014).

# OBJECTIVES

The cerebral cortex is the main structure for highest functions in mammals. The correct functionality of this structure depends on the correct generation of neurons, astrocytes and oligodendroglial cells and the proper execution of their respective differentiation programs. Disturbances in both processes could be pathogenic leading to common developmental disorders, such as intellectual disability and autism. Neuronal and glial cells are produced during embryonic and postnatal development directly from pluripotent progenitors named radial glial cells, or indirectly through intermediate progenitors with a more restricted fate. The general aim of this thesis was **to extend our understanding of the mechanisms driving neurogenesis and gliogenesis during the development of the cerebral cortex**. To address this general aim, we set two main objectives that we have developed according to previous data of the group and to data published by other groups. These two objectives are the following:

1. **To uncover how the transcriptome of radial glial cells changes during the neurogenic phase of cortical development, from E11 to E15, and the contribution of miRNA regulation to these changes**. In particular, we aimed to identify:
   1.1. The main mechanisms involved in the progression of neurogenesis.
   1.2. The miRNA-mRNA regulatory networks driving radial glial cell differentiation.
   1.3. The contribution of alternative splicing in generating transcript variability in radial glial cells.

2. **To provide further evidences on the pathological alterations underlying the neurological deficits associated to *DYRK1A* haploinsufficiency syndrome by analysing the glial phenotype of the *Dyrk1a*$^{+/-}$ mouse model.** In particular, we aimed to uncover possible alterations in:
   2.1. The generation of cortical astrocytes.
   2.2. The generation and differentiation of cortical oligodendroglial cells.
   2.3. The structure and composition of the myelin sheaths in the postnatal and adult brain.

# METHODS

# 1. Animals

Mice were maintained in ventilated or conventional cages in the animal facilities of the Parc Científic de Barcelona (PCB) and the Centre d'Investigació i Desenvolupament (CID-CSIC). Housing conditions were 12 hours light/dark cycles in controlled environmental conditions of humidity (60%) and temperature (22ºC±2ºC). Food and water were provided *ad libitum*.

All experimental procedures were carried out in accordance with the European Union guidelines (Directive 2010/63/UE) and the followed protocols were approved by the ethics committee of the PCB, CID, CSIC and the Generalitat de Catalunya.

## 1.1. Mouse strains

We used CD-1 wild-type and *Pax6*-GFP embryos as well as *Dyrk1a*$^{+/-}$ and *Dyrk1a*$^{+/+}$ littermate embryos at different developmental stages. We also used postnatal and young adult (age 2 months) *Dyrk1a*$^{+/-}$ and *Dyrk1a*$^{+/+}$ littermates.

CD-1 embryos were obtained from crosses between CD-1 animals (RjOrl:SWISS; Janvier Labs). *Pax6*-GFP embryos were obtained from crosses between CD-1 females and transgenic *Pax6*-GFP males. The *Pax6*-GFP mouse was kindly provided by Dr. David Price (University of Edinburg) and carries a YAC transgene (DTy54) expressing tau-GFP under the control of the human *PAX6* regulatory elements (Tyas et al., 2006). *Dyrk1a*$^{+/-}$ embryos and mice were obtained from crosses between C57BL/6JRjx129/Sv F1 females and *Dyrk1a*$^{+/-}$ males. Generation of the *Dyrk1a*$^{+/-}$ mouse model was described elsewhere (Fotaki *et al.*, 2002). Wild-type F1 females were generated in the PCB animal facility from parental C57BL/6JRj and 129/Sv mice (Janvier). Only females were considered at the adult stage in order to avoid sex-related variability.

To collect embryos and postnatal animals at the appropriate developmental stage, we set up controlled matings. Two to three females (6 weeks to 4 months of age) were placed in the same cage with one male. Females were checked for the presence of a copulation vaginal plug the following morning. Embryonic day (E) 0.5 was considered the day of the vaginal plug and the day of birth was defined as postnatal day (P) 0.

## 1.2. Genotyping

Animal genotyping was performed by polymerase chain reaction (PCR) using genomic DNA obtained from tail or ear-clip biopsies. DNA extraction from fresh or frozen tissue samples was done in 50 mM NaOH by heating at 98ºC for 30 min. Volume of incubation was adjusted according to tissue size; ie. tail biopsies (length ≈ 0.5 cm) from adult mice were incubated in 300 µl while ear-clip biopsies were incubated in 50 µl. The solution was neutralized by adding 1:10 volumes of 1 M Tris-HCl pH 8 and samples were centrifuged at maximum speed for 10 min. One µl of the supernatant was used for PCR with the primers and conditions indicated in **Table M1**. Electrophoresis of the PCR products was done in a 1.5% agarose gel containing Sybr® Safe DNA gel stain (Thermofisher).

**Table M1. Primers used for genotyping**

| Mouse model | Primer | Sequence 5'-3' | Ta (ºC) | Amplicon (bp)* |
|---|---|---|---|---|
| ***Pax6*-GFP** | Wt-IMR8545 (F) | AAAGTCGCTCTGAGTTGTTAT | 50 | 600/**275** |
| | Wt-IMR8546 (R) | GGAGCGGGAGAAATGGATATG | | |
| | Tau-GFP (F) | CCGTGTGCCTCAACCGTA | | |
| | Tau-GFP (R) | CACGGTTTACTGGGTCTGG | | |
| ***Dyrk1a*$^{+/-}$** | Dyrk1a-I4-(F) | ACAGTGAGGCTGTTCCTAGTGAAACTG | 58 | 250/**160** |
| | Dyrk1a-I5 (R) | ACGGCTTATGTTCTTCAACAGGTCAGG | | |
| | NeoT2 (F) | AAGACAATAGCAGGCATGCTGGGGATG | | |

All primers were used at 10 µM. *In bold the size of the mutant allele. bp: base pairs; F: forward; R: reverse; Ta: annealing temperature.

## 1.3. BrdU incorporation

For some experiments 5-bromo-2'-deocyuridine (BrdU, Sigma) was injected intraperitoneally in mice to label proliferating cells, or in pregnant females to label these cells in the embryos. Protocols for BrdU injection and sacrifice of the animals varied according to the experimental purpose and are detailed for each case in the Results section.

## 2. Cellular dissociation and FACS

RG cells were isolated by fluorescence-activated cell sorting (FACS) from the dorsal telencephalon of *Pax6*-GFP or wild-type CD-1 embryos collected at different developmental stages; from the beginning (E11.5) to the end (E17.5) of cortical neurogenesis (Kriegstein and Alvarez-Buylla, 2009).

*Pax6*-GFP embryos were distinguished from their wild-type siblings under a fluorescence binocular microscope (Leica MZ FLIII). *Pax6*-GFP whole brains were isolated and dorsal telencephalons dissected out and pooled (2 to 5 telencephalons per pool depending on the developmental stage) in dissociating media (DM). Enzymatic dissociation was done by incubating the tissue in papain-DNase solution (200 µl solution/telencephalon) for 10 min at 37ºC and soft agitation. Papain was inactivated by dilution with DM (1:2) and subsequent washes in DM. The DM was poured and replaced by HBSS-Glu media (100 µl/telencephalon). In this media, cells were further dissociated by gentle trituration: 30 up and downs passages using a p200 pipette tip. Dissociated cells were then filtered using a falcon tube with a cell strainer cap (BD Biosciences; BD falcon 12 x 75 mm), which was previously dampened with 500 µl of HBSS-Glu.

To isolate by FACS RG cells from wild-type telencephalons we used antibodies against the stem cell marker Prominin-1 (Weigmann et al., 1997; Corti et al., 2007). In this case, the dissected telencephalons were pooled (4 telencephalons/pool at E11.5 and 2 telencephalons/pool at E15.5) and incubated in HBSS-Glu with 5 mM EDTA for 5 min at 37ºC. Then, cells were mechanically dissociated by gently triturating: 20 up and downs passages through a p200 pipette tip. Cells were collected by centrifugation at 300 g for 10 min at 4ºC. Media was poured and cells were resuspended in 200 µl of incubation media (IM) and kept for 10 min at 4ºC in soft agitation to block unspecific antibody binding. Then, the anti-prominin-1-APC antibody (eBioscience; 17-1331-81) was added to the media at 0.2 mg/ml and incubated for 30 min at 4ºC. In one of the samples we added rat IgG1-APC instead of the antibody to define non-specific antibody fluorescence in the FACS. After the incubation, cells were centrifuged at 300 g for 10 min at 4ºC. Media with the antibody or IgG1 was poured and 1 ml of IM was added. Dissociated cells were filtered through a falcon tube with a cell strainer cap (BD Biosciences; BD falcon 12 x 75 mm) in which the filter was previously dampened with 500 µl of IM.

In both cases, the number of isolated cells was determined by using a Neubauer chamber and cells were diluted in IM solution to a final concentration of 2-3 x $10^6$ cells/ml.

Then, DAPI (20 ng/ml; Vector Labs) was added to identify and exclude dead cells. Sorting was done in the BD FACSAria$^{TM}$ Fusion (BD Biosciences) cytometer of the Cytometer Unit of Centres Científics i Tecnològics of the Universitat de Barcelona. We collected between 400,000 and 700,000 cells per tube; then collector tubes were centrifuged at 1000 g for 10 min at 4ºC and cell pellets immediately stored at -80ºC. The composition of the solutions used for cell dissociation and sorting is in **Table M2**.

**Table M2. Media for cell dissociation and sorting**

| **Dissociating media (DM)** | **Final concentration** |
|---|---|
| DMEM high glucose (#41965039, Thermo Fisher) | 99.5% (v/v) |
| HEPES 1M (Invitrogen) | 5 mM |
| **Papain-DNase solution** | **Final concentration** |
| DM | 100% (v/v) |
| N-acetyl cysteine (Sigma) | 1 mM |
| Papain (LS003124, Worthington) | 7 u/ml |
| DNase I recombinant (#4536282001, Life Technologies) | 12 mg/ml |
| **HBSS-Glu media** | **Final concentration** |
| HBSS, calcium, magnesium (#24020117, Thermo Fisher) | 99% (v/v) |
| HEPES 1M (Invitrogen) | 10 mM |
| D-(+)-Glucose (Sigma) | 0.6% (w/v) |
| **Incubation media (IM)** | **Final concentration** |
| DPBS, no calcium, no magnesium (#14200-075, Life Technologies) | 10% (v/v) |
| D-(+)-Glucose (Sigma) | 0.6% (w/v) |
| Fetal Bovine Serum (FBS; Thermo Fisher) | 2% (v/v) |
| $NaN_3$ (Sigma) | 0.02% (v/v) |

# 3. Gene expression analysis

## 3.1. RNA extraction

To extract RNA from FACS-isolated cells we used the miRNeasy Micro Kit (Quiagen). Cells were resuspended in 700 µl lysis buffer (provided by the kit) and homogenized using a syringe by passing the lysate through a 25-G needle at least 20 times. Total RNA, including small RNAs, was extracted from the lysates following the manufacture's indications.

To extract RNA from tissue, whole brains were harvested from embryos or mice after decapitation and the telencephalon was dissected out under a binocular microscope and immediately frozen in dry ice. Total RNA was extracted using the TriPure Isolation Reagent (Roche; 1ml/100 mg of starting tissue) following the manufacture's indications. Embryo samples were homogenized by mechanically trituration using a syringe and a 25-G needle and postnatal and adult samples were homogenized using a Polytron.

RNA extracted from cells or from telencephalons was treated with DNAse (#AM1906, Ambion) for 30 min at 37ºC to eliminate DNA contamination. RNA was quantified using a NanoDrop (Agilent) and its quality was assessed by RNA visualization in a 0.8% agarose gel. Quality assessment of the RNA used in RNA-seq experiments is explained in Section 3.2. All RNA samples were stored at -80ºC.

## 3.2. RNA sequencing

In this work we have performed RNA sequencing (RNA-seq) to evaluate differences in the gene expression profile of RGs along neurogenesis (E15.5 *vs* E11.5). We used total RNA samples to assess the expression of coding genes and alternative splicing (AS) forms, and small RNA-enriched fractions to assess the expression of miRNAs. Total RNA was prepared from FACS-isolated cells as described above (Section 3.1.).

### 3.2.1. Stranded mRNA-seq library preparation and sequencing

Strand-specific mRNA-seq libraries for the Illumina platform were generated and sequenced at the Genomics Unit of the Centre de Regulació Genòmica (CRG). The RNA quality was checked on a Bioanalyzer (Agilent) and only RNA with RNA integrity number values over 8 was used. High-quality total RNA was used as input for the so-called dUTP library preparation method using the TruSeq Stranded mRNA Sample Prep Kit v2 (Illumina, ref. RS-122-2101/2) according to the manufacturer's protocol. Briefly, the mRNA fraction was purified from total RNA by polyA capture, fragmented and subjected to first-strand cDNA synthesis with random hexamers in the presence of actinomycin D. The second-strand synthesis was performed incorporating dUTP instead of dTTP. Barcoded DNA adapters were ligated to both ends of the double-stranded cDNA and subjected to PCR amplification. The resultant library was checked on a Bioanalyzer (Agilent) and quantified by qPCR using the KAPA Library Quantification Kit (KapaBiosystems, ref. KK4835) prior to amplification with Illumina's cBot. The libraries were sequenced on an Illumina HiSeq 2500 (TruSeq v3 chemistry) to a length of 50 bp pair-ended. Around 40 - 50 million reads were obtained for each library with more than

98% aligned reads in all cases, between 71 - 75% of the reads were mapped univocally to genes. Triplicates were used for the analysis consisting in 3 pools of FACS-sorted cells obtained from 37 E11.5 embryos and from 30 E15.5 embryos (see **Table M3** for more details).

**Table M3. RNA samples used for RNA-seq experiments**

| Sample ID | N. embryos | N. cells | Usage |
|---|---|---|---|
| **E11**-CF9b | 16 | 550.000 | Strand-specific mRNA-seq library |
| **E11**-CF11 | 8 | 405.000 | Strand-specific mRNA-seq library |
| **E11**-CF13a | 13 | 600.000 | Strand-specific mRNA-seq library |
| **E11**-CF13b | 13 | 600.000 | Small RNA-seq library |
| **E11**-CF14 | 16 | 600.000 | Small RNA-seq library |
| **E11**-CF16 | 15 | 700.000 | Small RNA-seq library |
| **E15**-CF19-1b | 12 | 700.000 | Strand-specific mRNA-seq library |
| **E15**-CF19-2a | 11 | 700.000 | Strand-specific mRNA-seq library |
| **E15**-CF20e | 7 | 700.000 | Strand-specific mRNA-seq library |
| **E15**-CF19-2b | 11 | 700.000 | Small RNA-seq library |
| **E15**-CF20d | 7 | 700.000 | Small RNA-seq library |

ID: identification; N: number. E11 refers to embryonic day E11.5 and E15 to embryonic day E15.5.

### 3.2.2. Small RNA-seq library preparation and sequencing

Small RNA libraries were generated using TruSeq small RNA Sample Prep Kit (Illumina, ref. RS-200-0012) according to the manufacturer's protocol. Briefly, 700 - 900 ng of total RNA were used. First, 3' adapters and subsequently 5' adapters were ligated to the RNA. cDNA was synthesized using reverse transcriptase (SuperScript II, Invitrogen, ref. 18064-014) and a specific primer (RNA retrotranscription Primer) complementary to the 3' RNA adapter. cDNA was further amplified by PCR using indexed adapters supplied in the kit. Finally, libraries were size-selected using 6% Novex® TBE gels (Life Technologies, ref. EC6265BOX). Fragments with insert sizes of 18 to 36 bp were cut from the gel, and DNA was precipitated and eluted in 10 µl elution buffer. Final libraries were analyzed using Agilent High Sensitivity chip to estimate the quantity and check size distribution, and were then quantified by qPCR using the KAPA Library Quantification Kit (KapaBiosystems, ref. KK4835) prior to amplification with Illumina's cBot. Single-end sequencing was performed on an Illumina HiSeq 2000 platform. Around 11 - 15 million reads were obtained for each library with more than 83% aligned reads in all cases, between 35 - 50% reads were mapped to known miRNA genes. Triplicates (E11.5

samples) and duplicates (E15.5 samples) were used for the analysis. The triplicates were 3 pools of FACS-sorted cells obtained from 44 embryos and the duplicates 2 pools of FACS-sorted cells obtained from 18 embryos (see **Table M3** for more details).

## 3.3. Bioinformatic analysis

### 3.3.1. RNA-seq raw data analysis

Data from RNA-seq was analysed by the Bioinformatics Unit of the CRG (www.crg.eu/en/programmes-groups/bioinformatics-unit). For the miRNA analysis raw reads were evaluated for their quality by using FastQC (Andrews, 2010) and trimmed with Cutadapt (Martin, 2011) for removing the adapter. Trimmed reads were then aligned to reference genome (GRCm38 from iGenomes) using Bowtie2 (Langmead and Salzberg, 2012) with the option "--very-sensitive". Reads were associated to a given small non coding RNA (miRNAs, snoRNAs and snRNAs) and counted by HTSeq-count (Anders et al., 2015). In the case of miRNA transcripts (pre-miRs), reads were splited into two fragments and the mature miRNAs produced by each pre-miR (miRNA-5p or miRNA-3p) assigned according to the number of reads in the two fragments. Finally, the count matrix was fed to DESeq2 (Love et al., 2014) for calculating the differentially expresed genes. For the RNA analysis, paired ends were aligned to the same genome reference used for miRNA analysis using TopHat (Kim et al., 2013) and counted using HTSeq-count and the option "-m intersection-strict". The final count matrix was then analyzed using DESeq2 for calculating the differentially expressed genes. Low expressed genes (genes with zero counts in all the samples) and genes with standard deviation (SD) values 3 times higher than mean expression value of the replicates were not taken into consideration.

Fold-change (FC) values between E15.5 and E11.5 samples were expressed in log2. We considered differentially expressed mRNAs when adjusted (adj.) *p*-value (*p-value* after Benjamin-Hochberg correction) < 0.05 and log2 FC ≥ 1 (up-regulated) or log2 FC ≤ -1 (down-regulated). miRNAs were considered differentially expressed when adj. *p*-value < 0.01 and log2 FC ≥ 1.5 (up-regulated) or log2 FC ≤ -1.5 (down-regulated).

### 3.3.2. Expression data

Principal component analysis and clustered heatmaps were done with the ClustVis web resource (Metsalu and Vilo, 2015) using the log2 reads of each sample. Volcano plots

and density plots were created in GraphPad Prism®, Venn plots with BioVenn (Hulsen et al., 2008).

### 3.3.3. Identification of alternative splicing forms

The analysis of AS events was done in collaboration with the laboratory of Dr. Susana de la Luna (CRG, Barcelona) and using the software Vast-tools (Irimia et al., 2014; https://github.com/vastgroup/vast-tools) developed by Dr. Manuel Irimia (CRG, Barcelona). This software identifies and quantifies simple and complex exon skipping events, intron retention and alternative 5' and 3' splice site choices from RNA-seq data. For each event, the Vast-tools provides the percentage of alternative sequence inclusion (PSI) and a score value related to the number and quality of reads supporting the PSI. A sequence was considered an AS event when presented a $10 \leq PSI \leq 90$ in at least 10% of the samples with sufficient read coverage and/or a range of $PSI \geq 25$ across all samples with sufficient read coverage. Information about the AS events (genomic and sequence context, impact on the reading frame, mapping to protein structures, evolutionary conservation and primers for PCR validation) was found in the Vertebrate Alternative Splicing and Transcription Database (VastDB; Tapial et al., 2017; http://vastdb.crg.eu/).

### 3.3.4. miRNA target prediction

Bioinformatics prediction of targets modulated by differentially expressed miRNAs was done in collaboration with Dr. Ivan Conte (TIGEM, Naples). Targets were identified using an R script described in Agarwal et al., (2015) that interphases with TargetScan (targetscan.org).

### 3.3.5. Enrichment analyses

Functional enrichment analysis was performed using the Functional Annotation Clustering tool of the DAVID websource (Database for Annotation, Visualization and Integrated Discovery, Huang et al., 2007, version 6.8) with default parameters. Annotation categories used for the analysis included all Gene Ontology (GO) categories (biological function, cellular component and molecular function) and KEGG pathways, among others (OMIM, Keywords, Interpro). Significant modules were ranked according to their enrichment score. As background population we used the list of mRNAs detected in the RG cells.

Functional enrichment map was built in Cytoscape 3.7.1 (Shannon et al., 2003) using the EnrichmentMap app (Merico et al., 2010) with the following parameters: filter by gene expression, FDR cut-off = 0.01, *p*-value cut-off = 0.001; Jaccard + Overlap Combined option with cut-off = 0.375; Combined constant = 0.5. Annotations were assigned using the AutoAnnotate app (Kucera et al., 2016). Enrichment terms were obtained from DAVID chart for GO categories (Huang et al., 2007) using all the differentially expressed genes.

Enrichment analysis of TF-binding motifs was performed in EnrichR (Chen et al., 2013) using the TRANSFAC and JASPAR databases. TFs motif were ranked according to their combined score, which was calculated in the platform.

### 3.3.6. Protein-protein interactions

Assessment of protein-protein interactions was performed in STRING (Franceschini *et al.*, 2013) with the options “medium confidence” and “no more than 5 interactors in the first shell”. Interactions were based on textmining, experiments, databases, co-expression and co-ocurrence.

## 3.4. Reverse transcription and quantitative PCR

### 3.4.1 mRNAs

Reverse transcription (RT) from total RNA was done using the Transcriptor First Strand cDNA Synthesis Kit (Roche) and a mix of random hexamer primers and anchored-oligo(dT) primers, both provided in the kit. RTs were done with 100 ng of RNA extracted from isolated cells or with 1 µg of RNA extracted from brain tissue following manufacturer’s instructions.

Quantitative PCR (qPCR) was carried out with the Lightcycler 480 platform (Roche) using EvaGreen Dye (Niborlab). Reagents were mixed together with diluted cDNA following manufacturer’s instruction. Appropriate cDNA dilution was experimentally determined for each set of primers to allow acceptable detection. PCR conditions used were the following: 1 cycle at 95°C for 5 min; 40 cycles of 10 s at 95°C, 10 s at 60°C and 10 s at 72°C; 1 cycle at 95°C for 5 s; and 1 final cycle at 65°C for 1 min. Primers for mRNA qPCR are listed in **Table M4**. To design PCR primers we used the Primer Blast tool (Ye et al., 2012) in NCBI; with the following criteria: forward and reverse primers in different exons, amplicons of 70-200 bp and annealing temperatures between 59ºC and

61ºC. Data from qPCR was analysed with the LightCycler 489 Software release 1.5.0 and relative transcript levels calculated by the ΔΔCp method. As reference gene we used *Ribosomal protein s23* (*Rps23*), *Glyceraldehyde-3-phosphate dehydrogenase* (*Gapdh*) or *Peptidyl-prolyl isomerase* (*Ppia*).

Generally, qPCRs were performed in at least three independent biological samples per experimental condition (genotype or developmental stage). Due to the low yield of Prominin-1$^{+}$-FACS-isolated cells per embryo, only one biological sample was used to perform qPCRs with cDNA from these cells. Each sample was run in duplicate or triplicate. For validation of mRNA-seq results by qPCR we chose genes with expression values above 500 counts (mean normalized counts).

**Table M4. Primers for qPCR**

| Primer | 5'-3' Sequence | Amplicon (bp) |
|---|---|---|
| *Adamts20*-F<br>*Adamts20*-R | AGGTGTCTTCAACAGTGCCC<br>ATCGAGTTGTTTGACCCGCT | 240 |
| *Brn2*-F<br>*Brn2*-R | TCAAATGCCCTAAGCCCTCG<br>CGGGAGGGGTCATCCTTTTC | 126 |
| *Cdc34-F*<br>*Cdc34-R* | TTCGCTGCTGAATGAGCCC<br>AGTACTCGGCCAGCGTAGTG | 188 |
| *Cdk2-F*<br>*Cdk2-R* | TTCATGGATGCCTCTGCTCTC<br>TTCTGGGGCTTAAGGTCTCG | 128 |
| *Cnp1*-F<br>*Cnp1*-R | AGCAGGAGGTGGTGAAGAGAT<br>ACAACTGCAGCTCCTGATCG | 120 |
| *Col1a2*-F<br>*Col1a2*-R | TGGATACGCGGACTCTGTTG<br>GGCCCTTTCGTACTGATCCC | 87 |
| *Col3a1*-F<br>*Col3a1*-R | AAGGGCGAAGATGGCAAAGA<br>AGCTACTCCTCTGGGTCCTG | 183 |
| *CyclinD1*-F<br>*CyclinD1*-R | CACAACGCACTTTCTTTCCA<br>TGACTCCAGAAGGGCTTCAA | 88 |
| *Delta1*-F<br>*Delta1*-R | CGGCTCTTCCCCTTGTTCTAA<br>GGGGAGGAGGCACAGTCATC | 126 |
| *Dyrk1a*-F<br>*Dyrk1a*-R | ATCCAGCAACTGCTCCTCTG<br>CCGCTCCTTCTTATGACTGG | 140 |
| *Fezf2*-F<br>*Fezf2*-R | TATAACCTCACCCGCCACAT<br>TGTGTCTGCAGAGAGTGCTG | 103 |
| *Gfap*-F<br>*Gfap*-R | GTTACCAGGAGGCACTTGCT<br>GTAGGTGGCGATCTCGATGT | 131 |
| *Gria2*-F<br>*Gria2*-R | GCGACCTGACCTCAAAGGAG<br>TGATAGCAGTCACCTGCCAC | 152 |
| *Grin2b*-F<br>*Grin2b*-R | ATGCGCTCTCCCTTAATCTGTC<br>TTCATCTTCAGCTCGTCGACTC | 75 |
| *Hes1*-F<br>*Hes1*-R | TCTGACGACAGAAAGTCATCA<br>AGCTATCTTTCTTAAGTGCATC | 115 |
| *Hes5*-F | CCAAGGAGAAAAACCGACTG | 103 |

| | | |
|---|---|---|
| *Hes5*-R | AACTCCTGCTCCAGCAGCA | |
| *Kcna1*-F<br>*Kcna1*-R | TCTTCAAACTCTCCCGCCAC<br>AGTGCGACTCAGCTTCTTCC | 319 |
| *Kcnh3*-F<br>*Kcnh3*-R | CGCTAACACAGACACGGAGA<br>GGTGGATGCGGATGTAGTCT | 170 |
| *Kcnq3*-F<br>*Kcnq3*-R | CAGGAGACGTGGAGCAAGTCA<br>AGGTTTCCAGCAGCAAAAGCC | 345 |
| *Mag*-F<br>*Mag*-R | CGCGTCATTTGTACCTCCAG<br>GCACACAATGGCAATCAGGA | 141 |
| *Mash1*-F<br>*Mash1*-R | ACTTTGGAAGCAGGATGGCAG<br>CCCCTGTAGGTTGGCTGTCT | 136 |
| *Mbp*-F<br>*Mbp*-R | CTTCAAAGACAGGCCCTCAG<br>CCAGGTACTTGGATCGCTGT | 125 |
| *Mid1*-F<br>*Mid1*-R | CACAGAACTGGAGACTCTTTTGG<br>TGCCTTCTTTAATCTTTGTTCCA | 161 |
| *NeuroD1*-F<br>*NeuroD1*-R | GCTCCAGGGTTATGAGATCG<br>CGCTCTCGCTGTATGATTTG | 83 |
| *NeuroD6*-F<br>*NeuroD6*-R | CTCCAGGAGACGATGCGAC<br>ACGACAGACTCGTCAAACGG | 139 |
| *Nf1a*-F<br>*Nf1a*-R | CTTTGTACATGCAGCAGATT<br>TTCCTGCAGCTATTGGTGTTT | 176 |
| *Nf1b*-F<br>*Nf1b*-R | CGCATGGAGTCACTATTCCTG<br>ATAAAATGGCTGGCTCATGG | 94 |
| *Ntrk2*-F<br>*Ntrk2*-R | TGGTGCATTCCATTCACTGT<br>CTTGGCCATCAGGGTGTAGT | 192 |
| *Pax6*-F<br>*Pax6*-R | GGCGGTTAGAAGCACTTCAC<br>GCCTTCTGTACGCAAAGGTC | 86 |
| *Plp*-F<br>*Plp*-R | TTGGCGACTACAAGACCACC<br>AGCCATACAACAGTCAGGGC | 85 |
| *Ppia*-F<br>*Ppia*-R | ATGGCAAGACCAGCAAGAAG<br>TTACAGGACATTGCGAGCAG | 142 |
| *Rps23*-F<br>*Rps23*-R | CGTCAGGGTGCAGCTCATTA<br>GGCACGAACGCTGTGATCTT | 51 |
| *Satb2*-F<br>*Satb2*-R | TGCCCTCTCTCCCAGAGTATG<br>TCTGAAAGGTTCTCTCGCTCC | 149 |
| *Shank1*-F<br>*Shank1*-R | GGAGCCAGTTACATCCCAG<br>CCAGTTCTGAAAGATGCTGC | 111 |
| *Snap25*-F<br>*Snap25*-R | ACCAGTACCATGGCCGAAG<br>CGCCTTGCTCATCCAACAT | 172 |
| *Syt4*-F<br>*Syt4*-R | GGAGTTCTTTCAGCACCTCGG<br>CACTGAAGATGCCCACCACTG | 106 |
| *Zbtb20*-F<br>*Zbtb20*-R | AACGCAATGAATCCGAGGAGT<br>CCCAAACTGTTGCTCCACTGA | 140 |

All primers were used at 10 µM. bp: base pairs; F: forward; R: reverse.

### 3.4.2. miRNAs

Quantification of miRNAs was done using the TaqMan® Small RNA Assays kit (Applied Biosciences) following manufacturer's instructions. The kit provides a stem-looped primer for RT of the miRNA of interest and a sequence-specific TaqMan probe for qPCR amplification of the cDNA. qPCRs with TaqMan probes were ran in the Lightcycler 480 platform. PCR program consisted in a cycle of enzyme activation (10 min at 95ºC) followed by 40 cycles of 15 s at 95ºC plus 1 min at 60ºC. As for mRNAs, relative transcript levels were calculated by the ΔΔCp method and *Sno135* (*snoRNA135,* #001230, Applied Biosystems*)* was used as a reference gene for normalization. The TaqMan Assays used in this work are in **Table M5**.

For validation of small RNA-seq results by qPCR we chose miRNAs with expression values above 400 counts. Validations were performed in 3 independent biological preparations from GFP-FACs-isolated cells per developmental stage and one preparation from Prominin-1$^{+}$-FACS-isolated cells per stage. Samples were run in duplicate or triplicate.

**Table M5. TaqMan™ MicroRNA Assays for miRNA RT-qPCR**

| miRNA | Assay ID (Thermo Fisher) |
|---|---|
| mmu-let-7b-5p | #002619 |
| mmu-let-7d-5p | #002283 |
| mmu-let-7f-5p | #000382 |
| mmu-mir-23a-3p | #000399 |
| mmu-mir-98-5p | #000577 |
| mmu-mir-99b-5p | #000436 |
| mmu-mir-148a-3p | #000470 |
| mmu-mir-204-5p | #000508 |

## 3.5. Quantification of alternative splicing forms by PCR

Quantification of AS forms by conventional PCR was done in cDNA samples obtained from GFP- and Prominin-1$^{+}$-FACS-isolated cells (see Section 3.3.1 for RT). Primers and conditions are listed in **Table M6**. PCR products were resolved on 2-3% agarose gels. Image of the gel was taken using a Gene Genius Bioimaging System (Syngene). We quantified the amount of AS form relative to the total gene transcripts (AS plus reference form) using the Gel Analyzer tool of Fiji software (Schindelin et al., 2012). Three

independent biological samples from GFP- FACs-isolated cells and one from Prominin-1$^{+}$- FACs-isolated cells were evaluated per developmental stage.

For validation of mRNA-seq results, we chose AS forms with absolute PSI change (ΔPSI) > 25%, high expression values of the reference mRNA (above 500 counts in the RNA-seq) and PCR primers validated previously (**Table M6**).

## 4. Protein expression analysis

### 4.1. Brain lysates

Mouse brains were collected after cervical dislocation or decapitation in the case of embryos or early postnatal animals. The embryonic dorsal telencephalon and the cerebral hemispheres of postnatal and adult animals were dissected out under a binocular microscope and immediately frozen in dry ice. Total protein extracts were prepared by resuspension of the frozen tissue in 10 volumes of SDS-buffer (**Table M7**) and mechanic homogenization using a pipette tip (for embryo tissue) or a syringe (for postnatal and adult tissue). Then, samples were sonicated with 4 pulses of 30 s each in a Bioruptor (Diagenode), boiled for 15 min at 98ºC, centrifuged at 800 g at 4ºC for 10 min and the supernatants stored at -80ºC

Protein concentration was determined using a colorimetric assay (BCA Protein Assay Kit from Pierce, according to the manufacturer's indications). Absorbances were read in a Power Wave XS (Biotek).

**Table M6. PCR primers and conditions for quantification of alternative splicing forms**

| Primer | AS event ID | Sequence 5'-3' | Amplicon (bp)* | AS length (bp) | Ta (ºC) | Extension time | Source |
|---|---|---|---|---|---|---|---|
| *Abi*-AS-F | MmuEX0003242 | GCAAATATGGAGCGTCCTGT | 123/**138** | 15 | 58.9 | 30 sec | Zhang et al., 2012 |
| *Abi*-AS-R | | TCTCGACAATGTGCCAGTTC | | | | | |
| *Ank2*-AS-F | MmuEX0004899 | CCTTGTGAAACGCCATCGAC | 185/**284** | 99 | 62.8 | 45 sec | Zhang et al., 2012 |
| *Ank2*-AS-R | | CATTTTCACTGCGCAGGACC | | | | | |
| *Dctn1*-AS-F | MmuEX0013951 | CTACCCTGGTCTCTGGCATC | 91/**106** | 15 | 58.9 | 30 sec | Zhang et al., 2012 |
| *Dctn1*-AS-R | | AGTGGGGAGTCCTTCACCAG | | | | | |
| *Elmo2*-AS-F | MmuEX0016707 | TCCAACCAGGAGATCCAGAC | 156/**192** | 36 | 58.9 | 30 sec | Zhang et al., 2012 |
| *Elmo2*-AS-R | | GATTGGACGATTCCCTCTGA | | | | | |
| *Ergic3*-AS-F | MmuEX0017296 | AAACTTCCACTTTGCCCCTGG | 78/**93** | 15 | 62.0 | 30 sec | VastDB |
| *Ergic3*-AS-R | | TCAAGGCCAAAGCTCTGCAAG | | | | | |
| *Flna*-AS-F | MmuEX0019330 | AGGTGGAAGTTGTCATCCAG | 252/**309** | 57 | 59.0 | 45 sec | Zhang et al., 2012 |
| *Flna*-AS-R | | GCCCTTTGTGTACACCTTGAA | | | | | |
| *Macf1*-AS-F | MmuEX0027472 | AGGCAAAAACAGCTGGAAGA | 519/**846** | 327 | 59.0 | 45 sec | Zhang et al., 2012 |
| *Macf1*-AS-R | | CCTGTGTTCCATGACCTCCT | | | | | |
| *Scrib*-AS-F | MmuEX0041307 | GGCAGCCAGAATGAAGTCTC | 216/**291** | 75 | 59.0 | 45 sec | Zhang et al., 2012 |
| *Scrib*-AS-R | | CTCAGCTCCTCCACGAAATC | | | | | |
| *Ttc9c*-AS-F | MmuINT0167446 | GAGACTCAGGCCTCACTCACT | 356/**692** | 336 | 57.7 | 1 min | VastDB |
| *Ttc9c*-AS-R | | TGTTTTCTTGCTCCGGTGTGA | | | | | |

All primers were used at 10 μM. Number of PCR cycles was 35. AS: alternative splicing form; bp: base pairs; F: forward; R: reverse; Ta: annealing temperature. * In bold is the size of the amplicon including the AS form.

**Table M7. SDS-buffer composition**

| Components | Final concentration |
|---|---|
| Tris-HCl, pH 7.4 (Panreac) | 25 mM |
| EDTA (Panreac) | 1 mM |
| SDS (Panreac) | 1% (w/v) |
| Sodium pyrophosphate (PpiNa; Sigma) | 10 mM |
| Beta-glycerol phosphate (Sigma) | 20 mM |
| Sodium orthovanadate (Sigma) | 2 mM |
| Phenylmethylsulphonyl fluoride (PMSF; Sigma) | 2 mM |
| Protease inhibitor cocktail 7x, EDTA-free (#11836170001, Roche) | 1x |

## 4.2. Western blotting

Protein extracts (30 to 80 µg) were mixed with Laemmli buffer, heated for 5 min at 98ºC and resolved on a SDS-PAGE gel (7.5 to 14% acrylamide depending on the molecular weight of the protein of interest) at 125 V in running buffer. Proteins on the gel were transferred onto a nitrocellulose membrane (Hybond-ECL, Amersham). Transfer was performed in transfer buffer at 400 mA for 60 min in a cold chamber (4ºC). Correct protein transfer was checked by Ponceau staining (Sigma-Aldrich). Transferred membranes were washed in TBS-T buffer and blocked in TBS-T with 10% bovine serum albumin (BSA; w/v). Then, membranes were incubated overnight (ON) at 4ºC with the corresponding primary antibody diluted in 5% BSA - TBS-T. Membranes were washed in TBS-T and incubated 45 min at room temperature (rT) with the appropriated fluorescent secondary antibodies diluted in 5% BSA - TBS-T. After washes in TBS-T, infrared fluorescence was visualized in the LI-COR Odyssey IR Imaging System V3.0 (LI-COR Biosciences). The composition of the buffers used for western blotting is listed in **Table M8**. Primary and secondary antibodies together with dilutions used are listed in **Tables M9** and **M10**, respectively. Quantification of protein levels was done using the Odissey software version 3.0. We used GAPDH or Vinculin as loading control for the normalization of protein levels. Protein quantifications were done in a minimum of three independent lysates per experimental condition (genotype or developmental stage).

**Table M8. Buffers for western blotting**

| Laemmli buffer | Final concentration |
|---|---|
| Tris-HCl, pH 6.8 (Panreac) | 83 mM |
| SDS (Panreac) | 2% (w/v) |
| Glycerol (Sigma) | 10% (v/v) |
| Dithiothreitol (Sigma) | 100 mM |
| Bromophenol blue (Sigma) | 0.01% (v/v) |
| **Running buffer** | **Final concentration** |
| Tris-base (Panreac) | 25 mM |
| Glycine (Sigma) | 200 mM |
| SDS (Panreac) | 0.1% (w/v) |
| **Transfer buffer** | **Final concentration** |
| Tris-HCl, pH 8.3 (Panreac) | 25 mM |
| Glycine (Sigma) | 200 mM |
| Methanol (Panreac) | 20% (v/v) |
| **TBS-T buffer** | **Final concentration** |
| Tris-HCl, pH 7.5 (Panreac) | 10 mM |
| NaCl (Sigma) | 100 mM |
| Tween-20 (Sigma) | 0.1% (v/v) |

**Table M9. Primary antibodies used for western blotting**

| Primary antibody | Host | Working dilution | #Reference, provider |
|---|---|---|---|
| GAPDH | Mouse | 1:2000 | #mab374, Merck Millipore |
| MBP | Rat | 1:500 | #mab386, Merck Millipore |
| PLP | Rabbit | 1:1000 | #NB100-74503, Novus Biologicals |

**Table M10. Secondary antibodies used for western blotting**

| Secondary antibody | Host | Working dilution | Provider |
|---|---|---|---|
| anti-mouse IgG IRDye-800CW | Goat | 1:5000 | LICOR Biosciences |
| anti-rabbit IgG IRDye-680RD | Goat | 1:5000 | LICOR Biosciences |
| anti-goat IgG IRDye-680RD | Donkey | 1:5000 | LICOR Biosciences |

## 5. *In-utero* electroporations

*In-utero* electroporations were carried out following standard protocols (Saito and Nakatsuji, 2001; Matsui *et al.*, 2011) using a TSS20 ovodyne electroporator (Intracel) connected to the EP21 Current Amplifier (Intracel). Briefly, pregnant mice carrying E16.5 embryos were anesthetized using isofluorane and put face up on a heated pad. The uterus was exposed and the indicated plasmids diluted in phosphate buffer saline (PBS) containing 5% Fast Green FCF (Sigma-Aldrich) were injected into the lateral ventricle of the embryo brain with a fine glass micropipette. Five electrical pulses of 50 ms, 38 volts at an interval of 950 ms were delivered using 5 mm diameter electrodes (CUY650P5, Nepagene). Finally, the uterus was placed back into the abdominal cavity.

For Stat3 activity assays, a firefly luciferase reporter plasmid that contains sequences of the *Gfap* promoter (GFL1-pGL3) or its mutated version (GFL1-S-pGL3) was co-electroporated with a *Renilla* luciferase reporter plasmid (pRL-CMV) at a 30:1 ratio. Pregnant mice were sacrificed 14 hours after electroporation and embryos collected and processed for luciferase assay as describe in Section 8.

For tracking the progeny of RG cells, we used the Piggybac Transposon System. In this system, transposon-specific inverted terminal repeats (ITRs) enable the integration of a gene of interest, in our case the fluorescence protein GFP, into the genome (Wang et al., 2008b). The plasmid PB-GFP was co-electroporated with a plasmid expressing the PiggyBac transposase (PBase) that recognizes the ITR sequences in PB-GFP (Nagy *et al.*, 2011). Plasmids were co-electroporated at a 1:1 ratio. For these experiments, electroporated embryos developed until P5 and the pups were sacrificed and processed for immunofluorescence as described in Section 10.

DNA plasmids for electroporation were extracted and purified using NucleoBond® Xtra Midi Plus EF (Macherey-Nagel) following the manufacturer's indications. Purified DNA was reconstituted in sterile dd$H_2O$. A description of these plasmids is in **Table M11**.

## 6. Luciferase assays

The dorsal telencephalon of embryos electroporated with the reporter luciferase plasmid pGFL1-pGL3 or pGFL1-S-pGL3 and pRL-CMV was dissected out and stored at -80ºC until usage. Lysis of the tissue and preparation of the samples were done with the Dual-Luciferase Assay System (Promega) according to manufacturer's indications. Firefly and

*Renilla* luciferase activities were measured in an Orion II Microplate Luminometer (Berthold). Reporter luciferase values were normalised to the Renilla values.

**Table M11. Plasmids used for in-*utero* electroporations**

| Plasmid | Details | References |
|---|---|---|
| pPB-GFP | pCAG-driven GFP reporter flanked by ITRs | Nagy et al., 2011 |
| pPB transposase | pCAG-driven Piggybac transposase expression | Nagy et al., 2011 |
| GFL1-pGL3 | Luciferase reporter gene fused with the 2.5-kb GFAP promoter (GF1L) containing a STAT3-binding site | Nakashima *et al*., 1999 |
| GFL1-S-pGL3 | Luciferase reporter gene fused with the 2.5-kb GFAP promoter (GF1L) containing a mutated STAT3-binding site | Nakashima *et al*., 1999 |
| pRL-CMV | *Renilla* luciferase expression under the CMV enhancer/promoter | #E226A, Promega |

IRES, internal ribosomal entry site; ITRs, inverted terminal repeats.

## 7. Lysolecithin-induced focal demyelination

For lysolecithin (l-α-lysophosphatidylcholine or LPC)-induced demyelination in the CC we used ten- to twelve-week old *Dyrk1a*$^{+/-}$ female mice and their respective *Dyrk1a*$^{+/+}$ control littermates. Mice were anesthetized by intraperitoneal injection of a mixture of ketamine (0.13 mg/g; Imalgene) and xylazine (0.01 mg/kg, Rompun) diluted in 0.9% NaCl (Braun) and situated on a heated platform to maintain body temperature. Then, a longitudinal incision of the skin was performed in order to expose the skull and the mouse was positioned in a stereotaxic frame (Kopf). Stereotaxic coordinates for the location of CC in wild-type animals were deduced from the Paxinos and Franklin's atlas (Franklin and Paxinos, 2013) and were the following; 1.5 mm anterior to the Bregma, 1 mm lateral and 1.8 mm deep from the skull surface. Due to the smaller brain volume of *Dyrk1a*$^{+/-}$ mice, the stereotaxic coordinates in these mice had to be readjusted to 1.25 mm anterior to the Bregma, 1 mm lateral and 1.3 mm deep from the skull surface. A fine hole was drilled in the region of interest in the left hemisphere and demyelination was induced by stereotaxic injection of 2 µl of 1% LPC (Sigma) diluted in 0.9% NaCl using a Hamilton syringe. Control animals received vehicle solution (0.9% NaCl) instead of LPC. After injection the needle was kept in place for 5 min to reduce reflux along the needle track. Then, the animal was removed from the stereotaxic frame and the skin sutured. Ocular lubricant was administered to prevent corneal desiccation during surgery. The animals

were placed in the heated platform until they recovered from surgery and were treated for 2 days with Metacam (2 mg/kg) for pain therapy. The day of the injection was considered as day 0 post-lesion (DPL). Five, 14 or 21 DPL mice were perfused for histological analysis.

# 8. Histology and immunofluorescence

## 8.1. Tissue preparation

To obtain embryonic brain sections, heads were dissected and fixed by immersion in 4% (w/v) paraformaldehyde in PBS pH 7.4 (PFA – PBS) ON at 4ºC. To obtain postnatal and adult brain sections, mice were deeply anesthetised with $CO_2$ and transcardially perfused with 4% PFA – PBS at rT. Brains were removed and post-fixed at 4ºC ON in 4% PFA – PBS. Embryo heads and brains were then rinsed in PBS and processed to obtain either cryostat or vibratome sections.

For vibratome sectioning, brains were embedded in agarose of different percentages according to the age of the sample: embryo and P0 brains were embedded in 2% agarose; postnatal brains in 3-4% agarose and adult brains in 6% agarose. Embedded brains were cut in a Leica VT1000S vibratome and the slices (50 µm) were kept in PBS for short storage at 4ºC or placed in cryoprotective solution (**Table M12**) for long storage at -20ºC.

For cryostat sectioning of embryo heads, samples were cryoprotected in 30% (w/v) sucrose in PBS at 4ºC for 1 or 2 days until the head sunk indicating that it has absorbed enough to be isotonic to the sucrose. E11.5 heads were embedded in Tissue-Tek OCT (Sakura Finetek) and frozen at -30ºC in isopentane (Panreac). E13.5, E15.5 and E17.5 heads were directly frozen in isopentane at -30ºC and then loaded on an OCT-base. Head sections (20 µm) were obtained using a Leica CM3050S cryostat and collected serially on SuperFrost® slides (VWR). Slides were maintained at -20ºC until usage.

## 8.2. Immunofluorescence

Brain sections (vibratome or cryostat) used for immunofluorescence were washed in PBS. BrdU immunostaining required an additional treatment in order to denaturate the DNA. The treatment consisted in an incubation with 50% formamide diluted in 2X saline-

sodium citrate buffer at 64ºC for 10 min followed by an incubation in 2 N HCl at 37ºC for 30 min. The pH was then re-established by a 10 min incubation in 0.1 M boric acid (Panreac) at rT. Additionally, some antibodies required an antigen retrieval treatment that consisted in boiling the sections for 10 min in sodium citrate buffer. Antibodies that needed this treatment are indicated in **Table M13**. After these treatments (if needed), tissue sections or slides were permeabilised for 30 to 90 min with PBS - 0.2% Triton-X100 and incubated 60 min at rT in blocking solution. Then, samples were incubated ON at 4ºC with the corresponding primary antibody (or antibodies) diluted in incubating solution. After washing, samples were incubated with the secondary antibodies diluted in incubating solution for 60 min at rT. In some cases, an incubation with biotinylated secondary antibody (1:200, Vector Laboratories) followed by a 60 min incubation with Alexa fluor 488, 568 or 633-conjugated Streptavidin were done to amplify the staining signal. Cell nuclei were stained with DAPI (0.1 µg/ml; Vector Labs). Finally, samples were mounted either with Vectashield (Vector Labs) or with 2,2'-thiodiethanol (TDE; Sigma) mounting media, depending on the immersion objectives required for posterior imaging (glycerol or oil). The composition of the buffers used for immunofluorescence is listed in **Table M12** and details for the primary and secondary antibodies used are summarized in **Tables M13** and **M14**, respectively.

Immunofluorescences performed in demyelinated brains showed an increased background due to the inflammation process associated to the lesion. We used the Vector Mouse On Mouse (M.O.M) immunodetection Kit (Vector Laboratories) to reduce background of the antibodies CC1 and BrdU. In this case, M.O.M. blocking solution and M.O.M. diluent were used instead of blocking and incubating solution respectively, and a biotinylated anti-mouse IgG provided in the kit was used as secondary antibody.

In all cases, specificity of the immunoreaction was verified by omitting the primary antibody in samples processed in parallel. Samples used for the same assay were processed in parallel to avoid day-to-day variations in the immunostaining.

**Table M12. Buffers for histology and immunofluorescence**

| **Cryoprotective solution** | **Final concentration** |
|---|---|
| PBS | 40% |
| Glycerol (Sigma) | 30% |
| Ethylene glycol (Sigma) | 30% |
| **2x saline-sodium citrate buffer** | **Final concentration** |
| NaCl (Sigma) | 0.3 M |
| Tri-sodium citrate (Prolabo) | 30 mM |
| **Sodium citrate buffer, pH 6.0** | **Final concentration** |
| Citric acid monohydrate (Sigma) | 2 mM |
| Tri-sodium citrate (Prolabo) | 8 mM |
| **Blocking solution** | **Final concentration** |
| Triton-X100 (Sigma)* | 0.2% |
| FBS (Invitrogen) | 10% |
| PBS | 89.8% |
| **Incubating solution** | **Final concentration** |
| Triton-X100 (Sigma)* | 0.2% |
| FBS (Invitrogen) | 5% |
| PBS | 94.8% |

**Table M13. Primary antibodies used for immunofluorescence**

| **Primary antibody** | **Host** | **Dilution** | **#Reference, provider** |
|---|---|---|---|
| BrdU | Rat | 1:100 | #OBT0030G, AbD Serotec |
| CASPR (clone K65/35)* | Mouse | 1:200 | #75-001, NeuroMab |
| CC1 | Mouse | 1:200 | #OP80, Calbiochem |
| Collagen type-I* | Goat | 1:50 | #1310, Southern Biotech |
| COL3A1* | Rabbit | 1:200 | #ab7888, Abcam |
| Cyclin D1 | Rabbit | 1:100 | #RM-9104, Thermo scientific |
| DYRK1A | Mouse | 1:250 | #H00001859, Abnova |
| GFAP | Rabbit | 1:500 | #Z0334, DAKO |
| IBA1 | Rabbit | 1:600 | #019-19741, Wako |
| Laminin | Rabbit | 1:500 | #L9393, Sigma |
| MBP | Rat | 1:500 | #mab386, Merck Millipore |
| NAV1.6* | Rabbit | 1:200 | #ASC009, Alomone Labs |

| | | | |
|---|---|---|---|
| NEUN | Mouse | 1:500 | #mab377, Chemicon |
| NG2 | Rabbit | 1:500 | #ab5320, Merck Millipore |
| OLIG2 | Rabbit | 1:500 | #ab9610, Merck Millipore |
| PAX6 | Rabbit | 1:100 | #901301, Biolegend |
| PDGFRa (CD140a) | Rat | 1:100 | #558774, BD Pharmigen |
| SOX9 | Rabbit | 1:500 | Stolt *et al*., 2003[1] |

(*) Citrate pre-treatment needed. (1) Kindly provided by Dr. Wegner (Friedrich-Alexander-Universität Erlangen-Nürnberg, Erlangen, Germany).

**Table M14. Secondary antibodies used for immunofluorescence**

| Secondary antibody | Host | Dilution | Source |
|---|---|---|---|
| Alexa Fluor 488-conjugated anti-mouse | Donkey | 1:1000 | Life Technologies |
| Alexa Fluor 488-conjugated anti-rabbit | Goat | 1:1000 | Life Technologies |
| Alexa Fluor 488-conjugated anti-rat | Donkey | 1:1000 | Life Technologies |
| Alexa Fluor 488-conjugated anti-goat | Donkey | 1:1000 | Life Technologies |
| Alexa Fluor 568-conjugated anti-mouse | Donkey | 1:1000 | Life Technologies |
| Alexa Fluor 568-conjugated anti-rabbit | Donkey | 1:1000 | Life Technologies |
| Alexa Fluor 594-conjugated anti-mouse | Donkey | 1:1000 | Life Technologies |
| Alexa Fluor 594-conjugated anti-rabbit | Donkey | 1:1000 | Molecular Probes |
| Alexa Fluor 594-conjugated anti-rat | Goat | 1:1000 | Life Technologies |
| Alexa Fluor 633-conjugated anti-rabbit | Goat | 1:1000 | Life Technologies |
| Alexa Fluor 647-conjugated anti-rat | Donkey | 1:1000 | Life Technologies |

## 8.3. Luxol Fast Blue staining

Vibratome sections from LPC-induced demyelinated brains were mounted on gelatinized slides and dried ON at rT. The following morning, sections were rehydrated by rinsing them in $H_2O$ for 2 min twice. Then, sections were dehydrated in an ethanol gradient: 70% (v/v) EtOH for 2 min twice and 95% (v/v) EtOH for 30 s twice. Afterwards, slides were placed in a coplin jar with Luxol Fast Blue (LFB; Sigma) for 24 hours at 60ºC. Sections were rehydrated reversing the ethanol gradient, dipped for 1 min in 0.03% $LiCO_3$ (Fluka Chemika) in 70% EtOH and washed in water. The incubation with $LiCO_3$ was repeated until the staining reached the appropriate level for myelin visualization. Some sections were counter-stained with cresyl violet to visualize cell nuclei. Finally, sections were dehydrated again and mounted in *Eukitt* mounting medium (Sigma).

# 9. Image acquisition and analysis

Image acquisition was performed with the equipment of the Molecular Imaging Platform Unit (http://www.ibmb.csic.es/groups/molecular-imaging-platform) of the IBMB-CSIC. Wide-field images were collected in a Leica AF7000 motorized microscope using a Digital CCD camera ORCA-R2 for immunofluorescence or a DFC-550 colour camera for bright-field images. Confocal images were taken either in a confocal SP5 microscope using the Leica Confocal Software (LCS) or in a Zeiss LSM-780 microscope controlled under the LSM Software ZEN 2.1. Samples from the same experiment were imaged with the same microscopy and the same settings to reduce technical variability.

Images were analysed with the Fiji software (Schindelin et al., 2012) using the following commands and plug-in: *Cell counter*, to count features in a slice; *Measurement tool*, to define parameters such as area and integrated density; *Z-projection tool*, to obtain a unique image from z-series acquired at imaging; and *Find maxima*, to count automatically particles of high fluorescence.

Measurements in brain slices were done in images obtained from coronal brain sections. Quantifications in sections were performed in a minimum of three sections per animal and a minimum of three animals per experimental condition.

## 9.1. Cell counts

Cells in the embryonic telencephalon were quantified in confocal images. Quantification of PAX6+ cells in the dorsal telencephalon was performed in images collected using an HCX PL APO 40x/1.25-0.75 OIL CS objective in the SP5 microscope. Images were acquired as z-stacks of 4 µm thickness (step size = 1 µm, sum projection). Quantification of OLIG2+ and PDGFR$\alpha$+ cells in the embryonic LGE and dorsal telencephalon was performed in images collected using a 25x multi immersion objective in the Zeiss LSM-780 microscope. Images were acquired as z-stacks of 15 µm thickness (step size = 3 µm, max projection). Immunopositive cells in the dorsal telencephalon were counted in columns of 200 µm width in the lateral cortical wall and results were expressed as number of cells per column. Immunopositive cells in the LGE were counted in a 150 x 300 $\mu m^2$ rectangle drawn in the centre of the mantel zone and results were expressed in cell density.

Quantification of cells (NEUN+, OLIG2+, GFAP+, IBA1+) in the postnatal and adult neocortex was performed in wide-field images taken either with the 10x or the 20x objective. Immunopositive cells were counted in columns of 500 µm width in the somatosensory barrel cortex and results were expressed as number of cells per column.

Quantification of cells (GFAP+, OLIG2+) in electroporated brains was performed in confocal images collected using the 25x objective in the zeiss LSM-780 microscope. Up to 3 optical images were acquired per brain section at 15 µm intervals. Electroporated cells were counted outside of the proliferative zone (VZ and SVZ). Results were expressed as the percentage of cells immunopositive for a specific cell fate marker with respect to the total electroporated cells (GFP+).

Cell quantifications in the CC were done using confocal images sequentially acquired in the SP5 microscope using an HC PL APO 20x/0.70 CS objective. Images were collected as *z*-stacks of 25 µm thickness (step size = 5 µm, max projection). The region of interest was delimited generally in the centre of the CC except for the quantification of CC1+ cells at P7 that we also considered cells in the external capsule. Results were expressed as immunolabelled cells with respect to the total nuclei (DAPI+). In the case of the CC of induced demyelinated lesions, images were acquired as z-projections of 15 µm thickness (step size = 3 µm, max projection); except for the quantification of NG2+ cells, in which case images were acquired as z-stacks of 5 µm thickness (step size = 0.5 µm, sum projection) and 2x optical zoom. Region of interest was considered the area of the lesion (defined based on the acute local cell density) and results were expressed as number of cells per area.

## 9.2. Quantifications of nodes of Ranvier

The density and the length of nodes of Ranvier were quantified on images covering the centre of the CC collected in the Zeiss LSM-780 microscope. Only nodes in which a NAV1.6+ domain was flanked by 2 $CASPR^+$ domains were considered for the analysis.

To estimate node of Ranvier densities we used images of 64.2 $\mu m^2$ collected with the 40x Oil DIC objective, a 3x optical zoom and as z-stacks of 15 µm thickness (step size = 0.5 µm). Quantifications were done in the projected images and results were expressed as number of nodes per area.

To estimate the average length of the nodes of Ranvier we used images collected with the 63x Oil DIC objective, the pinhole set to 1 Airy unit for the CASPR

immunofluorescence signal, which resulted in an optical slice of 0.7 µm, and as z-stacks of 4.5 µm thickness. To allow posterior image deconvolution we used the following Nyquist settings: 2.1x optical zoom and 0.15 µm z-steps, which resulted in images with 15.9 pixels/µm resolution. Deconvolution was performed with the Huygens Professional Deconvolution Software (SVI). Deconvoluted stacks were processed with the 3D Object Counter plug-in (Bolte and Cordelieres, 2006) of Fiji. The 3D Object Counter resulted in a 3D map with the labelled (CASPR or NAV1.6) particles segmented and a report with the following measurements for each object: volume, length, integrated staining density and coordinates for the centre of masses, among others. Nodes present in the first or last images of the stack were not considered for the morphological analysis. Intra-paranodal length (L) was calculated as the Euclidean distance between two CASPR+ paranodes separated by a NAV1.6+ node according to the following equation:

$$L = \sqrt{(x_b - x_a)^2 + (y_b - y_a)^2 + (z_b - z_a)^2}$$

where (x,y,z) are the coordinates in three dimensions of the centre of masses of a paranode. For nodal length, we selected nodes that lay approximately parallel to the plane of the section: NAV1.6+ node with the 2 CASPR+ paranodes displayed together in at least eight slices. We generated a maximum intensity projection with the slices displaying the node. In the projected image, we drawn a line spanning both $CASPR^+$ paranodes and plotted the intensity profile (Plot profile command in Fiji). Nodal length was measured in the intensity profile as the distance between the half maximum intensity for each paranode. Quantifications were done at least in 50 particles per animal.

## 9.3. Immunolabelling quantifications

Labelling fluorescence intensity was evaluated using the *Integrated density function* (sum of intensity values of the pixels in a particular area or volume; https://imagej.nih.gov/ij/docs/guide/146-30.html#toc-Subsection-30.1) of the Fiji software. NAV1.6 labelling intensity in the nodes of Ranvier was evaluated in the segmented nodes obtained from the deconvoluted images described in section 10.2. Cyclin D1 labelling intensity in the PDGFRα+ cells was evaluated in images collected using the 25x multi immersion objective in the Zeiss LSM-780 microscope. Images were acquired as z-stacks of 5 µm thickness (step size = 1 µm, sum projection). To estimate COL1A2 and COL3A1 labelling intensity in the basal lamina we used immunofluorescence images collected with the 25x objective in the Zeiss LSM-780 microscope (z = 1). Measurements were done in up to 5 rectangles (50 x 5 $\mu m^2$) per

section distributed along the basal lamina of the lateral cortical wall. Intensity values were divided by the area or volume measured and were expressed as labelling index (L.I.) in arbitrary units (a.u.).

Labelled area in the demyelinated CC lesions was assessed with LFB staining or immunostaining against MBP. Bright-field images of LFB stainings were acquired with the 10x objective in the AF7000 microscope. Immunofluorescence images of MBP stainings were collected in the SP5 microscope using a HC PL APO 20x/0.70 CS objective as z-stacks of 5 µm thickness (steps size = 0.5 µm, sum projection). Images were converted to binary images by applying a threshold to distinguish between signal pixels and background. In the binary images, we assessed the area occupied by signal pixels within the area of the lesion. Results were expressed as the percentage of the labelled area with respect to the total lesioned area.

## 10. Transmission electron microscopy

The analysis of CC by transmission electron microscopy was done in the laboratory of Dr. Eduardo Fernández (Universidad Miguel Hernández, Alicante). Briefly, animals were deeply anesthetized and transcardially perfused with 4% PFA and 2% Glutaraldehyde in PBS at rT. Brains were removed and post-fixed in the same fixative at 4ºC for 24h. The brains were then segmented in the medial sagittal plane with the help of a stainless steel and trimmed to 2-3 mm thick segments. Sagital slices were washed in PBS, stained with 1% $OsO_4$, dehydrated in graded concentrations of ethanol and embedded in Epon 812 (Electron Microscopy Science). Serial 0.5 mm semi-thin sections were stained with toluidine blue and examined with a Leica DMB Microscope. Thin sections (60-80 nm thick) were obtained with a Reichert Ultracut ultramicrotome equipped with a diamond knife. Sections were stained with uranyl acetate and lead citrate, and examined with a JEOL JEM-1001 electron microscope. Digital images were acquired with a MegaViewIII camera. The image fields were analysed using the Fiji and a modified version of a software designed to study axonal morphometry (Fernandez et al., 1991). For morphometrical evaluation of axons, fibers taken at magnifications of 11,000x were examined. Only fibers with microtubules and neurofilaments sectioned perpendicular to their longitudinal axes were selected for analysis. Because it was difficult to automatically select the boundary between the nerve fibers and the surrounding background for small axons and thinly myelinated fibers using standard image analysis techniques, each image was analysed using a semiautomatic method. The axonal contour and the

external contour of the myelin sheath (fiber contour) were manually traced on enlarged images. A set of custom macros allowed the calculation of the length of a line, the cross-sectional area, and the lengths of the major and minor axes of the best fitting ellipse. Fiber diameters and axonal diameters were deduced from the fiber and axonal perimeters assuming a cylindrical shape of axons. These basic data were used to derive the g-ratio and myelin sheath thickness (Fernandez et al., 1991; Branner et al., 2001). A minimum of three embryos or mice of the same genotype were analysed in each experiment.

## 11. Statistical analysis

Statistical analysis of RNA-seq raw data is described in Section 3.3.1. Differences in the distribution of the RNA-seq data (represented in violin plots) were assessed with a two-tailed non-parametric Wilcoxon rank test performed with the R *stats* package (Team, 2013). Data other than RNA-seq data were analysed using the GraphPad Prism 6 software. Sample sizes (n) are indicated in the figure legends. The normal distribution of the values was assessed with a D'Agostino-Pearson omnibus normality test. Normal distributed data is presented as mean (standard deviation of the mean, S.E.M) in bar graphs or as mean (standard deviation, S.D.) in dot plots. When comparing 2 groups with normal distributed data, statistical analysis was carried out using a two-tailed, unpaired Student's t test (small n) or Welch's test (big n, unequal variances). For evaluation of more than 2 groups we used two-way ANOVA with Bonferroni post-hoc correction. Non-normal distributed data is presented as median (interquartile range) and statistical analysis was carried out using the non-parametric Mann-Whitney test. Differences were considered significant at $p$-values < 0.05: (*) $p < 0.05$; (**) $p < 0.01$; (***) $p < 0.001$.

# RESULTS

# 1. Developmentally regulated genes in dorsal telencephalon radial glial cells during neurogenesis

The distinct types of glutamatergic neurons are orderly generated, either directly or through IP divisions, from RGs of the dorsal telencephalon. During neurogenesis, the competence of these RG progenitors changes while they lose self-renewal potential. To understand which are the genetic networks underlying these changes, we have compared the expression of coding genes and miRNAs in FACS-sorted RGs isolated from the dorsal part of the mouse *Pax6*-GFP telencephalon at two developmental stages: E11.5, when RGs begin to divide asymmetrically to produce subplate neurons and layer VI neurons; and E15.5, when most RGs undergo asymmetric proliferative divisions to generate layers IV-II neurons (Greig et al., 2013). In addition, we have evaluated the contribution of AS in RGs gene expression variability.

## 1.1. miRNA-mRNA regulatory networks

### 1.1.1 Protein-coding transcripts

RNA-seq was performed in 3 biological replicates per developmental stage. Principal component analysis and heat map representation of the transcripts detected in RGs (22,432) showed that they cluster by developmental stage (**Fig R.1a,b**). Seventy-five percent of these transcripts corresponded to protein-coding genes (16,431). Differential expression analysis of the RNA-seq data indicated that 24.7% of the coding genes expressed in RGs (4,069) undergo changes in gene expression levels (log2 FC ≥ +1 or log2 FC ≤ -1; adj. *p*-value < 0.05) between E11.5 and E15.5 (**Fig R.1c,d**). Similar number of genes was down- and up-regulated (**Fig R.1d**). FC values for the top 25 down-regulated genes and the top 25 up-regulated genes were similar; log2 FC ranged from -8.62 to -5,56 in the downs and from 8.96 to 5.58 in the ups (**Fig R.1c** and **Annex 1**, Tables 1 and 2).

To validate the RNA-seq data, we assessed the expression changes of a set of 22 genes (8 down-regulated and 14 up-regulated) by RT-qPCR. This set included a few of the 25 top differentially expressed genes (*Kcnh3*, *Col3a1*, *Col1a2*) and differentially expressed genes with a much moderate log2 FC value, such as *Nfia*, *NeuroD1*, *Fezf2*, *Pax6* and *Delta* (**Fig R.2**). For this experiment we used RNA samples prepared from pools of *Pax6*-GFP FACS-sorted RGs different from the ones used for the RNA-seq. Correlation analysis of the RNA-seq and RT-qPCR results revealed a strong positive correlation

(Pearson's correlation, r = 0.98; p<0.0001) between these two sets of data (**Fig R.2**), thus supporting the reliability of the RNA-seq data.

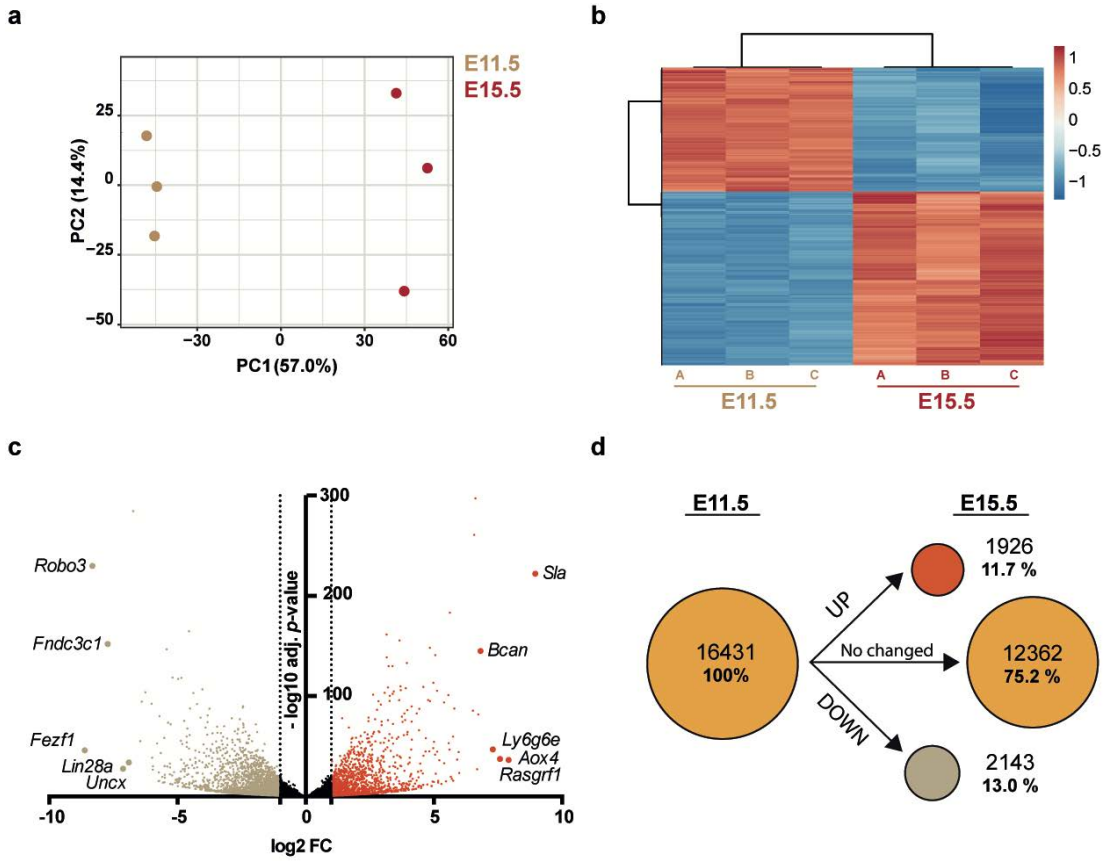


**Figure R.1. Differentially expressed genes in radial glia cells between E11.5 and E15.5. (a)** Principal component (PC) analysis of the transcripts detected by RNA-seq in E11.5 and E15.5 RGs. Notice that the relative variance among replicates from the same developmental stage (PC2) is smaller than the relative variance between stages (PC1). **(b)** Heatmap representing the relative expression of the 1,200 transcripts that show the highest difference in expression, according to the adjusted *p*-value, between E15.5 and E11.5. A, B and C indicate biological replicates. **(c)** Volcano plot showing the difference in gene expression between E15.5 and E11.5. Fold-changes (FC) are represented in log2 (x-axis) and adjusted *p*-values in -log10 (y-axis). Dashed lines indicate log2 FC = 1 and log2 FC = -1. Dots on the right and on the left of these lines represent transcripts differentially expressed during development: red dots up-regulated transcripts and brown dots down-regulated transcripts. The 5 most up- and down-regulated transcripts are indicated. **(d)** Representation of the up- and down-regulated protein-coding genes between E15.5 and E11.5. The total number of genes detected at E11.5 is indicated in the yellow circle on the left. The number and percentage of the genes with significant (red circle for up-regulated genes and brown circle for down-regulated genes) and non-significant (yellow circle on the right) changes in expression are indicated. The area of the circles is proportional to the number of genes. Genes are considered differentially expressed when log2 FC ≤ -1 or log2 FC ≥ +1 and adj. *p*-value < 0.05.

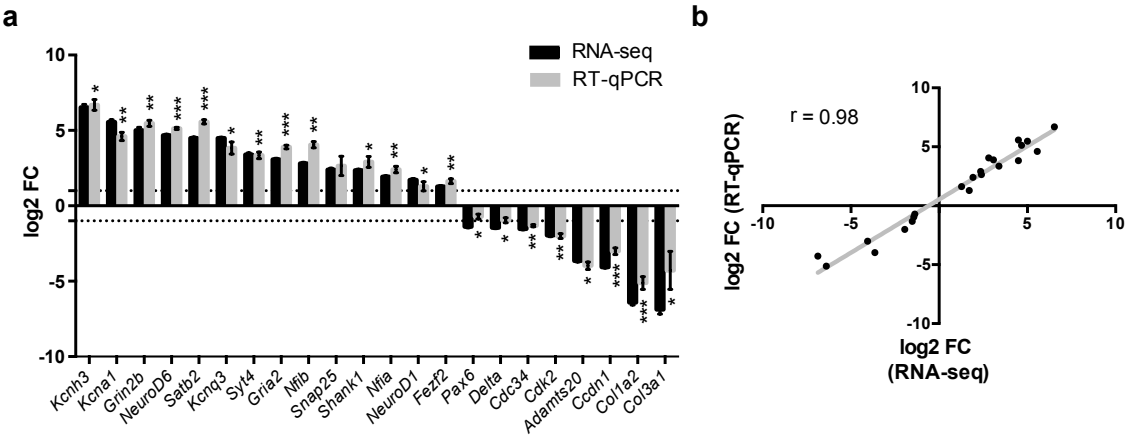


**Figure R.2. Validation of RNA-seq data by RT-qPCR. (a)** RT-qPCR values were normalized to *Rps23* expression. Log2 FC values correspond to the mean (S.E.M.). Dashed lines indicate log2 FC = 1 and log2 FC = -1. Values above and bellow theses lines are considered significantly different. n=3 samples each stage. Asterisks above the grey bars (RT-qPCR data) indicate the statistical significance; *p < 0.05, **p < 0.01, ***p < 0.001, Student's t-test. **(b)** Correlation analysis of the log2 FC values obtained by RNA-seq and RT-qPCR. Each dot corresponds to one of the 22 genes shown in panel a. Pearson's correlation, r = 0.98; p < 0.0001.

Among the top differentially expressed genes (see **Annex 1**, Tables 1 and 2) there are genes such as *Sla* (Src Like Adaptor), *Samd3* (Sterile Alpha Motif Domain Containing 3) or *Ly6g6e* (Lymphocyte antigen 6 complex) that do not have a known function in nervous system development. Others, such as the transcriptional regulators *Fezf1*, *Trnp1* and *Hmga2* (Nishino et al., 2008; Stahl et al., 2013; Eckler and Chen, 2014), do have a known role in neurogenesis or in other nervous system functions, as it is the case of *Robo3,* which is involved in axon guidance (Sabatier et al., 2004).

The enrichment map of the GO terms identified by DAVID revealed that genes whose expression changes significantly during neurogenesis clustered in 4 main groups: "cell cycle and DNA-binding", "WNT signalling", "synapse and ion channels" and "ECM" (**Fig R.3**). Among these functional clusters only "cell cycle and DNA-binding" and "WNT signalling" presented overlapping gene nodes**.** This is consistent with the roles of WNT signalling in cell cycle regulation and cortical neurogenesis (Harrison-Uy and Pleasure, 2012).

DAVID functional analysis of the **down-regulated genes** revealed enrichment in functions ("cell cycle", "DNA replication", "DNA damage and repair", "chromosome" and "DNA-binding") that are highly interconnected within the main cluster "cell cycle and DNA-binding" (**Fig R.3** and **R.4a** and **Annex 1**, Table 3). Violin plots showing the distribution of genes according to the FC revealed that a big proportion of the genes within the GOs Cell cycle (GO~0007049), DNA replication (GO~0006260) and DNA-

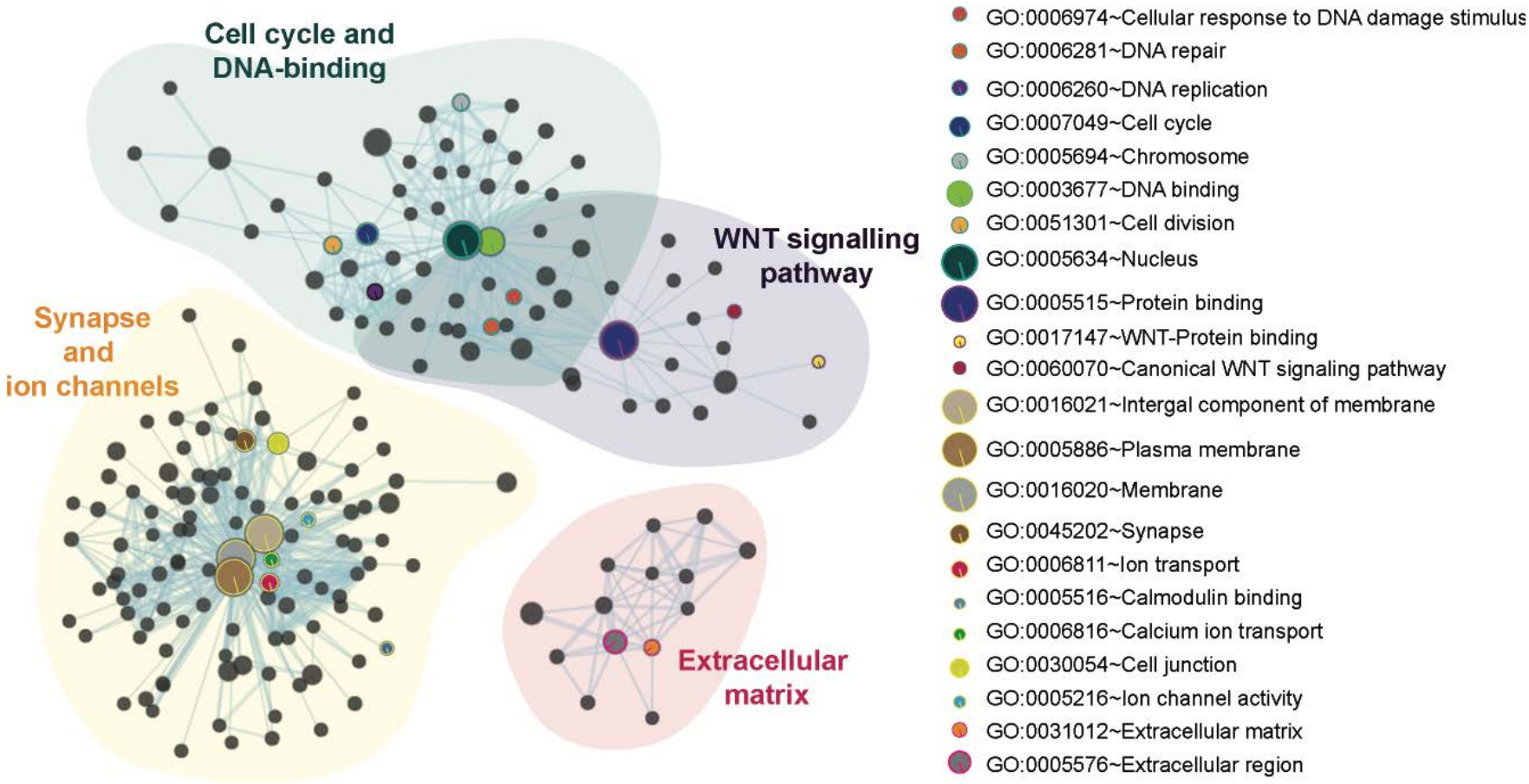


**Figure R.3. Functional enrichment map of the differentially expressed genes in radial glia cells between E11.5 and E15.5.** Functional interaction map for GO categories enriched in the genes differentially expressed in radial glial cells (E15.5 *vs* E11.5; log2 FC ≤ -1 or log2 FC ≥ +1; adj. *p*-value < 0.05). The functional analysis was performed in DAVID. Nodes represent categories and edges connect nodes sharing genes. Node size is proportional to the number of associated-genes and edge width to the number of genes shared between nodes.

damage response (GO~0006974) were down-regulated at E15.5 with respect to E11.5 (**Fig R.4b**). This is consistent with the fact that the replicative index of RGs decreases as neurogenesis progresses, mainly due to a progressive enlargement of the G1 phase of the cell cycle (Takahashi et al., 1995), and the need to safeguard genetic fidelity in RGs undergoing proliferative divisions for normal expansion of the neocortex (McKinnon, 2013).

Functional analysis of the down-regulated set of genes also revealed enrichment in ECM genes (**Fig R.3 and R.4a** and **Annex 1,** Table 3). However, genes included in this category (GO~0031012) do not undergo generalised down-regulation, but great portion of the differentially expressed ECM genes up-regulate at E15.5 (see violin plot in **Fig R.4b**), suggesting that some genes replace others between the stages analysed. Indeed, genes within this GO term are both among the 25 top down-regulated genes (*Col1a2* and *Col3a*1; **Annex 1**, Table 1) and the 25 top up-regulated ones (*Bcan* and *Adamstl3;* **Annex 1,** Table 2). Although the role of ECM in cortical neurogenesis is not well understood, some studies in the developing CNS indicated that it influences progenitor proliferation and differentiation (Long and Huttner, 2019). The difference in the expression of ECM genes here reported suggests that the composition of the ECM is key for the progression of the neurogenic program in the dorsal RGs.

The functional analysis of the **up-regulated genes** revealed a significant enrichment in functions associated to the main cluster “synapse and ion channels” (**Fig R.3** and **R.4c** and **Annex 1,** Table 4). Many of the up-regulated genes within this cluster encode calcium and potassium channels, such as *Kcnh3*, *Kcna1, Cacna1* and *Cacna1e;* and GABA and glutamate ionotropic receptor subunits, such as *Gabra1, Grin2b* and *Gria*. Violin plots of the distribution of genes according to the FC of all the expressed genes within the GOs Ion channel activity (GO~0005216), Calcium transport (GO~0006816), Calmodulin binding (GO~0005516) and Plasma membrane (GO~0005886) showed that these functions undergo extensive up-regulation; although they also include down-regulated genes at E15.5 (**Fig R.4d**). The temporal regulation of ion transport in RGs is consistent with previous studies showing that calcium-waves propagation through RGs and the bioelectrical membrane properties of these cells are relevant for the temporal progression of neurogenesis in the developing neocortex (Weissman et al., 2004; Vitali et al., 2018).

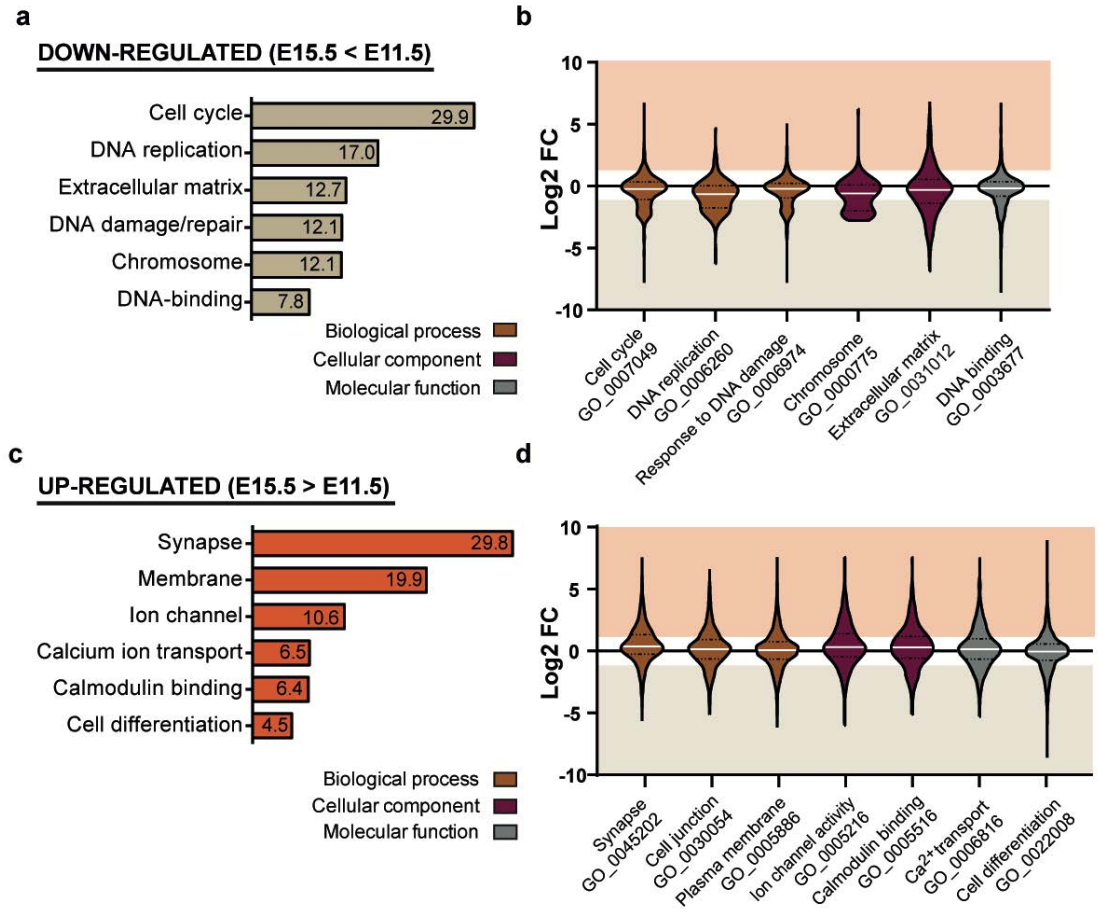


**Figure R.4. Functional enrichment analysis of the differentially expressed genes in radial glia cells between E11.5 and E15.5. (a, c)** Top 6 enriched functional clusters identified by DAVID of the down-regulated (a) and up-regulated (c) genes. Enrichment scores are indicated inside the bars. **(b, d)** Violin plots showing the log2 FC distribution of all differentially expressed genes within GO categories enriched in down-regulated (b) and up-regulated (d) genes. White solid line indicates the median and black dotted lines indicate the interquartile range. Colour indicates the type of GO category.

In addition, among the up-regulated genes at E15.5 we found a great amount of genes with well-established functions in neurons that are not expressed in neural progenitors, at least at the protein level. For instance, this is the case of genes encoding the postsynaptic scaffolding proteins SHANK1 and SHANK2, which function in glutamatergic synapses (Monteiro and Feng, 2017); the synaptosomal nerve-associated protein 25 (SNAP25) of the SNARE complex; and the calcium-binding synaptic vesicle proteins Synaptotagmin 1, 4 and 5, which are involved in neurotransmitter release (Adolfsen and Littleton, 2001). To provide further evidence that these neuronal genes are indeed expressed in RGs, we checked the expression changes of 3 of these genes (*Shank1*, *Snap25* and *Syt4*), together with 3 down-regulated genes (*Ccdn1*, *Col1a2* and *Col3a1*), by RT-qPCR in cells FACS-isolated from E11.5 and E15.5 wild-type embryos using an antibody against the stem cell apical marker Prominin-1 (**Fig R.5;** Weigmann et al., 1997;

Corti et al., 2007). This marker is expressed in ~80% of the *Pax6*-GFP+ cells isolated from the dorsal telencephalon of E15.5 embryos (**Fig R.5a,b**), indicating that the GFP+ cell samples used for the RNA-seq experiment were enriched in apical RG progenitors. In agreement, the log2 FCs of the genes tested in *Pax6*-GFP+ and Prominin-1+ cell samples showed a significant positive correlation (Pearson's correlation: r=0.99; p<0.0001; see **Fig R.5d**). This result confirmed the up-regulation of neuronal transcripts in the RGs along neurogenesis, implying that neuronal genes are already expressed in these progenitors. This is in accordance with recent studies describing that RGs express IP and neuronal genes that are necessarily not translated, a concept that is known as "transcriptional pre-patterning" (Albert and Huttner, 2018). Alternatively, some of the encoded proteins could have a function in non-neuron cells that is not known yet.

Next, we used the TRANSFAC/JASPAR databases in EnrichR to search for TF-binding motifs enriched in the promoter regions of the genes differentially expressed between E11.5 and E15.5. This analysis identified TEAD (TEA domain transcription factor) 2 and 4, TFAP2A (transcription factor AP-2 alpha), EGR1 (early growth response 1), SP1 (tans-acting transcription factor 1), RELA (RELA proto-oncogene, NF-kβ), PCBP1 (poly(rC) binding protein 1), MZF1 (myeloid zinc finger 1), E2F6 (E2F transcription factor 6) and ZBTB7A (zinc finger and BTB domain containing 7a) as key TFs for gene expression regulation in RGs (**Fig R.6a**). Protein interaction analysis revealed that, with the exception of E2F6, all these TFs are part of a highly interconnected network (**Fig R.6b**). Indeed, the expression of five of the interconnected genes, *Tfap2a*, *Egr1*, *Tead2, Tead4* and *Yap1*, was significantly lower in RGs at E15.5 than at E11.5 (table in **Fig R.6c**).

TEAD factors lack intrinsic transactivation activity and their activity depends on the nuclear availability of transcriptional coactivators YAP1 (also named YAP) and TAZ (Vassilev et al., 2001). In turn, YAP/TAZ location into the nucleus depends both on the phosphorylation by the Hippo pathway kinases LAST1/2 and on mechanical cues, including forces generated by cytoskeleton contractility, ECM rigidity and other fluid flows (Totaro et al., 2018). The Hippo signalling pathway regulates cell proliferation and survival (Varelas, 2014) and there is evidence that YAP/TAZ activity in neural progenitors maintains proliferation and inhibits differentiation (Cao et al., 2008; Lavado et al., 2013; Han et al., 2015). Our RNA-seq data supports that YAP-TEAD activity is higher during the proliferative phase (E11.5; **Fig R.6**) coinciding with increased gene expression of several ECM components (**Fig R.4a,b**). Moreover, functional analysis of the down-regulated genes using the KEGG database showed a significant enrichment in genes involved in "ECM-receptor interaction" (mmu04512; FDR = 1.28E-09) and in the "Hippo

signalling pathway" (mmu04390; FDR = 6,22E-08). In summary, these data are in agreement with previous studies indicating that YAP/TAZ transcriptional activity promotes self-renewal proliferative divisions in RGs and supports that both ECM components and Hippo signalling pathway participate in the regulation of this activity.

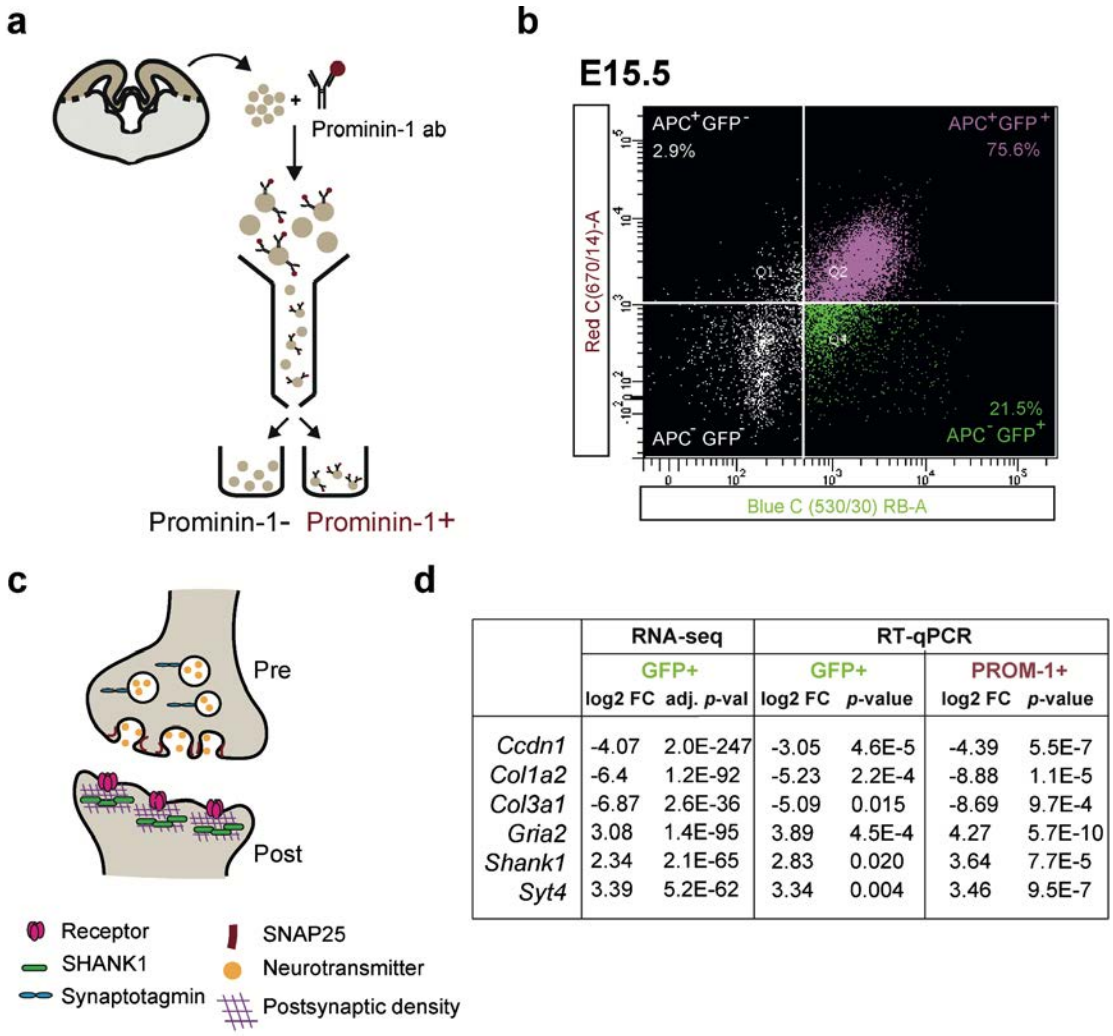


d

| | RNA-seq | | RT-qPCR | | | |
|---|---|---|---|---|---|---|
| | GFP+ | | GFP+ | | PROM-1+ | |
| | log2 FC | adj. *p*-val | log2 FC | *p*-value | log2 FC | *p*-value |
| *Ccdn1* | -4.07 | 2.0E-247 | -3.05 | 4.6E-5 | -4.39 | 5.5E-7 |
| *Col1a2* | -6.4 | 1.2E-92 | -5.23 | 2.2E-4 | -8.88 | 1.1E-5 |
| *Col3a1* | -6.87 | 2.6E-36 | -5.09 | 0.015 | -8.69 | 9.7E-4 |
| *Gria2* | 3.08 | 1.4E-95 | 3.89 | 4.5E-4 | 4.27 | 5.7E-10 |
| *Shank1* | 2.34 | 2.1E-65 | 2.83 | 0.020 | 3.64 | 7.7E-5 |
| *Syt4* | 3.39 | 5.2E-62 | 3.34 | 0.004 | 3.46 | 9.5E-7 |

**Figure R.5. Gene expression changes in Prominin-1 progenitors between E11.5 and E15.5.** **(a)** Scheme of the isolation of Prominin-1+ apical progenitors from E11.5 or E15.5 mouse dorsal telencephalons by FACS using an APC-conjugated anti-Prominin-1 antibody. **(b)** FACS plot showing the intensities of GFP and APC fluorescences in logarithmic scales of E15.5 *Pax6*-GFP+ cells incubated with APC-conjugated anti-Prominin-1 antibody. White lines represent the threshold established with control cells (*Pax6*-GFP- cells incubated with APC-conjugated IgGs). The percentage of positive and negative GFP and APC cells are indicated. **(c)** Scheme of a mature synapse showing the expression of SHANK, SNAP25 and Synaptotagmin proteins in the pre- and post-synaptic components. (**d**) Table comparing the log2 fold-changes (FC) of the indicated genes in FACS isolated *Pax6*-GFP+ (GFP+) and Prominin-1+ (PROM-1+) cells at E15.5 relative to E11.5. Gene expression changes were assessed by RNA-seq or RT-qPCR. RT-qPCRs were performed in triplicates using the same set of primers in both cell preparations. Log2 FC values correspond to the mean (S.E.M). *Pax6*-GFP+, n=3 samples each stage; Prominin-1+, n=1 sample each stage.

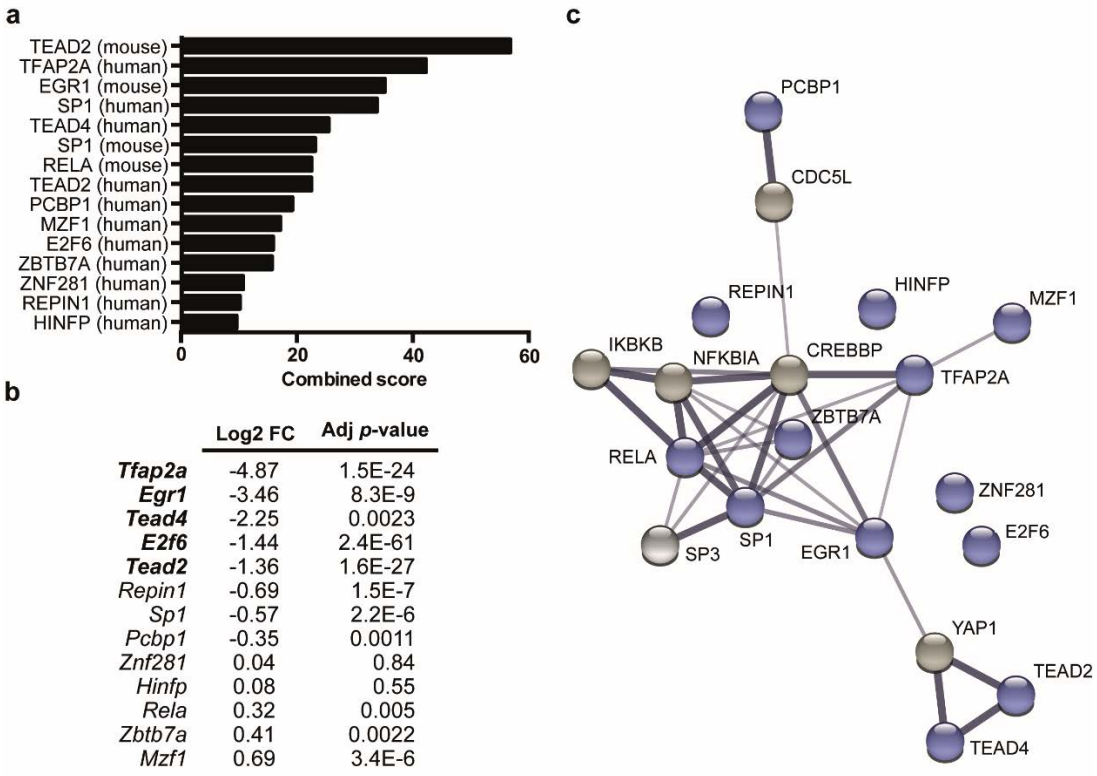


b

| | Log2 FC | Adj *p*-value |
|---|---|---|
| ***Tfap2a*** | -4.87 | 1.5E-24 |
| ***Egr1*** | -3.46 | 8.3E-9 |
| ***Tead4*** | -2.25 | 0.0023 |
| ***E2f6*** | -1.44 | 2.4E-61 |
| ***Tead2*** | -1.36 | 1.6E-27 |
| *Repin1* | -0.69 | 1.5E-7 |
| *Sp1* | -0.57 | 2.2E-6 |
| *Pcbp1* | -0.35 | 0.0011 |
| *Znf281* | 0.04 | 0.84 |
| *Hinfp* | 0.08 | 0.55 |
| *Rela* | 0.32 | 0.005 |
| *Zbtb7a* | 0.41 | 0.0022 |
| *Mzf1* | 0.69 | 3.4E-6 |

**Figure R.6. Enrichment analysis of transcription factor binding-motifs in the differentially expressed genes between E11.5 and E15.5 in radial glia cells. (a,b)** Top 15 transcription factor (TF) with binding motifs enriched in the promoter of the differentially expressed genes (log2 FC ≤ -1 or log2 FC ≥ +1; adj. *p*-value < 0.05) according to TRANSFAC/JASPAR analysis (a) and log2 FC and adj. *p*-values in the RNA-seq experiment (b). TFs binding motifs are shown according to their combined enrichment scores. Differentially expressed TFs are in bold. **(c)** Protein interaction network for the TFs determined using the STRING interaction tool. Blue balls represent input TFs and grey balls inferred TFs. Strength of the edges is proportional to the confidence of the interaction.

### 1.1.2. miRNAs

miRNAs have an important role regulating gene expression during cortical development (Barca-Mayo and De Pietri Tonelli, 2014). To provide some evidence of miRNAs contribution to the temporal gene expression changes that we have identified in mouse embryo RGs, we have performed a second RNA-seq experiment to detect the expression of miRNAs in the same RG samples that we used for the first experiment (*Pax6*-GFP+ RGs FACS-sorted from the dorsal telencephalon of E11.5 and E15.5 embryos). RNA-seq in this experiment was performed using 3 pools of E11.5 cells and 2 pools of E15.5 cells. Principal component analysis and heat map representation of the 1,262 short transcripts detected in these samples showed that they clustered by developmental stage (**Fig R.7a,b**). We mapped 722 of these short transcripts to miRNA genes (*mirs*). Due to the low number of biological replicates included in this experiment,

we considered differences in expression significant when the FC was equal or greater than 2.8 (log2 FC ≥ +1.5 or log2 FC ≤ -1.5) and the adj. *p*-value < 0.01. As shown in **Fig R.7c,d**, the levels of 16.5% of the expressed miRNA genes changed between E11.5 and E15.5 in the RGs.

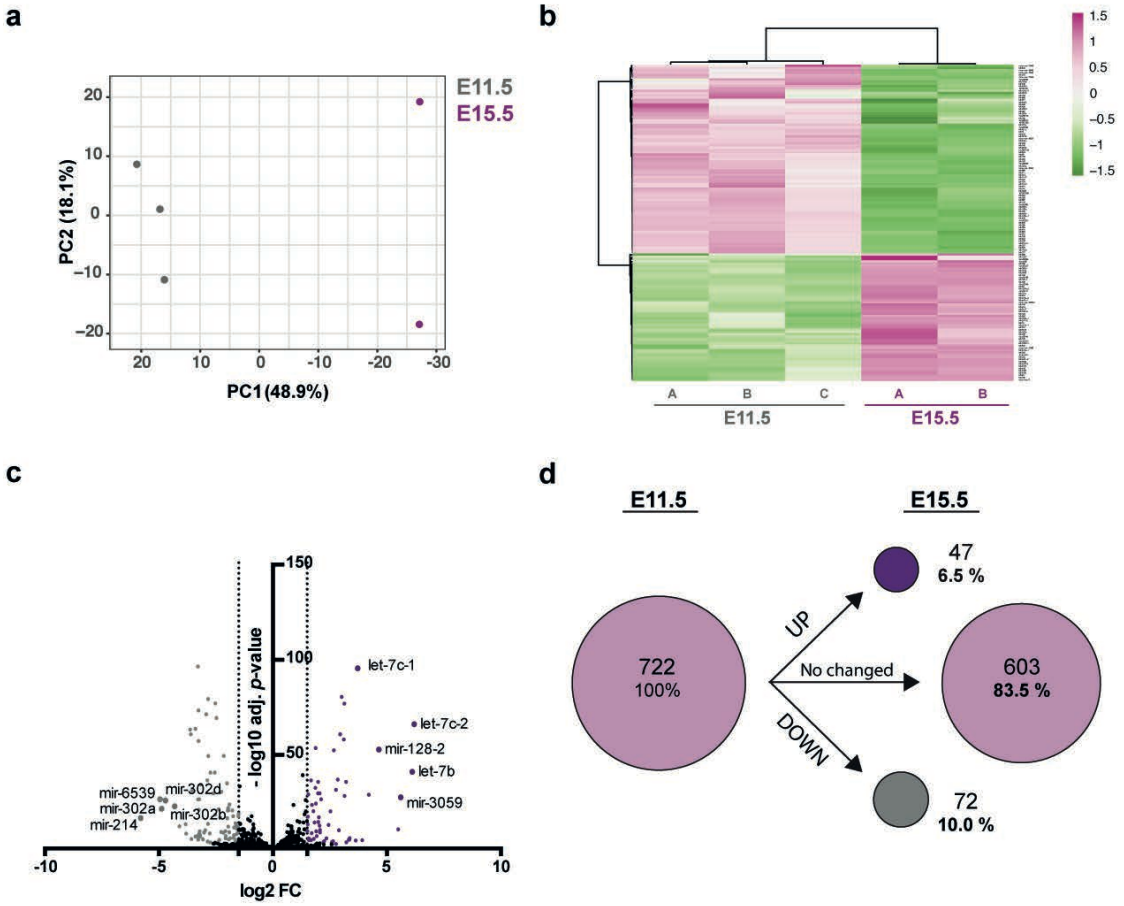


**Figure R.7. Differentially expressed microRNAs in radial glia cells between E11.5 and E115.5. (a)** Principal component (PC) analysis of the small RNAs detected by RNA-seq in E11.5 and E15.5 radial glia cells. Notice that the relative variance among replicates from the same stage (PC2) is smaller than the relative variance between stages (PC1). **(b)** Heatmap showing the relative expression of the differentially expressed small RNAs (log2 FC ≤ -1.5 or log2 FC ≥ +1.5; adj. *p*-value < 0.01) in the sequenced samples. **(c)** Volcano plot showing the expression changes between E15.5 and E11.5. Genes are distributed according to their log2 FC (x-axis) and adj. *p*-values in -log10 (y-axis). Dashed lines indicate log2 FC=1.5 and log2 FC =-1.5. Dots on the right (purple) and on the left (grey) of these lines indicate up-regulated and down-regulated small RNAs respectively. Black dots are RNAs with no significant changes in expression. The 5 most up- and down-regulated *mirs* (microRNA genes) are labelled. **(d)** Representation of the up- and down-regulated miRNA genes between E11.5 and E15.5. The total number of genes detected at E11.5 is indicated in the circle on the left. The number and percentage of genes with significant changes in expression (purple circle for up-regulated genes and grey circle for down-regulated genes) and with not significant changes (light purple circle in the right) at E15.5 are indicated. The area of the circles is proportional to the number of miRNA genes.

To validate the RNA-seq data we selected a set of 8 miRNAs (5 up-regulated, 1 down-regulated and 2 with not significant changes in expression) and performed RT-qPCRs with RNA obtained from E11.5 and E15.5 *Pax6*-GFP+ cells. The results showed a strong positive correlation between RNA-seq and RT-qPCR assays (Pearson's correlation, r=0.99; p<0.0001; see **Fig R.8**). The expression of 3 of these miRNAs, miR-204-3p, let-7b-5p and let-7d-5p, was also assessed by RT-qPCR using RNA obtained from E11.5 and E15.5 Prominin-1+ cells. Log2 FC values for these miRNAs in the Prominin-1+ samples (miR-204-3p, -6.61 ± 0.14; let-7b-5p, 4.07 ± 0.03; let-7d-5p, 3.29 ± 0.05) were in line with those obtained in the *Pax6*-GFP samples.

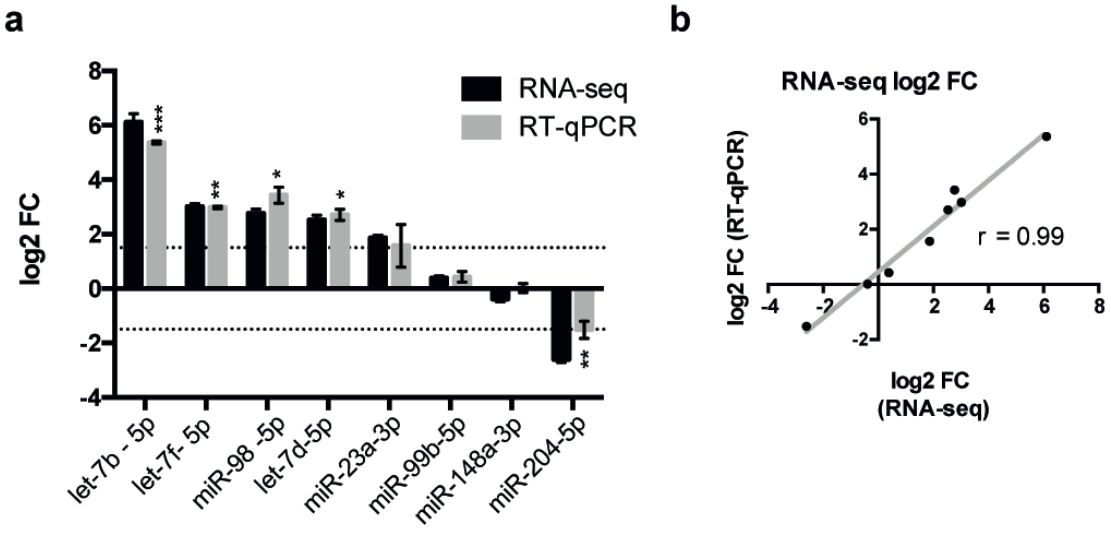


**Figure R.8. Validation of small RNA-seq data by RT-qPCR. (a)** RT-qPCR values were normalized to *Sno135* expression. Log2 FC values correspond to the mean (S.E.M.). Dashed lines indicate log2 FC = 1.5 and log2 FC = -1.5. Values above and bellow these lines are considered significantly different. n= 3 samples each stage. Asterisks above the grey bars (RT-qPCR data) indicate the statistical significance. *p<0.05, **p<0.01, ***p<0.001. Student's t test**. (b)** Correlation analysis of the log2 FC values obtained by RNA-seq and RT-qPCR. Each dot corresponds to one of the 8 genes shown in panel a. Pearson's correlation, r=0.99; p<0.0001.

Among the top 12 down-regulated miRNAs genes we found 4 of the 5 members of the *mir*-302/367 cluster (*mir-302a*, *mir-302b*, *mir-302d* and *mir-367*; **Annex 2**, Table 1), which are known to regulate self-renewal in pluripotent stem cells and NSCs (Wang et al., 2013; Yang et al., 2015). On the other hand, 10 of the 12 let-7 locus in mouse are up-regulated and 5 of them (*let-7c-2*, *let-7b*, *let-7c-1*, *let-7a-2* and *let-7f-2*) have log2 FC values greater than 3**.** Consistently, genes for miRNAs that clustered with some of these up-regulated let-7 (*mir-100*, *mir-99a* and *mir-98*) were also up-regulated at E15.5 (see **Annex 2,** Table 2). Let-7 miRNAs have an essential role in normal development and

there is evidence that they promote differentiation of NSCs (Rehfeld et al., 2015). The RBP LIN28 controls let-7 expression by blocking the biogenesis of these miRNAs; in turn, let-7 miRNAs repress LIN28 expression by binding to the UTR's of *Lin28a* and *Lin28b* genes (Newman et al., 2008; Rybak et al., 2008). This regulatory feedback loop is evolutionarily conserved and controls the balance between proliferation and differentiation during development (Rehfeld et al., 2015). In agreement with this, the expression of both *Lin28a* and *Lin28b* genes is significantly lower at E15.5 than at E11.5 (**Fig. R.1c** and data not shown). The coordinated up-regulation of let-7 miRNAs in E15.5 RG undergoing differentiative divisions and the concomitant down-regulation of *Lin28* genes in these cells are in line with published studies and supports that LIN28/let-7 axis has an important role modulating gene expression in RGs during neurogenesis.

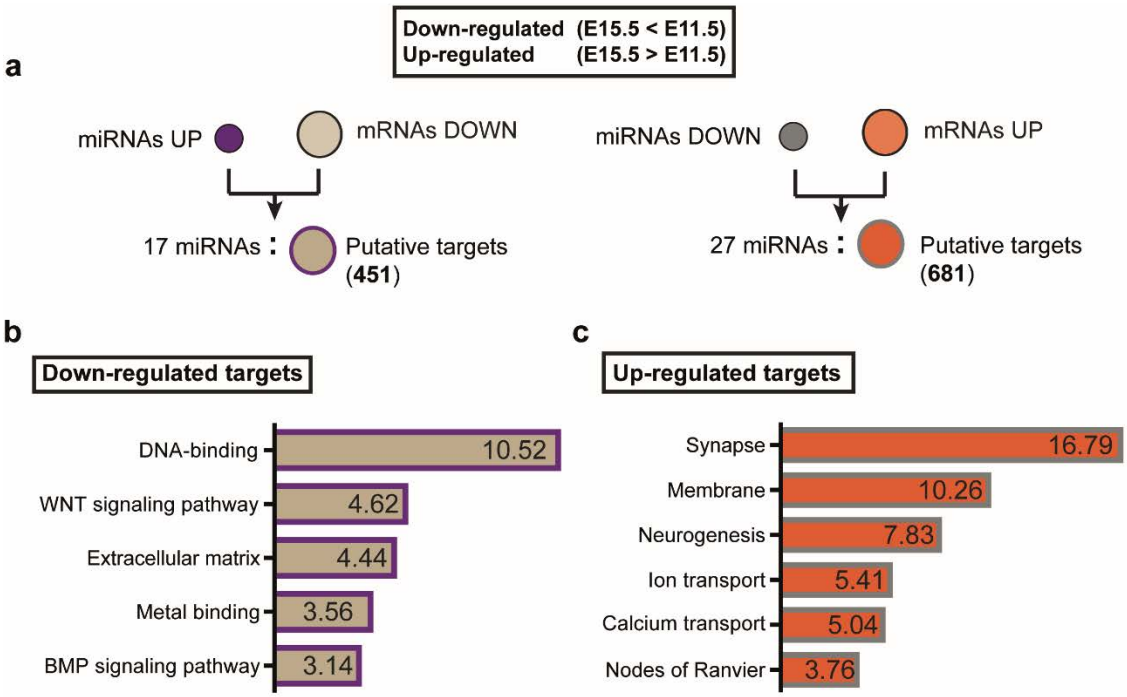


**Figure R.9. Functional enrichment analysis of microRNA targets. (a)** Summary of the integrated miRNA-mRNA analysis indicating the number of miRNAs and mRNAs used in the analysis and the number of predicted down-regulated (left) and up-regulated (right) targets. **(b, c)** Top enriched functional clusters identified by DAVID analysis of the down-regulated (b) and up-regulated (c) predicted targets. Enrichment scores are indicated inside the bars.

Next, we performed an integrated analysis of the mRNAs and miRNAs that showed expression changes during development using bioinformatics tools (Agarwal et al., 2015). mRNA degradation is the predominant mechanism by which miRNAs mediate repression of gene expression regulation (66-90% miRNA-mediated effects; Guo et al., 2010a; Eichhorn et al., 2014). Therefore, the strategy followed to uncover miRNA-mRNA

pairs assumes that expression of miRNAs and their targets is often negatively correlated (see **Fig R.9a**). This analysis revealed 2,204 possible miRNA-mRNA interactions involving 44 miRNAs and 1,032 predicted targets. The total number of predicted targets represent 6.9% of the coding genes that are expressed in RGs and 27.8% of the genes that were differentially expressed between E15.5 and E11.5 (see **Fig R.1d**).

DAVID analysis of the down-regulated targets revealed a very significant enrichment in DNA-binding and metal ion-binding genes, and ECM genes, and WNT and BMP signalling. (**Fig R.9b**; see **Annex 2,** Table 3).

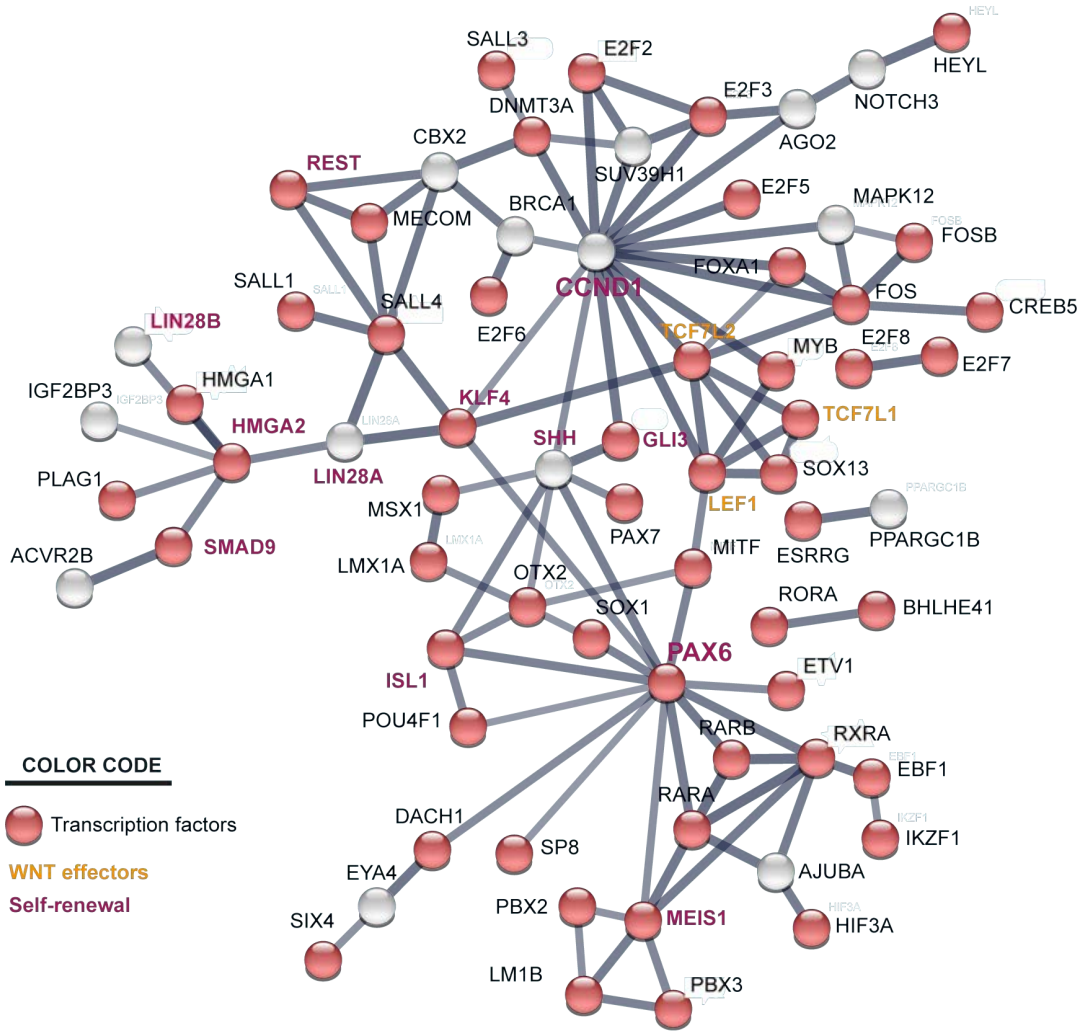


**Figure R.10. Protein-protein interaction network of predicted microRNA targets within the DNA-binding cluster**. Representation of the protein-protein interaction network for the genes within the DNA-binding cluster that are putative targets of microRNAs up-regulated at E15.5 compared to E11.5 (Fig R.9b). Network was determined using the STRING interaction tool. Red nodes correspond to transcription factors. WNT signalling pathway effectors are indicated in orange and proteins involved in neural stem self-renewal in pink. Strength of the edge is proportional to the confidence of the interaction.

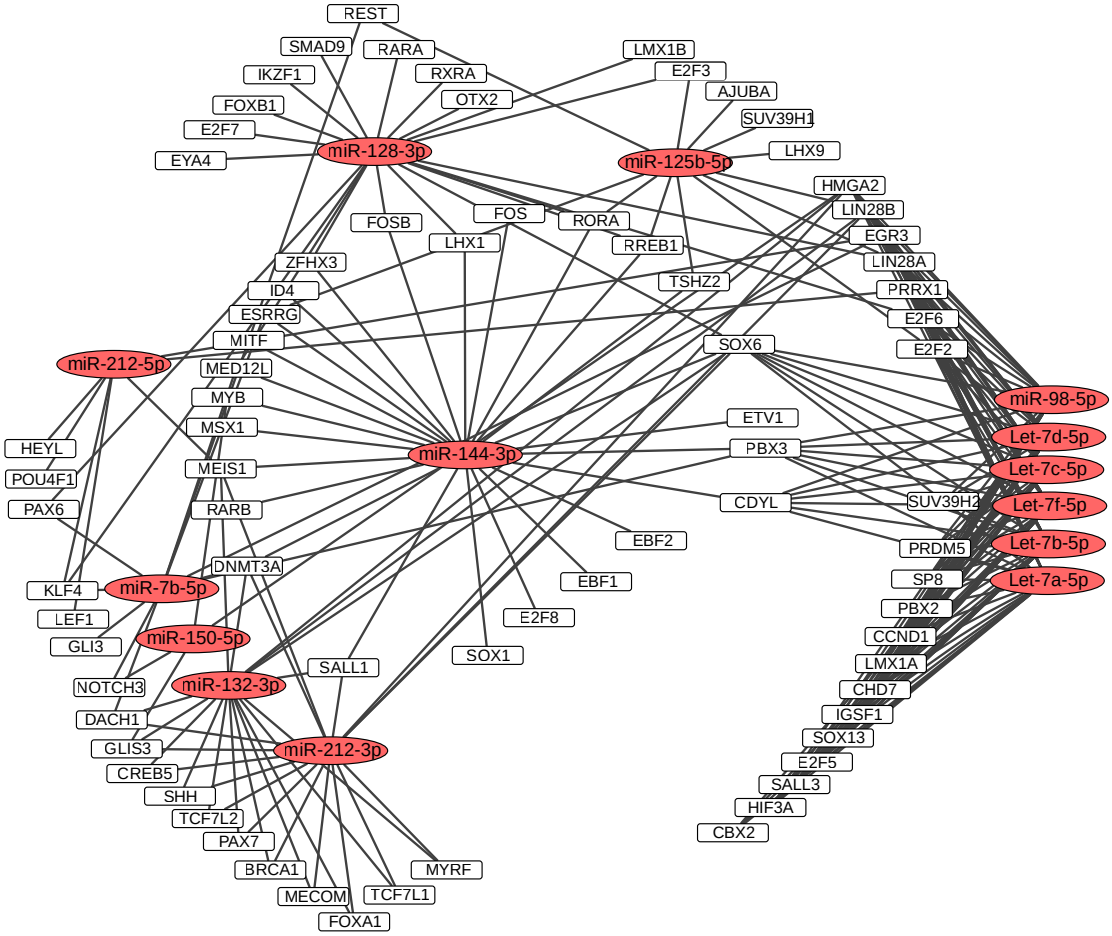


**Figure R.11. microRNA-mRNA network of down-regulated DNA-binding targets between E11.5 and E15.5.** Representation of the microRNA up-regulated at E15.5 compared to E11.5 and their predicted targets within the "DNA-binding cluster" (Fig R.9b). microRNAs are highlighted with red frames. The network was illustrated by Cytoscape.

Protein-protein interaction network of the coding genes within the "DNA-binding" cluster revealed a highly connected transcriptional network enriched in pluripotency pathways (*p*-value=9E-9; **Fig R.10**) Most of the genes in the network encode TFs. PAX6 is the most connected TF within the network. The expression of this TF is tightly regulated in the RGs of the dorsal telencephalon where it plays a critical role balancing self-renewal and neurogenesis (Manuel et al., 2015). Other TFs within the network, such as the PAX6 target HMGA2 and KLF4, promote RG self-renewal (Sansom et al., 2009; Moon et al., 2018). The protein Cyclin D1 (*Ccnd1*), which influences the fate of RG daughter cells by regulating the length of the cell cycle G1 phase (Lange et al., 2009; Najas et al., 2015), is the most connected hub of the network. The miRNAs that target network hubs are miRNAs of the let-7 family, miR-212-5p, miR-128-3p, miR-144-3p and the cluster miR-212/132. Interestingly, the RBPs LIN28A/B and the WNT effectors TCF7L2, TCF7L1 and LEF1 are also predicted targets of these miRNAs (**Fig R.11**). A few of these miRNA-

mRNA interactions have been shown to regulate RG behaviour *in vivo*. This is for instance the case of Cyclin D1 (Zhao et al., 2010) and LIN28A/B (Rybak et al., 2008) regulation by let-7 miRNAs.

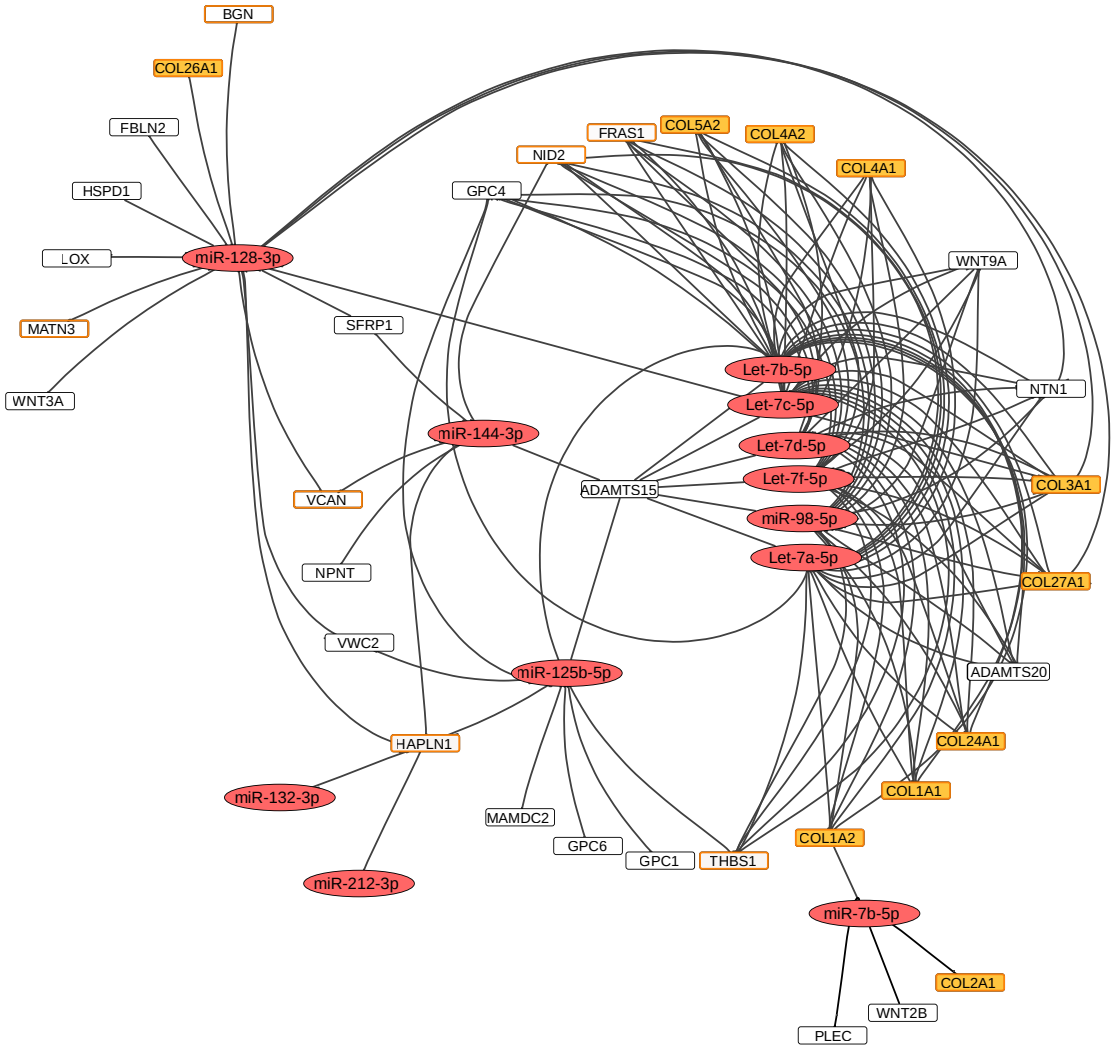


**Figure R.12. microRNA-mRNA network of down-regulated extracellular matrix targets between E11.5 and E15.5.** Representation of the microRNAs up-regulated at E15.5 compared to E11.5 and their predicted targets within the "Extracellular matrix" (ECM) cluster (Fig R.9b). microRNAs are highlighted with red frames. ECM-structural components are indicated with an orange frame and collagens with a filled orange boxes. The network was illustrated by Cytoscape.

The predicted targets of miRNAs within the "ECM" cluster are abundant in collagens and other structural components of the ECM like BGN (Biglican), FRAS1 (Fraser extracellular matrix complex subunit 1), MATN3 (Matrilin 3), NID2 (nidogen 2), THBS1 (Thrombospondin 1) and VCAN (Versican); also comprise ADAMTS15 and ADAMTS20, 2 proteins of the ADAMTS (A Desintegrin and Metalloproteinase with Thrombosponding motifs) family that mediate proteolytic degradation of other ECM components; and, 3

WNT proteins and SFRP1 (secreted Frizzle related protein 1), which is a soluble modulator of WNT signalling. ECM components bind morphogens such as WNTs, facilitating their storage and presentation to their ligands (Faissner and Reinhard, 2015). Representation of the miRNA-ECM network (**Fig R.12**) revealed that the miRNAs that have more connections are members of the let-7 family and miR-128-3p. Nine of the 10 collagen genes of the network are targeted by let-7 miRNAs. Regulation of collagen expression by these miRNAs in RGs has not been reported, but previous studies in other cellular contexts have shown that collagen transcripts are indeed bona-fide targets of several let-7 miRNAs (Witman et al., 2013; Su et al., 2014; Liu et al., 2016; Bi et al., 2017).

The miRNAs in the ECM network and in the DNA-binding network are the same with the exception of miR-150p, which is present only in the DNA-binding network. In both networks, the more connected miRNAs are the clusters let-7c/let-7b, let-7f/miR-98 and let-7d/let7a, miR-128-3p and miR-144-3p (compare networks in **Fig R.11** and **Fig. R.12**). Together, these results indicate that the up-regulation of a small set of miRNAs modulates the expression of a complex gene network that coordinate the self-renewal of the RGs with the ECM.

Functional analysis of the target genes of the down-regulated miRNAs showed a significant enrichment in “synapse” and “neurogenesis”. These two DAVID clusters were also the two top ones when all the up-regulated genes were considered (compare **Fig R.4c** with **Fig R.9c**). The following enriched clusters in the sub-set of miRNA targets were “ion/calcium transport” and “nodes of Ranvier” (**Fig R.9c**; **Annex 2,** Table 4). Representation of the miRNA-mRNA interaction network of the up-regulated “synapse” genes revealed a highly interconnected network that involved 24 miRNAs down-regulated during neurogenesis (**Fig R.13**). These 24 miRNAs target almost half of the total up-regulated genes annotated in the GO term synapse (GO:0045202). Moreover, 72% of the targets are putatively regulated by 2 or more miRNAs, and 38% by 3 or more miRNAs. The most connected miRNAs in the network were miR-449c and miR-449b, within the *mir*-449 cluster; miR-302a, miR-302b, miR-302d and miR-367, within the *mir*-302/367 cluster; and miR-448. As mentioned before, *mir*-302/367 promotes self-renewal divisions (Wang et al., 2013; Yang et al., 2015); the cluster *mir*-449 controls proper mitotic spindle orientation in the RGs (Fededa et al., 2016). The role of miR-448 has not been assessed in the developing CNS. Some of the predicted target genes are ion channels or neurotransmitter receptors. As already mentioned, some of these genes may contribute to maintain the electrical membrane potential of RGs, and therefore

neurogenesis. In addition, we also found miRNA targets that encode synapse proteins. These include the presynaptic proteins SNAP25, SYT 1/4/5 and SVOP (synaptic vesicle 2-related protein), and the postsynaptic proteins SHANK2 and NLGN1 (Neuroligin 1) (See **Fig R.12**). These data suggest that miRNAs could participate in the translational silencing of synapse-related genes.

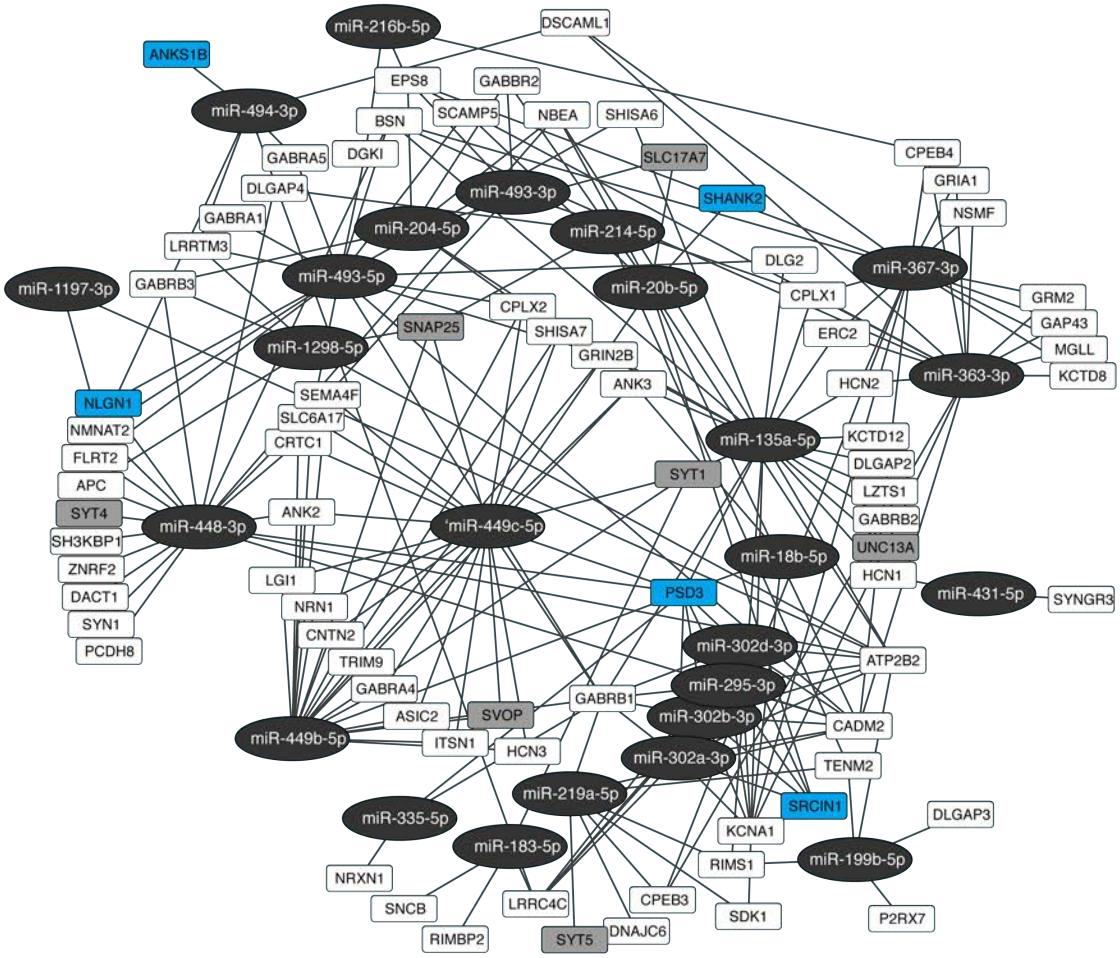


**Figure R.13. microRNA-mRNA network of up-regulated synapse targets between E11.5 and E15.5.** Representation of the microRNAs down-regulated at E15.5 compared to E11.5 and their predicted targets within the "Synapse" cluster (Fig R.9c). microRNAs are in black boxes and their targets within rectangles. Genes involved in the recycling of synaptic vesicles are in grey rectangles and genes expressed in the postsynaptic component in blue rectangles.

Down-regulated miRNAs also show highly overlapping targets related to neurogenesis (see representation of the network in **Fig R.14**). miRNAs that presented higher number of targets were again members of the *mir*-302/367 and *mir*-449 clusters. Among the putative targets we found the genes coding for the transcriptional regulators NEUROD1, SOX11 and MEF2C, which have important roles in the generation and/or specification of cortical excitatory neurons (Bergsland et al., 2006; Hevner et al., 2006; Li et al., 2008).

Together, these results suggest that regulation by miRNAs of the let-7 family, *mir*-302/367 and *mir*-449 clusters is important to maintain a balance between RG self-renewal and differentiation along the neurogenic period of cortical development.

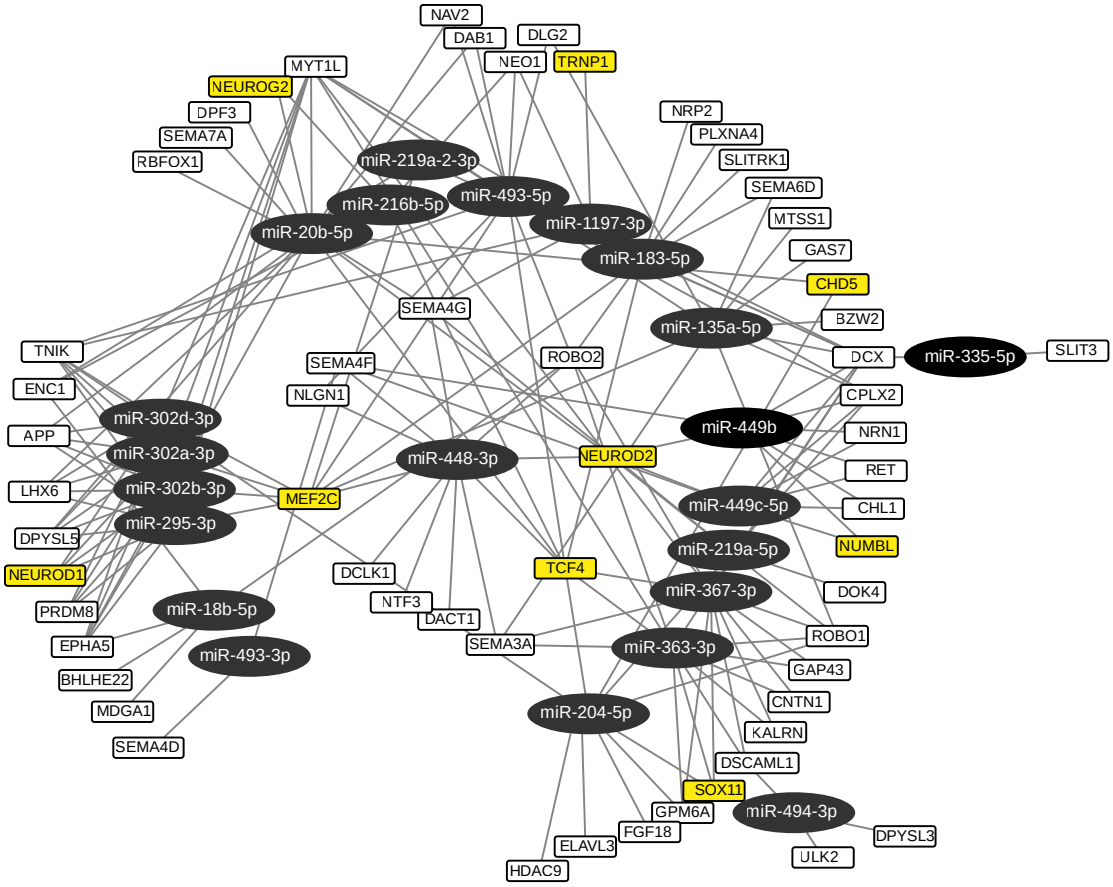


**Figure R.14. microRNA-mRNA network of up-regulated pro-neuronal targets between E11.5 and E15.5.** Representation of the microRNAs down-regulated at E15.5 compared to E11.5 and their predicted targets within the "Neurogenesis" cluster (Fig R.9c). microRNAs are in black boxes and their targets within rectangles. Yellow rectangles indicate genes with known roles in the generation and/or specification of cortical projection neurons.

## 1.2. Expression of collagens

The RNA-seq data indicated that the expression of several collagen genes decreases significantly in RGs as neurogenesis proceeds and that miRNAs of the let-7 family might contribute to this decrease. To provide evidence that these ECM proteins are indeed developmentally regulated in the mouse developing telencephalon, we first performed immunostainings against two of the most down-regulated collagens according to the RNA-seq, collagen type I and collagen type III (see **Annex 1**, Table 1) in sections of

E11.5, E13.5 and E15.5 embryos. Collagens are molecules composed by 3 polypeptide $\alpha$ chains that form a triple-helical structure. Collagen type I is an heterotrimer formed by 2 COL1A2 chains and 1 COL1A1 chain; while collagen type III is an homotrimer formed by 3 COL3A1 chains (Ricard-Blum, 2011). Both of these collagens are fibril-forming and are synthesized as protocollagen molecules that are submitted to numerous posttranslational modifications until they are deposited in the ECM and form supramolecular assemblies. In the developing cerebral cortex, collagens are deposited in the basal lamina presumably by RGs and they also accumulate in the meninges, where they are deposited by meningeal fibroblasts (Luo et al., 2011; Siegenthaler and Pleasure, 2011). In E11.5 embryos, collagen type I (COL1A1 and COL1A2) and COL3A1 immunofluorescences were high and restricted to the basal lamina and meninges. The staining pattern was maintained until E15.5 but collagen type I and COL3A1 fluorescence intensities in the basal lamina were significantly lower at E13.5 compared to E11.5 and almost undetectable at E15.5 **(Figs R.15** and **R.16)**. A significant decrease in their fluorescence intensity was also detected in the meninges of E15.5 brains. This reduction in collagen type I and III accumulation along neurogenesis correlates with the decreased expression of *Col1a1*, *Col1a2* and *Col3a1* genes detected by RNA-seq and by RT-qPCRs between E11.5 and E15.5 in the RGs (**Fig. R.2** and **R.5c**; **Annex 1**, Table 1; and data not shown).

Next, we compared the expression of 4 of the up-regulated let-7 and their predicted targets *Col1a1*, *Col1a2* and *Col3a1* in E11.5, E13.5 and E15.5 dorsal *Pax6*-GFP+ progenitors. The expression of let-7b-5p and let-7f-5p progressively increased from E11.5 to E15.5, whereas the expression of let-7d-5p and miR-98-5p reached maximum levels already at E13.5 (**Fig. R.17a**). Relative expression levels of the three collagen genes were higher at E13.5 than at E11.5 but they dropped significantly at E15.5 (**Fig. R.17b**). This drop is consistent with the low levels of collagen type I and III detected in the basal lamina of E15.5 embryos (**Figs R.15** and **R.16**).

These data support the idea that the composition of the ECM in structural collagens changes along the neurogenic phase of cortical development and suggest that repression of collagen genes in RGs by let-7 miRNAs contributes to these changes.

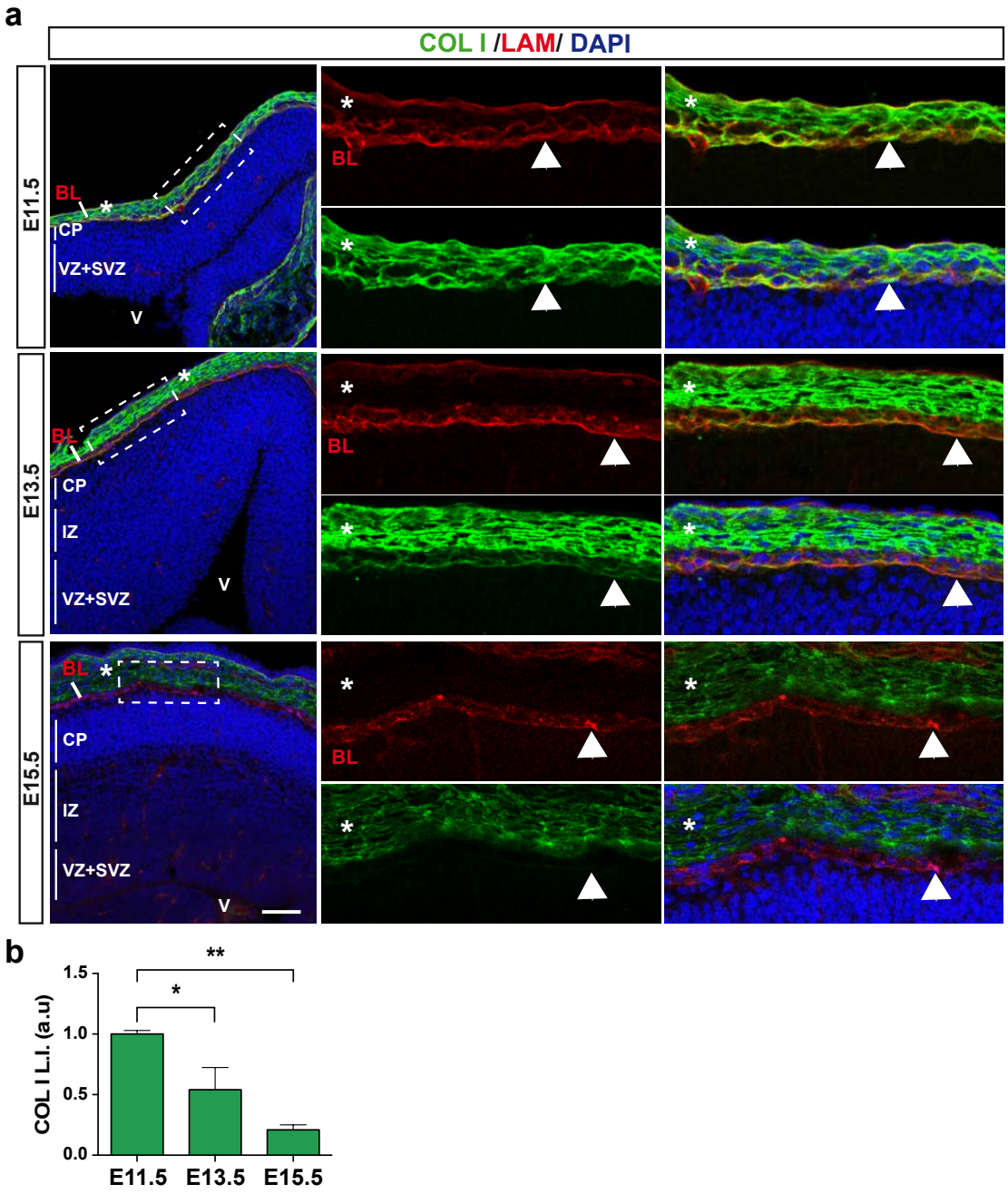


**Figure R.15. Expression of collagen I in the mouse dorsal telencephalon. (a)** Representative sections of the dorsal telencephalon from E11.5, E13.5 and E15.5 embryos immunostained against collagen type I (COL I; COL1A1 and COL1A2) and laminin. The nuclei are stained with DAPI. The dashed squares are magnified in the right panels. Laminin immunostaining defines the basal lamina (BL, pointed with arrowheads in the magnifications). Asterisks indicate the meninges. CP, cortical plate; IZ, intermediate zone; SVZ, subventricular zone; V, ventricle; VZ, ventricular zone. **(b)** Quantification of COL I labelling index (L.I.) in the BL at the indicated stages. Values correspond to the mean (S.E.M) and are expressed relative to E11.5 values that were arbitrary set as 1. n = 3 animals each stage. *p < 0.05, **p < 0.01, Student's t test. Scale bar: 100 µm.

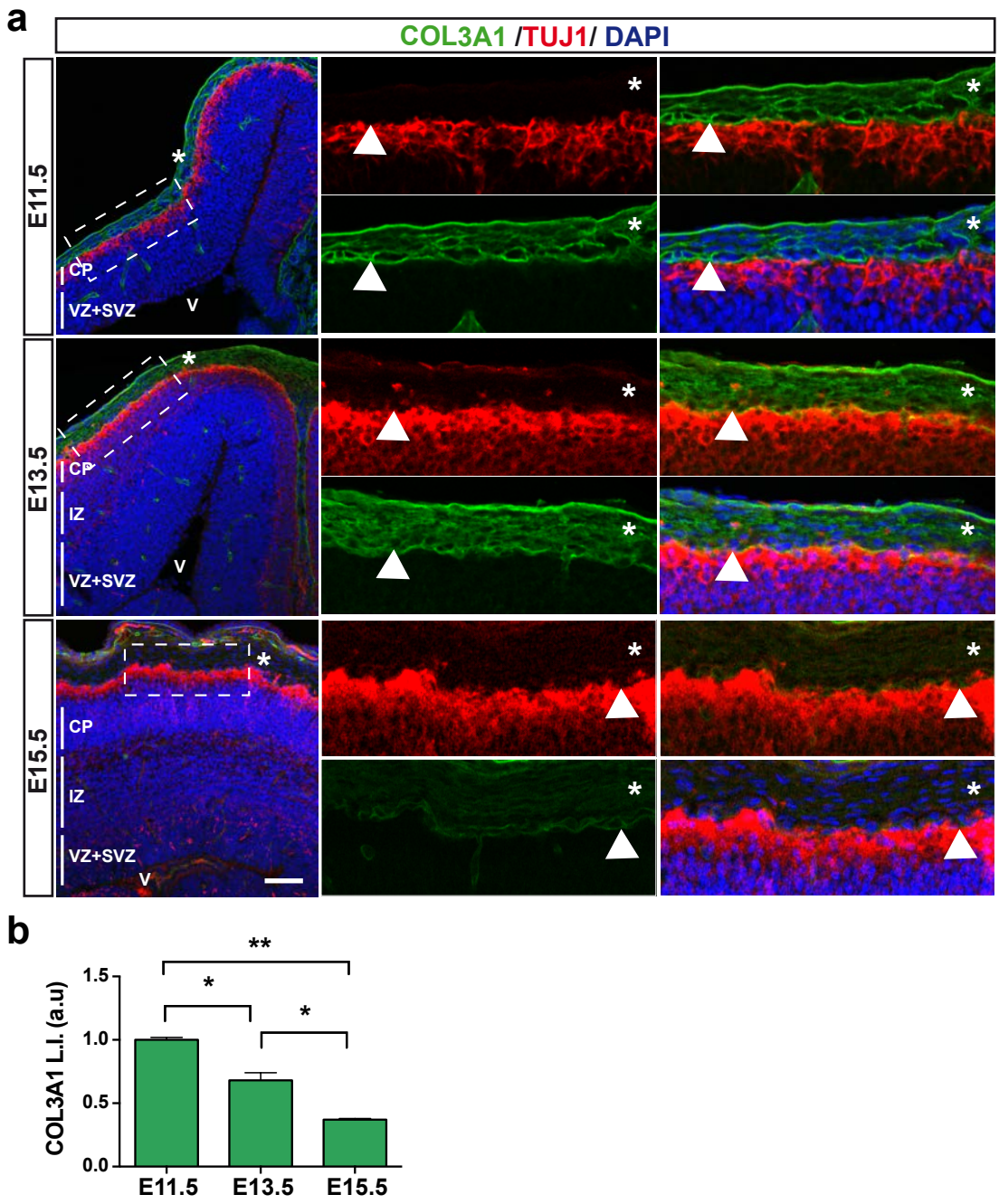


**Figure R.16. Expression of collagen III in the mouse dorsal telencephalon. (a)** Representative sections of the dorsal telencephalon from the indicated embryonic stages immunostained against collagen type III (COL3A1) and TUJ1. The nuclei are stained with DAPI. The dashed squares are magnified in the right panels. The basal lamina (BL, pointed with arrowheads in the magnifications) is located in the upper limit of TUJ1 immunostaining that defines the end of the cortical plate (CP in pictures on the left). Asterisks indicate the meninges. IZ, intermediate zone; SVZ, subventricular zone; V, ventricle; VZ, ventricular zone. **(b)** Quantification of COL3A1 labelling index (L.I.) in the BL at the indicated stages. Values correspond to the mean (S.E.M) and are expressed relative to E11.5 values that were arbitrary set as 1. n = 3 animals each stage. n = 3 animals each stage. *p < 0.05, **p < 0.01, Student's t test. Scale bar: 100 µm.

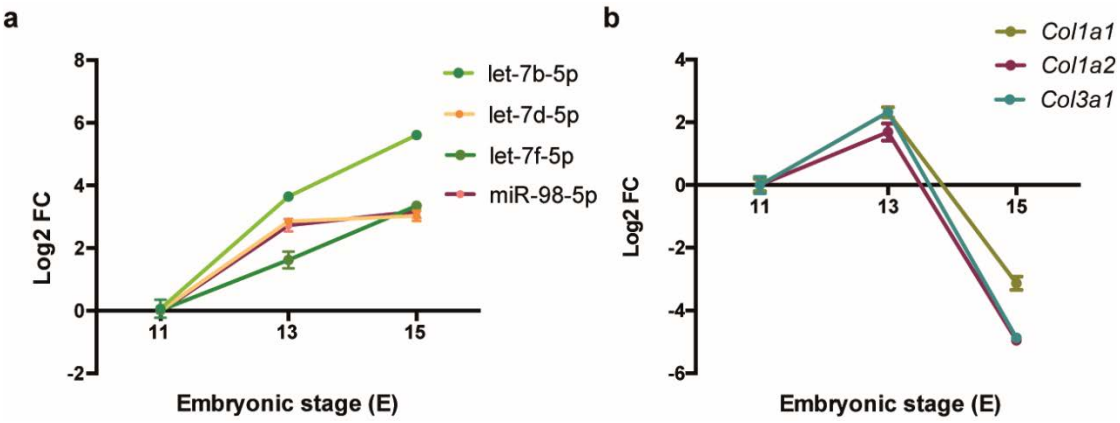


**Figure R.17. Expression of let-7 microRNAs and collagen genes in radial glia cells between E11.5 and E15.5. (a,b)** Expression of the indicated miRNA genes (a) and collagen genes (b) in *Pax6*-GFP cells isolated from the dorsal telencephalon of E11.5, E13.5 and E15.5 embryos. RT-qPCR values for mRNAs were normalized to *Rps23* and for miRNAs to *Sno135*. The graphs represent the expression changes at the indicated developmental stages relative to the expression at E11.5. Log2 FCs values correspond to the mean (S.E.M.). n = 2 samples each stage.

## 1.3. Alternatively spliced transcripts

AS events are controlled by multiple RBPs, the combined action of which creates a distribution of alternatively spliced products in a given cell type. Among the transcripts that we have detected by RNA-seq in E11.5 and E15.5 RGs, 434 encode RBPs, and ~20% of them were differentially expressed between E15.5 and E11.5. Among these RBP-coding genes we found 21 genes involved in AS regulation in the CNS (see **Annex 3**, Table 1), thus suggesting that the inclusion of the AS forms expressed in the RGs might change along neurogenesis. To provide evidence on this, we re-analysed the RNA-seq data using the software Vast-tools (Irimia et al., 2014). The result of this analysis revealed differences in the inclusion of 5,215 AS events (ΔPSI between E11.5 and E15.5 bigger than 10%) that affected 18.7% of the total coding genes expressed in RGs (3,078 genes). Interestingly, only 23.3% of the differentially expressed coding genes between E11.5 and E15.5 (717 genes) also showed developmental differences in the inclusion of AS events (**Fig R.18a**). This is consistent with other reports claiming that AS regulation and transcriptional regulation usually affect different sets of genes (Pan et al., 2004; Fagnani et al., 2007). Among the genes with regulated AS, 60% presented only 1 AS event, 37% between 2 and 4, and only 2 genes, *Aak1* and *Lrrc7*, presented 9 and 10 AS events, respectively (**Fig R.18b**). *Aak1* (AP2 Associated Kinase 1) encodes different protein isoforms of a kinase involved in several steps of the endocytic pathway

(Henderson and Conner, 2007), while *Lrrc7* (Leucine Rich Repeat Containing 7) encodes a postsynaptic scaffolding gene necessary for normal synaptic spine architecture and function that expresses alternatively spliced transcripts in the developing and mature CNS (Witte et al., 2018). Next, we checked for the type of AS events with differential inclusion between E11.5 than at E15.5. The number of AS events with decreased and increased inclusion was similar (2,332 vs 2,883; **Fig R.18c**). Distribution of AS types among the regulated events was similar and the most abundant AS type was intron retention followed by exon skipping, alternative donor and acceptor and microexons. It is noteworthy to mention that the inclusion of microexons in RGs was more frequent at E15.5 than at E11.5 (65 *vs* 8; see **Fig R.18c** and **Annex 3**, Tables 1 and 2).

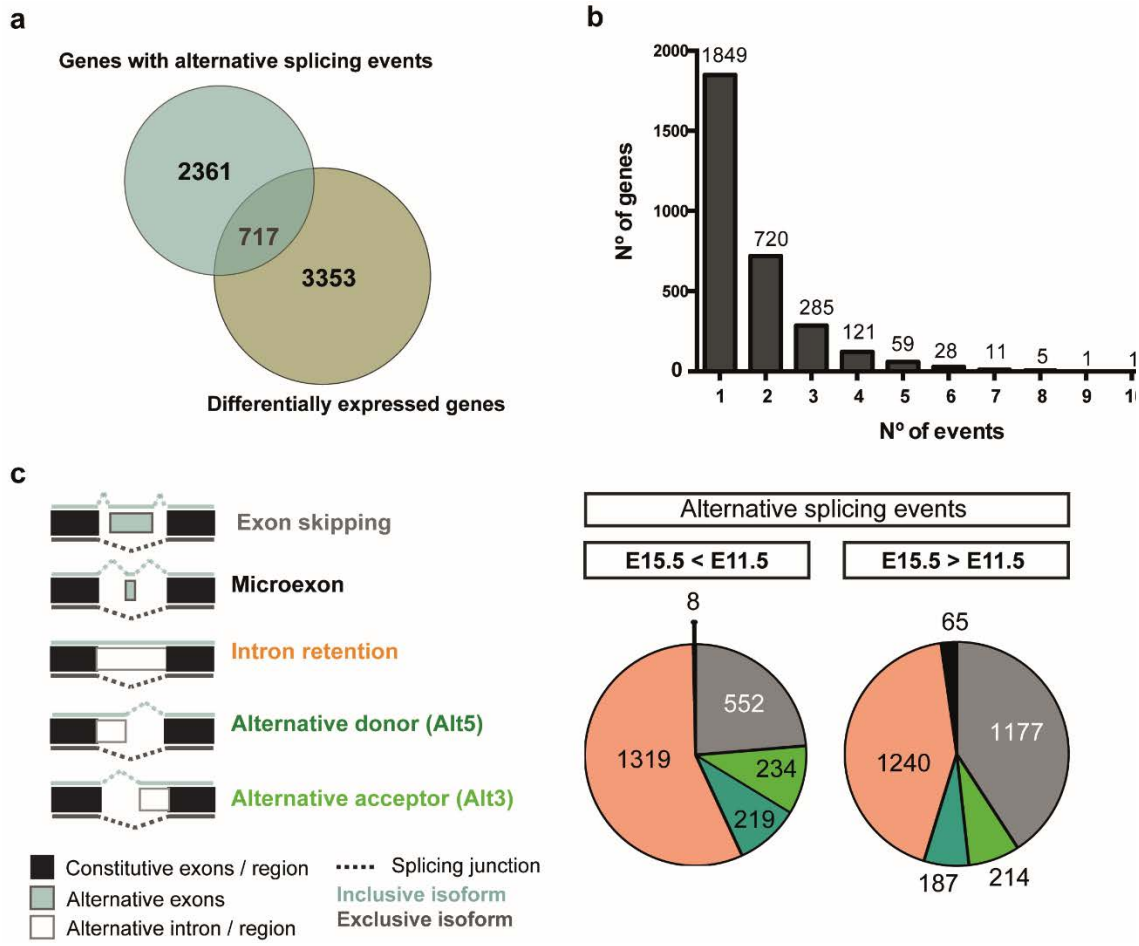


**Figure R.18. Differentially spliced transcripts in radial glia cells between E11.5 and E15.5.** **(a)** BioVenn plot indicating the overlap between the genes with differential expression between E11.5 and E15.5 and the genes presenting regulated alternative spliced (AS) events. **(b)** Distribution of the number of regulated AS events per gene. **(c)** Type and distribution of regulated AS events in radial glial cells between E11.5 and E15.5. Circle in the left shows AS events decreased inclusion at E15.5 than at E11.5, while circle on the right shows AS events with increased inclusion.

To validate the AS events detected by RNA-seq, we selected 9 AS annotated events (1 intron retention, 4 exon-skipping and 3 microexons) among the ones that showed appreciable ΔPSI values between E11.5 and E15.5 to be detected by RT-PCR. We performed RT-PCRs from total RNA isolated from E11.5 and E15.5 *Pax6*-GFP progenitors and Prominin-1 progenitors. The 9 AS events assessed by RT-PCR showed in the two type of progenitor samples developmental changes in the AS events that were in the same direction than the ones detected by RNA-seq (see **Fig R.19**), thus confirming the temporal regulation of these events in RGs.

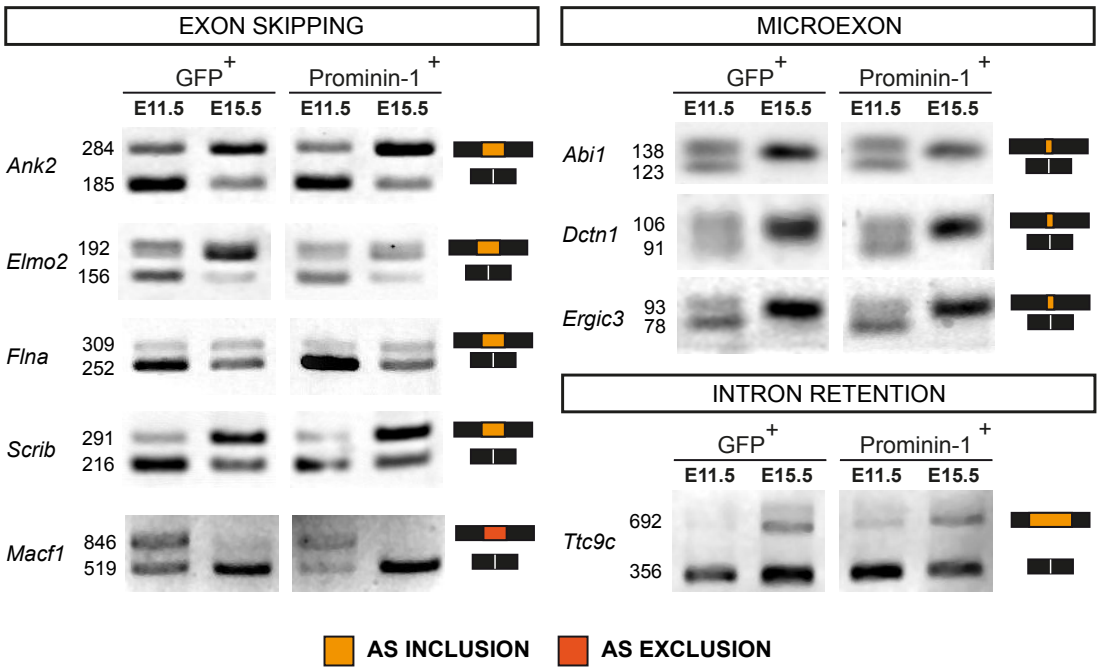


**Figure R.19. Validation of alternative spliced events by RT-PCR.** Representative RT-PCR assays validating 5 exon-skipping events, 3 microexon inclusions, and 1 intron retention event in the indicated genes. Numbers in the left indicate the length of the PCR product in base pairs (bp). Cassette inclusion is represented by an orange box flanked by black constitutive exons; cassette exclusion is represented by a red box. PCRs were performed in technical duplicates using 2 independent biological *Pax6*-GFP (GFP+) samples and a Prominin-1+ sample. The relative abundance of the PCR product in the different reactions was similar.

Functional enrichment analysis of the genes with regulated AS in RGs showed a significant enrichment in genes encoding ATP-binding proteins, synapse proteins and proteins involved in cytoskeleton organization, cilium biogenesis and DNA repair (**Fig R.20a** and **Annex 3,** Table 3). Different studies demonstrate that intron retention often results in the degradation of the intron-retaining transcript and, therefore, serve as a regulatory mechanism of gene expression levels (Jacob and Smith, 2017). Functional analysis among the genes with decreased intron retention at E15.5 revealed regulation

of genes coding metal ion binding, ATP binding and synapse proteins. This result suggests that intron-retention could be a mechanism extensively used by RGs to "silence" genes that need to be expressed in RG postmitotic daughters. Interestingly, genes with increased intron retention at E15.5 were enriched in completely different categories: "cilium biogenesis and degradation" and "microtubule" (**Fig R.20b,c**). The biogenesis of the cilium is important in the daughter cells retaining the RG-fate (Paridaen et al., 2013) and our result suggests that genes encoding ciliary proteins could be regulated by intron retention as neurogenesis proceeds.

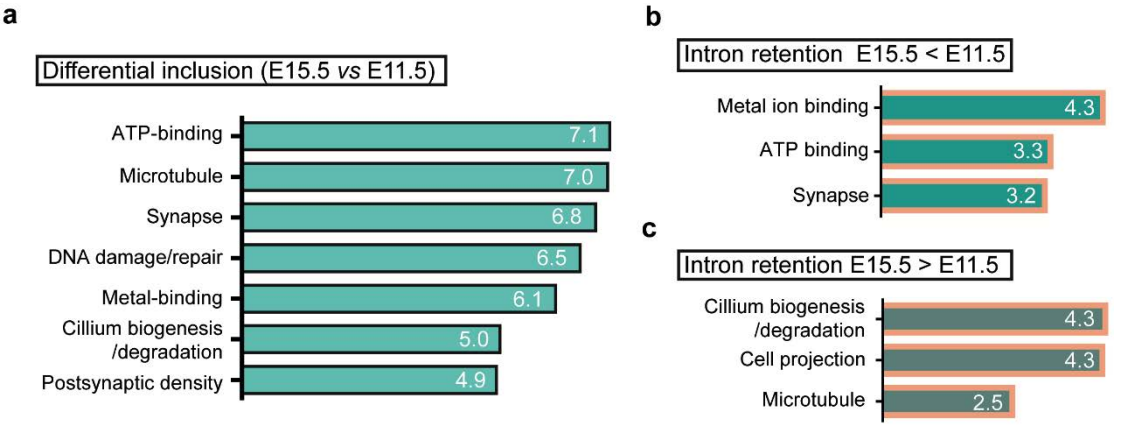


**Figure R.20. Functional enrichment analysis of the genes presenting of alternative spliced transcripts regulated between E11.5 and E15.5 in radial glia progenitors. (a)** DAVID functional enrichment of the 3,000 genes showing different frequencies in alternative spliced events between E15.5 and E11.5 (ΔPSI values higher than 10.3%). The top 7 functional categories are indicated**. (b,c)** DAVID enriched categories of the genes with decreased intron-retention events at E15.5 with respect to E11.5 (b) and increased intron-retention events at E15.5 (c). Enrichment scores are indicated inside the bars.

Overall, the data presented so far show that the genetic programs that balance the mode of division of RGs during neurogenesis are dynamic and regulated by miRNAs, specially by let-7 miRNAs and the miRNAs from the clusters *mir*-302/367 and *mir*-449. The data also suggest that AS is an important mechanism to accommodate the proteome of these progenitors to their mode of division.

## 2. Generation and differentiation of cortical macroglial cells in a mouse model of *DYRK1A* haploinsufficiency syndrome

The examination of the neocortex of the haploinsufficient *Dyrk1a*$^{+/-}$ mouse model has revealed alterations in the generation, morphology and synaptic connectivity of the excitatory neurons, phenotypes that could explain the neurological deficits associated to the human syndrome (Benavides-Piccione et al., 2005; Guedj et al., 2012; Arranz et al., 2019). In addition, adult *Dyrk1a*$^{+/-}$ mice present an excess of astrocytes in different brain regions, including the cortex (Fotaki et al., 2002; Guedj et al., 2012) and myelination defects in the CC (Balducci, 2012), suggesting that haploinsufficiency of DYRK1A also affects glial cells. This is in accordance with the gliosis and hypomyelination of the CC presented by children with a pathogenic *de novo* mutation in the *DYRK1A* gene (Ji et al., 2015; van Bon et al., 2016).

### 2.1. Astrocytes in the developing and adult *Dyrk1a*$^{+/-}$ neocortex

Quantification of astrocytes in the adult *Dyrk1a*$^{+/-}$ neocortex and hippocampus was performed by immunohistochemistry using antibodies against the astroglial marker GFAP (Guedj et al., 2012). GFAP in the mouse neocortex is expressed in a small population of astrocytes (Sofroniew and Vinters, 2010) and its cytosolic expression complicates the assignment of individual cell identity. To have an unbiased estimation of the astrocyte content in the adult *Dyrk1a*$^{+/-}$ neocortex we performed immunofluorescences using as a marker the TF SOX9. In addition to its nuclear localization, SOX9 has the advantage that it is expressed in all astrocytes outside of the adult neurogenic regions regardless of the brain functional status (Sun et al., 2017). The quantification of SOX9+ cells in the neocortex and hippocampus of young adult *Dyrk1a*$^{+/-}$ mice and their control littermates confirmed the increase in astrocyte numbers previously reported in *Dyrk1a*$^{+/-}$ mutants (**Fig R.21a-c, R.22a-c**; Guedj et al., 2012). Moreover, it suggests that the augmented GFAP immunostaining in the brain of these *Dyrk1a* mutants is not due to a pathological gliosis. As gliosis may also involve the hypertrophy and/or proliferation of microglial cells (Burda and Sofroniew, 2014), we next immunostained *Dyrk1a*$^{+/+}$ and *Dyrk1a*$^{+/-}$ brain sections with antibodies against the microglial marker IBA1 and counted the IBA1+ cells in the neocortex and hippocampus. We did not observe differences between genotypes in the number of IBA1+ cells nor in their morphology, which was the characteristic of resting microglia in both genotypes

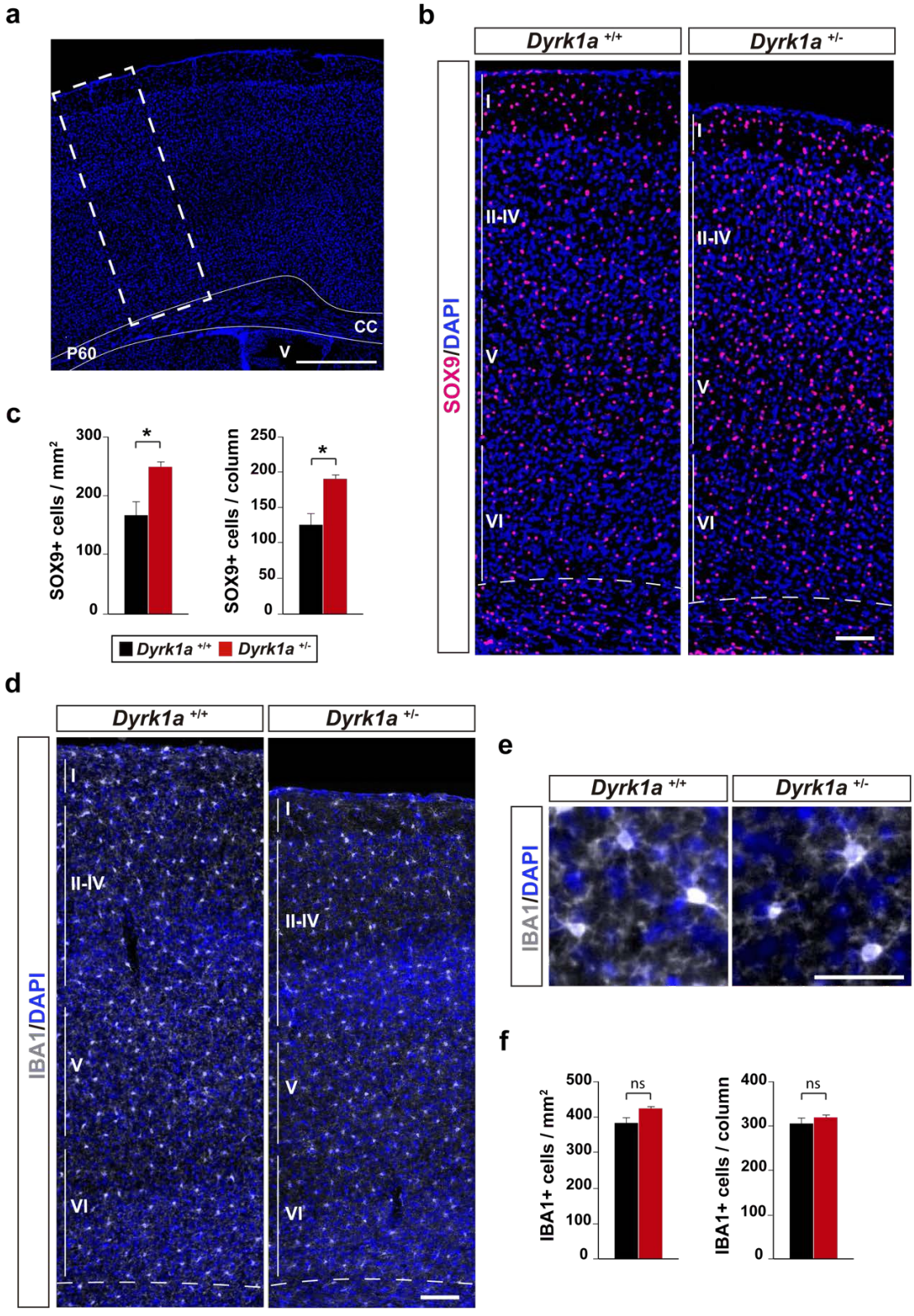


**Figure R.21. Number of astrocytes and microglial cells in adult *Dyrk1a*$^{+/+}$ and *Dyrk1a*$^{+/-}$ neocortices. (a)** Coronal brain section of an adult (P60) *Dyrk1a*$^{+/+}$ neocortex stained with DAPI. White rectangle indicates the region of the neocortex where quantifications in (c) and (f) were done and the *Corpus callosum* (CC) is delimited in continuous lines. V, ventricle. **(b, d)** Representative images of the *Dyrk1a*$^{+/+}$ and *Dyrk1a*$^{+/-}$ neocortices immunostained against SOX9 (b) or IBA1 (d) and the nuclei counterstained with DAPI. Cortical layers are indicated on

the left. **(c, f)** Histograms showing the density and the number of SOX9+ astrocytes (c) and IBA1+ microglial cells (f) in a 500 µm-wide column of the neocortex. Notice that both density and number of astrocytes in a column are increased in *Dyrk1a*$^{+/-}$ neocortices, whereas no differences are found in the microglial population. **(e)** Images showing a similar morphology of IBA1+ microglial cells in the two genotypes. Values correspond to the mean (S.E.M). SOX9+, n=5-4 animals each genotype; IBA+, n=3 each genotype. ns=not significant, **p*<0.05, Student's t-test. Scale bars = 500 µm (a), 100 µm (b, d), 50 µm (e).

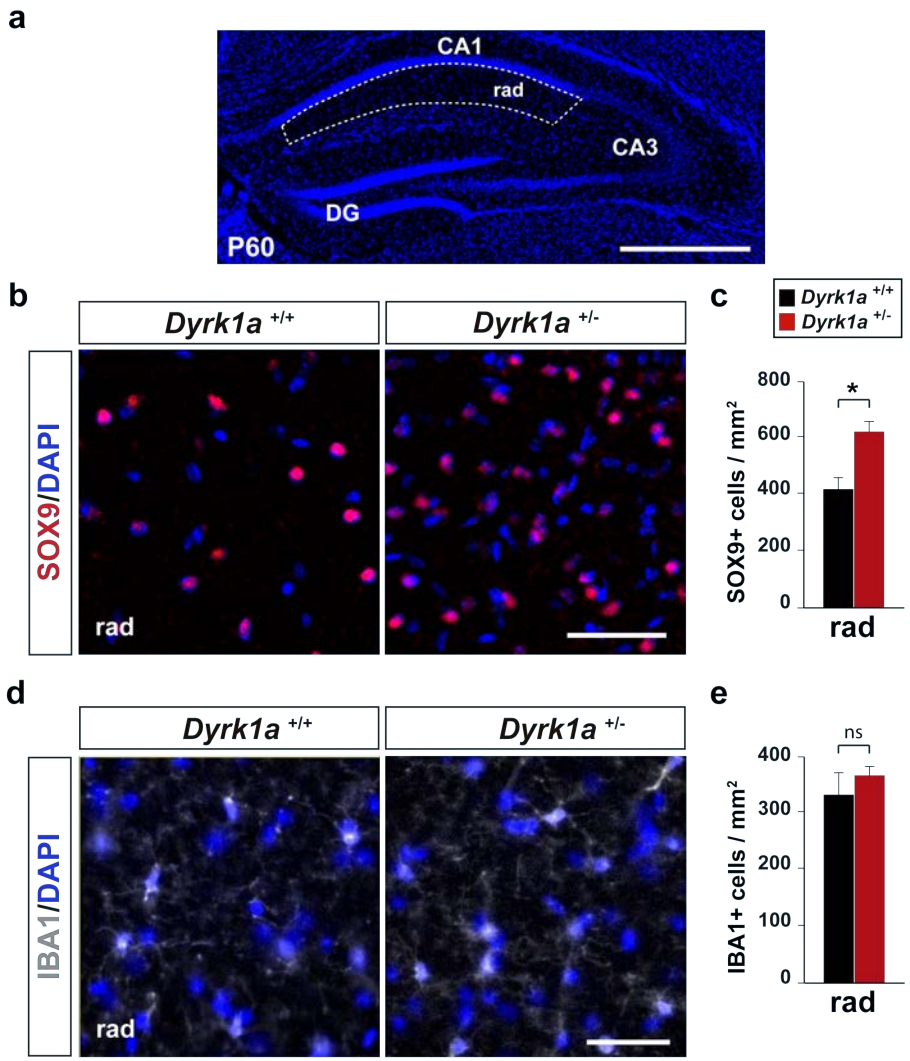


**Figure R.22. Number of astrocytes and microglial cells in adult *Dyrk1a*$^{+/+}$ and *Dyrk1a*$^{+/-}$ hippocampus. (a)** Coronal brain section of an adult (P60) *Dyrk1a*$^{+/+}$ hippocampus stained with DAPI. Dashed lines delimitate the *stratum radiatum* layer (rad) where quantifications in (c) and (e) were done. CA1, CA (*cornu ammonis*) area 1; CA3, CA area 3; GD, *dentate girus.* **(b, d)** Representative areas from *Dyrk1a*$^{+/+}$ and *Dyrk1a*$^{+/-}$ rad immunostained against SOX9 (b) or IBA1 (d) and the nuclei counterstained with DAPI. Scale bars = 500 µm (a), 50 µm (b, d). **(c, e)** Histograms showing the density of SOX9+ astrocytes (c) and IBA1+ microglial cells (e) in the rad. Notice that astrocyte density is increased in *Dyrk1a*$^{+/-}$ animals, whereas microglial densities are similar between genotypes. Values correspond to the mean (S.E.M). SOX9+, n=5-4 animals each genotype; IBA+, n=3 each genotype. **p*<0.05, ns=not significant, Student's t-test.

(**Fig R.21d-f, R.22d,e**). The immunostainings presented so far suggest that the increased number of astrocytes in *Dyrk1a*$^{+/-}$ brains result from a developmental defect. This is in agreement with the increased expression of the astroglial genes *Gfap* and *Aqp4* (aquaporin- 4; Rash et al., 1998) in postnatal *Dyrk1a*$^{+/-}$ neocortices (Arranz et al., 2019).

Cortical astrocytes are generated after birth mostly from RGs of the dorsal germinal layer and by local amplification of RG-derived astrocytes (Kriegstein and Alvarez-Buylla, 2009; Ge et al., 2012, see also **Fig R.23a**). Therefore, the astrocytes produced during development depend on the RGs available at the end of the neurogenic phase and their intrinsic capacity to differentiate into astrocytes. The onset of neurogenesis is advanced in the dorsal telencephalon of *Dyrk1a*$^{+/-}$ embryos leading to an increased production of neurons that is maintained until mid-neurogenesis (Najas et al., 2015; Arranz et al., 2019). This alteration may affect the timing of the neurogenic to gliogenic switch and/or the number of neural progenitors available at the onset of gliogenesis.

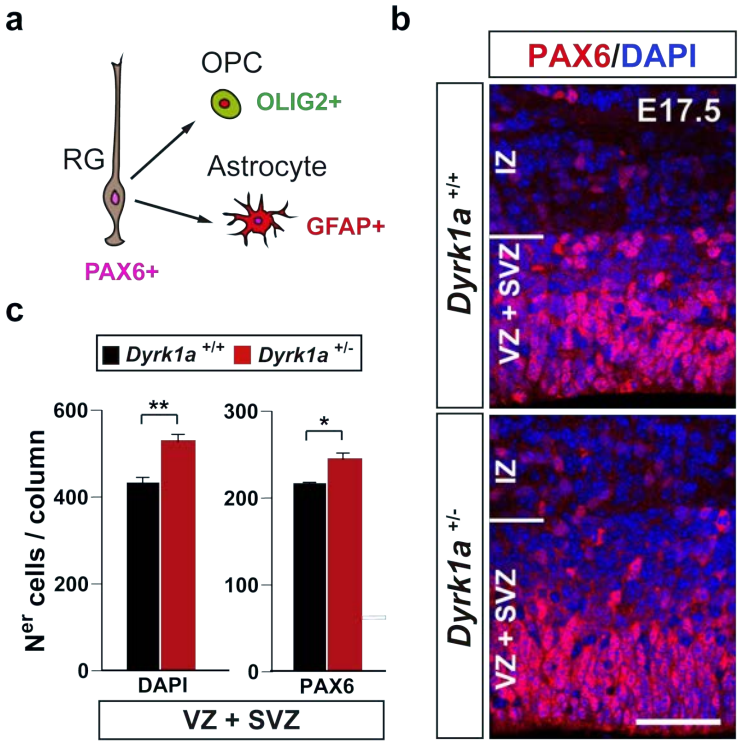


**Figure R.23. Neural progenitors in the dorsal telencephalon of E17.5 *Dyrk1a*$^{+/+}$ and *Dyrk1a*$^{+/-}$ embryos. (a)** Scheme indicating the cell lineage and the expression of PAX6, GFAP and OLIG2 in radial glial (RG) cells, astrocytes and oligodendrocyte precursor cells (OPC). **(b)** Representative coronal sections from *Dyrk1a*$^{+/+}$ and *Dyrk1a*$^{+/-}$ dorsal telencephalons immunostained against PAX6 and the nuclei counterstained with DAPI. IZ, intermediate zone; SVZ, subventricular zone; VZ, ventricular zone. Scale bar = 50 µm. **(c)** Histograms showing the number of total cells (DAPI), and PAX6+ cells in the VZ-SVZ of *Dyrk1a*$^{+/+}$ and *Dyrk1a*$^{+/-}$ embryos counted in 200 µm wide columns. Values correspond to the mean (S.E.M). n=4 animals each genotype. **p*<0.05, ***p*<0.01, Student's t test.

Classical BrdU-birthdating experiments performed by injecting BrdU in pregnant females at the end of dorsal neurogenesis (E17.5), indicated that cortical neurogenesis in the *Dyrk1a*$^{+/-}$ mutant (estimated as the number of neurons labelled for BrdU, BrdU+NEUN+ cells, in postnatal neocortices) ends at the correct time (**Fig R.24**). However, the dorsal germinal layer (VZ + SVZ) of E17.5 *Dyrk1a*$^{+/-}$ mutants contained more cells than the control germinal layer, and more RGs that still expressed the marker PAX6 (**Fig R.23b,c**).

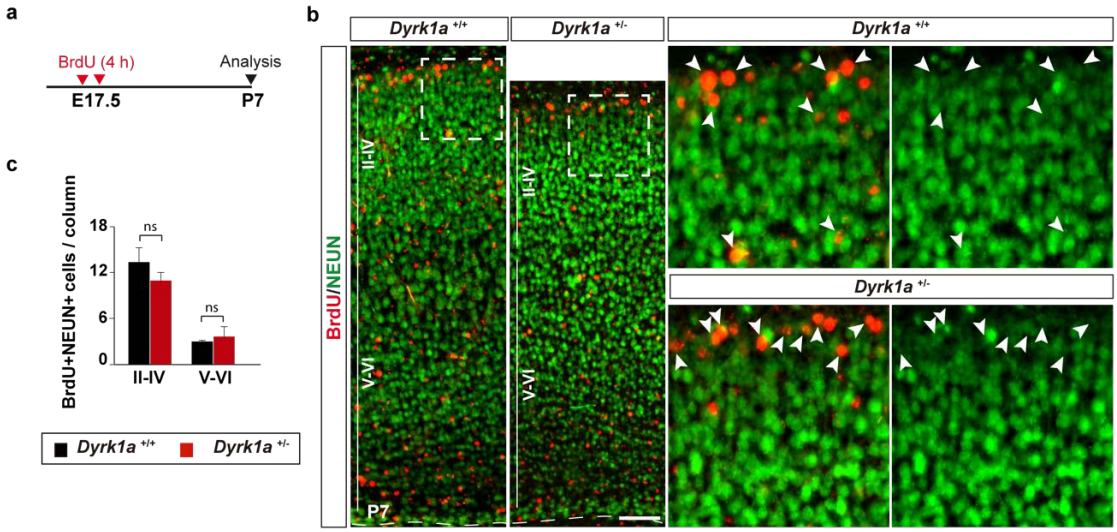


**Figure R.24. Neuron production in the dorsal telencephalon of E17.5 *Dyrk1a*$^{+/+}$ and *Dyrk1a*$^{+/-}$ embryos. (a)** Schedule of the BrdU-labeling protocol used to estimate neuron production in the developing neocortex at the end of the neurogenic period. **(b)** Representative images of the P7 *Dyrk1a*$^{+/+}$ and *Dyrk1a*$^{+/-}$ neocortex immunostained for BrdU and the neuronal marker NEUN. Cortical layers are indicated on the left. Dashed squares are magnified on the right to show double positive cells (arrowheads). Scale bar = 50 µm. **(c)** Histogram showing the number of BrdU+;NEUN+ neurons in a 500 µm wide column of the upper (II-IV) and lower (V-VI) layers. Notice that most of the double positive cells are in the upper layers in both genotypes. Values correspond to the mean (S.E.M). n=3 animals each genotype. ns=not significant, Student's t test.

Next, we visualize the astrocytes that populate the neocortices of postnatal *Dyrk1a*$^{+/-}$ mice and their control littermates by immunofluorescence. In this case we used GFAP as a marker instead of SOX9 because during development this TF is also expressed in neural progenitors (Stolt et al., 2003). In the developing wild-type neocortex, GFAP+ cells with the characteristic staining of a mature astrocyte were not detected until P5 (data not shown and **Fig R.25a**). In both *Dyrk1a*$^{+/+}$ and *Dyrk1a*$^{+/-}$ genotypes, there were many GFAP+ astrocytes in the white matter and in the most external layer of the cortical plate (layer I) but only few in the remaining cortical plate where most of them were in layer VI. Nonetheless, the number of astrocytes in layers II to VI was augmented in the *Dyrk1a*$^{+/-}$ brains (**Fig R.25a,b**). At P7 most of the astrocytes that populated these layers

in control brains remained in layer VI while in *Dyrk1a*$^{+/-}$ brains these cells were more abundant and populated the external layers (**Fig R.25c,d**).

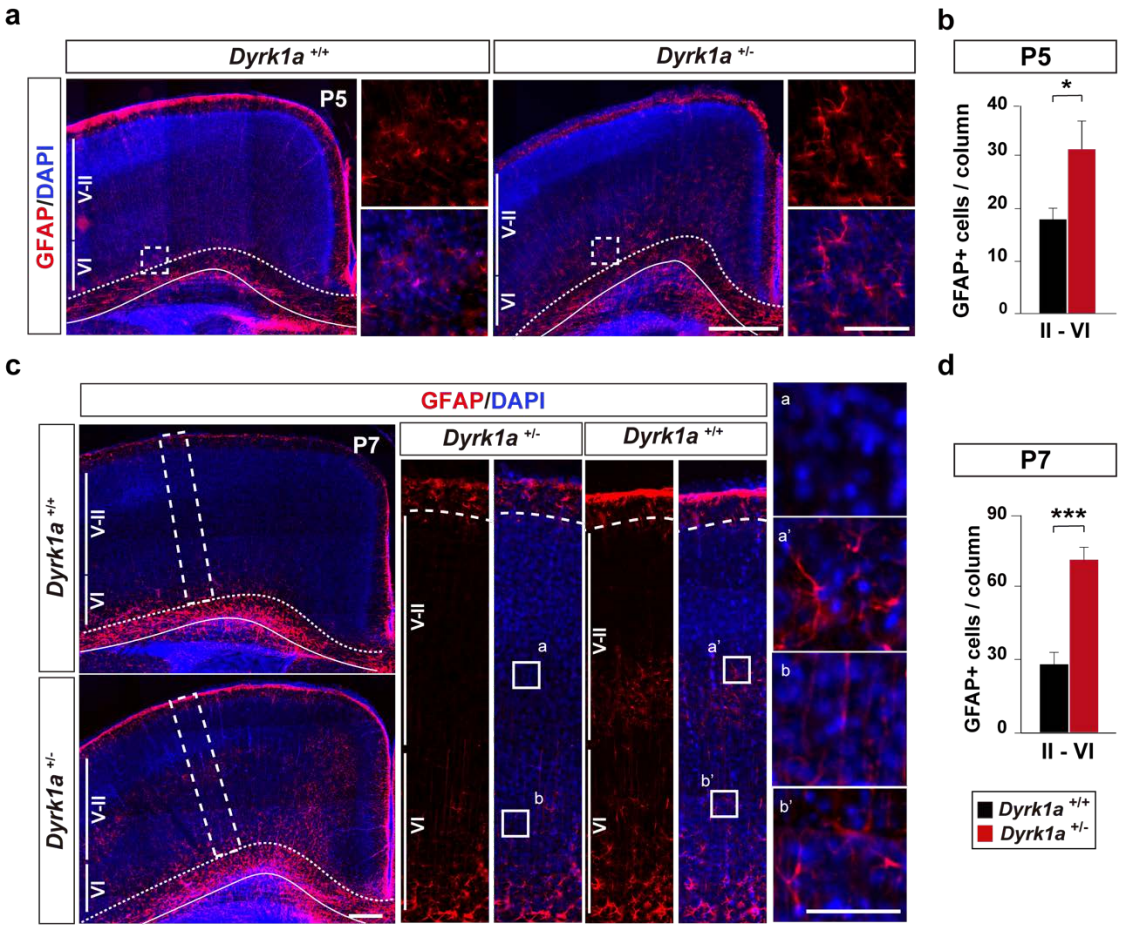


**Figure R.25. Cortical astrocytes in postnatal *Dyrk1a*$^{+/+}$ and *Dyrk1a*$^{+/-}$ brains. (a, c)** Representative images from *Dyrk1a*$^{+/+}$ and *Dyrk1a*$^{+/-}$ cerebral cortex at P5 (a) and at P7 (c) immunostained against GFAP and the nuclei counterstained with DAPI. White dashed lines indicate the border between layer VI and the white matter. Layers VI and V to II are indicated on the left. Boxed areas are magnified on the right panels. Scale bars: 500 µm and 100 µm (high magnifications). **(b, d)** Histograms show the number of GFAP+ astrocytes in a 500 µm wide column in P5 (b) and P7 (d) *Dyrk1a*$^{+/+}$ and *Dyrk1a*$^{+/-}$ brains. Notice that number of GFAP+ astrocytes is significantly increased in postnatal *Dyrk1a*$^{+/-}$ mice. Values correspond to the mean (S.E.M). P5, n=4 animals each genotype; P7, n=5-7. **p*<0.05, ****p*<0.001, Student's t test.

The data described so far indicate that the increased number of cortical neural progenitors available at the onset of gliogenesis may be the cause of the augmented number of astrocytes in *Dyrk1a*$^{+/-}$ neocortices. An increased astrogliogenic potential of the mutant progenitors may also explain this phenotype. Therefore, we performed *in utero* electroporations to compare the astrogliogenic potential of *Dyrk1a*$^{+/+}$ and *Dyrk1a*$^{+/-}$ apical progenitors. For this, we used the transposon PiggyBac system to label with GFP all the progeny of the electroporated progenitors (Nagy et al., 2011). Electroporations

were performed at E16.5 and the astroglial output of the electroporated progenitors was analysed in P5 neocortices using the glial marker GFAP (**Fig R.26a**). GFAP+GFP+ astrocytes in *Dyrk1a*$^{+/+}$ and *Dyrk1a*$^{+/-}$ neocortices were located in the white matter and in the cortical plate, mostly in layer I, and the astroglial output of the electroporated progenitors (% of GFAP+GFP+/GFP+ cells) that populated the cortical plate was similar in the two genotypes (**Fig R.26b,c**). Since VZ progenitors also generate OPCs (Bergles and Richardson, 2015; **Fig R.23a**) we immunostained the electroporated neocortices for the oligodendroglial marker OLIG2. We did not detected differences between genotypes neither in the distribution of cortical OLIG2+GFP+ oligodendroglia cells nor in the percentage of these cells with respect to the total number of GFP+ cells (% of OLIG2+GFP+/GFP+ cells; **Fig R.26d,e**). These results indicate that haploinsufficiency of *Dyrk1a* does not affect the capacity of dorsal progenitors to differentiate into glial cells. This is in agreement with published data showing that acute knockdown of *Dyrk1a* in E16.5 embryos using plasmids that express *Dyrk1a* shRNAs do not modify the astrocytic differentiation of dorsal neural progenitors (Kurabayashi et al., 2015). However, in the same paper, there is data showing that the overexpression of DYRK1A up-regulates the activity of the astrogliogenic transcription factor STAT3 in wild-type progenitors and that this up-regulation correlates with an increased astroglial differentiation of these progenitors. Therefore, we performed another set of *in utero* electroporations to evaluate STAT3 activity in E16.5 *Dyrk1a*$^{+/-}$ dorsal progenitors. For this, we used a STAT3-luciferase reporter plasmid that contains 2.5 kb of the GFAP promoter including a STAT3-binding motif (GL1-pGL3), and a version of this plasmid that has a mutated STAT3-binding motif (GL1-S-pGL3; see **Fig R.27a** and Nakashima et al., 1999) as a control. As expected, luciferase activity in the neocortices electroporated with GL1-pGL3 was significantly reduced in *Dyrk1a*$^{+/-}$ samples compared to the *Dyrk1a*$^{+/+}$ samples, indicating that the mutant progenitors show less STAT3 activity. Luciferase activities in the neocortices electroporated with the GL1-S-pGL3 were similar in the two genotypes (**Fig R.27b**). Together our electroporation data indicates that despite dorsal *Dyrk1a*$^{+/-}$ RGs has reduced STAT3 activity during the neurogenic-gliogenic switch, their astrogliogenic potential is preserved.

Collectively, our data indicate that the augmented astrogliogenesis observed in postnatal *Dyrk1a*$^{+/-}$ mutant mice is likely caused by the excess of progenitors in the germinal VZ-SVZ region at the onset of gliogenesis rather than an enhanced capacity of these progenitors to differentiate into glial cells.

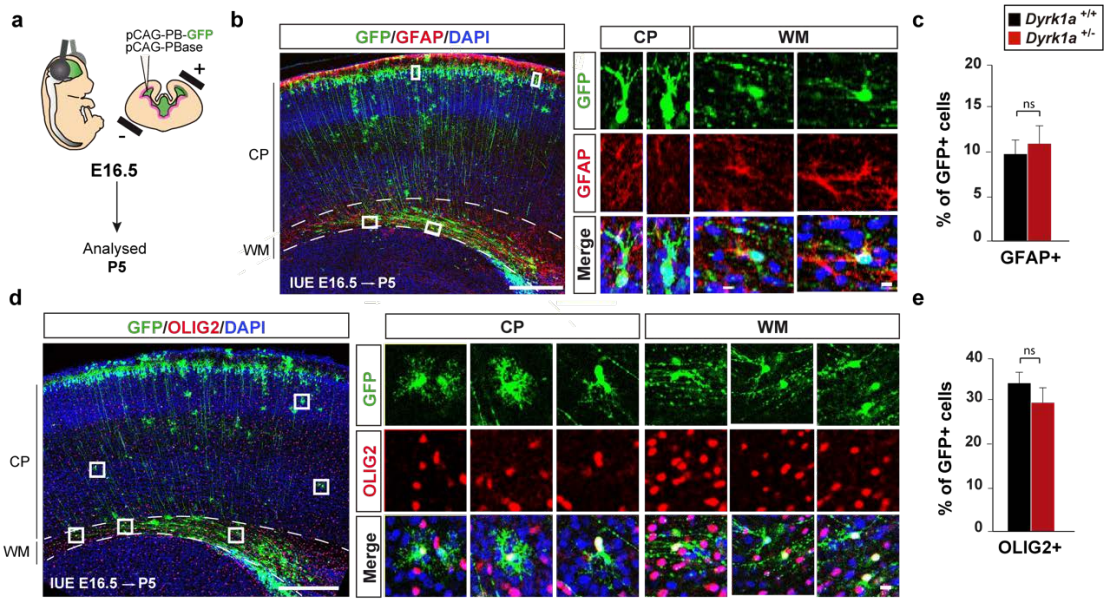


**Figure R.26. Differentiation of dorsal *Dyrk1a*$^{+/+}$ and *Dyrk1a*$^{+/-}$ progenitors into glial cells.** **(a)** Schematic representation of the *in-utero* electroporation experiment performed in E16.5 *Dyrk1a*$^{+/+}$ and *Dyrk1a*$^{+/-}$ embryos to evaluate the capacity of dorsal ventricular zone progenitors to generate GFAP+ astrocytes and OLIG2+ OPCs. **(b, d)** Representative coronal sections from P5 electroporated *Dyrk1a*$^{+/+}$ brains immunostained for GFAP (b) or OLIG2 (d). The nuclei are counterstained with DAPI. Notice that GFAP+GFP+ cells are mostly situated in the upper cortical layers (layers I and II), whereas OLIG2+;GFP+ cells are distributed along the white matter (WM) and the cortical plate (CP). Dashed lines delimitate the WM. Right panels in b and d show magnification of the boxed cells. Scale bars: 500 µm and 10 µm (magnification panels). **(c, e)** Histograms showing the percentage of electroporated GFP+ cells that are GFAP+ (c) or OLIG2+ (e). Values correspond to the mean (S.E.M). GFAP, n=6-3 animals each genotype; OLIG2, n=6-3 animals. ns=not significant, Student's t test.

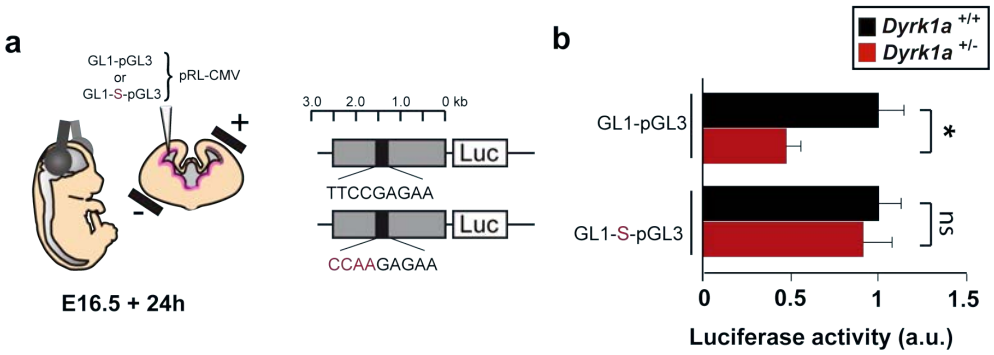


**Figure R.27. Stat3 activity in dorsal *Dyrk1a*$^{+/+}$ and *Dyrk1a*$^{+/-}$ cortical progenitors. (a)** Scheme illustrating the *in-utero* electroporation experiment and luciferase (Luc) reporter plasmids used to estimate Stat3 activity in the dorsal telencephalon of E16.5 *Dyrk1a*$^{+/+}$ and *Dyrk1a*$^{+/-}$ embryos. Grey and black boxes in GL1-pGL3 and GL1-S-pGL3 plasmids indicate the GFAP promoter (GL1) and the STAT3 binding site, respectively. The mutated sequence in GL1-S-pGL3 is indicated in red. **(b)** Histogram showing relative GL1-pGL3 and GL1-S-pGL3 luciferase values normalized to the *Renilla* values in the *Dyrk1a*$^{+/+}$ and *Dyrk1a*$^{+/-}$ neocortices. Notice that Stat3 activity is significantly reduced in the mutant neocortex. Values correspond to the mean (S.E.M). GL1-pGL3, n=9-6 embryos each genotype; GL1-S-pGL3, n=6-7 each genotype. *$p$<0.05, ns=not significant, Student's t test.

## 2.2. Oligodendrogenesis in the *Dyrk1a*$^{+/-}$ forebrain

Cortical OPCs are first produced in the embryo from ventral VZ progenitors and later on, starting around birth, from dorsal VZ progenitors (Bergles and Richardson, 2015; **Fig I.11**). There is evidence that alterations in the neurogenic program of these progenitors may influence the onset of dorsal OPC production (Toma and Hanashima, 2015). Therefore, it is possible that the neurogenic alterations reported in the dorsal telencephalon of *Dyrk1a*$^{+/-}$ embryos (Najas et al., 2015; Arranz et al., 2019) have an impact in the firsts OPCs produced in the dorsal germinal layer. To test this possibility, we immunostained E17.5 *Dyrk1a*$^{+/+}$ and *Dyrk1a*$^{+/-}$ neocortices for the OPC markers OLIG2 and PDGFR$\alpha$ and counted OLIG2+ cells and OLIG2+PDGFR$\alpha$+ OPCs in the VZ-SVZ region and in the intermediate zone, where the delaminated OPCs migrate to reach the cortical plate (**Fig R.28a**). In both genotypes there were fewer OLIG2+PDGFR$\alpha$+ cells than OLIG2+ cells, but *Dyrk1a*$^{+/-}$ neocortices had significantly less OLIG2+ cells in the VZ-SVZ and less OLIG2+ and OLIG2+PDGFR$\alpha$+ OPCs in the intermediate zone than control neocortices (**Fig R.28b**). At E18.5, the abundance of OLIG2+ and OLIG2+PDGFR$\alpha$+ OPCs in the VZ-SVZ and intermediate zone was similar in the two genotypes (**Fig R.28b,c**). Collectively, this experiment indicates that the onset of dorsal oligodendrogenesis is slightly delayed in *Dyrk1a*$^{+/-}$ mutant brains. Interestingly, E17.5 transgenic embryos overexpressing DYRK1A show more OPCs in the dorsal telencephalon than their wild-type littermates (Najas et al., 2015).

Since DYRK1A is also expressed in progenitors of the embryo ventral telencephalon and the overexpression of DYRK1A affects the production of cortical interneurons (Najas, 2014), which are also generated from ventral neural progenitors (Bandler et al., 2017), we next examined the generation of OPCs in the LGE at E15.5, when the production of OPCs in this region begins (second wave of OPC production; Bergles and Richardson, 2015). LGE OPCs are generated in the VZ from progenitors that express OLIG2 and migrate dorsally to populate the neocortex (**Fig R.29a**). These committed progenitors maintain high levels of OLIG2 when delaminate from the VZ and move to the mantel zone, where they start to express other OPC markers such as PDGFR$\alpha$ (**Fig R.29b**). We detected OLIG2+ and OLIG2+PDGFR$\alpha$+ OPCs in the LGE mantel zone of *Dyrk1a*$^{+/-}$ embryos but the number of these OPCs was significantly lower than in the control embryos (**Fig R.29b,c**), indicating that oligodendrogenesis from LGE progenitors is affected in these mutants.

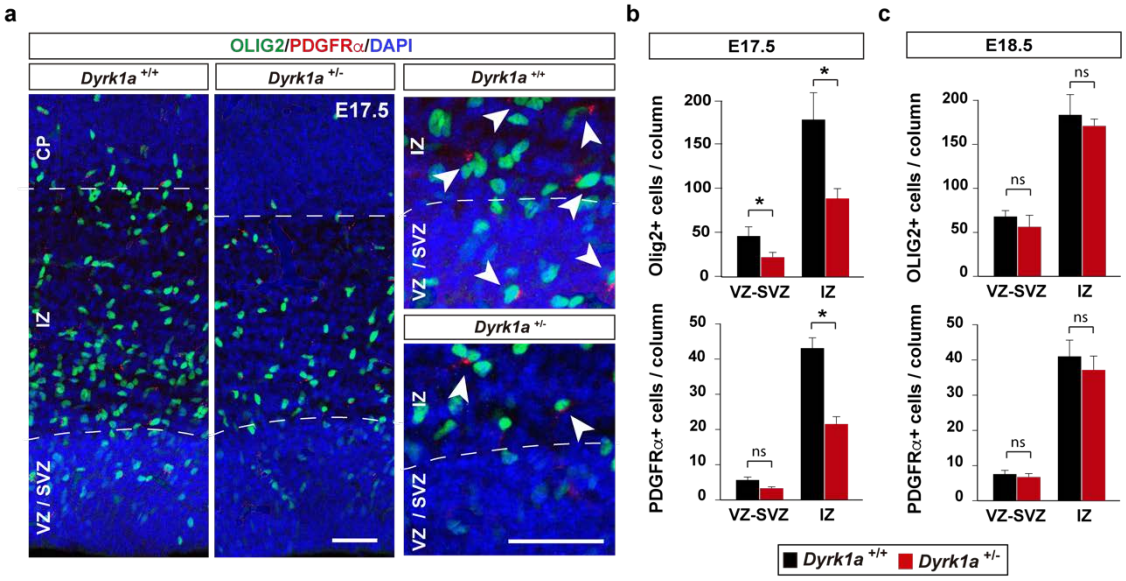


**Figure R.28. OPCs in the dorsal telencephalon of *Dyrk1a*$^{+/+}$ and *Dyrk1a*$^{+/-}$ embryos at the onset of gliogenesis. (a)** Representative coronal sections from E17.5 *Dyrk1a*$^{+/+}$ and *Dyrk1a*$^{+/-}$ dorsal telencephalons immunostained against OLIG2 and PDGFRα and the nuclei counterstained with DAPI. Right panels correspond to magnifications of the ventricular – subventricular zone (VZ-SVZ) region and the intermediate zone (IZ). Arrowheads point to OLIG2+ PDGFRα+ OPCs. Dashed lines indicate the limits between the VZ-SVZ region and the IZ and between the IZ and the cortical plate (CP). Scale bars: 50 µm. **(b, c)** Histograms showing the number of OLIG2+ cells and PDGFRα+ cells in 200 µm wide columns of the dorsal telencephalon at E17.5 (b) and E18.5 (c). Notice that differences in OPC numbers between genotypes are significant at E17.5 but not at E18.5. Values correspond to the mean (S.E.M). E17.5, n=3-4 embryos each genotype; E18.5, n=7-4. *$p$<0.05, ns=not significant, Student's t test.

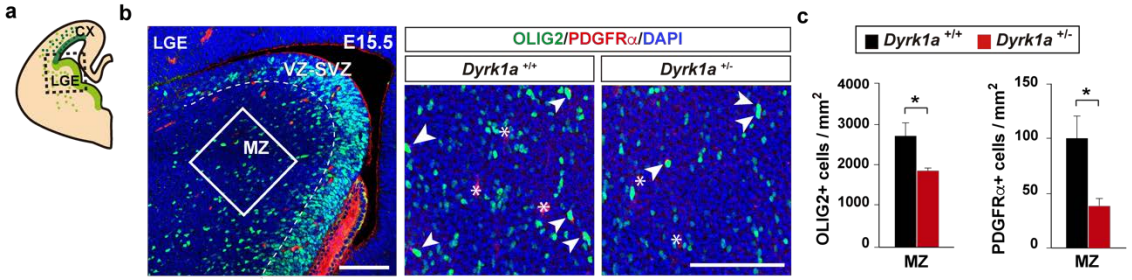


**Figure R.29. OPCs in the lateral ganglionic eminence of E15.5 *Dyrk1a*$^{+/+}$ and *Dyrk1a*$^{+/-}$ embryos. (a)** Scheme indicating the lateral ganglionic eminence (LGE) in a coronal brain section. **(b)** Representative coronal sections from LGEs immunostained against OLIG2 and the nuclei counterstained with DAPI. The dashed line delimitates the ventricular - subventricular zone (VZ and SVZ). The square in the centre indicates the area of the mantel zone (MZ) where cells were counted. The right panels show representative sections from *Dyrk1a*$^{+/+}$ and *Dyrk1a*$^{+/-}$ MZs immunostained against OLIG2 and PDGFRα. Asterisks indicate blood vessels labelled with anti-PDGFRα. Arrowheads point to OLIG2+PDGFRα+ OPCs. Scale bars: 100 µm. **(c)** Histograms show the density of all OLIG2+ cells (left) and OLIG2+PDGFRα+ cells (right) in the MZ of *Dyrk1a*$^{+/+}$ and *Dyrk1a*$^{+/-}$ embryos. Notice the significant reduction of these cells in mutant *Dyrk1a*$^{+/-}$ embryos. Values correspond to the mean (S.E.M.) n=3-4 each genotype. *$p$<0.05, Student's t test.

OPCs generated in the ventral and dorsal germinal zones proliferate and migrate away from these zones to populate the grey and white matter before differentiation into myelinating oligodendrocytes (Bergles and Richardson, 2015). To assess whether the defects in OPC production detected in the *Dyrk1a*$^{+/-}$ model affect the time in which OPCs reach the target axons, we counted the number of these cells (OLIG2+ cells) in the main axonal tract, the CC, of *Dyrk1a*$^{+/-}$ mutants and wild-type littermates at different developmental stages; from E17.5 to P10. At E17.5 and P0, when the CC is populated only by ventral OPCs, *Dyrk1a*$^{+/-}$ mutants presented fewer OLIG2+ cells than the wild-types. The difference between genotypes is still significant at P7, when the first OPCs generated in the dorsal telencephalon arrive to the CC, but not at P10, a developmental stage in which OLIG2+ cells in the *Dyrk1a*$^{+/-}$ CC reached normal levels (**Fig R.30**). This result is consistent with the significant deficit in ventral OPC production in *Dyrk1a*$^{+/-}$ embryos (**Fig R.29**) and indicates that this deficit is compensated by postnatal OPCs.

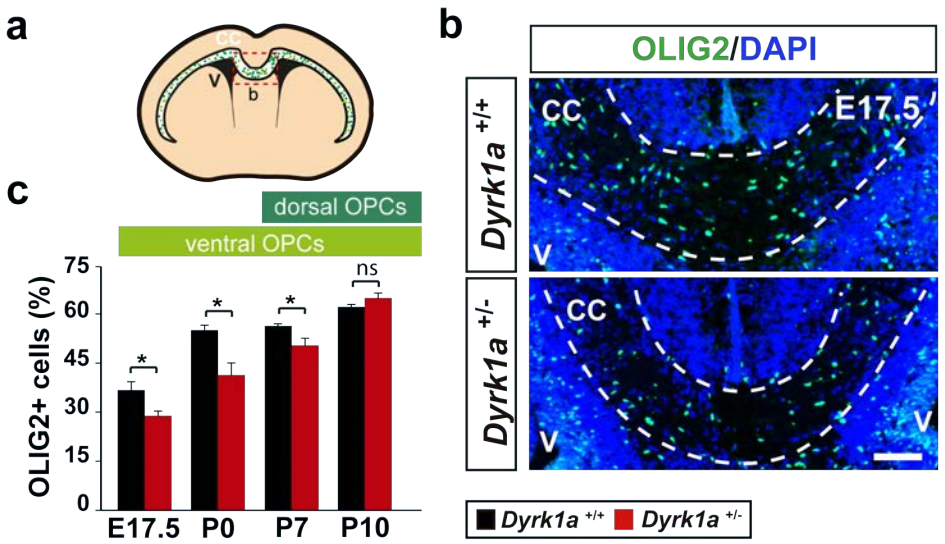


**Figure R.30. OPC numbers in the *Dyrk1a*$^{+/+}$ and *Dyrk1a*$^{+/-}$ *corpus callosum* during development. (a)** Schematic representation of a coronal brain section at the level of the *corpus callosum* (CC). Green dots represent OPCs populating the CC. Red dashed square indicates the region of the CC where cells were quantified from E17.5 to P10. **(b)** Representative images from E17.5 *Dyrk1a*$^{+/+}$ and *Dyrk1a*$^{+/-}$ CC*s* immunostained against OLIG2 and the nuclei counterstained with DAPI. White dashed lines delimitate the CC. Scale bar: 100 µm. V, ventricle. **(c)** Histogram showing the percentage of cells that are OLIG2+ in the *Dyrk1a*$^{+/+}$ and *Dyrk1a*$^{+/-}$ CC. The contribution of ventral and dorsal OPCs in the different developmental stages is indicated. Notice that the percentage of OLIG2+ OPCs in the *Dyrk1a*$^{+/-}$ CC is reduced from E17.5 to P7 reaching normal numbers at P10. Values correspond to the mean (S.E.M). E17.5, n=7 animals each genotype; P0, n=4-3; P7, n= 5-7; P10, n=7-8. **p*<0.05, ns=not significant, Student's t test. Scale bar: 100 µm.

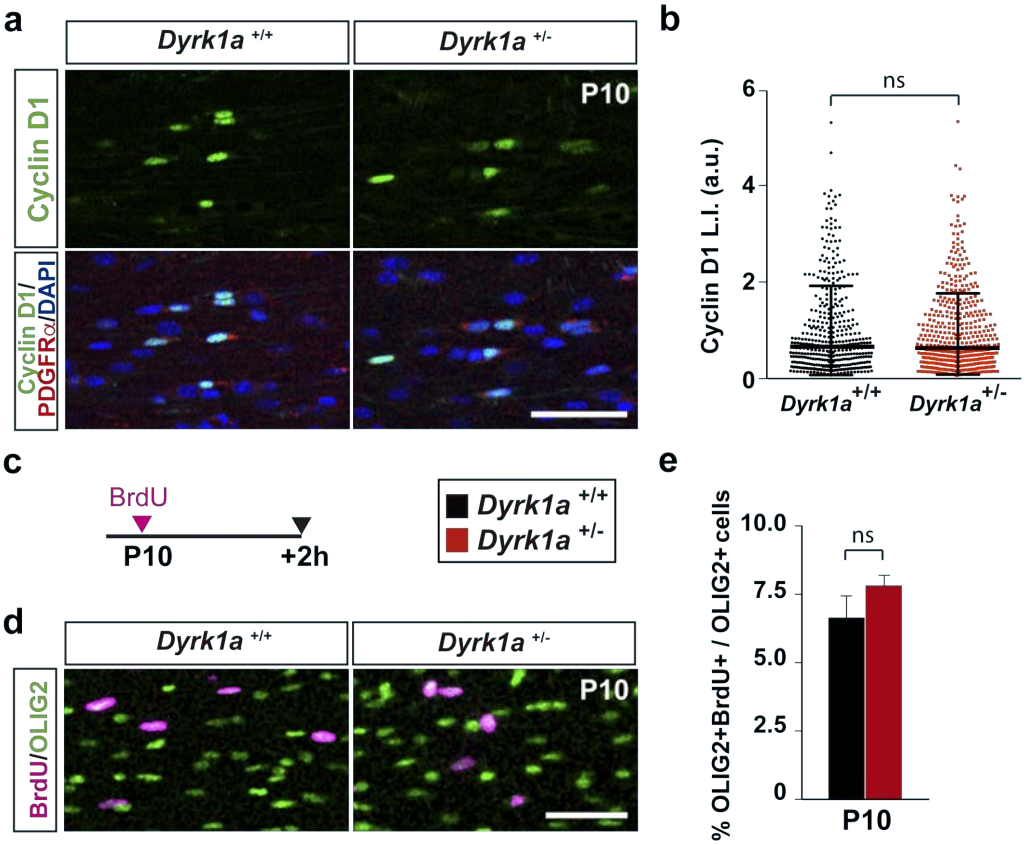


**Figure R.31. Proliferative OPCs in the postnatal *Dyrk1a*$^{+/+}$ and *Dyrk1a*$^{+/-}$ *corpus callosum*.** **(a)** Representative images from P10 *Dyrk1a*$^{+/+}$ and *Dyrk1a*$^{+/-}$ *corpus callosum* (CC) immunostained against Cyclin D1 and PDGFRα and the nuclei counterstained with DAPI. **(b)** Plot showing Cyclin D1 labelling index (L.I) values for individual PDGFRα+ cells in the CCs of the indicated genotype. The bars indicate the median and the interquartile range. n=409-500 cells each genotype (3 animals per genotype). ns=not significant, Mann-Whitney test. a.u., arbitrary units. **(c)** Schedule of the BrdU-labeling protocol used to estimate the fraction of proliferative OPCs in the CC. **(d)** Representative images from P10 *Dyrk1a*$^{+/+}$ and *Dyrk1a*$^{+/-}$ CC immunostained against OLIG2 and BrdU. **(e)** Histogram showing the percentage of OLIG2+ cells immunolabelled for BrdU. Values are the mean (S.E.M). n=7-8 animals each genotype. ns=not significant, Student's t test. Scale bars: 50 µm.

DYRK1A phosphorylates Cyclin D1 in Thr286, a phosphorylation event that promotes Cyclin D1 degradation *via* the ubiquitin-proteasome pathway (Chen et al., 2013b; Najas et al., 2015). Postnatal OPCs express DYRK1A (unpublished data of the group) and there is evidence that Cyclin D1 is necessary for the proliferation of these OPCs (Nobs et al., 2014). Therefore, it is possible that similarly to what occurs in *Dyrk1a*$^{+/-}$ PAX6+ RGs (Najas et al., 2015), *Dyrk1a*$^{+/-}$ OPCs have an excess of nuclear Cyclin D1 and consequently shorter cell cycles. To test for this possibility, we immunostained P10 *Dyrk1a*$^{+/+}$ and *Dyrk1a*$^{+/-}$ brains for Cyclin D1. Nuclear Cyclin D1 labelling indexes in callosal PDGFRα+ OPCs did not shown differences between genotypes (**Fig R.31a,b**). Moreover, *in vivo* labelling of proliferative cells with a short pulse of BrdU showed similar

percentages of cycling oligodendroglial cells (% OLIG2+BrdU+/OLIG2+ cells) in the CC of P10 *Dyrk1a* mutants than in the wild-types (**Fig R.31c-e**). These results suggest that the normalization of OPC numbers in the postnatal *Dyrk1a*$^{+/-}$ CC is likely the result of the developmental plasticity of cells of the oligodendroglial lineage (Bergles and Richardson, 2015) rather than a specific cell cycle defect in these mutant progenitors. Consistently, the neocortex of young adult *Dyrk1a*$^{+/-}$ mice presented normal numbers of oligodendroglial cells (OLIG2+ cells; **Fig R.32**).

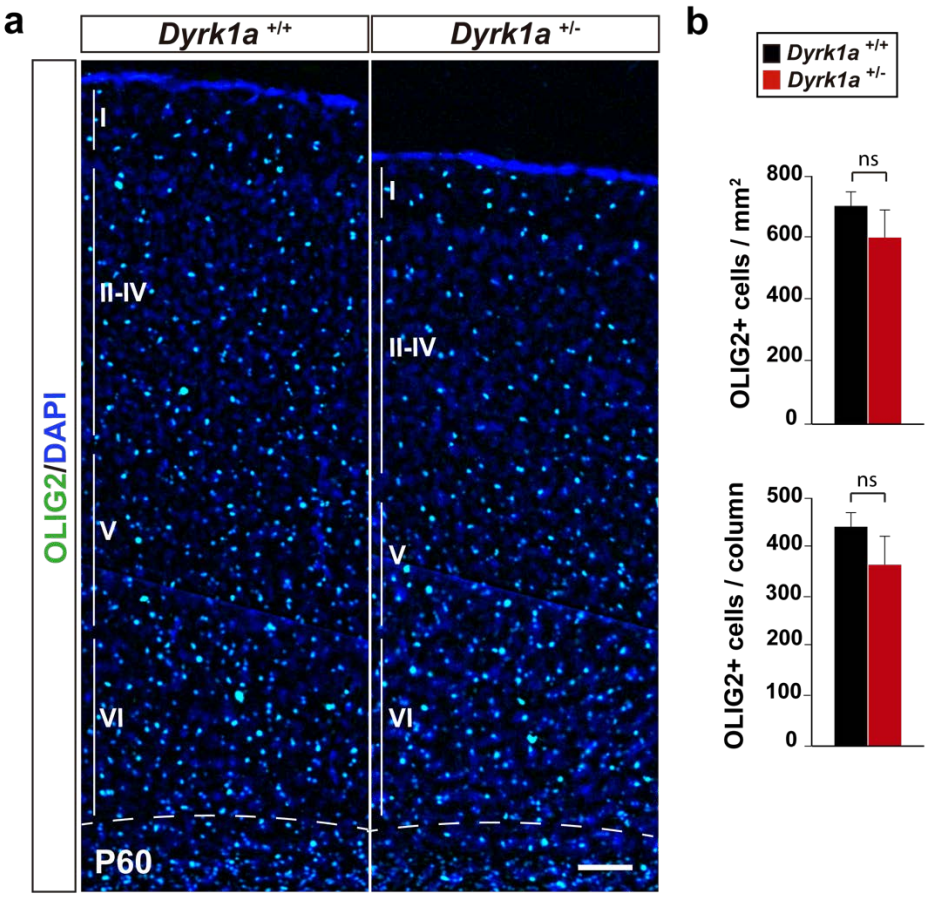


**Figure R.32. Number of oligodendrocytes in the adult *Dyrk1a*$^{+/+}$ and *Dyrk1a*$^{+/-}$ neocortex. (a)** Representative areas from P60 *Dyrk1a*$^{+/+}$ and *Dyrk1a*$^{+/-}$ neocortices immunostained against OLIG2 and the nuclei counterstained with DAPI. Cortical layers are indicated on the left. Scale bar = 100 µm. **(b)** Histograms showing the density of OLIG2+ cells (upper) and the number of these cells in 500 µm-wide columns (lower). Notice that the content of OLIG2+ cells is similar in *Dyrk1a*$^{+/+}$ and *Dyrk1a*$^{+/-}$ neocortices. Values correspond to the mean (S.E.M). n=4-3 animals each genotype. ns=not significant, Student's t-test.

## 2.3. Differentiation of oligodendroglial precursors in the developing *Dyrk1a*$^{+/-}$ cerebral cortex

Next, we examined whether the delay of *Dyrk1a*$^{+/-}$ OPCs in populating the postnatal CC affects the differentiation program of these progenitors. To this end, we immunolabelled P7 brain sections for OLIG2 and the oligodendrocyte marker CC1 (Bhat et al., 1996; see **Fig I.10**). In the wild-types, CC1 expression in the CC progressively decreased from the ventral to the dorsal part of the brain and it was almost undetectable in the CC central region (**Fig R.33a**). The same ventral to dorsal CC1 expression gradient was observed in the CC of *Dyrk1a*$^{+/-}$ mutants but these CCs contained less oligodendrocytes (% of CC1+/total cells and % of CC1+OLIG2+/OLIG2+ cells) than the wild-types (**Fig R.33a,b**). Consistently, at this developmental stage, the area of the *Dyrk1a*$^{+/-}$ CC immunolabelled for MBP was significantly reduced (**Fig R.33c,d**).

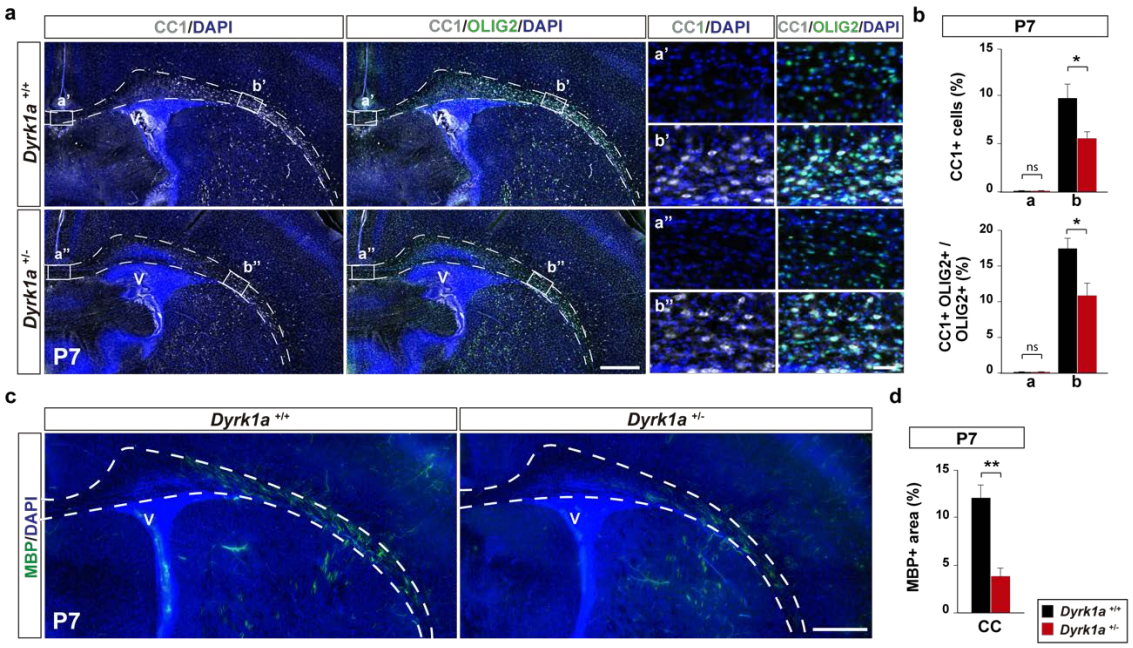


**Figure R.33. Differentiating oligodendrocytes in the corpus callosum of P7 *Dyrk1a*$^{+/+}$ and *Dyrk1a*$^{+/-}$ mice. (a)** Representative coronal brain sections from *Dyrk1a*$^{+/+}$ and *Dyrk1a*$^{+/-}$ animals showing the *corpus callosum* (CC, delimitated by dashed lines) immunostained against CC1 and OLIG2 and the nuclei counterstained with DAPI. Solid squares show the areas where cells were counted and are magnified on the right panels. **(b)** Histograms showing the percentage of CC1+ cells (upper) and the percentage of OLIG2+ cells expressing CC1 (lower) in the areas indicated with boxes in (a). Notice that *Dyrk1a*$^{+/-}$ animals have less CC1+ oligodendrocytes in the lateral CC than control mice. **(c)** Representative coronal brain sections immunostained against MBP and the nuclei counterstained with DAPI. Dashed lines delimitate the area for MBP quantifications. **(d)** Histogram showing the percentage of the CC area labelled with MBP in *Dyrk1a*$^{+/+}$ and *Dyrk1a*$^{+/-}$ sections. Values correspond to the mean (S.E.M). CC1, n= 5-7 animals each genotype; MBP, n=4-5. **p*<0.05, ***p*<0.01, ns=not significant, Students t test. Scale bars: 500 µm (a, c), 50 µm (magnification panel in a). V, ventricle.

CC1+ oligodendrocytes start to populate the central part of the CC around P10 (**Fig R.34a,b**). In both *Dyrk1a*$^{+/+}$ and *Dyrk1a*$^{+/-}$ brains the percentage of callosal differentiated oligodendroglial cells (% CC1+OLIG2+/OLIG2+ cells) similarly increased from P10 to P60 (**Fig R.34c**). These results suggest that the differentiation program in *Dyrk1a* mutant oligodendroglial cells is delayed.

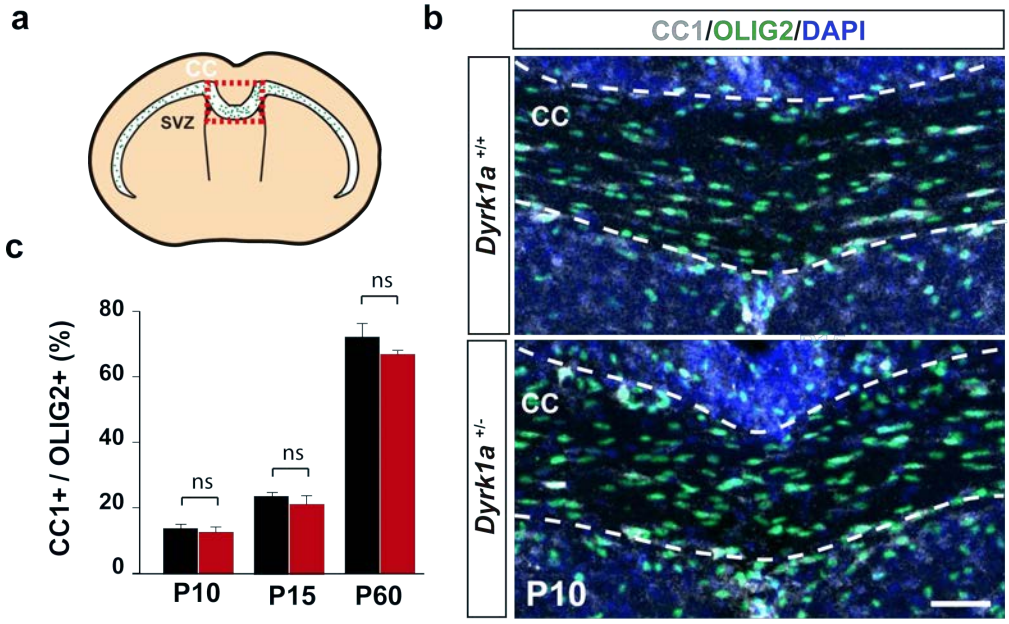


**Figure R.34. Differentiating oligodendrocytes in the postnatal *corpus callosum* of *Dyrk1a*$^{+/+}$ and *Dyrk1a*$^{+/-}$ mice. (a)** Schematic representation of a postnatal brain section. Green dots indicate the OPCs that populate the *corpus callosum* (CC) and the red dashed square the center of the CC where cells were counted. **(b)** Representative images from P10 *Dyrk1a*$^{+/+}$ and *Dyrk1a*$^{+/-}$ CCs immunostained against OLIG2 and CC1 and the nuclei counterstained with DAPI. White dashed lines delimitate the CC. Scale bar: 50 µm. V, ventricle. **(c)** Histogram showing the percentage of OLIG2+ cells immunolabelled for CC1 in the CC of *Dyrk1a*$^{+/+}$ and *Dyrk1a*$^{+/-}$ mice at the indicated developmental stages. Values correspond to the mean (S.E.M). P10, n= 7-8 animals each genotype; P15, n= 6-4; P60, n=6. Differences between genotypes are not significant, Student's t test, in any of the developmental stages.

Next, we asked whether *Dyrk1a*$^{+/-}$ pre-myelinating oligodendrocytes differentiate into normal myelin-forming oligodendrocytes. Since the most active phase of callosal myelination in the mouse brain takes place between P14 and P45 (Sturrock, 1980), we first checked the expression of the myelin proteins MBP, MAG (Myelin Associated Glycoprotein) and PLP and in the cerebral cortex of *Dyrk1a*$^{+/-}$ mice at the onset and mid-stage of this phase. In the cerebral cortex of P16 and P28 *Dyrk1a*$^{+/-}$ mice, the expression of *Mbp*, *Mag* and *Plp* genes was similar than in the wild-types (**Fig R.35a**). In line, we did not find differences between genotypes when relative levels of MBPs isoforms and PLP

were measured by immunobloting at P19 (**Fig R.35**). Thus, the expression of myelin proteins in *Dyrk1a*$^{+/-}$ brains at the onset of myelination is not significantly affected.

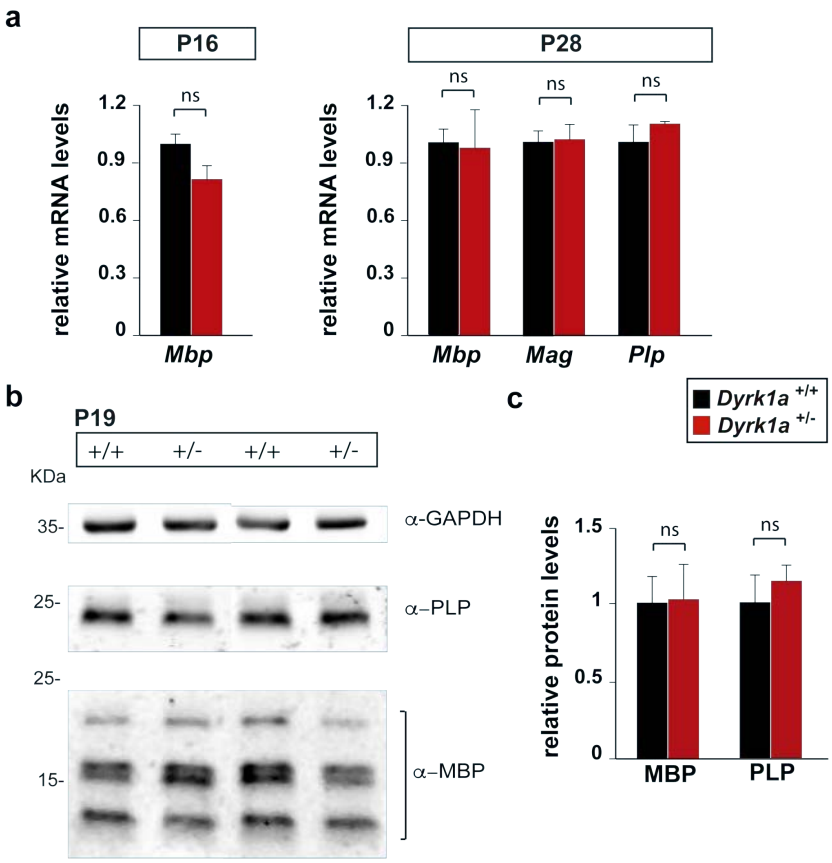


**Figure R.35. Expression of myelin proteins in the postnatal *Dyrk1a*$^{+/+}$ and *Dyrk1a*$^{+/-}$ cerebral cortex. (a)** Relative mRNA levels for *Mbp*, *Mag* and *Plp* at the indicated stages in *Dyrk1a*$^{+/+}$ and *Dyrk1a*$^{+/-}$ samples. *Ppia* was used as a reference gene. **(b)** Representative immunoblot of extracts prepared from P19 *Dyrk1a*$^{+/+}$ and *Dyrk1a*$^{+/-}$ cerebral cortices and probed with the indicated antibodies. **(c)** Histogram showing MBP and PLP protein levels in *Dyrk1a*$^{+/+}$ and *Dyrk1a*$^{+/-}$ samples. Values are normalized to GAPDH levels and correspond to the mean (S.E.M) expressed relative to wild-type values arbitrary set as 1. n=3 animals each genotype. ns= not significant, Student's t test.

Next, we used transmission electron microscopy to analyse the myelin sheaths in the CC of P19 *Dyrk1a*$^{+/-}$ and wild-type littermates. In both genotypes, the percentage of myelinated axons was similar with values (*Dyrk1a*$^{+/+}$, 6.6±0.8%; *Dyrk1a*$^{+/-}$, 4.7±0.9%; **Fig R.36a,b**) that are consistent with published data (Sturrock, 1980). The densities of unmyelinated and myelinated axons were also similar in the two genotypes (**Fig R.36a,b**), but the myelinated mutant axons showed smaller diameters (calibres) and smaller G-ratios (axon diameter/fiber diameter; **Fig R.36c,d**). In the adult *Dyrk1a*$^{+/-}$ brains, myelinated axons of the CC also have smaller diameters but the G-ratios are

normal and the proportion of myelinated axons is decreased (Balducci, 2012 and unpublished data of the group). As oligodendrocytes myelinate axons above a certain diameter and signals from the axon are key for myelination (Bradl and Lassmann, 2010), it is likely that differences in the neuron population largely contribute to the callosal phenotype just described.

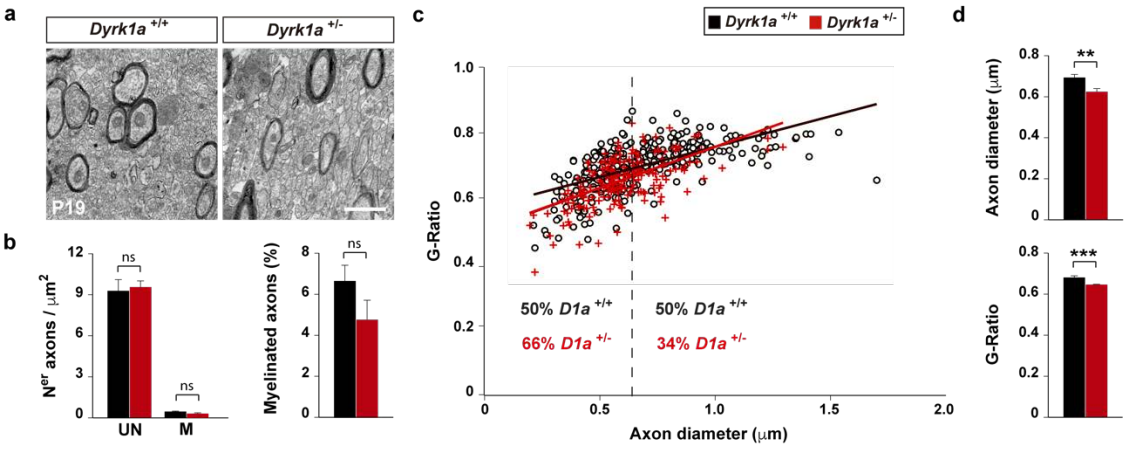


**Figure R.36. Myelination of the *corpus callosum* in P19 *Dyrk1a*$^{+/+}$ and *Dyrk1a*$^{+/-}$ mice. (a)** Representative electron micrographs of transverse sections of the *Dyrk1a*$^{+/+}$ and *Dyrk1a*$^{+/-}$*corpus callosum* (CC). Scale bar: 1 µm. **(b)** Histograms showing the density of myelinated (M) and unmyelinated (UM) axons (left) and the percentage of myelinated axons (right). Values are the mean (S.E.M). **(c)** Scattered plot of g-ratios of individual fibers relative to their respective axon diameter. The dashed line indicates the mean value for *Dyrk1a*$^{+/+}$ axon diameter and the numbers at both sides of this line the percentage of axons bellow (left) or above (right) this mean value for each genotype. **(d)** Histograms showing the mean diameter (upper) and mean g-ratio (lower) for CC axons in *Dyrk1a*$^{+/+}$ and *Dyrk1a*$^{+/-}$ mice. Histogram values correspond to the mean (S.E.M). b, n= 3-2 animals each genotype; c-d, n=398-200 axons from 3-2 animals each genotype. ***p*<0.01, ***p*<0.001, ns=not significant, Student's t test.

## 2.4. Myelin characteristics in the adult *Dyrk1a*$^{+/-}$ cerebral cortex

To further characterize the phenotype of the myelinated axons in *Dyrk1a*$^{+/-}$ brains we looked for possible differences in the expression of the two main myelin proteins, MBP and PLP, in the adult CNS. As shown in **Fig R.37a**, the expression of *Mbp* and *Plp* genes in the cerebral cortex of adult *Dyrk1a*$^{+/-}$ mice was similar to the wild-types, and the levels of the different MBP isoforms in the mutants were also normal. However, the levels of PLP were significantly augmented in the mutant cortices (**Fig R.36b,c**). This result suggests that the biogenesis of PLP and/or its transport to the myelin sheath in *Dyrk1a*$^{+/-}$ oligodendrocytes is impaired.

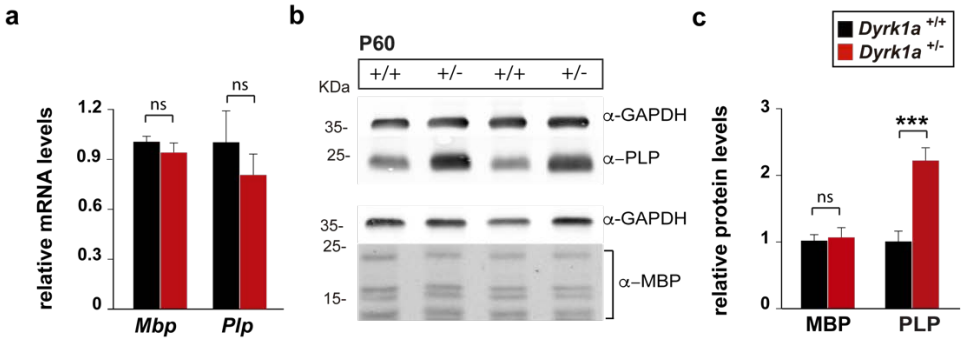


**Figure R.37. Expression of myelin proteins in the adult *Dyrk1a*$^{+/+}$ and *Dyrk1a*$^{+/-}$ cerebral cortex. (a)** Relative mRNA levels for *Mbp* and *Plp* at P60 in *Dyrk1a*$^{+/+}$ and *Dyrk1a*$^{+/-}$ samples. *Ppia* was used as a reference gene. Differences between genotypes are not statistically significant, Student's t test**. (b)** Representative immunoblots of extracts prepared from P60 *Dyrk1a*$^{+/+}$ and *Dyrk1a*$^{+/-}$ cerebral cortices and probed with the indicated antibodies. **(c)** Histogram shows MBP and PLP protein levels in the P60 *Dyrk1a*$^{+/+}$ and *Dyrk1a*$^{+/-}$ cerebral cortices. Values are normalized to GAPDH protein levels and correspond to the mean (S.E.M) expressed relative to wild-type values arbitrary set as 1. Notice the increased levels of PLP protein in the cerebral cortex of *Dyrk1a*$^{+/-}$ mice. a, n=3 animals each genotype; MBP, n=7-8 each genotype; PLP, n=11 each genotype. ****p*<0.001, ns= not significant, Student's t test.

Deficits in oligodendrocyte maturation and myelination may lead to impaired formation of the nodes of Ranvier (Ulzheimer et al., 2004; Tanaka et al., 2009; Ritter et al., 2013), therefore we immunostained adult *Dyrk1a*$^{+/+}$ and *Dyrk1a*$^{+/-}$ brain sections for the voltage-gated sodium channel $Na_v1.6$ (NAV1.6), the major sodium channel isoform at node of Ranvier (Caldwell et al., 2000), and for CASPR (Contactin-Associated Protein 1), which marks the paranode region (Rios et al., 2000). Quantifications of the nodes of Ranvier in the CC of these animals did not show differences between genotypes in node of Ranvier densities (**Fig R.38a,b**). However, the immunolabelled nodes were shorter in *Dyrk1a*$^{+/-}$ mice than in control ones (**Fig R.38c-d**). The measurement of the intraparanodal distance confirmed that the mutant nodes were shorter than the controls (**Fig R.38c,e**). Moreover, average NAV1.6 labelling index in the mutant nodes was significantly diminished (**Fig R.38f**), suggesting that these nodes have less NAV1.6 sodium channels.

The overexpression of PLP in humans causes a dysmyelinating disorder (Pelizaeus-Merzbacher disease; (Garbern et al., 1999) and premature oligodendrocyte cell death in the mouse (Kagawa et al., 1994). On the other hand, there is evidence that structural changes at the node of Ranvier and altered functions of proteins at this site, including the voltage-gated sodium channel $Na_v1.6$, are important players in neurological disorders such as autism and epilepsy syndromes (Arancibia-Carcamo and Attwell, 2014). Therefore, it is possible that the excess of PLP and the alterations at the node of

Ranvier detected in the neocortex of adult *Dyrk1a*$^{+/-}$ mice contribute to some of the neurological phenotypes in *DYRK1A* haploinsufficiency syndrome.

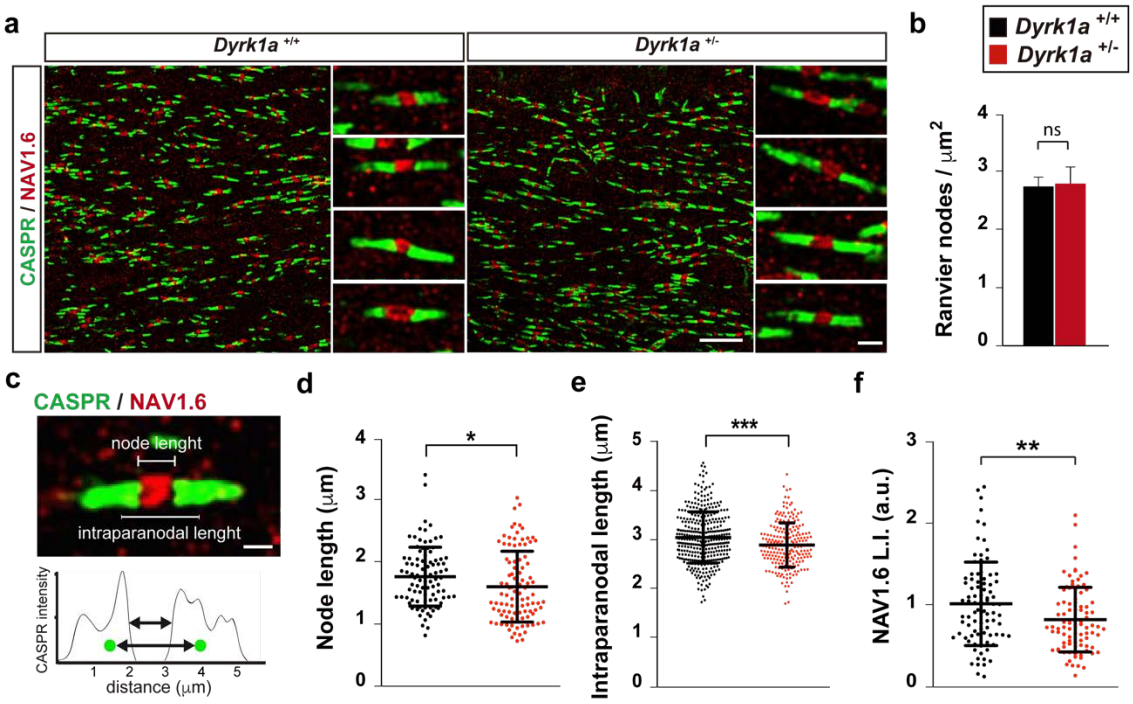


**Figure R.38. Nodes of Ranvier in the corpus callosum of *Dyrk1a*$^{+/+}$ and *Dyrk1a*$^{+/-}$ adult mice.** **(a)** Representative images showing nodes of Ranvier in the *Dyrk1a*$^{+/+}$ and *Dyrk1a*$^{+/-}$ *corpus callosum* (CC). Nodes are labelled with NAV1.6 antibodies and paranodes with CASPR antibodies. Some of the nodes are magnified in the right panels. **(b)** Histogram shows the density of nodes of Ranvier. Values correspond to the mean (S.E.M). n=5-4 animals each genotype. ns= not significant, Student's t test. **(c)** Confocal image showing a single node of Ranvier and the intensity profile of CASPR immunostaining at the paranodes. Arrows indicate the distances measured in the intensity profile to determine node length (d) and intraparanodal length (e). Green dots in the intensity profile represent the centre of masses for each paranode as determined by 3D object reconstruction. Scale bar: 10 µm, 1 µm (magnifications in a and c). **(d, e)** Scatter dot plot showing node length (d) and intraparanodal length (f) values for individual nodes of Ranvier in *Dyrk1a*$^{+/+}$ and *Dyrk1a*$^{+/-}$ CCs. **(f)** Scatter dot plot showing NAV1.6 labeling index (L.I.) values for individual nodes of Ranvier normalized to the mean *Dyrk1a*$^{+/+}$ value arbitrary set to 1. Bars show mean (S.D). Node length, n= 95-100 nodes; intraparanodal length, n=356-217 nodes; NAV1.6 L.I., n=88-90 nodes. *Dyrk1a*$^{+/+}$, n=3; *Dyrk1a*$^{+/-}$, n=2. *$p$<0.05; **$p$<0.01; **$p$<0.001, Welch's test.

## 2.5. Differentiation of adult *Dyrk1a*$^{+/-}$ callosal oligodendroglial precursors induced by focal demyelination

The defects in the differentiation program of *Dyrk1a*$^{+/-}$ mutant OPCs described above may, at least in part, result from the decreased levels of DYRK1A protein in these progenitors. Given that brain OPCs continue to express DYRK1A in the adulthood (see

**Fig R.39** for the expression of DYRK1A in adult callosal OPC immunolabelled for NG2), we used a model of focal demyelination in adult *Dyrk1a*$^{+/-}$ mice and their wild-type littermates to evaluate the differentiation capability of the OPCs. Demyelinating lesions were induced by injecting the toxin LPC into the CC and mice were sacrificed at different DPL (see schedule of the experiment in **Fig R.40a**). In this model, the demyelinating lesion induces the proliferation of OPCs in the surrounding parenchyma. These OPCs then migrate to the lesion (see the increased cell densities of the demyelinated CC in LPC-injected animals compared with SHAM animals 5 DPL; **Fig R.40b,c**) where they differentiate into mature oligodendrocytes.

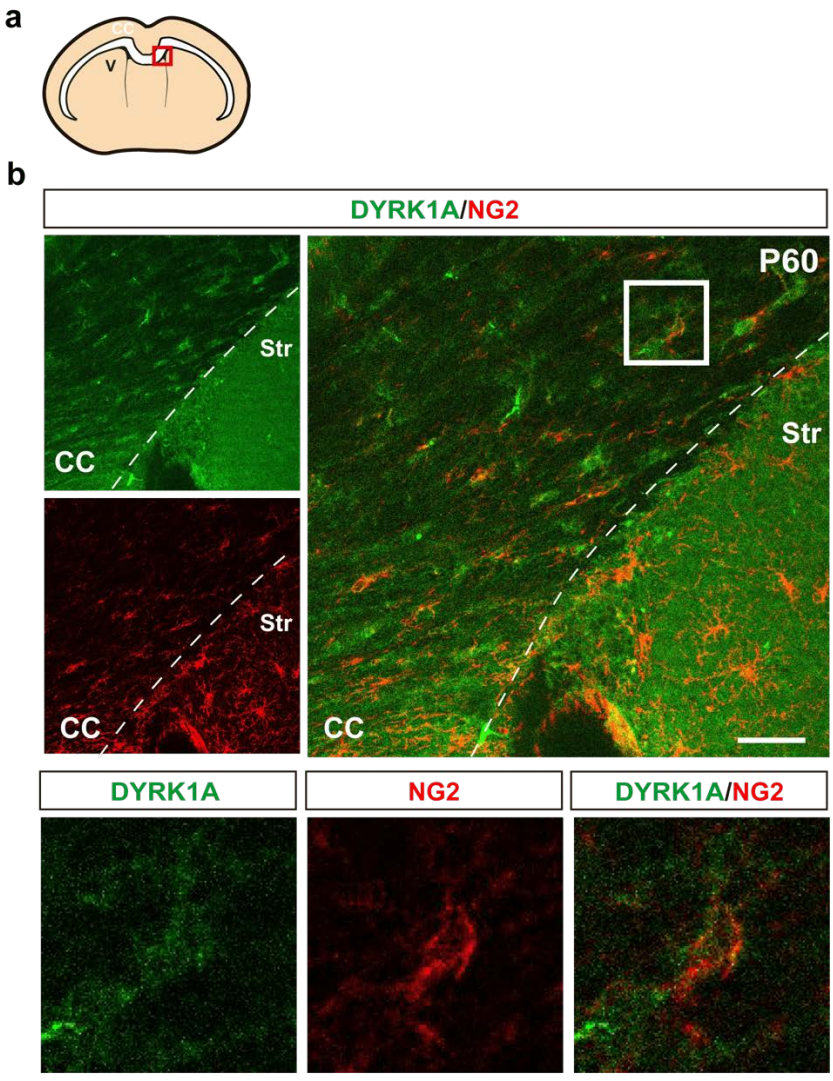


**Figure R.39. Expression of DYRK1A in adult OPCs. (a)** Schematic representation of a coronal section from an adult mouse brain. Red square indicates the area of the corpus callosum (CC) shown in (b). **(b)** Representative image from a wild-type brain immunostained against NG2 and DYRK1A. Dashed line indicates the limit between the CC and the striatum (Str). The lower panels show a magnification of the boxed region. Notice that NG2+ OPCs express DYRK1A. Scale bar: 50 µm.

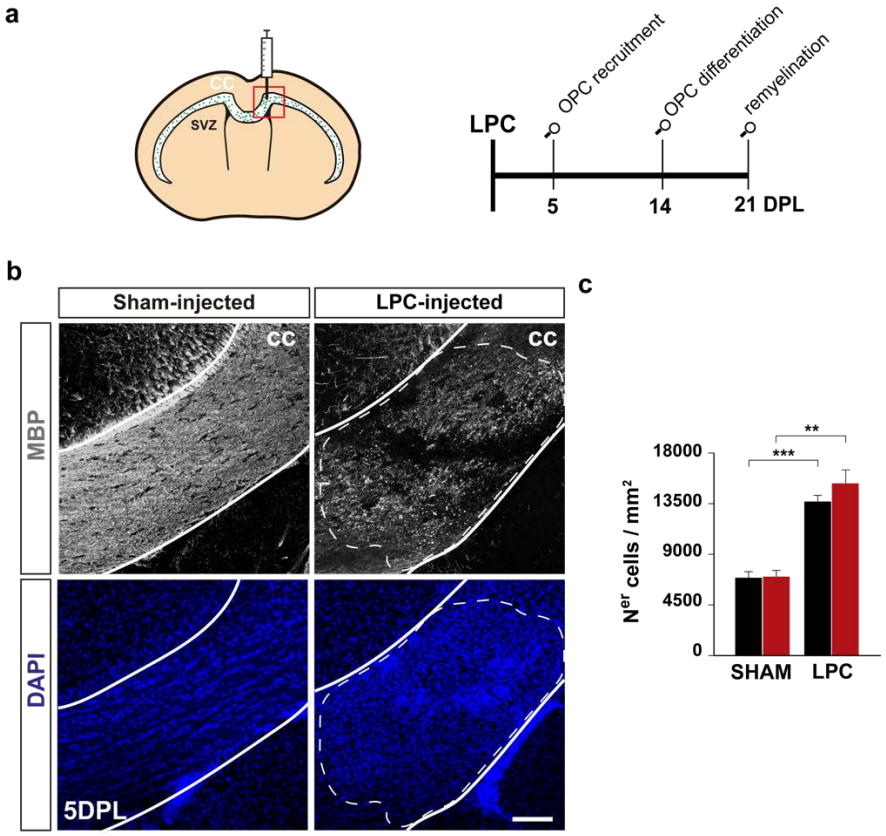


**Figure R.40. Lysolecithin-induced focal demyelination model. (a)** Schematic representation of a coronal section from the adult brain (left) and schedule of the measurements performed in brain sections after lysolecithin (LPC) injections (right). Green dots represent oligodendrocytes populating the corpus callosum (CC) and the red square indicates the region of the CC where LPC was injected. DPL, day post-lesion. **(b)** Representative images from sham saline- and LPC-injected *Dyrk1a*$^{+/+}$ CC at 5 DPL immunostained against MBP and the nuclei counterstained with DAPI. White solid lines delimitate the CC. Dashed lines show the boundaries of the LPC lesion. Notice that the LPC-injected brain shows depletion of MBP staining and increased cell density compared to the sham-injected brain. Scale bar: 100 µm. **(c)** Histogram showing the cell density in the sham- and LPC-injected *Dyrk1a*$^{+/+}$ and *Dyrk1a*$^{+/-}$ CCs at 5 DPL. We used two-way ANOVA to analyze possible interaction between treatment and genotype and found that the effect of the LPC injection in cellular density is not significantly different between genotypes ($p>0.35$, Two-way ANOVA with Bonferrori post-hoc test). Values correspond to the mean (S.E.M). Sham, n=5-3 animals each genotype; LPC, n=10-6 each genotype. $^{**}p<0.01$, $^{***}p<0.001$, Student's t test.

*Dyrk1a*$^{+/-}$ neocortices showed similar densities of OPCs (OLIG2+CC1- cells) than their wild-type littermates (*Dyrk1a*$^{+/+}$, 152.5±13.0 cells/mm$^2$; *Dyrk1a*$^{+/-}$, 162.8±40.0 cells/mm$^2$; Student t-test=0.76). Therefore, we can compare the proliferation and differentiation capacities of *Dyrk1a*$^{+/-}$ and wild-type OPCs by analysing their recruitment within the demyelinated areas and how they proliferate and differentiate using cell markers. In both genotypes there were many OLIG2+ cells in the demyelinated area of the CC at 5 DPL, but the density of these cells was augmented in *Dyrk1a*$^{+/-}$ mutant animals (**Fig R.41a,b**). We detected few OLIG2+ cells expressing the differentiation marker CC1 in both

*Dyrk1a*$^{+/+}$ and *Dyrk1a*$^{+/-}$ LPC-treated sections (data not shown). Moreover, in both genotypes the density of cells that expressed the OPC marker NG2 was significantly higher in LPC-treated animals than in the SHAM condition (**Fig R.41c**). As with the OLIG2+ cells, the density of NG2+ OPCs in the demyelinated area was augmented in *Dyrk1a*$^{+/-}$ mutant animals (**Fig R. 41a,c**). These results suggest that mutant OPCs arrived faster to the injured area and/or they over proliferate.

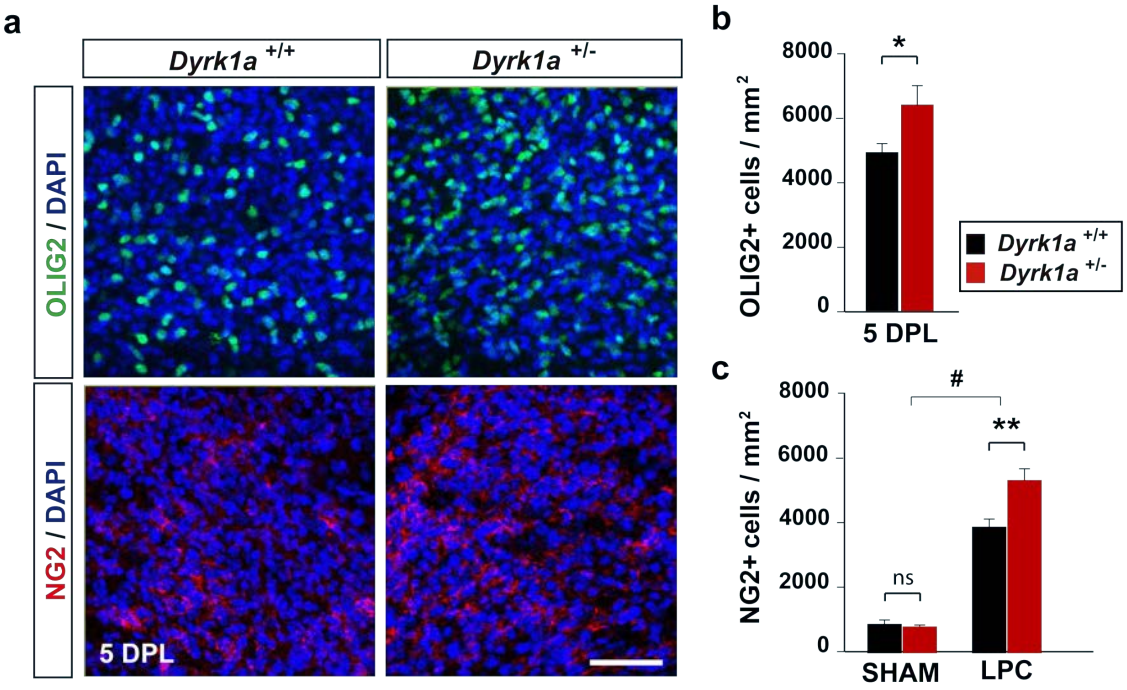


**Figure R.41. Recruitment of OPCs in the demyelinated corpus callosum of *Dyrk1a*$^{+/+}$ and *Dyrk1a*$^{+/-}$ mice. (a)** Representative images from sections immunostained against NG2 and OLIG2 and the nuclei counterstained with DAPI showing the lesion site at 5 days post-lesion (DPL). **(b)** Histogram showing the density of NG2+ OPCs in the sham- and LPC-injected *Dyrk1a*$^{+/+}$ and *Dyrk1a*$^{+/-}$ mice. Notice that recruitment of NG2+ OPCs is enhanced in the lesion site of the *Dyrk1a*$^{+/-}$ CC and that the effect of the LPC injection in NG2 density is significantly different between genotypes (# $p<0.05$, Two-way ANOVA with Bonferroni post-hoc test). **(c)** Histogram showing the density of OLIG2+ cells in the lesion site at 5 DPL. Values correspond to the mean (S.E.M). NG2, sham, n=6-3 animals each genotype; LPC, n=10-5 each genotype. OLIG2, n=4-7 each genotype. *$p<0.05$, **$p<0.01$, Student's t test. Scale bar: 50 µm.

Next, we asked for the differentiation program of the OPCs that were recruited to the injured area. To this end, we immunostained LPS-treated brain sections for OLIG2 and CC1 at 14 DPL. In contrast to the analysis performed at 5 DPL, we did not find differences between *Dyrk1a*$^{+/+}$ and *Dyrk1a*$^{+/-}$ section in the density of OLIG2+ cells nor in the percentage of postmitotic OLIG2+ cells (% of CC1+OLIG2+/OLIG2+ cells; **Fig R.42a,b**), suggesting that part of the recruited OPCs in the mutant condition detected 5 DPL could not differentiate, and consequently died by apoptosis, or proliferate at rates lower than

in the wild-types. Therefore, we labelled with BrdU the proliferative OPCs of demyelinated animals (see schedule of BrdU injections in **Fig R.42c**) and counted the BrdU+ oligodendroglial cells (OLIG2+ cells) and the BrdU+ cells that expressed the marker CC1 at 14 DPL. BrdU-labelled OPCs generated similar numbers of oligodendroglial cells (BrdU+OLIG2+ cells) and similar numbers of oligodendrocytes (BrdU+OLIG2+CC1+ cells) in the two genotypes, suggesting that the OPCs that migrated into the lesion in the mutants proliferate and differentiate normally. The fact that there were not differences between genotypes in the numbers of cells that expressed active Caspase-3 at 14 DPL (*Dyrk1a*$^{+/+}$, 17.8±5.6 cells/mm$^2$; *Dyrk1a*$^{+/-}$, 26.8±11.6 cells/mm$^2$, Student t-test=0.48), indicates that mutant OPCs that did not differentiate died before that stage.

Finally, we injected the demyelinating toxin in another set of *Dyrk1a*$^{+/-}$ animals and their wild-type littermates to evaluate the capacity of the mutant oligodendrocytes to fully differentiate into myelin-forming cells. In this experiment, animals were sacrificed 21 DPL and the presence of myelin-forming oligodendrocytes in the demyelinated CC evaluated by MBP immunostaining and by LFB staining, to label the phospholipids in the myelin sheaths. Both genotypes showed similar MBP and LFB staining patterns, which covered similar percentage of the total injured area, around 80% and 60%, respectively (**Fig R.43**).

Collectively, the results obtained in the LPC-induced re-myelination model indicate that *Dyrk1a*$^{+/-}$ OPCs are able to proliferate and differentiate normally. Therefore, these results support the hypothesis that the oligodendroglial phenotype in the *Dyrk1a*$^{+/-}$ haploinsufficient model described above results from a developmental defect in the production of OPCs and from the alterations that these mutants show in the neuron and astroglial populations.

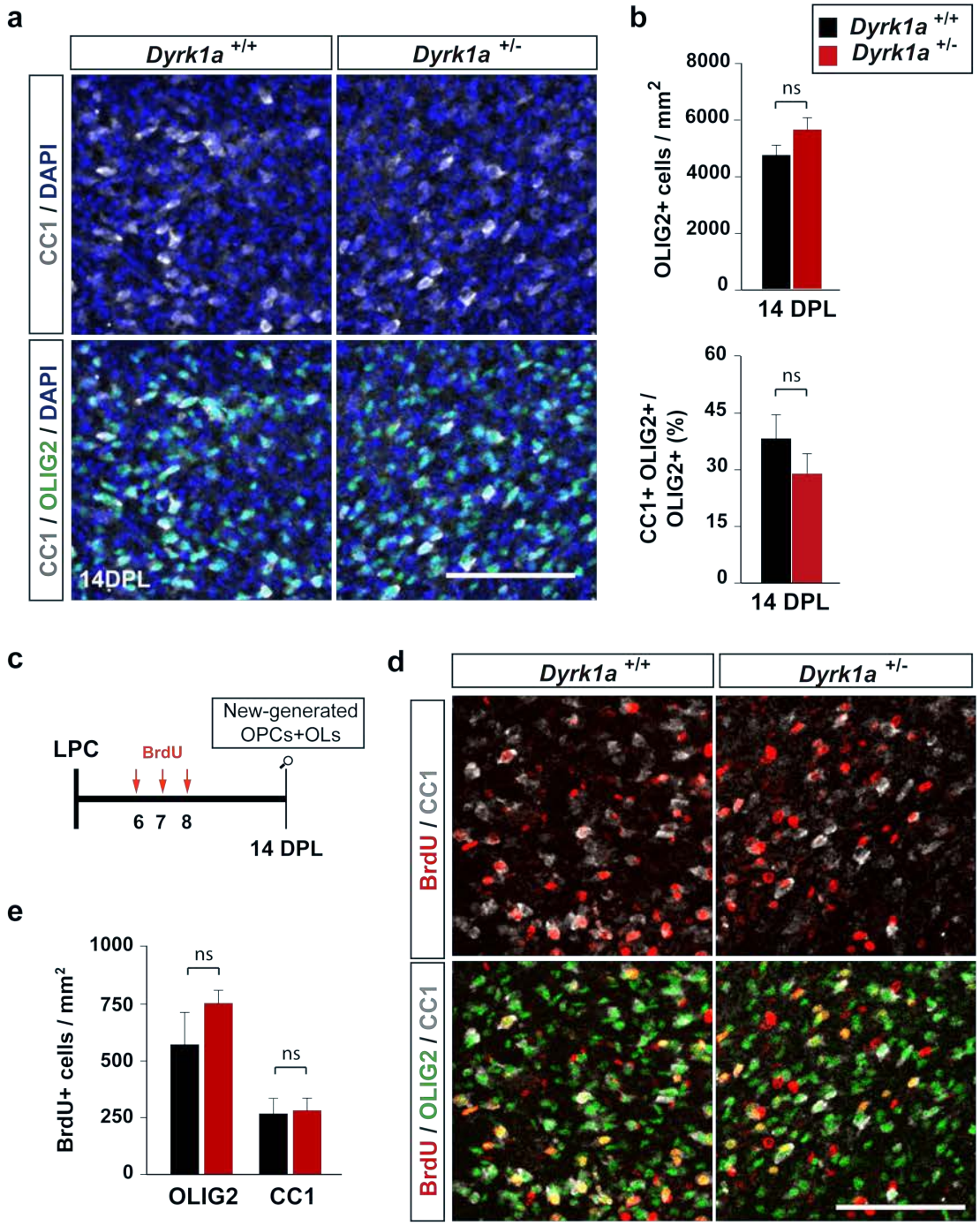


**Figure R.42. Differentiated oligodendrocytes in the demyelinated corpus callosum of *Dyrk1a*$^{+/+}$ and *Dyrk1a*$^{+/-}$ mice 14 days post-lesion.** **(a)** Representative images from the lesion site of sections immunostained against CC1 and OLIG2 and the nuclei counterstained with DAPI. **(b)** Histograms showing the density of OLIG2+ cells (upper) and the percentage of OLIG2+ cells that express CC1 (lower) in the lesion site. **(c)** Schedule of the BrdU-labeling protocol used to label OPC proliferation in response to the lesion. **(d)** Representative images from the lesion site of sections immunostained against BrdU, OLIG2 and CC1. **(e)** Histograms showing the density of BrdU+ cells that express OLIG2 (all the cells from the oligodendroglial lineage, upper) and the percentage of OLIG2+ expressing CC1 (oligodendrocytes, lower). Values are the mean (S.E.M). OLIG2, CC1, BrdU n=8-4 animals each genotype; ns=not significant, Student's t test. Scale bars: 50 µm.

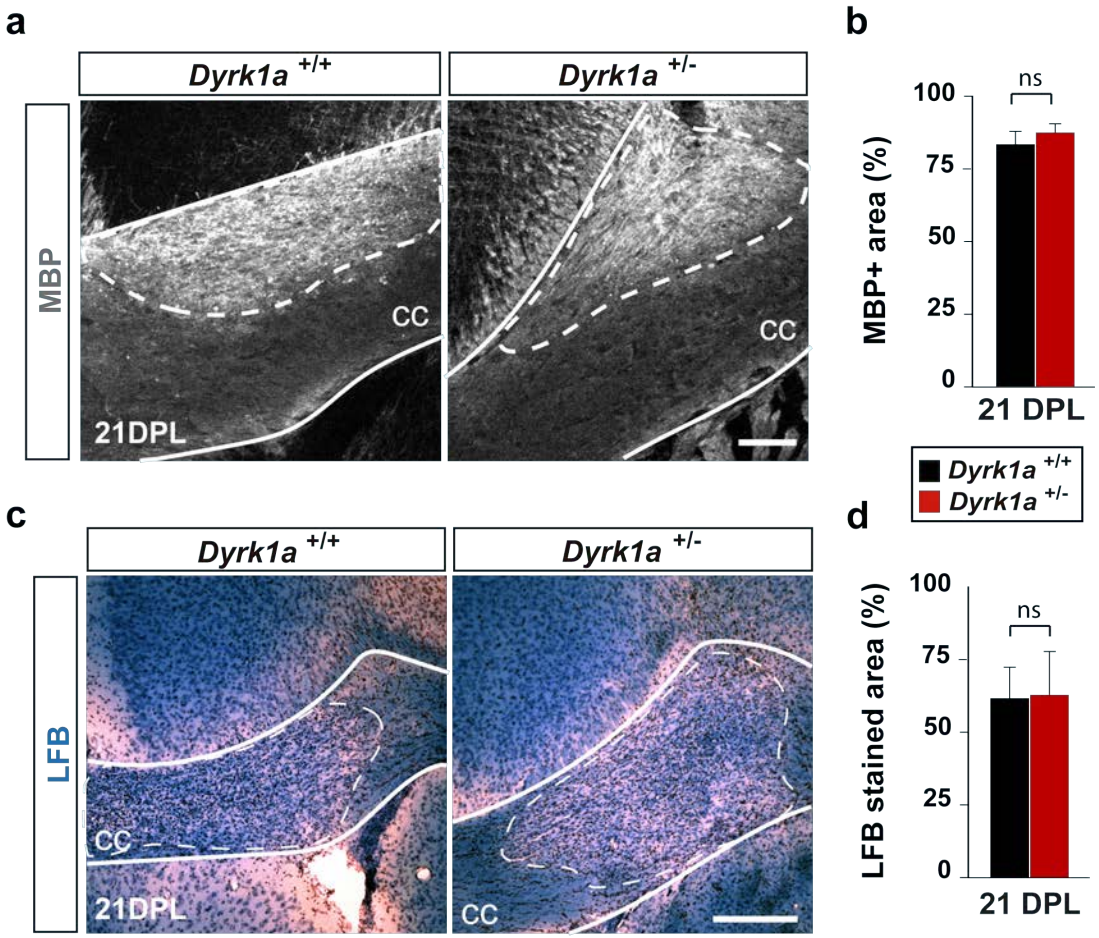


**Figure R.43. Remyelination of the *Dyrk1a*$^{+/+}$ and *Dyrk1a*$^{+/-}$ corpus callosum 21 days post-lesion. (a, c)** Representative images from the corpus callosum (CC) immunostained for MBP (a) or stained with Luxol Fast Blue (LFB, c). White solid lines delimitate the CC and the dashed lines show the boundaries of the LPC lesion. Nuclei in (c) are counterstained with cresyl violet. Scale bars: 100 µm. **(b, d)** Histograms showing the percentage of the injured area immunostained for MBP (b) or labeled with LFB (d). Values are the mean (S.E.M). MBP, n=5-4 animals each genotype; LFB, n=4-3 each genotype. ns=not significant, Student's t test.

# DISCUSSION

## 1. Gene expression changes in radial glial cells during neurogenesis

Although the cellular processes involved in cortical neurogenesis have been particularly studied, the knowledge about the gene networks underling these processes is still limited. Here we show that during neurogenesis (from E11.5 to E15.5) the expression of protein-coding genes, alternative-spliced mRNAs and miRNAs substantially changes. Around 25% of the protein-coding genes show differential expression levels between E11.5 and E15.5, and 25% of them are putatively regulated at the post-transcriptional level by miRNAs. Moreover, AS regulation affects almost 20% of the expressed protein-coding genes. Notably, there is little overlap between the genes regulated by AS and the genes regulated at the transcriptional level and by miRNAs (see summary of the RNA-seq data in **Fig D.1**).

These extensive changes in expression were in a way anticipated considering that during embryonic development, RGs experience important changes in morphology, cell cycle parameters and mode of division, and produce daughters that acquire different morphologies, layer position and express different sets of genes (Martynoga et al., 2012; Florio and Huttner, 2014).

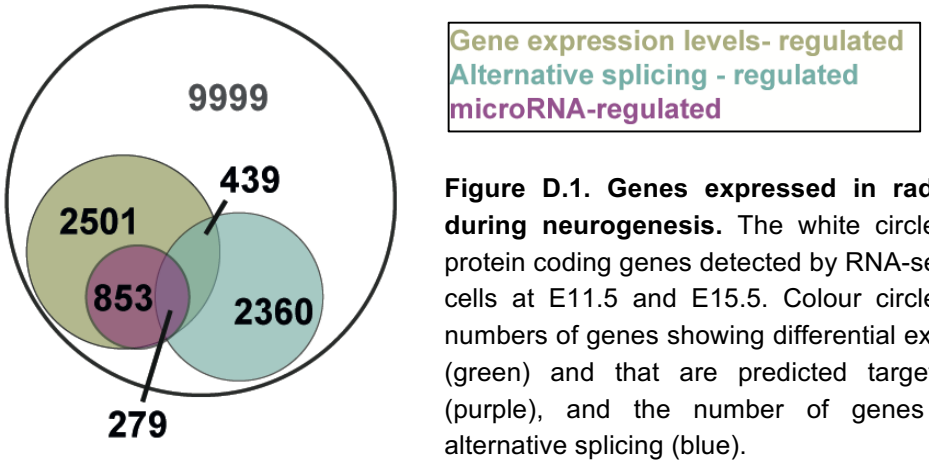


**Figure D.1. Genes expressed in radial glial cells during neurogenesis.** The white circle indicates the protein coding genes detected by RNA-seq in radial glial cells at E11.5 and E15.5. Colour circles indicate the numbers of genes showing differential expression levels (green) and that are predicted targets of miRNAs (purple), and the number of genes regulated by alternative splicing (blue).

To the best of our knowledge, this study is the first to integrate such a comprehensive information about the coordinated regulation of coding genes, miRNAs and AS events in cortical RGs during the progression of neurogenesis. Overall, we have generated a large gene expression database that can be useful for the study of genetic networks and their regulation during neurogenesis.

## 1.1. Cell cycle

We have shown that genes with lower expression levels at E15.5 than at E11.5 are mainly associated to cell cycle (see Fig R.4). Cell cycle parameters in RGs are highly regulated. For instance, the duration of the cell cycle increases dramatically from E11 (~8h) to E15 (~17.5h) mainly due to the lengthening of the G1 phase (Takahashi et al., 1995; Calegari et al., 2005). Moreover, RGs undergoing proliferative divisions have longer S phases than those undergoing asymmetric neurogenic divisions (Arai et al., 2011). Like other progenitors, the decision of a RG to proliferate or exit the cell cycle to become a neuron is taken at G1 (Dehay and Kennedy, 2007). To proliferate, cells must overcome the check point at the G1/S transition, which requires the sequential activation of cyclin-dependent kinases (CDKs) and their associated cyclins (Cooper and Hausman, 2009). The overexpression of CDK4/6 or their partner cyclin D1 in RGs shortens G1 phase, speeding up the cell cycle and increasing the symmetric proliferative divisions, which results in the expansion of the RG pool (Lange et al., 2009; Pilaz et al., 2009). These observations indicate a correlation between the duration of the cell cycle phase G1 and the mode of RG divisions. In line with these observations, we found that the expression of cyclins, CDKs and several components of the E2F family of TFs, which are part of the CDK4/6-cyclin D pathway and activate the transcription of genes important for the progression of the cell cycle (Duronio and Xiong, 2013), is higher at E11.5, when RGs proliferate fast and self-renewal divisions are abundant, than at E15.5 when these divisions diminish.

In addition to genes involved in the regulation of cell cycle progression, we found several down-regulated genes that are components of the DNA replication (*Pcna*, *Orc1*, *Rfc1*/3, *Gns1*-3, etc.) or DNA repair (*Brca1*/2, *Msh6*, etc.) machineries. DNA replication and repair occur during S-phase. DNA replication is a primary source of DNA damage during neurogenesis and higher replicative rates entail larger DNA damage. Therefore, the concomitant down-regulation of DNA replication and repair genes is consistent with the fact that the requirement for DNA repair decreases as the replicative rate reduces during neurogenesis (McKinnon, 2013). Since errors in the DNA sequence in postmitotic cells would be less deleterious than in cycling progenitors, this also provides an explanation for the shorter S-phase duration of progenitors exiting the cell cycle (Arai et al., 2011), which may expend less time repairing (McKinnon, 2013).

One of the top enriched categories that came up from the functional analysis of the differentially expressed genes is WNT signalling (see Fig R.3). WNT/β-Catenin signalling promotes cell cycle progression through transcriptional up-regulation of target genes

such as those encoding Cyclin D proteins and c-Myc (Niehrs and Acebron, 2012). Moreover, many evidences indicate that beyond its role in transcriptional activation, this signalling pathway plays other roles in the mitotic cycle, for example in the positioning of the mitotic spindle and centrosomal separation at the onset of spindle formation (Bryja et al., 2017). There is evidence that WNT signalling also plays an important role in the decision of RGs to proliferate or differentiate. For example, the constitutive activation of the WNT pathway in early cortical progenitors results in a gross expansion of the cortical surface area due to a decreased cell cycle exit (Chenn and Walsh, 2002). Conversely, conditional deletion of β-Catenin from these progenitors leads to a premature cell cycle exit and differentiation (Woodhead et al., 2006). According to the proliferative role of WNT/β-Catenin signalling in RGs, we found that the main transcriptional effector genes of the pathway (*Lef1*, *Tcf7*, *Tcf7l1* and *Tcf7l2*) and several WNT receptors (*Fzd4*, *Fzd5*, *Fzd6*, *Fzd8*, *Fzd10*) are down-regulated during development. Consistent with the relevant role that it plays during neurogenesis, defects in different components of the WNT signalling have been strongly implicated in autism and intellectual disability (Krumm et al., 2014; Kwan et al., 2016).

miRNAs have important roles in regulating stem cell self-renewal and differentiation (Gangaraju and Lin, 2009). There is evidence that some miRNAs control this balance by targeting the cell cycle machinery (Wang and Blelloch, 2011; Shim and Nam, 2016). In embryonic stem cells (ESCs), *mir*-290 and *mir*-302 clusters promote G1/S phase transition by targeting repressors of the CDK2-Cyclin E axis (Wang and Blelloch, 2011). In accordance, we found that members of the *mir*-290 clusters (*mir*-295 and *mir*-293) and *mir*-302 cluster (*mir*-302a, *mir*-302b, *mir*-302d and *mir*-367) are among the most down-regulated miRNAs between E11.5 and E15.5, a period in which the G1 phase in these cells is significantly enlarged (see Annex 2, Table 1). This observation indicates that in rapidly dividing stem cells these two miRNA clusters promote G1/S phase transition, thereby maintaining their high proliferative rates. On the contrary, let-7 miRNAs in NSCs accumulate as neurogenesis advances (Wulczyn et al., 2007; Zhao et al., 2010; Ni et al., 2014) targeting regulators of cell cycle progression such as Cyclin D1, *Hmga2* and *Tlx*, thereby promoting cell cycle exit and neuronal differentiation (Zhao et al., 2010; Zhao et al., 2013; Xia and Ahmad, 2016). In agreement with this, we found up-regulation of all let-7 miRNAs in E15.5 RGs and a concomitant down-regulation of Cyclin D1, *Hmga2* and other let-7 targets (see Annex 2, Table 2). These targets and the targets of other up-regulated miRNAs at E15.5 (miR-212-5p, miR-128-3p, miR-144-3p and the miRNAs of the cluster *mir*-212/132) form a protein-protein interaction network of DNA-binding proteins involved in pluripotency pathways (see networks in Fig R.10 and

Fig R.11). Remarkably, Cyclin D1 is the most connected protein in the network, which includes several E2Fs (E2F2/3/5/6/7/8) and WNT effectors (LEF1, TCF7L1, TCF7L2). This predicted miRNA:mRNA interaction network highlights the importance of miRNA regulation for RG differentiation during neurogenesis.

## 1.2. Electrical activity

Quite unexpectedly, we found that the top enriched functional category among the up-regulated genes in E15.5 RGs is synapse, which is highly represented by genes encoding for ion channels (see Fig R.4). In particular, we found up-regulation of genes encoding for subunits of the GABA(A) receptor (9 genes out of 22 expressed) and AMPA (3 out of 4) and NMDA (4 out of 7) glutamatergic receptors, as well as for voltage-gated potassium (18 out of 64) and calcium (11 out of 26) channels. In addition to the well-known roles of these ion channels in synaptic transmission and neuron depolarization, both ligand- and voltage-gated ion channels also have a function in non-excitable cells, including RGs. The concerted action of these two types of ion channels, together with ion pumps and exchangers, is key for the establishment of the resting membrane potential and other bioelectric parameters (Spitzer, 2006; Aprea and Calegari, 2012). Interestingly, a strong correlation between the bioelectric membrane properties and the proliferative behaviour of distinct cell types has been reported (Blackiston et al., 2009; Aprea and Calegari, 2012; Urrego et al., 2014). In the developing rat neocortex neural progenitors start to depolarize in response to GABA and glutamate, presumably secreted by postmitotic neurons and IPs, before the formation of functional synapsis (LoTurco et al., 1995; Ma and Barker, 1995). GABA-induced depolarization increases intracellular Ca2+ concentration by activation of voltage-dependent calcium channels affecting DNA synthesis (LoTurco et al., 1995). Moreover, Weissman et al. (2004) reported spontaneous calcium waves propagated through the RGs that are necessary to sustain proliferation of VZ progenitors at late neurogenesis. Our data are in agreement with a higher requirement of RGs for ligand-gated and calcium ion channels at late stages of the neurogenic phase. In consistency with a higher requirement in calcium ion channels, we found significant up-regulation of genes encoding for calmodulin-binding proteins (*i.e. Camk2b*, *Camk4*, *Camk1d,* etc*.)* involved in calcium signalling pathway (Toth et al., 2016). Of note, several of the up-regulated GABA(A) receptor subunits are putative targets of a group of down-regulated miRNAs that includes clusters *mir*-449 and *mir*-302/367 (see miRNA:mRNA network in Fig R.13), suggesting their potential contribution to restrain GABA responses at early neurogenic stages.

Progression through cell cycle is influenced by membrane potential, which is mainly dependent of potassium currents (Blackiston et al., 2009; Urrego et al., 2014). Hyperpolarized cells, such as neurons or muscle cells, do not show mitotic activity and hyperpolarization in cycling cells induces cell cycle arrest (Cone, 1971). Moreover, membrane potential seems to be cell cycle dependent (Sachs et al., 1974; Boonstra et al., 1981). The extensive changes in the expression of genes encoding for potassium channels reported here indicates that the link between membrane potential and cell cycle progression also operates in RGs. Indeed, it has been recently shown that RGs become more hyperpolarized as neurogenesis proceeds and that the progressive increase in RG hyperpolarization regulates the switch from direct to indirect neurogenic divisions and the competence of RGs to generate distinct types of projection neurons (Vitali et al., 2018). Thus, it is tempting to speculate that the progressive hyperpolarization of RGs relies on a precise regulation of many different potassium channel genes.

## 1.3. Extracellular matrix and YAP-TEAD activity

One of the most relevant findings from our transcriptome analysis is that RGs show extensive changes along development in the expression of genes encoding for structural ECM components (see Fig R.3 and R.4). Due to their polarized morphology and the specific localization of ECM-rich membranes at the apical and basal sides of the telencephalon, RGs had not been traditionally considered active players in the formation and maintenance of the ECM. Instead, RGs were considered recipients of ECM cues, which they sense by means of ECM-receptors, i.e. integrins. Therefore, changes in the ECM-receptors expression, rather than in the ECM composition, were considered responsible for the changes in the ECM signalling during neurogenesis (Lathia et al., 2007; Kazanis and ffrench-Constant, 2011). However, transcriptomic analyses have brought to light that neural progenitors express genes coding for ECM structural proteins, including laminins and collagens (Arai et al., 2011; Fietz et al., 2012). In addition to the genes encoding ECM components, we also detected significant changes in the expression of many ECM-receptor genes. Among the down-regulated genes at E15.5 we found genes encoding for integrins (8 genes out of 17 expressed), proteoglycans (16 out of 34) and collagens (19 out of 38). We confirmed by immunostaining that collagen type I and III, that show greater changes in gene expression, are down-regulated in the basal membrane. In line with an extensive collagen and proteoglycan removal, we also found transcriptional up-regulation of matrix proteinases (matrix metalloproteinases and adamalysins), which are enzymes driving matrix cleavage and degradation. In addition, other ECM structural proteins, such as the proteoglycans Versican and Tenascin C and

6 other collagen genes, were up-regulated between E11.5 and E15.5, possibly replacing the components removed (see Annex 1, Table 2). Overall, our data indicate that the composition of the ECM changes along neurogenesis and that RGs modulate cell-autonomously the ECM properties. Moreover, the location of RG-produced collagens in the basal membrane implies that RGs show vesicular transport routes to secrete the collagens to the basal lamina.

Several of the ECM-regulated genes along development are associated to human disease and cortical malformations. For instance, *Adamtsl3*, an adamalysin gene involved in schizophrenia (Dow et al., 2011) is significantly up-regulated in E15.5 RGs (Log2 FC = 5.6, adj. *p*-value = 4.8E-181). Also, mutations in *COL3A1,* the collagen gene that shows the greatest down-regulation along development (Log2 FC = -6.9, adj. *p*-value = 2.6E-36), cause the vascular Ehlers-Danlos disease, which is characterized by cortical cobblestone-like malformations frequently accompanied of cognitive delay (Horn et al., 2017; Jorgensen et al., 2015). This association between developmental-regulated genes and genes involved in cortical malformations further supports the notion that ECM composition is critical for the proper development and function of the cerebral cortex.

Besides providing structural support, ECM plays pivotal roles in the regulation of stem cell proliferation/differentiation during development and in cancer (Lu et al., 2011b). In line with our results, different works reported an association between poor ECM-cell interactions and decreased proliferation in the developing neocortex (Arai et al., 2011; Fietz et al., 2012; Stenzel et al., 2014). RGs transduce biochemical and mechanical external cues through different signalling pathways (Arulmoli et al., 2015; Guilak et al., 2009; Iwashita et al., 2019; Long and Huttner, 2019). Interestingly, among the regulated genes between E11.5 and E15.5, we have found a very significant enrichment in targets of the YAP-TEAD transcriptional complex. YAP-TEAD activity promotes proliferation in many different cell types including neural progenitors of the developing neocortex (Cappello et al., 2013; Lavado et al., 2013; Zhao et al., 2008). In cell culture models, rigid ECM favours the location of YAP in the nucleus, where it activates transcription through binding with TEAD TFs, while more compliant matrices favour the location of YAP in the cytoplasmic (inactive) compartment. YAP localization into the nucleus involves remodelling of the actin cytoskeleton, which is in intimate contact with membrane receptors able to sense both biochemical and mechanical cues (Dupont, 2016). Activation of the Hippo kinases LATS1/2 in response to extracellular cues induces LAST1/2-phosphorylation of YAP (and TAZ) promoting its cytoplasmic retention and, eventually, its ubiquitination and degradation (Meng et al., 2016). Moreover, the

cytoskeleton, which is mechanically linked to the nucleus, can stretch the nuclear pores allowing the entry of YAP into the nucleus in a Hippo-independent manner (Elosegui-Artola et al., 2016; 2017). Indeed, human pluripotent stem cells cultured in soft substrates present low levels of nuclear YAP and differentiate into neurons even in the presence of pluripotency factors (Musah et al., 2014). We here show that the abundance of collagen type I (COL1A1 and COL1A2) and III (COL3A1) proteins in the basal lamina decreases radically during neurogenesis, likely reducing ECM stiffness. COL3A1 regulates cortical development and lamination through the binding of the receptor GPR56 (Luo et al., 2011), and there is evidence that signalling through this type of G protein receptors results in the inhibition of LATS1/2 activity and the accumulation of YAP into the nucleus (Yu et al., 2012). Therefore, it is likely that GRP56-mediated signalling in RGs decreases along neurogenesis, dampening YAP activity. The idea that YAP activity in neural progenitors decreases as neurogenesis advances is supported by different studies showing that nuclear YAP promotes proliferative divisions (Cao et al., 2008; Cappello et al., 2013; Lavado et al., 2013).

In summary, our results suggest a model in which ECM stiffness and ECM-receptor signalling in RG contribute to restrain YAP-TEAD activity at late neurogenesis, thereby allowing differentiation (see model in **Fig D.2**).

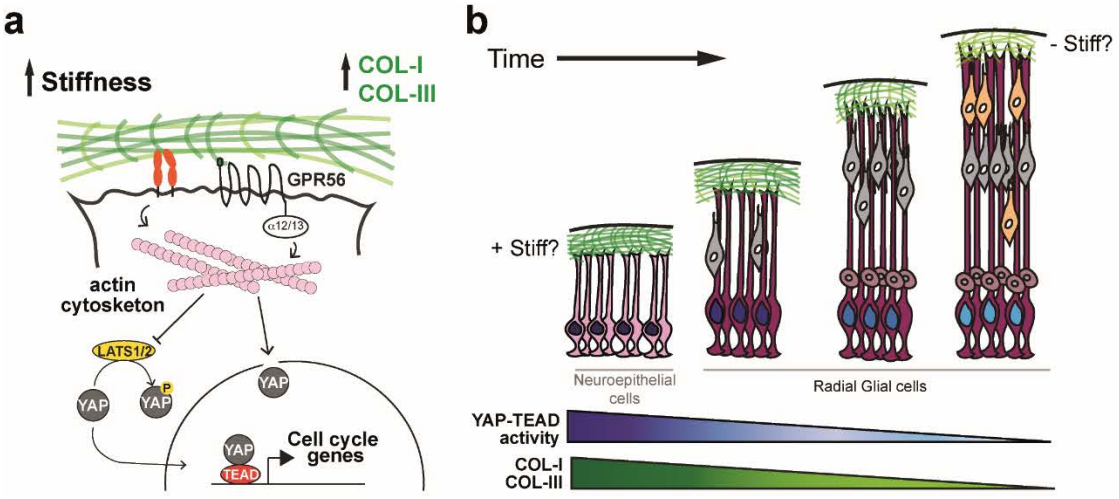


**Figure D.2. ECM-driven regulation of YAP-TEAD activity in radial glial cells. (a)** Schematic representation of the extracellular matrix components involved in YAP –TEAD activity regulation in radial glial cells. **(b)** Scheme showing the accumulation of collagen type I (COL-I) and collagen type III (COL-III) in the basal lamina along neurogenesis and the expected impact of ECM stiffness in the activity of YAP-TEAD in radial glial cells (garnet cells). White cells represent intermediate progenitors and yellow and orange cells neurons.

Multiple evidences indicate that WNT/β-Catenin signalling and the Hippo pathway are mutually regulated (Totaro et al., 2018). For instance, in mouse ESCs WNT signalling promotes YAP nuclear accumulation, while cytosolic YAP promotes β-catenin degradation, thereby inhibiting WNT signalling (Azzolin et al., 2014). Our data indicates that in RGs both YAP activity and WNT signalling are highly regulated. In addition, we found that many regulated ECM genes are putative miRNA targets and that the same miRNA network involved in the regulation of cell cycle and WNT signalling genes also targets ECM genes, especially collagens and other structural components (see miRNA:mRNA networks in Fig R.11 and R.12). This miRNA network includes members of the let-7 family. In cancer stem cells, let-7 miRNAs reduce proliferation by targeting collagen genes (Makino et al., 2013; Su et al., 2014; Liu et al., 2016). Thus, a similar mechanism may operate in RGs to promote differentiation as neurogenesis advances. Collectively, our data strongly suggests that miRNA regulation in these progenitors is relevant for the precise integration of extracellular cues with progression through the cell cycle.

## 1.4. Alternative splicing

Our RNA-seq data revealed large AS regulation in RGs, which affects almost 20% of the expressed protein-coding genes. Indeed, the expression of several genes encoding for RBP involved in AS changes significantly between the two analysed developmental stages, and some of these genes, for example *Nova1*, *Rbm20*, *Elavl2*, *Elavl3*, *Celf2*, *Srrm4* and *Khdrbs2*, are themselves regulated by AS. Most of the RBP-coding genes that were up-regulated at E15.5 have a role in neuronal migration and maturation (Vuong et al., 2016). The function in NSCs of the 12 down-regulated RBP genes involved in AS is unknown with the exception of *Ptbp1* and of *Qk*, which are involved in maintaining NSC fates (Vuong et al., 2016; Hayakawa-Yano et al., 2017). Hence, our data suggest that during early neurogenesis AS in RGs is controlled by additional RBPs not yet identified. One possible candidate is RBM47 because in our RNA-seq experiment *Rbm47* is the most down-regulated gene at E15.5 (Log2 = -4.75, *p*-value = 1.9E-11), and the knockdown of *rbm47* in zebrafish results in severe headless and small head phenotypes (Guan et al., 2013).

It is interesting to note that in RGs only 23.3% of the genes with AS-regulated events show differences in gene expression levels between E11.5 and E15.5 (see **Fig D.1**).

This observation is in agreement with previous reports claiming that AS and transcriptional regulation modulate the expression of different gene sets in order to define cell- and tissue-specific profiles (Pan et al., 2004; Fagnani et al., 2007). In line, we found that the functional overlapping of these two sets of genes is low (see **Fig D.3**).

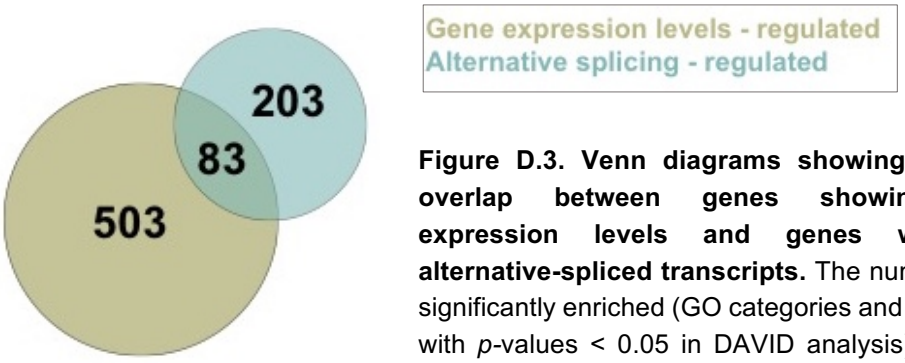


**Figure D.3. Venn diagrams showing the functional overlap between genes showing differential expression levels and genes with regulated alternative-spliced transcripts.** The number of functions significantly enriched (GO categories and KEGG pathways with *p*-values < 0.05 in DAVID analysis) for each set of genes is indicated.

We also found that intron retention is the most regulated splicing type in RGs. Intron retention usually results in the introduction of premature termination codons and it is most often associated to down-regulation of gene expression *via* non-sense mediated mRNA decay (Ge and Porse, 2014). However, the overlap between the genes with regulated intron retention and the differentially expressed genes is very low in RGs (data not shown), suggesting quite the opposite. Intron retention is also a mechanism for controlling the subcellular location of transcripts in polarized cells (Ortiz et al., 2017) and to generate new transcripts upon a stimulus (i.e. neuronal activity or cellular stress; Shalgi et al., 2014; Boutz et al., 2015; Mauger et al., 2016); therefore, many of the regulated intron retention events in RGs might be associated to these functions. Intron retention has been also proposed to reduce the transcripts that are less or not required for the physiology of the cell. For instance, during neuron differentiation intron retention in synapse genes inversely correlates with the expression of these genes (Braunschweig et al., 2014). Our RNA-seq revealed that intron retention events decrease between E11.5 and E15.5 in 37 up-regulated genes coding for postsynaptic proteins: among them, *Snap25*, *Shank1*, *Shank2* and *Stx1a* (see Annex 3, Table 6). Therefore, it is likely that at least for a subset of genes, non-sense mediated mRNA decay induced by intron retention is the mechanisms that RGs use to restrain the levels of non-needed transcripts.

Interestingly, genes showing more intron retention at E15.5 than at E11.5 are enriched in cilium related functions. Among them we found elementary members of the

ciliogenesis route, such as *Cep164*, *Cep290 and Mark4,* which are involved in the first steps of the formation of the axoneme (Bernabe-Rubio and Alonso, 2017). In RG asymmetric divisions, the daughter cell that re-assembles the cilium faster is the one that retains the RG phenotype, while the other differentiates (Paridaen et al., 2013). Moreover, there is evidence that cells committed to differentiate assemble a transitory basolateral cilium, instead of the apical one, after the centriole docks to the lateral plasma membrane (Wilsch-Brauninger et al., 2012). Therefore, an appealing possibility is that transcripts retaining the intron are not translated until the docking occurs. In conclusion, our data provide evidence that AS is an additional mechanism for establishing asymmetric fates between RG daughters.

An unexpected finding of our study is the different microexon expression pattern in E11.5 and E15.5 RGs. The inclusion of microexons usually preserves the ORF and affects protein domains involved in protein interactions (Irimia et al., 2014). In the CNS, most microexons show neuron-specific splicing patterns and display high inclusion during axonogenesis and synaptogenesis (Irimia et al., 2014). We here reported 65 microexons showing increased inclusion in E15.5 RGs compared to E11.5, and 8 with decreased inclusion at E15.5. Accordingly, we found changes in the expression of *Srrm4, Rbfox1/2/3* and *Ptbp1*, which encode for the RBPs involved in microexon regulation (Irimia et al., 2014; Li et al., 2015). Neural microexon inclusions are misregulated in autistic brains (Irimia et al., 2014). Interestingly, we found that some of these misregulated microexons, including microexons affecting *Dtna*, *Shank2*, *Robo1*, *Apbb1* and Slc43a2, are developmentally regulated in RGs.

## 1.5. Transcriptional pre-patterning

Another unanticipated finding of this study is that a large part of transcriptional and post-transcriptional developmental changes occurs in synapse-related genes. As we have mentioned before, some of the detected genes included in the “synapse” GO category have known functions in neural progenitors (i.e. ionotropic GABA and glutamate receptor genes). However, for other synaptic genes (i.e. *Snap25*, *Svop*, *Syt3*, *Psd3*, etc.), there is no information regarding the possible function of the encoded proteins in RGs. Similarly, we found that genes coding for transcription factors that are key for the specification of cortical excitatory neurons, such as *Satb2*, *Cux2*, *Fezf2*, *Ctip2* and *Pou3f2* (Molyneaux et al., 2007) are already expressed in RGs. Of note, all these neuronal-genes are significantly up-regulated at E15.5 compared to E11.5.

In the recent years, several groups have reported the presence of mRNAs coding for neuronal-specific proteins in neural progenitors (Guo et al., 2013; Eckler et al., 2015; Telley et al., 2016; Yoon et al., 2017). Although the function of these neuronal transcripts is still not clear, an accepted hypothesis is that progenitors are “transcriptionally pre-patterned” to rapidly generate neurons (Yoon et al., 2017; Albert and Huttner, 2018). This hypothesis may explain the abundance of neuronal transcripts at E15.5, where most RG divisions are differentiative.

The most accepted hypothesis in cortical development is that neuronal-transcripts in RGs are up-regulated according to the generation time of each neuron subtype, and then down-regulated when that subtype is no longer generated (Kwan et al., 2012; Greig et al., 2013). However, single cell RNA-seq and FISH analyses have shown that throughout the neurogenic period RGs co-express mRNAs encoding for different neuron subtypes (deep and upper layer neurons; Telley et al., 2016; Zahr et al., 2018). We have found up-regulation at E15.5 of genes encoding for TFs expressed in upper-layer neurons (*Satb2*, *Cux2*, *Pou3f2* and *Mef2c*) as well as TF genes specific for lower-layer neurons (*Fezf2*, *Ctip2* and *Sox5*), mostly generated before E15.5 (Molyneaux et al., 2007). Although our RNA-seq experiment was performed with the entire RG population, these observations support the findings of Telley et al. (2016) and Zahr et al. (2018).

We found that 25 out of the 27 miRNAs that are down-regulated during development target synapse-related genes and neuronal-transcriptional specifiers, indicating that miRNA regulation is important for repressing the expression of neural genes during early neurogenesis. It suggests that some neuronal mRNAs are already detected in RGs and that their expression is repressed post-transcriptionally. This hypothesis is supported by two recent reports. In the first one, the authors showed that the mRNAs of neuron-specific TFs (*Satb2*, *Otx1*, *Tbr2*, *NeuroD1*, etc.) are tagged with an epitranscriptomic mark, an $N^6$-methyladenosine ($m^6A$) that subjects them to rapid decay (Yoon et al., 2017). In the second one, the authors reported the existence of a translational repression complex formed by the protein 4E-T and the RBP Pumilio2 (Pum2/4E-T complex) that represses neuron genes (Zahr et al., 2018).

# 2. Effects of *DYRK1A* haploinsufficiency in the generation and differentiation of glial cells

In the second part of this thesis, we showed that *Dyrk1a* haploinsufficiency alters the generation of glial cells and myelination during cortical development, resulting in defects in the glial populations and in the interactions glia – axon that persist until adulthood. Our observations suggest that several of these defects are likely promoted by disturbances in the behaviour of embryonic dorsal RGs and in the neuronal population generated by these progenitors (Benavides-Piccione et al., 2005; Martinez de Lagran et al., 2012; Najas et al., 2015; Arranz et al., 2019).

Neurons and glial cells work together to develop, maintain and assure the correct functionality of the cerebral circuits. Therefore, the alterations here reported in the development of glial populations may contribute to the neurological features of individuals with *DYRK1A*-related syndrome, which include traits of the autistic spectrum, intellectual disability and epilepsy.

## 2.1. Astrogliogenesis

The brain of both human and mice carrying *DYRK1A* loss-of-function mutations shows increased number of astrocytes. Our experiments in the mouse *Dyrk1a*$^{+/-}$ cortex indicate that this excess is not the consequence of a pathological glial reactivity, but rather to an enhanced astrogliogenesis during development. The number of astrocytes in the mutant cortex is already increased at P5, when the astrocytes generated in the dorsal VZ/SVZ germinal layer reach the cortex and start to expand locally (Ge et al., 2012). Fate-mapping analyses showed that the astroglial potential of dorsal *Dyrk1a*$^{+/-}$ RGs at late embryonic stages is normal (see Fig R.27). However, *Dyrk1a*$^{+/-}$ embryos showed more RGs in the dorsal germinal layer than the controls (see Fig R.23). This excess of RGs does not correlate with an augmented production of late cortical neurons (see Fig R.24) or perinatal cell death (unpublished data of the group), and are not likely to remain as adult NSCs because this population is not increased in young *Dyrk1a*$^{+/-}$ SVZs (Ferron et al., 2010). Based on these observations and the fact that part of the RGs transform directly into astrocytes (Kriegstein and Alvarez-Buylla, 2009), we propose that this small excess of RGs observed in the dorsal *Dyrk1a*$^{+/-}$ telencephalon just before the gliogenic phase contributes to the augmented number of astrocytes observed in postnatal mutants. Of note, RG-derived astrocytes proliferate in the cortex at postnatal stages (Ge

et al., 2012). Therefore, small differences in the number of RG-derived astrocytes might be enhanced in the *Dyrk1a*$^{+/-}$ postnatal cortex.

The increased astrogliogenesis observed in the *Dyrk1a*$^{+/-}$ mutant model seems to argue against the pro-astrogliogenic role of DYRK1A proposed by Kurabayashi et al. (2015). In this work, the authors show that the overexpression of DYRK1A in the developing mouse cerebral cortex enhances astrogliogenesis and the transcriptional activity of STAT proteins, effects that seem to be mediated by DYRK1A phosphorylation of the JAK pathway effector STAT3 in a residue that promotes its dimerization and activation (Levy and Darnell, 2002). In accordance, our luciferase-reporter assay indicated that STAT3 activity in *Dyrk1a*$^{+/-}$ RGs is reduced by 50%, although, as already mentioned, this reduction does not significantly affect their astrogliogenic potential. In response to BMP proteins, activated STAT3 forms the STAT3-SMAD1-P300 co-activity complex, which initiates the expression of astrocyte-specific genes, such as *Gfap*, by binding of the complex to their promoters. Methylation of the STAT binding element within the *Gfap* promoter inhibits the association of activated STAT3 with the promoter, thereby repressing transcription of the *Gfap* gene during neurogenesis (Nakashima et al., 1999; Fukuda et al., 2007). Moreover, demethylation of *Gfap* and other genes that are essential for the JAK-STAT signalling is considered a key mechanism to control both the magnitude and timing of astroglial differentiation (Takizawa et al., 2001). Previous data of the group showed that during neurogenesis, the CpGs that lie within the STAT3 binding site ttcCGagaa in the *Gfap* promoter (see scheme in Fig R.27) and two additional CpGs surrounding this site are less methylated in *Dyrk1a*$^{+/-}$ dorsal telencephalon than in the controls (Balducci, 2012), indicating that mutant RGs are more prone to respond to pro-astrogliogenic factors activating the STAT3-SMAD1-P300 complex. However, the expression of *Gfap* in the cerebral cortex of P0 *Dyrk1a*$^{+/-}$ mice is not altered (Balducci, 2012), which argues against the possibility of an advanced astrogliogenesis in the *Dyrk1a*$^{+/-}$ model and suggests that the precocious demethylation of *Gfap* gene in the mutant condition may compensate for the deficit of DYRK1A-mediated phosphorylation of STAT3. Taking all these considerations together, we propose that the astrogliogenic potential of *Dyrk1a*$^{+/-}$ dorsal RGs is preserved and that the enhanced number of astrocytes in the postnatal *Dyrk1a* haploinsufficient mouse results from the larger pool of RGs available for astrocyte differentiation at the end of the neurogenic period.

## 2.2. Oligodendrogenesis

The population of OPCs in the *Dyrk1a*$^{+/-}$ developing telencephalon is also altered. In the ventral domain, we detected reduced OPC production in the LGE at E15.5, the peak of oligodendrogenesis in this region. Part of the ventral-generated OPCs migrates gradually to the dorsal telencephalon to populate cortical structures, including the CC (Richardson et al., 2006). Consistently, the number of OPCs arriving into the dorsal telencephalon is reduced at E17.5 and in the CC at perinatal stages (see Fig R.28 and Fig R.30). At late embryonic stages, dorsal neural progenitors generate OPCs that spread throughout the cortex. In the *Dyrk1a*$^{+/-}$ embryo the onset of dorsal OPC generation is slightly delayed but the addition of dorsal-generated OPCs at postnatal stages finally compensates the initial deficit in callosal OPCs.

In the developing telencephalon, oligodendrogenesis is modulated by intrinsic and extrinsic mechanisms. Dorsal RGs display a very deterministic intrinsic program controlling proliferation, neurogenesis and gliogenesis. Alterations in one of these phases may impact in the subsequent one (Gao et al., 2014; Toma and Hanashima, 2015). Therefore, it is plausible that the delay in the onset of dorsal oligodendrogenesis is related to the alterations in the neurogenic program reported in the *Dyrk1a*$^{+/-}$ dorsal telencephalon (Najas et al., 2015). In fact, Tg*Dyrk1a* embryos, carrying 3 *Dyrk1a* alleles, show the opposite phenotype, an advanced neurogenic program that correlates with and advanced OPC production (Najas et al., 2015). Given that *Dyrk1a* dosage imbalance affects the timing of ventral neurogenesis and the number and subtype of generated interneurons (unpublished data of the group and Arranz, 2016), a similar situation could account for the deficits detected in ventral oligodendrogenesis, where neurogenesis and gliogenesis are overlapped and there is evidence that the two phases are coupled (Petryniak et al., 2007; Chapman et al., 2013).

One of the extrinsic molecules that regulates ventral oligodendrogenesis is SHH (Tekki-Kessaris et al., 2001). The generation of OPCs from ventral progenitors is almost abolished in the absence of SHH, both *in vitro* and *in vivo* (Nery et al., 2001; Tekki-Kessaris et al., 2001; Fuccillo et al., 2004). The exact interplay between DYRK1A and SHH seems complex, but several evidences support that DYRK1A phosphorylates GLI1, one of the major effectors of the SHH pathway, promoting its nuclear retention and in consequence, enhancing its transcriptional activity (Mao et al., 2002; Schneider et al., 2015). Therefore, a putative reduction in GLI1 activity in the *Dyrk1a*$^{+/-}$ ventral telencephalon could affect the generation of OPCs. Moreover, it has been recently proposed that the arrival of ventral GABAergic interneurons to the dorsal telencephalon

coincides with the onset of dorsal oligodendrogenesis and that those neurons secrete factors, such as SHH, that modulate dorsal generation of OPCs (Voronova et al., 2017; Winkler et al., 2018). Thus, a possible alteration in the number and subtype of cortical GABAergic interneurons may contribute to the delayed dorsal oligodendrogenesis in the *Dyrk1a*$^{+/-}$ model.

Despite the deficit in cortical OPCs detected in the *Dyrk1a*$^{+/-}$ model at embryonic and perinatal stages, this population reaches normal numbers in the CC at P10 and in the adult neocortex. Embryonic and early postnatal cortical OPCs express DYRK1A (unpublished data of the group) and their proliferation is dependent on Cyclin D1 (Nobs et al., 2014), which binds to CDK4/6 promoting their activity, and thereby G1 to S phase transition. DYRK1A promotes cyclins D degradation in several cellular contexts, including dorsal RGs (Chen et al., 2013; Najas et al., 2015; Thompson et al., 2015). However, the postnatal normalization of *Dyrk1a*$^{+/-}$ OPCs does not seem to result from an altered Cyclin D1 turnover in these progenitors (Nobs et al., 2014), since the levels of nuclear Cyclin D1 in the OPCs of the mutant CC are not significantly altered. The fact that variations in the dosage of DYRK1A significantly changes the nuclear levels of Cyclin D1 in neurogenic RG progenitors but not in OPCs indicates that the action of DYRK1A controlling Cyclin D1 turnover is cell-type specific.

OPCs communicate with each other and are able to sense deficits in OPC densities, promoting their proliferation until reaching the appropriated density (Zhang and Miller, 1996; Yang et al., 2011). The short-term BrdU incorporation experiment performed at P10 indicates that the pool of proliferating OPCs in the *Dyrk1a*$^{+/-}$ postnatal cerebral cortex is normal. Therefore, it is likely that the plastic property of these progenitors gradually compensates the OPC deficit observed in the telencephalon of *Dyrk1a*$^{+/-}$ embryos and postnatal animals younger than P10.

## 2.3. Oligodendrocyte differentiation

The alterations in the generation of OPCs in the *Dyrk1a*$^{+/-}$ telencephalon are associated to a delay in the appearance of oligodendrocytes in the CC. This phenotype could be the consequence of an impaired oligodendroglial differentiation program. However, this possibility is unlikely because differentiated oligodendrocytes in the CC reach normal numbers by P10, when differentiation in this structure is still incipient (see Fig R.32). In the LPC-induced focal demyelination model, the process triggered by the demyelinating insult recapitulates some aspects of developmental oligodendroglial differentiation and

myelination, including OPCs proliferation, migration and expression of differentiating markers (Bradl and Lassmann, 2010). In the adult *Dyrk1a*$^{+/-}$ CC, OPC differentiation into oligodendrocytes induced by the demyelinating insult is normal and timely, which supports that the differentiation process is not grossly impaired in *Dyrk1a* haploinsufficient OPCs. Instead, we propose that the delay in differentiation most likely results from the delay in the generation of OPCs in the embryonic germinal zones. In fact, in other unrelated mutant mice, such as *Nkx6*.1, *Gli2* and *Axin2* mutants, reduced or delayed generation of OPCs has been associated to delayed appearance of differentiating oligodendrocyte markers (Liu et al., 2003; Qi et al., 2003; Dai et al., 2014). Thus, the phenotype of these three mutants and the one of the *Dyrk1a* haploinsufficient mutant reported here is consistent with the established concept that oligodendroglia differentiation is dictated by a cell-intrinsic timer (Durand and Raff, 2000), and suggest the possibility that this "intrinsic timer", which dictates the differentiation of cultured OPCs *in vitro* (Gao et al., 1997), also operates *in vivo.* Nonetheless, several lines of evidence indicate that the density of oligodendroglial cells and the differentiation state of the neighbouring cells also influence the differentiation timing of an OPC (Yang et al., 2011; Huang et al., 2013). Thus, both the deficit in OPCs during embryonic development and the delay of the OPCs in reaching the appropriate density at postnatal stages may contribute to the delay in OPC differentiation observed in the *Dyrk1a*$^{+/-}$ model.

## 2.4. Myelination

The ultrastructural analysis of the *Dyrk1a*$^{+/-}$ CC at the onset of myelination, P19, showed an increased thickness of the myelin sheet in relation to the axonal calibre (reduced G-ratio) in comparison to the control CC. However, G-ratios in the mutant CC are normalized by P60. According to the current model of myelin biogenesis, proposed by Snaideiro et al. (2014; see introduction section 1.2.5), during myelination oligodendrocytes expand a tongue of uncompacted myelin that wraps around the axon and compacts progressively from the outer layers (the first synthesized) to the inner ones (the lasts to be formed). Therefore, it is possible that the increased G-ratio transiently observed in the *Dyrk1a*$^{+/-}$ CC at P19 reflects a delay in the compaction of myelin, likely as a consequence of the general delay in the differentiation program. Consistent with this hypothesis, the expression of the gene encoding for MBP, which plays a major role in myelin compaction, is decreased in *Dyrk1a*$^{+/-}$ cerebral cortices before the onset of myelination (at P0 and P7; Arranz et al., 2019), but both MBP transcripts and protein levels normalize in the mutant cortices at later postnatal stages (see Fig R.35).

Although the CC of P60 *Dyrk1a*$^{+/-}$ mice show normal densities of differentiated oligodendrocytes (Fig R.34) and myelinated axons have normal G-ratios (Balducci, 2012), the number of callosal axons that are myelinated is 30% lower in the mutant mice than in the controls (unpublished data of the group). Since myelination is still very active at P60 (Sturrock, 1980), the deficit in myelinated axons could be a consequence of the general delay in oligodendrocyte differentiation. Impairments in the communication of the axon-oligodendrocyte tandem could also explain this deficit. An important difference between the CC of P60 *Dyrk1a*$^{+/-}$ and control mice is that the axonal density is significantly augmented in the mutant condition (Balducci, 2012), which is in accordance with the augmented number of callosal neurons (layer II-III neurons) detected in P60 *Dyrk1a*$^{+/-}$ neocortices (Arranz et al., 2019). Therefore, as the *Dyrk1a*$^{+/-}$ CC has normal oligodendrocyte numbers, the ratio of callosal oligodendrocytes per axon is lower in the mutant condition than in the controls. *Dyrk1a* dosage imbalance affects the morphology of dendrites in cultured neurons and in the mouse, probably because of the role of DYRK1A in the regulation of actin cytoskeleton and microtubule dynamics (Martinez de Lagran et al., 2012): the size and complexity of the dendritic arbour are reduced in cortical projection neurons of the adult *Dyrk1a*$^{+/-}$ neocortex (Benavides-Piccione et al., 2005), and the overexpression of autism-related *Dyrk1a* truncated mutations in cultured cortical neurons causes reduction of the axon length and affects dendrite development (Dang et al., 2018). Our analysis revealed that in *Dyrk1a*$^{+/-}$ postnatal mice, the axon diameter of callosal neurons is reduced (see Fig R.36). Since factors secreted by axons to promote myelination depend on the characteristics of the neuron, including the electrical activity received (Tomassy et al., 2016), it is probable that the alterations reported in the *Dyrk1a*$^{+/-}$ neuronal population impact on the axonal secretory profile perturbing its capability to promote myelination. Of note, factors secreted by astrocytes contribute to accommodate the environment for myelination (Domingues et al., 2016). Therefore, the increased density of astrocytes in the developing *Dyrk1a*$^{+/-}$ cortex may also contribute the hypomyelination in the *Dyrk1a* mutant model.

Unexpected findings arose when analysing the relative levels of the most abundant CNS myelin proteins. Firstly, we found that during myelination the cerebral cortex of *Dyrk1a*$^{+/-}$ mice present normal MBP protein levels (observed by western blot), despite the percentage of myelinated axons in the mutated CC is reduced. This could reflect an abnormal distribution of MBP between the distinct regions of the mutant cortex (for example, less MBP in the CC but more in other regions). Another interesting possibility is that oligodendrocytes synthesize normal amounts of MBP but do not extend myelin sheets because of impaired communication with the axons. The second striking finding

was that *Dyrk1a*$^{+/-}$ cortices contain twice as much PLP protein than the wild-types, which means that protein composition (MBP / PLP ratio) is severely disturbed in the mutant cortices, which may compromise myelin functionality and integrity. PLP is not essential for the biosynthesis of myelin membranes, but it is necessary for myelin maintenance and axonal integrity (Luders et al., 2019). Interestingly, alterations in the levels of PLP in the CNS are the cause of Pelizaeus-Merzbacher disease (MIM 312080), being the duplication of the wild-type *PLP* gene the most frequent genetic cause (60-70% of the cases, Osorio and Goldman, 2018). Pelizaeus-Merzbacher disease is characterized by severe hypomyelination of the CNS and variable psychomotor and cognitive delay (Osorio and Goldman, 2018). The pathogenic mechanisms of PLP overexpression have been assessed in mice models carrying supernumerary copies of *Plp1* that reproduce the major phenotypes of the disease, including demyelination and cognitive deficits. Importantly, the severity of the phenotype directly correlates with PLP overexpression levels (Kagawa et al., 1994; Readhead et al., 1994; Tanaka et al., 2009). In the brains of mice showing moderate PLP overexpression, myelination seems to progress normally during the first months, but at middle age demyelination proceeds rapidly and, ultimately, axonal degeneration leads to death around 1 year of age (Kagawa et al., 1994; Inoue et al., 1996; Anderson et al., 1998; Tanaka et al., 2006). Transgenic *Plp1* oligodendrocytes accumulate excessive PLP protein together with cholesterol in late endosomes/lysosomes and autophagosomes, perturbing the trafficking routes and resulting in arrest of oligodendrocyte maturation and premature cell death (Kagawa et al., 1994; Readhead et al., 1994; Anderson et al., 1998; Cerghet et al., 2001). Based on the phenotype of *Plp1* transgenic mice, it is tempting to speculate that increased PLP levels in the CNS may contribute to the hypomyelination detected in the CC of young adult *Dyrk1a*$^{+/-}$ mice. In fact, it is likely that increased PLP protein accumulation exacerbates the myelin deficit over time in these mice. It is worthy to mention that the impact on myelin integrity is not expected to be as severe in the *Dyrk1a*$^{+/-}$ mutant as in the *Plp1* transgenic animals because: 1) unlike to what has been reported in young *Plp1* transgenic mice, the cerebral cortex of P60 *Dyrk1a*$^{+/-}$ mutants does not exhibit astroglial and microglial reactivity (Fig R.21-22) and 2) *Dyrk1a*$^{+/-}$ mice show normal life expectancy. Nonetheless, considering the aberrant levels of PLP detected in young *Dyrk1a*$^{+/-}$, it would be important to take into account this myelin alteration when assessing the progression of the disease in individual with *DYRK1A* haploinsufficiency syndrome.

Despite the accumulation of PLP protein, the levels of *Plp1* transcripts in P28 and P60 mutant cortices are not altered, indicating that gene transcription is not affected. Therefore, PLP accumulation in the mutants has to be the consequence of alterations in

post-transcriptional mechanisms involved in the synthesis and/or degradation of the protein. Although this last possibility is unlikely because of the long half-life of PLP protein in the CNS (50% turnover in 6 months; Luders et al., 2019). Interestingly, the *Plp1* gene encodes two protein isoforms, DM20 and PLP, which are predominantly expressed in OPCs and in mature oligodendrocytes, respectively. The two products are generated from the same transcript by AS (Nave et al., 1987). Since we have not assessed the protein levels of DM20 and DYRK1A is known to interact with several splicing factors, one possibility is that the deficit of DYRK1A levels in the mutant oligodendrocytes favours the PLP spliced isoform. Alterations in the DM20 / PLP ratio have been reported in some of the patients affected from Pelizaeus-Merzbacher disease (Regis et al., 2009). More work is required to elucidate how haploinsufficiency of *DYRK1A* affects the levels of the two *PLP* encoding isoforms and myelination.

The alterations in myelin in the cerebral cortex of *Dyrk1a*$^{+/-}$ mice are accompanied by alterations in the nodes of Ranvier. Nodes in the *Dyrk1a*$^{+/-}$ CC are shorter and show weakened NAV1.6 expression levels (Fig R.38). *In silico* modelling predicts that alterations in nodal length and $Na^+$ channel density impact on the conduction velocity along single axons (Arancibia-Carcamo et al., 2017). Supporting this prediction, several studies in mutant mice models reported a correlation between nodal modifications and alterations in the conduction velocity (see for instance, Ritter et al., 2013; Sanz-Rodriguez et al., 2018). Additionally, loss-of-function mutations in the human gene coding for NAV1.6 (*SCN8A*) have been associated to intellectual disability and seizures (O'Brien and Meisler, 2013; Blanchard et al., 2015). NAV1.6 is a voltage-dependent sodium channel that regulates neuronal excitability and is highly concentrated in the axon initial segments and the nodes of Ranvier (Caldwell et al., 2000). A recent study proposed that reduction of NAV1.6 levels leads to alterations in the synchrony of thalamo-cortical networks triggering seizures (Makinson et al., 2017). Given that the effects of reduced NAV1.6 levels are region-specific, it would be of interest to assess whether the alteration in NAV1.6 levels in the CC of *Dyrk1a*$^{+/-}$ mice is limited to this region or affects other brain regions. Future work should be oriented to confirm the deficit of NAV1.6 in the *Dyrk1a*$^{+/-}$ cerebral cortex and the functional implications of this deficit.

In conclusion, our data suggest that myelination defects in the *Dyrk1a*$^{+/-}$ cortices arise during development from the combination of a delayed oligodendroglial differentiation program and alterations in the axonal population. Moreover, it is possible that cell autonomous defects in the oligodendrocytes also contribute to disturb the axon-oligodendrocyte communication.

## 2.5. Functional consequences of the glial phenotype in *DYRK1A* haploinsufficiency syndrome

Abnormalities in glial cells are being recognised as an important component of neurological developmental disorders (see introduction section 1.3). Similar to the phenotype here described in the *Dyrk1a*$^{+/-}$ mice, increased astrogliogenesis has been observed in mouse models for DS, Rett Syndrome, Fragile X syndrome and others disorders with intellectual disability and autism such as Noonan syndrome or Costello syndrome (Mito and Becker, 1993; Gauthier et al., 2007; Paquin et al., 2009; Andoh-Noda et al., 2015; Lee et al., 2019). These animal models point out the importance of producing an adequate number of cell populations during development to assure the proper wiring and function of the cortical circuits. Given that defects in connectivity are thought to underlie intellectual disability and autism (Hu et al., 2014), special focus must be put on understanding how defects in the astrocyte population affect the development and function of synapsis. Little is known about the molecular implications of excessive astrocytes during development, although it is tempting to speculate that astroglial secreted factors may be found in excess in affected brains. Related with the role of astrocytes in neurotransmitter clearing at synapses, it has been shown that a reduction in astrocyte numbers disturbs the glutamate/GABA balance in the context of neuropsychiatric disorders such as depression and schizophrenia (Takahashi et al., 2015; Mahmoud et al., 2019). In addition, there is evidence that brain astrocytes in Rett syndrome, Fragile X syndrome and Down Syndrome are not only augmented but also functionally impaired, failing to promote normal dendritic development and synaptogenesis in healthy neurons (Garcia et al., 2010; Jacobs et al., 2010; Williams et al., 2014). Functional impairment in these cases has been associated to aberrant gene expression profiling (Okabe et al., 2012; Chen et al., 2014a; Wallingford et al., 2017). DYRK1A is involved in transcription (Di Vona et al., 2015) and, interestingly, transcriptomic analyses show that *DYRK1A* expression is high during astrocyte development in both mice and human in comparison to other CNS populations (Zhang et al., 2014; 2016b). Therefore, it is possible that *Dyrk1a* dosage imbalance alters the gene expression profile of astrocytes. It would be interesting to evaluate experimentally if this is the case and to what extend do astrocytes contribute to the neuronal phenotype observed in *Dyrk1a*$^{+/-}$ mutants.

The presence of abnormalities in white matter volume and structure has also been consistently demonstrated in the brain of individuals with intellectual disability, autism and other psychiatric diseases (Fields, 2008; Groen et al., 2011; Olmos-Serrano et al., 2016). Myelination allows for the rapid, efficient and integrated transmission of the

electrical activity and myelin deficits have detrimental effects in brain connectivity. In particular, some of the myelin alterations here reported in the *Dyrk1a*$^{+/-}$ cortex, including hypomyelination, shorter nodal length and aberrant myelin protein composition, have been associated to reduced nerve conduction velocity, reduced range of cortical synchrony and axonal loss in other mouse models (for examples see Robaglia-Schlupp et al., 2002; Michailov et al., 2004; Lee et al., 2011; Ritter et al., 2013; Makinson et al., 2017; Sanz-Rodriguez et al., 2018). Therefore, it would be interesting to test whether *Dyrk1a* haploinsufficient brains show these functional deficits. If reproduced in the human brains, the defects in myelination reported in the *Dyrk1a*$^{+/-}$ mouse model must play an essential role in the cognitive delay, epilepsy and autistic traits associated to *DYRK1A* haploinsufficiency syndrome.

The maturation of cortical circuits is extended to postnatal stages. Connectivity maps are established within the second to third postnatal week in rodents; while in humans, this process extends until adolescence in some regions. Since the classic studies of Hubel and Wiesel (Wiesel and Hubel, 1963a,b) consisting in the assessment of cortical cytoarchitecture of the cat brain after visual deprivation, it is widely recognized that early sensory postnatal experience shapes cortical circuitries (Stein et al., 2009; Levelt and Hubener, 2012; Mount and Monje, 2017). In this context, it is interesting to highlight that alterations in the developing *Dyrk1a*$^{+/-}$ cortex affect the neuronal and glial populations, likely disturbing the processing of sensory inputs and, in consequence, the experience-dependent maturation of circuits.

Inhibition of DYRK1A activity is a successful therapeutic strategy to ameliorate the cognitive deficits associated to Down Syndrome (Guedj et al., 2014; de la Torre et al., 2014; 2016). However, in the case of *DYRK1A* haploinsufficiency in which there is deficient DYRK1A enzymatic activity, a therapeutic approach directed to enhance this activity is challenging, not only because of the difficulty of finding specific drugs, but also for the difficulty of reaching appropriate, non-pathological, DYRK1A levels. Moreover, detrimental effects of *DYRK1A* haploinsufficiency in corticogenesis arise very early in embryonic development. In fact, we propose that defects in the generation and differentiation of glial cells are, at least in part, consequence of the defects that occur ahead in the generation of neuronal populations. Therefore, therapies must be applied as soon as possible to overcome the primary defects. Unfortunately, prenatal treatments tend to be risky because of the invasiveness and possible teratogenic effects. Nevertheless, the results obtained in the present work allow us to propose therapeutic targets to alleviate some of the specific alterations of the *DYRK1A*$^{+/-}$ brains after birth.

For instance, one possible target is the myelin protein PLP, which is increased at young adult stages in the haploinsufficient mice brains. Interestingly, some therapeutic strategies ameliorate PLP overexpression-induced neuropathology in Pelizaeus-Merzbacher disease. For instance, the postnatal intake of the dietary supplement curcumin improved the motor phenotype and preserved myelinated axons in affected *Plp1*-transgenic mouse (Epplen et al., 2015). Similarly, in this mouse model dietary cholesterol supplementation reduced PLP accumulation, increased myelin content and reduced motor defects (Saher et al., 2012). Early postnatal treatments oriented to promote OPC proliferation and differentiation could also be a good therapeutic strategy for *DYRK1A*-haploinsuficient individuals. In this regard, several evidences indicate that adenosine-based drugs, working by enhancing adenosine signalling, are promising candidates to treat myelin deficits in autism-related syndromes (Shen et al., 2018). It would be interesting to assess the possible benefit of these treatments to improve the quality of life in *DYRK1A* haploinsufficient individuals.

# CONCLUSIONS

## OBJECTIVE 1: Transcriptome analysis in cortical neurogenic radial glial cells

- Twenty-five percent of the protein-coding genes detected by RNA-seq in radial glial cells show differential expression levels during neurogenesis, and 28% of the differentially expressed genes are putative targets of developmentally-regulated miRNAs.
- Differentially expressed genes are significantly enriched in genes encoding proteins involved in cell cycle regulation and WNT signalling, synapse and ion transport proteins, as well as components and regulators of the extracellular matrix.
- The miRNAs that up-regulate during neurogenesis include most of the let-7 family members, the cluster *mir*-212/132, and miR-128-3p, miR-144-3p, and miR-125-5p. These miRNAs are part of the miRNA-mRNAs networks involved in the regulation of proliferation and extracellular matrix composition.
- The miRNAs that down-regulate during neurogenesis include miR-448 and the clusters *mir*-449 and *mir*-302/367. These miRNAs are part of a miRNA network regulating genes encoding ion transport and synapse proteins and regulators of neurogenesis.
- Differentially expressed genes show a significant enrichment in TEAD2 targets, pointing to the importance of YAP-TEAD transcriptional regulation in radial glial cells.
- Alternative splicing is highly regulated during neurogenesis, affecting the expression of alternative-spliced transcripts in 19% of the protein-coding genes expressed in radial glial cells.
- Genes regulated by alternative splicing are functionally associated to ATP-binding, synapse, cytoskeleton organization, cilium biogenesis and DNA repair.

## OBJECTIVE 2: Glial phenotype in the *Dyrk1a*$^{+/-}$ mouse model

- Astrogliogenesis in the postnatal *Dyrk1a*$^{+/-}$ neocortex is enhanced, likely due to an enlarged pool of neural progenitors at the end of the neurogenic phase. This leads to an increased number of cerebral cortex astrocytes that is maintained until the adulthood.
- In the *Dyrk1a*$^{+/-}$ embryo, ventral oligodendrogenesis is impaired, which correlates with a perinatal deficit of callosal oligodendroglial progenitors and a delayed oligodendroglial differentiation.
- The deficit in oligodendroglial cells and differentiated oligodendrocytes in the *Dyrk1a*$^{+/-}$ cortex normalizes during the second postnatal week.

- At the onset of myelination, *Dyrk1a*$^{+/-}$ callosal axons show a reduction in axon calibre and an increase in myelin thickness.
- In the adult *Dyrk1a*$^{+/-}$ cerebral cortex, the PLP/MBP ratio is augmented and the nodes of Ranvier are shorter and show decreased expression of the sodium channel NAV1.6.
- The glial phenotype described here may affect the synaptic function and nerve impulse conductivity, contributing to the intellectual disability and epilepsy that are associated to the *DYRK1A*-related syndrome.

# ANNEXES

# Annex 1

**Table 1. Top 25 down-regulated coding genes in radial glial cells (E15.5 *vs* E11.5)**

| Gene | Log2 FC | Adj. *p*-value | Description |
|---|---|---|---|
| *Fezf1* | -8.62 | 3.2E-45 | FEZ Family Zinc Finger 1. Transcriptional repressor. |
| *Robo3* | -8.32 | 1.4E-230 | Roundabout Guidance Receptor 3. Transmembrane receptor. |
| *Hmga2* | -7.81 | 0.00 | High Mobility Group AT-Hook 2. Component of the enhanceosome. |
| *Fndc3c1* | -7.72 | 1.1E-152 | Fibronectin type III domain containing protein 3C1. |
| *Lin28a* | -7.13 | 2.4E-27 | Lin28 homologue A. RNA-binding protein. |
| *Uncx* | -6.90 | 2.1E-33 | UNC Homeobox. Transcription factor. |
| *Col3a1* | -6.87 | 2.6E-36 | Collagen Type III Alpha 1 Chain. Fibrillar collagen. |
| *Crabp2* | -6.73 | 3.0E-285 | Cellular Retinoic Acid Binding Protein 2. Retinoic acid signalling. |
| *Samd3* | -6.45 | 1.9E-54 | Sterile Alpha Motif Domain Containing 3. Unknown function. |
| *Col1a2* | -6.40 | 1.2E-92 | Collagen Type I Alpha 2 Chain. Fibrillar collagen. |
| *Gmnc* | -6.26 | 1.9E-102 | Geminin Coiled-Coil Domain Containing. Chromatin binding protein. |
| *Sulf1* | -6.19 | 1.2E-186 | Sulfatase 1. Extracellular heparan sulfate endosulfatase. |
| *Ebf2* | -6.02 | 8.9E-226 | EBF Transcription Factor 2. |
| *Ano1* | -6.01 | 3.0E-91 | Anoctamin 1. Calcium-activated chloride channel. |
| *Dlk1* | -5.99 | 4.9E-38 | Delta Like Non-Canonical Notch Ligand 1. Transmembrane protein. |
| *Vwa2* | -5.97 | 2.8E-26 | Von Willebrand Factor A Domain Containing 2. Structural component. |
| *Otx2* | -5.96 | 8.4E-30 | Orthodenticle Homolog 2. Transcription factor. |
| *Clic6* | -5.80 | 4.7E-52 | Clhoride Intracellular Channel 6. Chloride channel. |
| *Olig3* | -5.74 | 3.6E-15 | Oligodendrocyte Transcription Factor 3. Transcription factor. |
| *Hs3st3a1* | -5.73 | 9.5E-24 | Heparan Sulfate-Glucosamine 3-Sulfotransferase 3A1. |
| *Qprt* | -5.72 | 1.9E-15 | Quinolinate Phosphoribosyltransferase. |
| *Barhl2* | -5.70 | 5.8E-79 | BarH Like Homeobox 2. Transcriptional regulator. |
| *Th* | -5.66 | 1.3E-42 | Tyrosine Hydroxylase. |
| *Tfap2b* | -5.59 | 2.6E-19 | Transcription Factor AP-2 Beta. |
| *Hbb-bh1* | -5.56 | 9.2E-14 | Hemoglobin Z beta-like embryonic chain. Oxidoreductase. |

**Table 2. Top 20 up-regulated coding genes in radial glial cells (E15.5 *vs* E11.5)**

| Gene | Log2 FC | Adj. *p*-value | Description |
|---|---|---|---|
| *Sla* | 8.96 | 7.8E-223 | Src Like Adaptor. Inhibition of T-cell receptor signalling. |
| *Aox4* | 7.91 | 7.3E-36 | Aldehyde oxidase 4. Retinoic acid signalling. |
| *Rasgrf1* | 7.58 | 7.6E-37 | Ras Protein Specific Guanine Nucleotide Releasing Factor 1. |
| *Nos1* | 7.56 | 0.00 | Nitric Oxide Synthase 1. |
| *Ly6g6e* | 7.30 | 3.4E-46 | Lymphocyte Antigen 6 Family Member G6E. Signal transduction. |
| *Bcan* | 6.82 | 8.8E-146 | Brevican, chondroitin sulfate proteoglycan. |
| *Tiam2* | 6.78 | 0.0E+00 | T Cell Lymphoma Invasion and Metastasis 2. Guanine nucleotide exchange factor. |
| *Trnp1* | 6.73 | 2.6E-80 | TIM1-Regulated Nuclear Protein 1. DNA binding protein. |
| *Tac2* | 6.69 | 8.1E-27 | Tachykinin 2. Neurotransmitter. |
| *Ndrg1* | 6.62 | 7.3E-298 | N-Myc Downstream Regulated 1. Hydrolase activity. |
| *Abcc8* | 6.57 | 2.8E-261 | ATP-Binding Cassette Subfamily C Member 8. Transporter. |
| *Kcnh3* | 6.53 | 9.3E-84 | Potassium Voltage-Gated Channel Subfamily H Member 3. |
| *Dync1i1* | 6.22 | 1.7E-214 | Dynein Cytoplasmic 1 Intermediate Chain 1. Microtubule binding. |
| *Nr4a3* | 6.14 | 9.9E-236 | Nuclear Receptor Subfamily 4 Group A Member 3. Transcriptional activator. |
| *Jakmip1* | 6.01 | 1.1E-248 | Janus Kinase And Microtubule Interacting Protein 1. |
| *Cryab* | 5.99 | 4.6E-23 | Crystallin Alpha B. Chaperone. |
| *Gpr12* | 5.96 | 1.5E-43 | G Protein-Coupled Receptor 12. |
| *Adra2c* | 5.91 | 3.0E-36 | Adrenoreceptor Alpha 2C. |
| *Itprid1* | 5.80 | 1.9E-86 | ITPR Interacting Domain Containing 1. Signalling receptor. |
| *2810459M11Rik* | 5.75 | 1.0E-58 | Uncharacterized Protein C2orf72. |
| *Fam43b* | 5.70 | 2.0E-17 | Protein FAM43B. Function not known. |
| *Glt28d2* | 5.66 | 1.6E-19 | Glycosyltransferase 28 domain-containing 2. |
| *Adamtsl3* | 5.63 | 4.8E-181 | ADAMTS-like protein. Glycoprotein. |
| *Rgs6* | 5.61 | 4.8E-46 | Regulator of G protein signalling 6. GTPase-activity. |
| *Htra1* | 5.58 | 2.1E-52 | HtrA Serine Peptidase 1. |

**Table 3. DAVID functional enrichment analysis of the down-regulated genes**

| **CELL CYCLE** | **Enrichment Score: 29.9** | | |
|---|---|---|---|
| **Category** | **Term** | **Count** | ***p*-value** |
| UP_KEYWORDS | Cell cycle | 191 | 5.85E-41 |
| GOTERM_BP_DIRECT | GO:0007049~cell cycle | 188 | 2.90E-37 |
| UP_KEYWORDS | Mitosis | 99 | 2.10E-29 |
| UP_KEYWORDS | Cell division | 117 | 2.88E-26 |
| GOTERM_BP_DIRECT | GO:0007067~mitotic nuclear division | 100 | 8.77E-26 |
| GOTERM_BP_DIRECT | GO:0051301~cell division | 117 | 5.30E-24 |
| **DNA REPLICATION** | **Enrichment Score: 17.0** | | |
| **Category** | **Term** | **Count** | **p-value** |
| UP_KEYWORDS | DNA replication | 49 | 2.58E-21 |
| GOTERM_BP_DIRECT | GO:0006260~DNA replication | 56 | 8.67E-20 |
| KEGG_PATHWAY | mmu03030:DNA replication | 23 | 4.70E-12 |
| **EXTRACELLULAR MATRIX** | **Enrichment Score: 12.7** | | |
| **Category** | **Term** | **Count** | **p-value** |
| GOTERM_CC_DIRECT | GO:0005578~proteinaceous extracellular matrix | 84 | 2.41E-15 |
| UP_KEYWORDS | Extracellular matrix | 68 | 1.12E-14 |
| GOTERM_CC_DIRECT | GO:0031012~extracellular matrix | 75 | 8.29E-13 |
| GOTERM_CC_DIRECT | GO:0005604~basement membrane | 37 | 8.01E-11 |
| **DNA DAMAGE/REPAIR** | **Enrichment Score: 12.1** | | |
| **Category** | **Term** | **Count** | **p-value** |
| UP_KEYWORDS | DNA damage | 88 | 4.72E-14 |
| UP_KEYWORDS | DNA repair | 77 | 9.97E-14 |
| GOTERM_BP_DIRECT | GO:0006281~DNA repair | 84 | 3.21E-12 |
| GOTERM_BP_DIRECT | GO:0006974~cellular response to DNA damage stimulus | 100 | 1.76E-11 |
| **CHROMOSOME** | **Enrichment Score: 12.1** | | |
| **Category** | **Term** | **Count** | **p-value** |
| GOTERM_CC_DIRECT | GO:0000775~chromosome, centromeric region | 56 | 2.87E-17 |
| GOTERM_CC_DIRECT | GO:0005694~chromosome | 91 | 2.40E-15 |
| UP_KEYWORDS | Chromosome | 92 | 2.44E-14 |
| UP_KEYWORDS | Centromere | 49 | 3.08E-14 |
| UP_KEYWORDS | Kinetochore | 37 | 6.88E-12 |
| GOTERM_CC_DIRECT | GO:0000776~kinetochore | 43 | 1.58E-11 |
| GOTERM_BP_DIRECT | GO:0007059~chromosome segregation | 34 | 6.11E-10 |
| GOTERM_CC_DIRECT | GO:0000777~condensed chromosome kinetochore | 29 | 5.71E-08 |
| **DNA-BINDING** | **Enrichment Score: 7.7** | | |
| **Category** | **Term** | **Count** | **p-value** |
| UP_KEYWORDS | DNA-binding | 277 | 1.18E-20 |
| GOTERM_MF_DIRECT | GO:0003677~DNA binding | 307 | 5.70E-18 |
| UP_KEYWORDS | Nucleus | 624 | 3.90E-14 |

| | | | |
|---|---|---|---|
| GOTERM_MF_DIRECT | GO:0043565~sequence-specific DNA binding | 119 | 8.27E-11 |
| GOTERM_BP_DIRECT | GO:0045944~positive regulation of transcription from RNA polymerase II promoter | 164 | 5.51E-07 |
| UP_KEYWORDS | Activator | 102 | 2.63E-05 |
| UP_KEYWORDS | Transcription regulation | 242 | 1.98E-04 |
| GOTERM_MF_DIRECT | GO:0003700~transcription factor activity. sequence-specific DNA binding | 129 | 2.10E-04 |
| UP_KEYWORDS | Transcription | 247 | 3.68E-04 |
| GOTERM_BP_DIRECT | GO:0006351~transcription. DNA-templated | 245 | 0.0193 |
| GOTERM_BP_DIRECT | GO:0006355~regulation of transcription, DNA-templated | 278 | 0.0554 |

**Table 4. DAVID functional enrichment analysis of the up-regulated genes**

| **SYNAPSE** | **Enrichment Score: 29.8** | | |
|---|---|---|---|
| **Category** | **Term** | **Count** | ***p*-value** |
| GOTERM_CC_DIRECT | GO:0045202~synapse | 169 | 6.71E-48 |
| UP_KEYWORDS | Synapse | 134 | 6.89E-44 |
| UP_KEYWORDS | Cell junction | 157 | 6.39E-26 |
| GOTERM_CC_DIRECT | GO:0045211~postsynaptic membrane | 78 | 3.93E-23 |
| GOTERM_CC_DIRECT | GO:0030054~cell junction | 159 | 2.86E-22 |
| UP_KEYWORDS | Postsynaptic cell membrane | 64 | 2.95E-20 |
| **MEMBRANE** | **Enrichment Score: 16.6** | | |
| **Category** | **Term** | **Count** | ***p*-value** |
| GOTERM_CC_DIRECT | GO:0005886~plasma membrane | 573 | 1.12E-43 |
| UP_KEYWORDS | Membrane | 862 | 4.24E-32 |
| GOTERM_CC_DIRECT | GO:0016020~membrane | 833 | 4.76E-20 |
| UP_KEYWORDS | Transmembrane helix | 627 | 8.13E-20 |
| UP_KEYWORDS | Transmembrane | 628 | 1.03E-19 |
| GOTERM_CC_DIRECT | GO:0016021~integral component of membrane | 627 | 2.87E-18 |
| UP_KEYWORDS | Glycoprotein | 454 | 1.76E-16 |
| UP_SEQ_FEATURE | Topological domain: Cytoplasmic | 361 | 3.61E-16 |
| UP_SEQ_FEATURE | Transmembrane region | 509 | 3.86E-16 |
| UP_SEQ_FEATURE | Glycosylation site:N-linked (GlcNAc...) | 403 | 3.46E-13 |
| UP_SEQ_FEATURE | Topological domain: Extracellular | 272 | 9.63E-12 |
| UP_KEYWORDS | Signal | 403 | 1.54E-10 |
| UP_SEQ_FEATURE | Signal peptide | 312 | 5.38E-08 |
| UP_KEYWORDS | Disulfide bond | 301 | 2.18E-07 |
| UP_SEQ_FEATURE | Disulfide bond | 240 | 1.32E-06 |
| **ION CHANNEL** | **Enrichment Score: 10.3** | | |
| **Category** | **Term** | **Count** | ***p*-value** |
| UP_KEYWORDS | Ion channel | 95 | 1.77E-21 |
| GOTERM_MF_DIRECT | GO:0005216~ion channel activity | 63 | 5.71E-21 |
| GOTERM_BP_DIRECT | GO:0006811~ion transport | 120 | 2.81E-15 |
| INTERPRO | IPR005821:Ion transport domain | 42 | 2.94E-15 |
| UP_KEYWORDS | Ion transport | 124 | 3.56E-15 |
| GOTERM_BP_DIRECT | GO:0034765~regulation of ion transmembrane transport | 48 | 6.64E-15 |
| UP_KEYWORDS | Voltage-gated channel | 47 | 5.08E-14 |
| GOTERM_MF_DIRECT | GO:0005244~voltage-gated ion channel activity | 46 | 1.52E-13 |
| UP_KEYWORDS | Potassium | 41 | 2.51E-12 |
| UP_KEYWORDS | Potassium transport | 38 | 5.67E-12 |
| GOTERM_MF_DIRECT | GO:0005267~potassium channel activity | 32 | 6.82E-12 |
| GOTERM_CC_DIRECT | GO:0008076~voltage-gated potassium channel complex | 32 | 9.88E-12 |

| | | | |
|---|---|---|---|
| UP_KEYWORDS | Potassium channel | 29 | 1.04E-11 |
| GOTERM_BP_DIRECT | GO:0006813~potassium ion transport | 41 | 1.83E-11 |
| GOTERM_BP_DIRECT | GO:0071805~potassium ion transmembrane transport | 33 | 2.18E-11 |
| GOTERM_MF_DIRECT | GO:0005249~voltage-gated potassium channel activity | 28 | 4.77E-10 |
| REACTOME_PATHWAY | R-MMU-1296072:R-MMU-1296072 | 20 | 1.36E-09 |
| GOTERM_BP_DIRECT | GO:0055085~transmembrane transport | 71 | 1.94E-08 |
| UP_SEQ_FEATURE | Short sequence motif: Selectivity filter | 22 | 2.31E-08 |
| INTERPRO | IPR003131:Potassium channel tetramerisation-type BTB domain | 20 | 2.90E-07 |
| INTERPRO | IPR027359: Voltage-dependent potassium channel, four helix bundle domain | 20 | 4.16E-07 |
| GOTERM_MF_DIRECT | GO:0005251~delayed rectifier potassium channel activity | 14 | 6.43E-06 |
| UP_SEQ_FEATURE | Region of interest: Segment H5 (pore-forming) | 12 | 1.64E-05 |
| INTERPRO | IPR003968: Potassium channel. voltage dependent, Kv | 12 | 2.90E-05 |
| UP_KEYWORDS | Transport | 225 | 7.32E-04 |
| GOTERM_BP_DIRECT | GO:0006810~transport | 215 | 0.0025 |

| **CALCIUM ION TRANSPORT** | **Enrichment Score: 6.5** | | |
|---|---|---|---|
| **Category** | **Term** | **Count** | ***p*-value** |
| UP_KEYWORDS | Calcium transport | 30 | 6.17E-09 |
| GOTERM_BP_DIRECT | GO:0070588~calcium ion transmembrane transport | 28 | 4.16E-08 |
| GOTERM_BP_DIRECT | GO:0006816~calcium ion transport | 37 | 4.64E-08 |
| UP_KEYWORDS | Calcium channel | 22 | 1.07E-07 |
| GOTERM_MF_DIRECT | GO:0005262~calcium channel activity | 25 | 1.12E-06 |
| GOTERM_MF_DIRECT | GO:0005245~voltage-gated calcium channel activity | 13 | 4.77E-04 |

| **CALMODULIN BINDING** | **Enrichment Score: 6.4** | | |
|---|---|---|---|
| **Category** | **Term** | **Count** | ***p*-value** |
| GOTERM_MF_DIRECT | GO:0005516~calmodulin binding | 46 | 4.49E-09 |
| UP_KEYWORDS | Calmodulin-binding | 36 | 1.62E-07 |
| UP_SEQ_FEATURE | Region of interest: Calmodulin-binding | 16 | 8.48E-05 |

| **CELL DIFFERENTIATION** | **Enrichment Score: 4.5** | | |
|---|---|---|---|
| **Category** | **Term** | **Count** | ***p*-value** |
| UP_KEYWORDS | Neurogenesis | 73 | 9.25E-17 |
| UP_KEYWORDS | Differentiation | 89 | 3.88E-04 |
| GOTERM_BP_DIRECT | GO:0030154~cell differentiation | 94 | 0.0145 |
| UP_KEYWORDS | Developmental protein | 101 | 0.1665 |
| GOTERM_BP_DIRECT | GO:0007275~multicellular organism development | 101 | 0.3666 |

# Annex 2

**Table 1. miRNA genes down-regulated in radial glial cells (E15.5 *vs* E11.5)**

| ***mir* name** | **log2 FC** | **adj *p*-value** | ***mir* name** | **log2 FC** | **adj *p*-value** |
|---|---|---|---|---|---|
| *mir-214* | -5.78 | 5.6E-15 | *mir-540* | -2.55 | 1.7E-29 |
| *mir-6539* | -4.94 | 6.4E-23 | *mir-375* | -2.52 | 3.1E-15 |
| *mir-302a* | -4.88 | 3.4E-19 | *mir-92-2* | -2.52 | 1.5E-55 |
| *mir-302d* | -4.71 | 7.6E-23 | *mir-124a-3* | -2.50 | 0.0084 |
| *mir-302b* | -4.31 | 1.0E-19 | *mir-341* | -2.38 | 1.5E-15 |
| *mir-295* | -4.08 | 3.0E-10 | *mir-6546* | -2.38 | 0.0025 |
| *mir-199b* | -3.82 | 3.5E-11 | *mir-6399* | -2.33 | 3.9E-04 |
| *mir-200b* | -3.79 | 7.8E-08 | *mir-493* | -2.31 | 7.9E-14 |
| *mir-449c* | -3.63 | 2.9E-57 | *mir-494* | -2.26 | 1.7E-22 |
| *mir-758* | -3.60 | 8.4E-47 | *mir-7220* | -2.26 | 2.9E-08 |
| *mir-183* | -3.55 | 1.1E-26 | *mir-219-2* | -2.17 | 1.1E-07 |
| *mir-367* | -3.44 | 1.3E-04 | *mir-335* | -2.16 | 1.0E-31 |
| *mir-205* | -3.40 | 1.7E-04 | *mir-153* | -2.09 | 7.1E-04 |
| *mir-18b* | -3.40 | 5.9E-52 | *mir-217* | -2.07 | 1.5E-05 |
| *mir-450b* | -3.28 | 3.5E-73 | *mir-433* | -2.02 | 1.5E-23 |
| *mir-1197* | -3.28 | 2.8E-22 | *mir-666* | -2.00 | 3.5E-12 |
| *mir-31* | -3.26 | 1.2E-60 | *mir-337* | -1.99 | 5.1E-15 |
| *mir-135a-1* | -3.26 | 7.4E-49 | *mir-155* | -1.97 | 1.9E-15 |
| *mir-216b* | -3.24 | 4.5E-17 | *mir-1193* | -1.96 | 2.0E-09 |
| *mir-1298* | -3.23 | 1.1E-05 | *mir-134* | -1.95 | 4.5E-15 |
| *mir-653* | -3.20 | 4.7E-08 | *mir-665* | -1.92 | 7.0E-07 |
| *mir-200a* | -3.20 | 2.9E-04 | *mir-667* | -1.90 | 3.6E-17 |
| *mir-449b* | -3.17 | 4.9E-06 | *mir-34c* | -1.78 | 2.5E-14 |
| *mir-182* | -3.17 | 1.0E-26 | *mir-92b* | -1.74 | 1.9E-17 |
| *mir-96* | -3.15 | 5.4E-06 | *mir-7082* | -1.70 | 1.3E-06 |
| *mir-429* | -3.06 | 1.9E-04 | *mir-379* | -1.70 | 2.8E-08 |
| *mir-448* | -3.01 | 1.9E-07 | *mir-377* | -1.64 | 8.2E-11 |
| *mir-216a* | -2.96 | 3.0E-08 | *mir-7648* | -1.64 | 0.0021 |
| *mir-363* | -2.92 | 3.7E-50 | *mir-449a* | -1.61 | 1.6E-08 |
| *mir-106a* | -2.87 | 1.5E-31 | *mir-410* | -1.61 | 1.2E-07 |
| *mir-20b* | -2.84 | 4.5E-57 | *mir-34b* | -1.59 | 1.1E-05 |
| *mir-431* | -2.83 | 1.1E-35 | *mir-3072* | -1.59 | 8.5E-04 |
| *mir-5128* | -2.83 | 8.3E-12 | *mir-673* | -1.54 | 1.2E-06 |
| *mir-293* | -2.78 | 0.0024 | *mir-411* | -1.54 | 2.5E-08 |
| *mir-679* | -2.74 | 5.2E-32 | *mir-323* | -1.52 | 1.7E-11 |
| *mir-204* | -2.61 | 9.7E-39 | *mir-541* | -1.50 | 2.9E-12 |

**Table 2. miRNA genes up-regulated in radial glial cells (E15.5 *vs* E11.5)**

| ***mir* name** | **log2 FC** | **adj *p*-value** | ***mir* name** | **log2 FC** | **adj *p*-value** |
|---|---|---|---|---|---|
| *let*-7c-2 | 6.19 | 2.4E-57 | *mir*-701 | 2.05 | 4.5E-10 |
| *let*-7b | 6.11 | 8.3E-27 | *mir*-383 | 2.05 | 1.1E-06 |
| *mir*-3059 | 5.59 | 8.3E-27 | *mir*-125b-1 | 2.05 | 1.6E-24 |
| *mir*-128-2 | 4.65 | 1.5E-53 | *mir*-3085 | 2.01 | 2.2E-22 |
| *mir*-2137 | 4.21 | 5.1E-24 | *mir*-150 | 2.01 | 0.0029 |
| *let*-7c-1 | 3.72 | 1.2E-69 | *let*-7i | 1.99 | 4.8E-11 |
| *mir*-6769b | 3.31 | 2.7E-04 | *mir*-3099 | 1.98 | 7.6E-25 |
| *mir*-122a | 3.29 | 0.0011 | *let*-7g | 1.98 | 1.6E-21 |
| *let*-7a-2 | 3.20 | 1.4E-26 | *mir*-7b | 1.91 | 2.8E-07 |
| *mir*-100 | 3.15 | 1.5E-23 | *let*-7a-1 | 1.89 | 9.5E-07 |
| *mir*-99a | 3.13 | 5.9E-62 | *mir*-101a | 1.89 | 1.3E-28 |
| *mir*-128-1 | 3.11 | 6.9E-103 | *mir*-708 | 1.87 | 3.7E-55 |
| *let*-7f-2 | 3.02 | 3.6E-59 | *mir*-23a | 1.86 | 2.3E-23 |
| *mir*-125b-2 | 2.95 | 1.3E-47 | *mir*-218-2 | 1.78 | 2.4E-04 |
| *let*-7j | 2.87 | 1.7E-08 | *mir*-672 | 1.77 | 3.9E-15 |
| *mir*-195 | 2.85 | 1.1E-27 | *mir*-193 | 1.70 | 4.1E-06 |
| *mir*-98 | 2.77 | 2.4E-24 | *mir*-181c | 1.67 | 1.5E-36 |
| *mir*-132 | 2.67 | 4.1E-61 | *mir*-1247 | 1.67 | 0.0016 |
| *mir*-144 | 2.58 | 2.4E-04 | *mir*-486 | 1.58 | 2.6E-04 |
| *let*-7d | 2.53 | 1.4E-15 | *mir*-22 | 1.55 | 5.2E-30 |
| *mir*-124a-1 | 2.43 | 1.4E-09 | *mir*-181a-1 | 1.53 | 3.6E-15 |
| *mir*-5129 | 2.33 | 2.5E-04 | *mir*-338 | 1.53 | 2.0E-16 |
| *mir*-7066 | 2.16 | 5.2E-04 | *mir*-500 | 1.51 | 1.9E-08 |
| *mir*-212 | 2.11 | 2.1E-18 | | | |

**Table 3. DAVID functional enrichment analysis of the putative targets of the up-regulated miRNAs**

| **DNA-BINDING** | **Enrichment Score: 10.5** | | |
|---|---|---|---|
| **Category** | **Term** | **Count** | ***p*-value** |
| UP_KEYWORDS | DNA-binding | 93 | 1.36E-15 |
| GOTERM_BP_DIRECT | GO:0045944~positive regulation of transcription from RNA polymerase II promoter | 75 | 1.59E-15 |
| GOTERM_MF_DIRECT | GO:0003677~DNA binding | 101 | 2.24E-13 |
| UP_KEYWORDS | Transcription regulation | 99 | 2.88E-13 |
| UP_KEYWORDS | Transcription | 101 | 3.52E-13 |
| GOTERM_MF_DIRECT | GO:0043565~sequence-specific DNA binding | 50 | 2.99E-12 |
| GOTERM_BP_DIRECT | GO:0006355~regulation of transcription, DNA-templated | 113 | 3.74E-11 |
| GOTERM_BP_DIRECT | GO:0006351~transcription, DNA-templated | 101 | 3.98E-11 |
| UP_KEYWORDS | Activator | 45 | 1.44E-09 |
| GOTERM_MF_DIRECT | GO:0003700~transcription factor activity, sequence-specific DNA binding | 55 | 5.83E-09 |
| UP_KEYWORDS | Nucleus | 160 | 1.77E-06 |
| GOTERM_CC_DIRECT | GO:0005634~nucleus | 190 | 1.87E-04 |
| **WNT SIGNALING PATHWAY** | **Enrichment Score: 4.6** | | |
| **Category** | **Term** | **Count** | ***p*-value** |
| GOTERM_BP_DIRECT | GO:0060070~canonical Wnt signaling pathway | 16 | 1.45E-08 |
| KEGG_PATHWAY | mmu05217:Basal cell carcinoma | 12 | 1.51E-06 |
| KEGG_PATHWAY | mmu04390:Hippo signaling pathway | 17 | 3.61E-05 |
| GOTERM_BP_DIRECT | GO:0016055~Wnt signaling pathway | 18 | 5.83E-05 |
| UP_KEYWORDS | Wnt signaling pathway | 16 | 8.47E-05 |
| KEGG_PATHWAY | mmu04310:Wnt signaling pathway | 15 | 2.04E-04 |
| KEGG_PATHWAY | mmu04916:Melanogenesis | 10 | 0.0053 |
| **EXTRACELLULAR MATRIX** | **Enrichment Score: 4.4** | | |
| **Category** | **Term** | **Count** | ***p*-value** |
| GOTERM_CC_DIRECT | GO:0005578~proteinaceous extracellular matrix | 31 | 5.28E-10 |
| UP_KEYWORDS | Extracellular matrix | 24 | 2.75E-08 |
| GOTERM_MF_DIRECT | GO:0005201~extracellular matrix structural constituent | 11 | 8.23E-08 |
| UP_SEQ_FEATURE | Domain: Fibrillar collagen NC1 | 7 | 1.01E-07 |
| KEGG_PATHWAY | mmu04512:ECM-receptor interaction | 16 | 1.83E-07 |
| INTERPRO | IPR000885:Fibrillar collagen, C-terminal | 7 | 2.01E-07 |
| SMART | SM00038:COLFI | 7 | 8.80E-07 |
| KEGG_PATHWAY | mmu04151:PI3K-Akt signaling pathway | 29 | 2.25E-06 |
| GOTERM_CC_DIRECT | GO:0005576~extracellular region | 63 | 3.44E-06 |
| UP_KEYWORDS | Secreted | 58 | 5.10E-06 |
| UP_SEQ_FEATURE | Propeptide:N-terminal propeptide | 5 | 9.51E-06 |
| GOTERM_MF_DIRECT | GO:0048407~platelet-derived growth factor binding | 6 | 1.31E-05 |

| | | | |
|---|---|---|---|
| UP_SEQ_FEATURE | Propeptide:C-terminal propeptide | 5 | 2.17E-05 |
| GOTERM_CC_DIRECT | GO:0005581~collagen trimer | 11 | 3.93E-05 |
| KEGG_PATHWAY | mmu04510:Focal adhesion | 20 | 5.24E-05 |
| GOTERM_CC_DIRECT | GO:0031012~extracellular matrix | 21 | 6.45E-05 |
| INTERPRO | IPR001007:von Willebrand factor, type C | 8 | 8.07E-05 |
| SMART | SM00214:VWC | 8 | 1.22E-04 |
| INTERPRO | IPR008160:Collagen triple helix repeat | 10 | 1.33E-04 |
| UP_KEYWORDS | Collagen | 10 | 2.05E-04 |
| KEGG_PATHWAY | mmu04974:Protein digestion and absorption | 11 | 2.34E-04 |
| UP_KEYWORDS | Hydroxylation | 10 | 4.01E-04 |
| GOTERM_BP_DIRECT | GO:0030199~collagen fibril organization | 7 | 6.42E-04 |
| UP_SEQ_FEATURE | Domain:VWFC | 5 | 0.0012 |
| KEGG_PATHWAY | mmu04611:Platelet activation | 13 | 0.0013 |
| UP_SEQ_FEATURE | region of interest:Triple-helical region | 5 | 0.0015 |
| GOTERM_BP_DIRECT | GO:0071230~cellular response to amino acid stimulus | 7 | 0.0047 |
| GOTERM_CC_DIRECT | GO:0005615~extracellular space | 43 | 0.0067 |
| UP_SEQ_FEATURE | Glycosylation site:O-linked (Gal...) | 3 | 0.011 |
| KEGG_PATHWAY | mmu05146:Amoebiasis | 9 | 0.016 |
| GOTERM_MF_DIRECT | GO:0046332~SMAD binding | 4 | 0.20 |

**METAL-BINDING** **Enrichment Score: 3.6**

| Category | Term | Count | *p*-value |
|---|---|---|---|
| UP_KEYWORDS | Metal-binding | 120 | 2.43E-05 |
| UP_KEYWORDS | Zinc | 81 | 1.18E-04 |
| GOTERM_MF_DIRECT | GO:0046872~metal ion binding | 120 | 2.96E-04 |
| UP_KEYWORDS | Zinc-finger | 57 | 0.0068 |

**BMP SIGNALING PATHWAY** **Enrichment Score: 3.1**

| Category | Term | Count | *p*-value |
|---|---|---|---|
| GOTERM_BP_DIRECT | GO:0030509~BMP signaling pathway | 10 | 1.69E-04 |
| KEGG_PATHWAY | mmu04350:TGF-beta signaling pathway | 11 | 3.22E-04 |
| UP_KEYWORDS | Chondrogenesis | 4 | 0.0070 |

**Table 4. DAVID functional enrichment analysis of the putative targets of the down-regulated miRNAs**

| **SYNAPSE** | **Enrichment Score: 16.8** | | |
|---|---|---|---|
| **Category** | **Term** | **Count** | ***p*-value** |
| GOTERM_CC_DIRECT | GO:0045202~synapse | 82 | 1.72E-27 |
| UP_KEYWORDS | Synapse | 63 | 1.87E-23 |
| UP_KEYWORDS | Cell junction | 75 | 8.33E-17 |
| GOTERM_CC_DIRECT | GO:0030054~cell junction | 76 | 2.00E-14 |
| GOTERM_CC_DIRECT | GO:0045211~postsynaptic membrane | 36 | 5.90E-12 |
| UP_KEYWORDS | Postsynaptic cell membrane | 30 | 5.83E-11 |
| **MEMBRANE** | **Enrichment Score: 10.3** | | |
| **Category** | **Term** | **Count** | ***p*-value** |
| UP_KEYWORDS | Cell membrane | 189 | 2.04E-24 |
| GOTERM_CC_DIRECT | GO:0005886~plasma membrane | 248 | 2.87E-24 |
| UP_KEYWORDS | Membrane | 360 | 1.17E-19 |
| GOTERM_CC_DIRECT | GO:0016020~membrane | 366 | 4.66E-17 |
| UP_KEYWORDS | Glycoprotein | 195 | 3.28E-11 |
| UP_KEYWORDS | Transmembrane | 258 | 5.93E-11 |
| UP_KEYWORDS | Transmembrane helix | 257 | 7.39E-11 |
| UP_SEQ_FEATURE | Topological domain:Cytoplasmic | 161 | 3.78E-10 |
| GOTERM_CC_DIRECT | GO:0016021~integral component of membrane | 257 | 4.07E-09 |
| UP_SEQ_FEATURE | Transmembrane region | 219 | 4.50E-09 |
| UP_SEQ_FEATURE | Topological domain:Extracellular | 124 | 3.30E-08 |
| UP_SEQ_FEATURE | Glycosylation site:N-linked (GlcNAc...) | 170 | 9.76E-07 |
| UP_KEYWORDS | Disulfide bond | 125 | 7.09E-05 |
| UP_KEYWORDS | Signal | 147 | 0.0029 |
| UP_SEQ_FEATURE | Disulfide bond | 98 | 0.0033 |
| UP_SEQ_FEATURE | Signal peptide | 121 | 0.0081 |
| **NEUROGENESIS** | **Enrichment Score: 7.8** | | |
| **Category** | **Term** | **Count** | ***p*-value** |
| GOTERM_BP_DIRECT | GO:0007399~nervous system development | 63 | 4.95E-21 |
| UP_KEYWORDS | Neurogenesis | 42 | 8.89E-15 |
| UP_KEYWORDS | Differentiation | 48 | 8.91E-06 |
| GOTERM_BP_DIRECT | GO:0030154~cell differentiation | 49 | 0.0012 |
| UP_KEYWORDS | Developmental protein | 54 | 0.0022 |
| GOTERM_BP_DIRECT | GO:0007275~multicellular organism development | 55 | 0.0110 |
| **ION TRANSPORT** | **Enrichment Score: 5.4** | | |
| **Category** | **Term** | **Count** | ***p*-value** |
| GOTERM_MF_DIRECT | GO:0005216~ion channel activity | 33 | 2.85E-13 |
| UP_KEYWORDS | Ion channel | 45 | 1.13E-12 |
| INTERPRO | IPR005821:Ion transport domain | 23 | 1.68E-10 |
| UP_KEYWORDS | Ion transport | 55 | 8.15E-09 |

| | | | |
|---|---|---|---|
| GOTERM_BP_DIRECT | GO:0034765~regulation of ion transmembrane transport | 23 | 3.23E-08 |
| UP_KEYWORDS | Voltage-gated channel | 22 | 8.46E-08 |
| GOTERM_BP_DIRECT | GO:0006811~ion transport | 52 | 1.15E-07 |
| GOTERM_MF_DIRECT | GO:0005244~voltage-gated ion channel activity | 21 | 7.15E-07 |
| GOTERM_MF_DIRECT | GO:0005267~potassium channel activity | 15 | 3.85E-06 |
| GOTERM_BP_DIRECT | GO:0055085~transmembrane transport | 34 | 9.11E-06 |
| UP_KEYWORDS | Potassium channel | 13 | 9.77E-06 |
| GOTERM_BP_DIRECT | GO:0071805~potassium ion transmembrane transport | 15 | 1.13E-05 |
| GOTERM_BP_DIRECT | GO:0006813~potassium ion transport | 18 | 1.60E-05 |
| UP_KEYWORDS | Potassium transport | 16 | 1.83E-05 |
| GOTERM_MF_DIRECT | GO:0005249~voltage-gated potassium channel activity | 13 | 3.45E-05 |
| GOTERM_BP_DIRECT | GO:0042391~regulation of membrane potential | 15 | 3.71E-05 |
| UP_KEYWORDS | Potassium | 16 | 6.73E-05 |
| GOTERM_CC_DIRECT | GO:0008076~voltage-gated potassium channel complex | 13 | 8.03E-05 |
| UP_SEQ_FEATURE | Short sequence motif:Selectivity filter | 10 | 3.70E-04 |
| UP_KEYWORDS | Transport | 96 | 0.002 |
| GOTERM_BP_DIRECT | GO:0006810~transport | 93 | 0.011 |
| UP_SEQ_FEATURE | Region of interest:Segment H5 (pore-forming) | 5 | 0.020 |
| INTERPRO | IPR003968:Potassium channel, voltage dependent, Kv | 5 | 0.023 |
| GOTERM_MF_DIRECT | GO:0005251~delayed rectifier potassium channel activity | 5 | 0.043 |

| **CALCIUM TRANSPORT** | **Enrichment Score: 5.0** | | |
|---|---|---|---|
| **Category** | **Term** | **Count** | ***p*-value** |
| UP_KEYWORDS | Calcium transport | 18 | 5.94E-08 |
| KEGG_PATHWAY | mmu04020:Calcium signaling pathway | 22 | 2.03E-05 |
| GOTERM_BP_DIRECT | GO:0006874~cellular calcium ion homeostasis | 13 | 6.30E-04 |

| **NODES OF RANVIER** | **Enrichment Score: 3.8** | | |
|---|---|---|---|
| **Category** | **Term** | **Count** | ***p*-value** |
| GOTERM_CC_DIRECT | GO:0033268~node of Ranvier | 8 | 1.81E-06 |
| GOTERM_CC_DIRECT | GO:0043194~axon initial segment | 6 | 1.24E-04 |
| GOTERM_CC_DIRECT | GO:0033270~paranode region of axon | 4 | 0.023 |

# Annex 3

**Table 1. Genes coding RNA binding proteins involved in alternative splicing differentially expressed in radial glial cells (E15.5 *vs* E11.5)**

| Gene | Log2 FC | Adj. *p*-value | Gene | Log2 FC | Adj. *p*-value |
|---|---|---|---|---|---|
| *Rbm47* | -4.75 | 1.9E-11 | ***Rbfox1*** | **3.92** | **5.2E-136** |
| *Mbnl3* | -3.18 | 1.1E-37 | ***Khdrbs2*** | **2.84** | **9.4E-94** |
| *Rbm20* | -2.16 | 3.1E-25 | ***Rbfox3*** | **1.93** | **3.5E-45** |
| ***Nova1*** | **-1.65** | **5.8E-43** | ***Celf2*** | **1.80** | **8.4E-35** |
| ***Qk*** | **-1.40** | **3.2E-14** | *Rbm24* | 1.53 | 2.4E-31 |
| *Rbm46* | -1.39 | 0.047 | ***Rbfox2*** | **1.41** | **2.3E-51** |
| *Rbm38* | -1.29 | 2.1E-19 | ***Srrm4*** | **1.40** | **4.2E-50** |
| ***Ptbp1*** | **-1.22** | **1.2E-29** | ***Elavl2*** | **1.17** | **1.1E-16** |
| *Rbm15* | -1.17 | 5.7E-24 | ***Elavl3*** | **1.12** | **1.2E-39** |
| *Rbms2* | -1.12 | 1.2E-29 | | | |
| *Ptbp3* | -1.10 | 1.3E-09 | | | |
| *Rbm43* | -1.01 | 0.001 | | | |

Genes are considered differentially expressed when log2 FC ≤ -1 or log2 FC ≥ +1 and adj. p-value < 0.05. In bold are the genes coding for RNA binding proteins with reported roles in the central nervous system (Vuong et al., 2016).

**Table 2. Top 25 alternative splicing events with decreased inclusion between E11.5 and E15.5 in radial glial cells**

| Gene | Events per gene | Coordinates | Type of event | Length | ΔPSI |
|---|---|---|---|---|---|
| *Cyp4f16* | 3 | chr17:32673940-32674141 | Alt3 | 3 | -74.79 |
| *Serinc4* | 1 | chr2:121278242-121278367 | Intron retaining | 126 | -74.60 |
| *Nin* | 5 | chr12:71143119-71145239 | Exon skipping | 2121 | -74.32 |
| *Ablim1* | 5 | chr19:57121415-57121555 | Exon skipping | 141 | -64.87 |
| *Mcm9* | 4 | chr10:53325915-53325996 | Exon skipping | 82 | -61.29 |
| *Map3k7* | 2 | chr4:32081849-32081929 | Exon skipping | 81 | -57.57 |
| *Mcm9* | 4 | chr10:53322154-53322269 | Exon skipping | 116 | -56.76 |
| *Clip1* | 8 | chr5:124077303-124077419 | Exon skipping | 117 | -55.46 |
| *Erbb4* | 3 | chr1:68336817-68336891 | Exon skipping | 75 | -54.10 |
| *Phf21a* | 4 | chr2:92191858-92192021 | Exon skipping | 164 | -53.88 |
| *Gad1* | 2 | chr2:70422477-70422556 | Exon skipping | 80 | -53.58 |
| *Dtnb* | 5 | chr12:3773551-3773640 | Exon skipping | 90 | -51.76 |
| *Lsamp* | 2 | chr16:42151357-42151392 | Exon skipping | 36 | -50.26 |
| *Phactr1* | 1 | chr13:43154940-43155146 | Exon skipping | 207 | -50.08 |
| *Cacna1c* | 7 | chr6:118588445-118588528 | Exon skipping | 84 | -47.64 |
| *Pcdh9* | 1 | chr14:93959797-94284915 | Intron retaining | 325119 | -46.68 |
| *Mcm9* | 4 | chr10:53327471-53328115 | Exon skipping | 645 | -46.50 |
| *Myo5a* | 3 | chr9:75040191-75040271 | Exon skipping | 81 | -45.90 |
| *Macf1* | 6 | chr4:123074337-123074663 | Exon skipping | 327 | -45.76 |
| *Slc6a17* | 1 | chr3:107280337-107294337 | Intron retaining | 14001 | -45.63 |
| *Arfgap1* | 5 | chr2:180715103-180715179 | Alt3 | 6 | -45.51 |
| *Ap1g2* | 4 | chr14:55723419-55723495 | Exon skipping | 77 | -45.07 |
| *Zfp949* | 3 | chr9:88447554-88447674 | Exon skipping | 121 | -44.22 |
| *Lgals8* | 4 | chr13:12553508-12553757 | Alt5 | 186 | -44.21 |
| *Cadm2* | 2 | chr16:66731630-66731749 | Exon skipping | 120 | -43.10 |

Alt5, alternative donor; Alt3, alternative acceptor.

**Table 3. Top 25 alternative splicing events with increased inclusion between E11.5 and E15.5 in radial glial cells**

| Gene | Events per gene | Coordinates | Type of event | Length | ΔPSI |
|---|---|---|---|---|---|
| *Fbn2* | 2 | chr18:58267384-58267411 | Exon skipping | 28 | 95.65 |
| *Nin* | 5 | chr12:71123268-71123328 | Exon skipping | 61 | 78.61 |
| *Pls3* | 1 | chrX:73045056-73045082 | Exon skipping | 27 | 75.27 |
| *Osbpl6* | 5 | chr2:76393947-76394039 | Exon skipping | 93 | 73.04 |
| *Ablim1* | 5 | chr19:57125620-57125724 | Exon skipping | 105 | 70.76 |
| *Hook2* | 2 | chr8:87522285-87522290 | Microexon | 6 | 68.35 |
| *Dtna* | 1 | chr18:23758904-23758912 | Microexon | 9 | 67.83 |
| *Shank2* | 6 | chr7:151593961-151593981 | Exon skipping | 21 | 67.41 |
| *Epb4.1l3* | 4 | chr17:69623222-69623257 | Exon skipping | 36 | 66.62 |
| *Sh3glb2* | 5 | chr2:30201579-30201593 | Microexon | 15 | 64.55 |
| *Vav2* | 4 | chr2:27140359-27140373 | Microexon | 15 | 64.38 |
| *Erbb4* | 3 | chr1:68337013-68337057 | Exon skipping | 45 | 63.09 |
| *Zdhhc20* | 2 | chr14:58468982-58469017 | Exon skipping | 36 | 62.91 |
| *Homer1* | 2 | chr13:94156300-94156335 | Exon skipping | 36 | 61.98 |
| *Dock9* | 5 | chr14:121943798-121943805 | Microexon | 8 | 61.82 |
| *Tmem184b* | 2 | chr15:79194088-79194108 | Exon skipping | 21 | 61.56 |
| *Itpr1* | 7 | chr6:108381455-108381490 | Exon skipping | 36 | 61.17 |
| *Lrrfip1* | 5 | chr1:93006932-93007024 | Exon skipping | 93 | 60.63 |
| *Cadm2* | 2 | chr16:66953519-66953545 | Exon skipping | 27 | 60.22 |
| *Atp8a1* | 2 | chr5:68147889-68147933 | Exon skipping | 45 | 59.46 |
| *Scrib* | 2 | chr15:75878352-75878426 | Exon skipping | 75 | 59.29 |
| *Lepre1* | 6 | chr4:118912311-118912366 | Exon skipping | 56 | 59.29 |
| *Ptprk* | 5 | chr10:28281913-28281948 | Exon skipping | 36 | 58.92 |
| *Mef2a* | 3 | chr7:74389407-74389430 | Exon skipping | 24 | 58.90 |
| *Ssr1* | 1 | chr13:38074964-38074978 | Microexon | 15 | 58.16 |

**Table 4. DAVID functional enrichment analysis of the genes with differential inclusion of alternative splicing events between E11 and E15**

| **ATP-BINDING** | **Enrichment Score: 7.1** | | |
|---|---|---|---|
| **Category** | **Term** | **Count** | ***p*-value** |
| UP_KEYWORDS | ATP-binding | 327 | 8.93E-14 |
| GOTERM_MF_DIRECT | GO:0005524~ATP binding | 347 | 2.37E-10 |
| UP_SEQ_FEATURE | nucleotide phosphate-binding region:ATP | 227 | 1.14E-09 |
| UP_KEYWORDS | Serine/threonine-protein kinase | 114 | 1.43E-09 |
| UP_KEYWORDS | Kinase | 178 | 1.81E-09 |
| UP_KEYWORDS | Nucleotide-binding | 379 | 1.88E-09 |
| INTERPRO | IPR011009:Protein kinase-like domain | 145 | 4.52E-09 |
| GOTERM_MF_DIRECT | GO:0000166~nucleotide binding | 422 | 2.54E-08 |
| GOTERM_MF_DIRECT | GO:0004674~protein serine/threonine kinase activity | 118 | 2.55E-08 |
| INTERPRO | IPR008271:Serine/threonine-protein kinase, active site | 93 | 7.06E-08 |
| UP_SEQ_FEATURE | domain:Protein kinase | 128 | 1.72E-07 |
| GOTERM_MF_DIRECT | GO:0016301~kinase activity | 172 | 2.08E-07 |
| GOTERM_BP_DIRECT | GO:0016310~phosphorylation | 157 | 2.99E-07 |
| INTERPRO | IPR000719:Protein kinase, catalytic domain | 129 | 3.56E-07 |
| GOTERM_BP_DIRECT | GO:0006468~protein phosphorylation | 146 | 6.90E-07 |
| SMART | SM00220:S_TKc | 107 | 1.60E-06 |
| INTERPRO | IPR017441:Protein kinase, ATP binding site | 102 | 3.17E-06 |
| UP_KEYWORDS | Transferase | 335 | 3.38E-06 |
| GOTERM_MF_DIRECT | GO:0004672~protein kinase activity | 134 | 3.47E-06 |
| UP_SEQ_FEATURE | binding site:ATP | 132 | 2.62E-05 |
| UP_SEQ_FEATURE | active site:Proton acceptor | 151 | 7.61E-05 |
| GOTERM_MF_DIRECT | GO:0016740~transferase activity | 307 | 2.05E-04 |
| **MICROTUBULE** | **Enrichment Score: 7.0** | | |
| **Category** | **Term** | **Count** | ***p*-value** |
| GOTERM_CC_DIRECT | GO:0005874~microtubule | 100 | 1.55E-09 |
| GOTERM_MF_DIRECT | GO:0008017~microtubule binding | 65 | 1.61E-07 |
| UP_KEYWORDS | Microtubule | 75 | 2.89E-06 |
| **SYNAPSE** | **Enrichment Score: 6.8** | | |
| **Category** | **Term** | **Count** | ***p*-value** |
| GOTERM_CC_DIRECT | GO:0045202~synapse | 144 | 5.13E-11 |
| UP_KEYWORDS | Synapse | 99 | 3.63E-07 |
| UP_KEYWORDS | Cell junction | 157 | 1.82E-06 |
| GOTERM_CC_DIRECT | GO:0030054~cell junction | 165 | 1.71E-05 |
| **DNA DAMAGE/REPAIR** | **Enrichment Score: 6.5** | | |
| **Category** | **Term** | **Count** | ***p*-value** |
| UP_KEYWORDS | DNA damage | 99 | 3.03E-08 |
| GOTERM_BP_DIRECT | GO:0006281~DNA repair | 96 | 1.07E-07 |

| | | | |
|---|---|---|---|
| UP_KEYWORDS | DNA repair | 81 | 1.05E-06 |
| GOTERM_BP_DIRECT | GO:0006974~cellular response to DNA damage stimulus | 114 | 2.45E-06 |

| **METAL-BINDING** | **Enrichment Score: 6.1** | | |
|---|---|---|---|
| **Category** | **Term** | **Count** | ***p*-value** |
| UP_KEYWORDS | Zinc-finger | 336 | 5.31E-08 |
| UP_KEYWORDS | Zinc | 427 | 1.58E-07 |
| UP_KEYWORDS | Metal-binding | 634 | 9.95E-07 |
| GOTERM_MF_DIRECT | GO:0046872~metal ion binding | 639 | 6.40E-05 |

| **CILLIUM BIOGENESIS/DEGRADATION** | **Enrichment Score: 5.0** | | |
|---|---|---|---|
| **Category** | **Term** | **Count** | ***p*-value** |
| GOTERM_BP_DIRECT | GO:0042384~cilium assembly | 46 | 2.87E-06 |
| GOTERM_BP_DIRECT | GO:0060271~cilium morphogenesis | 56 | 3.09E-06 |
| UP_KEYWORDS | Cilium biogenesis/degradation | 46 | 6.71E-06 |
| GOTERM_BP_DIRECT | GO:0030030~cell projection organization | 46 | 1.44E-04 |

| **POSTSYNAPTIC DENSITY** | **Enrichment Score: 4.9** | | |
|---|---|---|---|
| **Category** | **Term** | **Count** | ***p*-value** |
| GOTERM_CC_DIRECT | GO:0014069~postsynaptic density | 83 | 3.30E-10 |
| UP_KEYWORDS | Synapse | 99 | 3.63E-07 |
| GOTERM_CC_DIRECT | GO:0045211~postsynaptic membrane | 53 | 0.0107 |
| UP_KEYWORDS | Postsynaptic cell membrane | 43 | 0.0122 |

The analysis was done with 3,000 genes. Genes with ΔPSI values between 10.0% and 10.3% were not considered.

**Table 5. DAVID functional enrichment analysis of the genes with increased intron retention events between E15.5 and E11.5**

| **CILLIUM BIOGENESIS/DEGRADATION** | **Enrichment Score: 4.31** | | |
|---|---|---|---|
| **Category** | **Term** | **Count** | ***p*-value** |
| UP_KEYWORDS | Cilium biogenesis/degradation | 24 | 3.92E-06 |
| GOTERM_BP_DIRECT | GO:0060271~cilium morphogenesis | 27 | 1.29E-05 |
| GOTERM_BP_DIRECT | GO:0030030~cell projection organization | 23 | 9.76E-05 |
| GOTERM_BP_DIRECT | GO:0042384~cilium assembly | 21 | 1.09E-04 |
| GOTERM_CC_DIRECT | GO:0005929~cilium | 29 | 5.00E-04 |
| **CELL PROJECTION** | **Enrichment Score: 4.25** | | |
| **Category** | **Term** | **Count** | ***p*-value** |
| UP_KEYWORDS | Cell projection | 69 | 2.92E-06 |
| UP_KEYWORDS | Cilium | 27 | 1.49E-05 |
| GOTERM_CC_DIRECT | GO:0042995~cell projection | 68 | 4.33E-05 |
| GOTERM_CC_DIRECT | GO:0005929~cilium | 29 | 5.00E-04 |
| GOTERM_CC_DIRECT | GO:0036064~ciliary basal body | 17 | 5.95E-04 |
| **MICROTUBULE** | **Enrichment Score: 2.51** | | |
| **Category** | **Term** | **Count** | ***p*-value** |
| GOTERM_CC_DIRECT | GO:0005874~microtubule | 36 | 3.15E-04 |
| UP_KEYWORDS | Microtubule | 27 | 0.0043 |
| GOTERM_MF_DIRECT | GO:0008017~microtubule binding | 20 | 0.0222 |

**Table 6. DAVID functional enrichment analysis of the genes with decreased intron retention events between E15.5 and E11.5**

| **METAL ION BINDING** | **Enrichment Score: 4.29** | | |
|---|---|---|---|
| **Category** | **Term** | **Count** | ***p*-value** |
| UP_KEYWORDS | Zinc | 167 | 5.93E-06 |
| UP_KEYWORDS | Zinc-finger | 131 | 1.11E-05 |
| UP_KEYWORDS | Metal-binding | 238 | 6.07E-05 |
| GOTERM_MF_DIRECT | GO:0046872~metal ion binding | 233 | 0.0018 |
| **ATP BINDING** | **Enrichment Score: 3.28** | | |
| **Category** | **Term** | **Count** | ***p*-value** |
| UP_KEYWORDS | ATP-binding | 120 | 2.55E-06 |
| UP_KEYWORDS | Nucleotide-binding | 144 | 8.68E-06 |
| GOTERM_MF_DIRECT | GO:0005524~ATP binding | 126 | 5.41E-05 |
| UP_KEYWORDS | Kinase | 67 | 7.48E-05 |
| GOTERM_MF_DIRECT | GO:0000166~nucleotide binding | 154 | 1.59E-04 |
| UP_SEQ_FEATURE | nucleotide phosphate-binding region:ATP | 82 | 1.64E-04 |
| UP_KEYWORDS | Serine/threonine-protein kinase | 42 | 2.55E-04 |
| GOTERM_BP_DIRECT | GO:0016310~phosphorylation | 60 | 2.84E-04 |
| INTERPRO | IPR011009:Protein kinase-like domain | 53 | 3.05E-04 |
| UP_SEQ_FEATURE | active site:Proton acceptor | 62 | 3.18E-04 |
| GOTERM_MF_DIRECT | GO:0016301~kinase activity | 64 | 5.87E-04 |
| INTERPRO | IPR017441:Protein kinase, ATP binding site | 40 | 7.55E-04 |
| INTERPRO | IPR000719:Protein kinase, catalytic domain | 48 | 9.25E-04 |
| GOTERM_MF_DIRECT | GO:0004674~protein serine/threonine kinase activity | 42 | 0.0015 |
| UP_SEQ_FEATURE | domain:Protein kinase | 46 | 0.0018 |
| GOTERM_BP_DIRECT | GO:0006468~protein phosphorylation | 53 | 0.0020 |
| GOTERM_MF_DIRECT | GO:0004672~protein kinase activity | 50 | 0.0021 |
| INTERPRO | IPR008271:Serine/threonine-protein kinase, active site | 33 | 0.0023 |
| UP_KEYWORDS | Transferase | 120 | 0.0035 |
| SMART | SM00220:S_TKc | 37 | 0.0077 |
| UP_SEQ_FEATURE | binding site:ATP | 47 | 0.0114 |
| GOTERM_MF_DIRECT | GO:0016740~transferase activity | 110 | 0.0141 |
| **SYNAPSE** | **Enrichment Score: 3.17** | | |
| **Category** | **Term** | **Count** | ***p*-value** |
| GOTERM_CC_DIRECT | GO:0045202~synapse | 60 | 2.92E-07 |
| GOTERM_CC_DIRECT | GO:0014069~postsynaptic density | 37 | 4.50E-07 |
| UP_KEYWORDS | Synapse | 39 | 3.46E-04 |
| GOTERM_CC_DIRECT | GO:0045211~postsynaptic membrane | 24 | 0.0070 |
| GOTERM_CC_DIRECT | GO:0030054~cell junction | 54 | 0.0486 |

# BIBLIOGRAPHY

Aaku-Saraste, E., Hellwig, A., and Huttner, W.B. (1996). Loss of occludin and functional tight junctions, but not ZO-1, during neural tube closure--remodeling of the neuroepithelium prior to neurogenesis. Dev Biol 180, 664-679.

Adolfsen, B., and Littleton, J.T. (2001). Genetic and molecular analysis of the synaptotagmin family. Cell Mol Life Sci 58, 393-402.

Agarwal, V., Bell, G.W., Nam, J.W., and Bartel, D.P. (2015). Predicting effective microRNA target sites in mammalian mRNAs. Elife 4.

Albert, M., and Huttner, W.B. (2018). Epigenetic and Transcriptional Pre-patterning-An Emerging Theme in Cortical Neurogenesis. Front Neurosci 12, 359.

Allen, N.J., and Eroglu, C. (2017). Cell Biology of Astrocyte-Synapse Interactions. Neuron 96, 697-708.

Allen, N.J., and Lyons, D.A. (2018). Glia as architects of central nervous system formation and function. Science 362, 181-185.

Almeida, R.G., Czopka, T., Ffrench-Constant, C., and Lyons, D.A. (2011). Individual axons regulate the myelinating potential of single oligodendrocytes in vivo. Development 138, 4443-4450.

Altafaj, X., Martin, E.D., Ortiz-Abalia, J., Valderrama, A., Lao-Peregrin, C., Dierssen, M., and Fillat, C. (2013). Normalization of Dyrk1A expression by AAV2/1-shDyrk1A attenuates hippocampal-dependent defects in the Ts65Dn mouse model of Down syndrome. Neurobiol Dis 52, 117-127.

Alvarez, M., Altafaj, X., Aranda, S., and de la Luna, S. (2007). DYRK1A autophosphorylation on serine residue 520 modulates its kinase activity via 14-3-3 binding. Mol Biol Cell 18, 1167-1178.

Alvarez, M., Estivill, X., and de la Luna, S. (2003). DYRK1A accumulates in splicing speckles through a novel targeting signal and induces speckle disassembly. J Cell Sci 116, 3099-3107.

Anders, S., Pyl, P.T., and Huber, W. (2015). HTSeq--a Python framework to work with high-throughput sequencing data. Bioinformatics 31, 166-169.

Anderson, T.J., Schneider, A., Barrie, J.A., Klugmann, M., McCulloch, M.C., Kirkham, D., Kyriakides, E., Nave, K.A., and Griffiths, I.R. (1998). Late-onset neurodegeneration in mice with increased dosage of the proteolipid protein gene. J Comp Neurol 394, 506-519.

Andoh-Noda, T., Akamatsu, W., Miyake, K., Matsumoto, T., Yamaguchi, R., Sanosaka, T., Okada, Y., Kobayashi, T., Ohyama, M., Nakashima, K., et al. (2015). Differentiation of multipotent neural stem cells derived from Rett syndrome patients is biased toward the astrocytic lineage. Mol Brain 8, 31.

Andrews, S. (2010). FastQC: a quality control tool for high throughput sequence data. .

Angevine, J.B., Jr., and Sidman, R.L. (1961). Autoradiographic study of cell migration during histogenesis of cerebral cortex in the mouse. Nature 192, 766-768.

Aprea, J., and Calegari, F. (2012). Bioelectric state and cell cycle control of Mammalian neural stem cells. Stem Cells Int 2012, 816049.

Arai, Y., Funatsu, N., Numayama-Tsuruta, K., Nomura, T., Nakamura, S., and Osumi, N. (2005). Role of Fabp7, a downstream gene of Pax6, in the maintenance of neuroepithelial cells during early embryonic development of the rat cortex. J Neurosci 25, 9752-9761.

Arai, Y., Pulvers, J.N., Haffner, C., Schilling, B., Nusslein, I., Calegari, F., and Huttner, W.B. (2011). Neural stem and progenitor cells shorten S-phase on commitment to neuron production. Nat Commun 2, 154.

Arancibia-Carcamo, I.L., and Attwell, D. (2014). The node of Ranvier in CNS pathology. Acta Neuropathol 128, 161-175.

Arancibia-Carcamo, I.L., Ford, M.C., Cossell, L., Ishida, K., Tohyama, K., and Attwell, D. (2017). Node of Ranvier length as a potential regulator of myelinated axon conduction speed. Elife 6.

Aranda, S., Alvarez, M., Turro, S., Laguna, A., and de la Luna, S. (2008). Sprouty2-mediated inhibition of fibroblast growth factor signaling is modulated by the protein kinase DYRK1A. Mol Cell Biol 28, 5899-5911.

Aranda, S., Laguna, A., and de la Luna, S. (2011). DYRK family of protein kinases: evolutionary relationships, biochemical properties, and functional roles. FASEB J 25, 449-462.

Arque, G., Fotaki, V., Fernandez, D., Martinez de Lagran, M., Arbones, M.L., and Dierssen, M. (2008). Impaired spatial learning strategies and novel object recognition in mice haploinsufficient for the dual specificity tyrosine-regulated kinase-1A (Dyrk1A). PLoS One 3, e2575.

Arranz, J. (2016). Caracterización de las alteraciones estructurales y funcionales de la cortezaa cerebral de ratones mutantes de pérdida y ganancia de función de DYRK1A.

https://dialnet.unirioja.es/servlet/tesis?codigo=128087. In Facultat de Biologia (Barcelona, Universitat de Barcelona), p. 190.

Arranz, J., Balducci, E., Arato, K., Sanchez-Elexpuru, G., Najas, S., Parras, A., Rebollo, E., Pijuan, I., Erb, I., Verde, G., et al. (2019). Impaired development of neocortical circuits contributes to the neurological alterations in DYRK1A haploinsufficiency syndrome. Neurobiol Dis 127, 210-222.

Arron, J.R., Winslow, M.M., Polleri, A., Chang, C.P., Wu, H., Gao, X., Neilson, J.R., Chen, L., Heit, J.J., Kim, S.K., et al. (2006). NFAT dysregulation by increased dosage of DSCR1 and DYRK1A on chromosome 21. Nature 441, 595-600.

Arulmoli, J., Pathak, M.M., McDonnell, L.P., Nourse, J.L., Tombola, F., Earthman, J.C., and Flanagan, L.A. (2015). Static stretch affects neural stem cell differentiation in an extracellular matrix-dependent manner. Sci Rep 5, 8499.

Ayoub, A.E., Oh, S., Xie, Y., Leng, J., Cotney, J., Dominguez, M.H., Noonan, J.P., and Rakic, P. (2011). Transcriptional programs in transient embryonic zones of the cerebral cortex defined by high-resolution mRNA sequencing. Proc Natl Acad Sci U S A 108, 14950-14955.

Azzolin, L., Panciera, T., Soligo, S., Enzo, E., Bicciato, S., Dupont, S., Bresolin, S., Frasson, C., Basso, G., Guzzardo, V., et al. (2014). YAP/TAZ incorporation in the beta-catenin destruction complex orchestrates the Wnt response. Cell 158, 157-170.

Bachoo, R.M., Kim, R.S., Ligon, K.L., Maher, E.A., Brennan, C., Billings, N., Chan, S., Li, C., Rowitch, D.H., Wong, W.H., et al. (2004). Molecular diversity of astrocytes with implications for neurological disorders. Proc Natl Acad Sci U S A 101, 8384-8389.

Balducci, E. (2012). Effect of DYRK1A dose reduction on the transcriptome of the developing mouse cerebral cortex: implications in gliogenesis. https://dialnet.unirioja.es/servlet/tesis?codigo=140864. In Departament de Ciències Experimentals i de la Salut (TDX, Universitat Pompeu Fabra), p. 244.

Ballas, N., Lioy, D.T., Grunseich, C., and Mandel, G. (2009). Non-cell autonomous influence of MeCP2-deficient glia on neuronal dendritic morphology. Nat Neurosci 12, 311-317.

Bandeira, F., Lent, R., and Herculano-Houzel, S. (2009). Changing numbers of neuronal and non-neuronal cells underlie postnatal brain growth in the rat. Proc Natl Acad Sci U S A 106, 14108-14113.

Bandler, R.C., Mayer, C., and Fishell, G. (2017). Cortical interneuron specification: the juncture of genes, time and geometry. Curr Opin Neurobiol 42, 17-24.

Barca-Mayo, O., and De Pietri Tonelli, D. (2014). Convergent microRNA actions coordinate neocortical development. Cell Mol Life Sci 71, 2975-2995.

Barnabe-Heider, F., Wasylnka, J.A., Fernandes, K.J., Porsche, C., Sendtner, M., Kaplan, D.R., and Miller, F.D. (2005). Evidence that embryonic neurons regulate the onset of cortical gliogenesis via cardiotrophin-1. Neuron 48, 253-265.

Bartel, D.P. (2004). MicroRNAs: genomics, biogenesis, mechanism, and function. Cell 116, 281-297.

Bartzokis, G., Lu, P.H., Tingus, K., Mendez, M.F., Richard, A., Peters, D.G., Oluwadara, B., Barrall, K.A., Finn, J.P., Villablanca, P., et al. (2010). Lifespan trajectory of myelin integrity and maximum motor speed. Neurobiol Aging 31, 1554-1562.

Bauer, N.G., Richter-Landsberg, C., and Ffrench-Constant, C. (2009). Role of the oligodendroglial cytoskeleton in differentiation and myelination. Glia 57, 1691-1705.

Bayraktar, O.A., Fuentealba, L.C., Alvarez-Buylla, A., and Rowitch, D.H. (2014). Astrocyte development and heterogeneity. Cold Spring Harb Perspect Biol 7, a020362.

Becker, W., and Sippl, W. (2011). Activation, regulation, and inhibition of DYRK1A. FEBS J 278, 246-256.

Becker, W., Weber, Y., Wetzel, K., Eirmbter, K., Tejedor, F.J., and Joost, H.G. (1998). Sequence characteristics, subcellular localization, and substrate specificity of DYRK-related kinases, a novel family of dual specificity protein kinases. J Biol Chem 273, 25893-25902.

Benavides-Piccione, R., Dierssen, M., Ballesteros-Yanez, I., Martinez de Lagran, M., Arbones, M.L., Fotaki, V., DeFelipe, J., and Elston, G.N. (2005). Alterations in the phenotype of neocortical pyramidal cells in the Dyrk1A+/- mouse. Neurobiol Dis 20, 115-122.

Bergles, D.E., and Richardson, W.D. (2015). Oligodendrocyte Development and Plasticity. Cold Spring Harb Perspect Biol 8, a020453.

Bergsland, M., Werme, M., Malewicz, M., Perlmann, T., and Muhr, J. (2006). The establishment of neuronal properties is controlled by Sox4 and Sox11. Genes Dev 20, 3475-3486.

Bernabe-Rubio, M., and Alonso, M.A. (2017). Routes and machinery of primary cilium biogenesis. Cell Mol Life Sci 74, 4077-4095.

Bernstein, E., Kim, S.Y., Carmell, M.A., Murchison, E.P., Alcorn, H., Li, M.Z., Mills, A.A., Elledge, S.J., Anderson, K.V., and Hannon, G.J. (2003). Dicer is essential for mouse development. Nat Genet 35, 215-217.

Bertrand, N., Medevielle, F., and Pituello, F. (2000). FGF signalling controls the timing of Pax6 activation in the neural tube. Development 127, 4837-4843.

Betizeau, M., Cortay, V., Patti, D., Pfister, S., Gautier, E., Bellemin-Menard, A., Afanassieff, M., Huissoud, C., Douglas, R.J., Kennedy, H., et al. (2013). Precursor diversity and complexity of lineage relationships in the outer subventricular zone of the primate. Neuron 80, 442-457.

Bhat, R.V., Axt, K.J., Fosnaugh, J.S., Smith, K.J., Johnson, K.A., Hill, D.E., Kinzler, K.W., and Baraban, J.M. (1996). Expression of the APC tumor suppressor protein in oligodendroglia. Glia 17, 169-174.

Bi, S., Chai, L., Yuan, X., Cao, C., and Li, S. (2017). MicroRNA-98 inhibits the cell proliferation of human hypertrophic scar fibroblasts via targeting Col1A1. Biol Res 50, 22.

Bian, S., Hong, J., Li, Q., Schebelle, L., Pollock, A., Knauss, J.L., Garg, V., and Sun, T. (2013). MicroRNA cluster miR-17-92 regulates neural stem cell expansion and transition to intermediate progenitors in the developing mouse neocortex. Cell Rep 3, 1398-1406.

Birey, F., Kokkosis, A.G., and Aguirre, A. (2017). Oligodendroglia-lineage cells in brain plasticity, homeostasis and psychiatric disorders. Curr Opin Neurobiol 47, 93-103.

Blackiston, D.J., McLaughlin, K.A., and Levin, M. (2009). Bioelectric controls of cell proliferation: ion channels, membrane voltage and the cell cycle. Cell Cycle 8, 3527-3536.

Blanchard, M.G., Willemsen, M.H., Walker, J.B., Dib-Hajj, S.D., Waxman, S.G., Jongmans, M.C., Kleefstra, T., van de Warrenburg, B.P., Praamstra, P., Nicolai, J., et al. (2015). De novo gain-of-function and loss-of-function mutations of SCN8A in patients with intellectual disabilities and epilepsy. J Med Genet 52, 330-337.

Bolte, S., and Cordelieres, F.P. (2006). A guided tour into subcellular colocalization analysis in light microscopy. J Microsc 224, 213-232.

Boonstra, J., Mummery, C.L., Tertoolen, L.G., Van Der Saag, P.T., and De Laat, S.W. (1981). Cation transport and growth regulation in neuroblastoma cells. Modulations of K+ transport and electrical membrane properties during the cell cycle. J Cell Physiol 107, 75-83.

Boutz, P.L., Bhutkar, A., and Sharp, P.A. (2015). Detained introns are a novel, widespread class of post-transcriptionally spliced introns. Genes Dev 29, 63-80.

Boutz, P.L., Stoilov, P., Li, Q., Lin, C.H., Chawla, G., Ostrow, K., Shiue, L., Ares, M., Jr., and Black, D.L. (2007). A post-transcriptional regulatory switch in polypyrimidine tract-binding proteins reprograms alternative splicing in developing neurons. Genes Dev 21, 1636-1652.

Bozzi, Y., Casarosa, S., and Caleo, M. (2012). Epilepsy as a neurodevelopmental disorder. Front Psychiatry 3, 19.

Bradl, M., and Lassmann, H. (2010). Oligodendrocytes: biology and pathology. Acta Neuropathol 119, 37-53.

Branca, C., Shaw, D.M., Belfiore, R., Gokhale, V., Shaw, A.Y., Foley, C., Smith, B., Hulme, C., Dunckley, T., Meechoovet, B., et al. (2017). Dyrk1 inhibition improves Alzheimer's disease-like pathology. Aging Cell 16, 1146-1154.

Branner, A., Stein, R.B., and Normann, R.A. (2001). Selective stimulation of cat sciatic nerve using an array of varying-length microelectrodes. J Neurophysiol 85, 1585-1594.

Braunschweig, U., Barbosa-Morais, N.L., Pan, Q., Nachman, E.N., Alipanahi, B., Gonatopoulos-Pournatzis, T., Frey, B., Irimia, M., and Blencowe, B.J. (2014). Widespread intron retention in mammals functionally tunes transcriptomes. Genome Res 24, 1774-1786.

Britanova, O., de Juan Romero, C., Cheung, A., Kwan, K.Y., Schwark, M., Gyorgy, A., Vogel, T., Akopov, S., Mitkovski, M., Agoston, D., et al. (2008). Satb2 is a postmitotic determinant for upper-layer neuron specification in the neocortex. Neuron 57, 378-392.

Bronicki, L.M., Redin, C., Drunat, S., Piton, A., Lyons, M., Passemard, S., Baumann, C., Faivre, L., Thevenon, J., Riviere, J.B., et al. (2015). Ten new cases further delineate the syndromic intellectual disability phenotype caused by mutations in DYRK1A. Eur J Hum Genet 23, 1482-1487.

Bryja, V., Cervenka, I., and Cajanek, L. (2017). The connections of Wnt pathway components with cell cycle and centrosome: side effects or a hidden logic? Crit Rev Biochem Mol Biol 52, 614-637.

Buratti, E., De Conti, L., Stuani, C., Romano, M., Baralle, M., and Baralle, F. (2010). Nuclear factor TDP-43 can affect selected microRNA levels. FEBS J 277, 2268-2281.

Burda, J.E., and Sofroniew, M.V. (2014). Reactive gliosis and the multicellular response to CNS damage and disease. Neuron 81, 229-248.

Burns, K.A., Murphy, B., Danzer, S.C., and Kuan, C.Y. (2009). Developmental and post-injury cortical gliogenesis: a genetic fate-mapping study with Nestin-CreER mice. Glia 57, 1115-1129.

Bushong, E.A., Martone, M.E., Jones, Y.Z., and Ellisman, M.H. (2002). Protoplasmic astrocytes in CA1 stratum radiatum occupy separate anatomical domains. J Neurosci 22, 183-192.

Cai, J., Qi, Y., Hu, X., Tan, M., Liu, Z., Zhang, J., Li, Q., Sander, M., and Qiu, M. (2005). Generation of oligodendrocyte precursor cells from mouse dorsal spinal cord independent of Nkx6 regulation and Shh signaling. Neuron 45, 41-53.

Caldwell, J.H., Schaller, K.L., Lasher, R.S., Peles, E., and Levinson, S.R. (2000). Sodium channel Na(v)1.6 is localized at nodes of ranvier, dendrites, and synapses. Proc Natl Acad Sci U S A 97, 5616-5620.

Calegari, F., Haubensak, W., Haffner, C., and Huttner, W.B. (2005). Selective lengthening of the cell cycle in the neurogenic subpopulation of neural progenitor cells during mouse brain development. J Neurosci 25, 6533-6538.

Campos, L.S., Duarte, A.J., Branco, T., and Henrique, D. (2001). mDll1 and mDll3 expression in the developing mouse brain: role in the establishment of the early cortex. J Neurosci Res 64, 590-598.

Cao, X., Pfaff, S.L., and Gage, F.H. (2008). YAP regulates neural progenitor cell number via the TEA domain transcription factor. Genes Dev 22, 3320-3334.

Cappello, S., Gray, M.J., Badouel, C., Lange, S., Einsiedler, M., Srour, M., Chitayat, D., Hamdan, F.F., Jenkins, Z.A., Morgan, T., et al. (2013). Mutations in genes encoding the cadherin receptor-ligand pair DCHS1 and FAT4 disrupt cerebral cortical development. Nat Genet 45, 1300-1308.

Carmody, D.P., and Lewis, M. (2010). Regional white matter development in children with autism spectrum disorders. Dev Psychobiol 52, 755-763.

Castro, D.S., Martynoga, B., Parras, C., Ramesh, V., Pacary, E., Johnston, C., Drechsel, D., Lebel-Potter, M., Garcia, L.G., Hunt, C., et al. (2011). A novel function of the proneural factor Ascl1 in progenitor proliferation identified by genome-wide characterization of its targets. Genes Dev 25, 930-945.

Cerghet, M., Bessert, D.A., Nave, K.A., and Skoff, R.P. (2001). Differential expression of apoptotic markers in jimpy and in Plp overexpressors: evidence for different apoptotic pathways. J Neurocytol 30, 841-855.

Chakrabarti, L., Galdzicki, Z., and Haydar, T.F. (2007). Defects in embryonic neurogenesis and initial synapse formation in the forebrain of the Ts65Dn mouse model of Down syndrome. J Neurosci 27, 11483-11495.

Chandran, S., Kato, H., Gerreli, D., Compston, A., Svendsen, C.N., and Allen, N.D. (2003). FGF-dependent generation of oligodendrocytes by a hedgehog-independent pathway. Development 130, 6599-6609.

Chapman, H., Waclaw, R.R., Pei, Z., Nakafuku, M., and Campbell, K. (2013). The homeobox gene Gsx2 controls the timing of oligodendroglial fate specification in mouse lateral ganglionic eminence progenitors. Development 140, 2289-2298.

Charizanis, K., Lee, K.Y., Batra, R., Goodwin, M., Zhang, C., Yuan, Y., Shiue, L., Cline, M., Scotti, M.M., Xia, G., et al. (2012). Muscleblind-like 2-mediated alternative splicing in the developing brain and dysregulation in myotonic dystrophy. Neuron 75, 437-450.

Chen, B., Wang, S.S., Hattox, A.M., Rayburn, H., Nelson, S.B., and McConnell, S.K. (2008). The Fezf2-Ctip2 genetic pathway regulates the fate choice of subcortical projection neurons in the developing cerebral cortex. Proc Natl Acad Sci U S A 105, 11382-11387.

Chen, C., Jiang, P., Xue, H., Peterson, S.E., Tran, H.T., McCann, A.E., Parast, M.M., Li, S., Pleasure, D.E., Laurent, L.C., et al. (2014a). Role of astroglia in Down's syndrome revealed by patient-derived human-induced pluripotent stem cells. Nat Commun 5, 4430.

Chen, E.Y., Tan, C.M., Kou, Y., Duan, Q., Wang, Z., Meirelles, G.V., Clark, N.R., and Ma'ayan, A. (2013a). Enrichr: interactive and collaborative HTML5 gene list enrichment analysis tool. BMC Bioinformatics 14, 128.

Chen, J.Y., Lin, J.R., Tsai, F.C., and Meyer, T. (2013b). Dosage of Dyrk1a shifts cells within a p21-cyclin D1 signaling map to control the decision to enter the cell cycle. Mol Cell 52, 87-100.

Chen, V.S., Morrison, J.P., Southwell, M.F., Foley, J.F., Bolon, B., and Elmore, S.A. (2017). Histology Atlas of the Developing Prenatal and Postnatal Mouse Central Nervous System, with Emphasis on Prenatal Days E7.5 to E18.5. Toxicol Pathol 45, 705-744.

Chen, Y., Bian, S., Zhang, J., Zhang, H., Tang, B., and Sun, T. (2014b). The Silencing Effect of microRNA miR-17 on p21 Maintains the Neural Progenitor Pool in the Developing Cerebral Cortex. Front Neurol 5, 132.

Chenn, A., and Walsh, C.A. (2002). Regulation of cerebral cortical size by control of cell cycle exit in neural precursors. Science 297, 365-369.

Chenn, A., and Walsh, C.A. (2003). Increased neuronal production, enlarged forebrains and cytoarchitectural distortions in beta-catenin overexpressing transgenic mice. Cereb Cortex 13, 599-606.

Chenn, A., Zhang, Y.A., Chang, B.T., and McConnell, S.K. (1998). Intrinsic polarity of mammalian neuroepithelial cells. Mol Cell Neurosci 11, 183-193.

Chettouh, Z., Croquette, M.F., Delobel, B., Gilgenkrants, S., Leonard, C., Maunoury, C., Prieur, M., Rethore, M.O., Sinet, P.M., Chery, M., et al. (1995). Molecular mapping of 21 features associated with partial monosomy 21: involvement of the APP-SOD1 region. Am J Hum Genet 57, 62-71.

Choi, H.K., and Chung, K.C. (2011). Dyrk1A Positively Stimulates ASK1-JNK Signaling Pathway during Apoptotic Cell Death. Exp Neurobiol 20, 35-44.

Conboy, J.G. (2017). Developmental regulation of RNA processing by Rbfox proteins. Wiley Interdiscip Rev RNA 8.

Cone, C.D., Jr. (1971). Unified theory on the basic mechanism of normal mitotic control and oncogenesis. J Theor Biol 30, 151-181.

Cooper, G.M., and Hausman, R.E. (2009). The Cell: A molecular approach, 18a edn (Washington, D. C. : ASM Press).

Corti, S., Nizzardo, M., Nardini, M., Donadoni, C., Locatelli, F., Papadimitriou, D., Salani, S., Del Bo, R., Ghezzi, S., Strazzer, S., et al. (2007). Isolation and characterization of murine neural stem/progenitor cells based on Prominin-1 expression. Exp Neurol 205, 547-562.

Costa, A.C., Walsh, K., and Davisson, M.T. (1999). Motor dysfunction in a mouse model for Down syndrome. Physiol Behav 68, 211-220.

Courcet, J.B., Faivre, L., Malzac, P., Masurel-Paulet, A., Lopez, E., Callier, P., Lambert, L., Lemesle, M., Thevenon, J., Gigot, N., et al. (2012). The DYRK1A gene is a cause of syndromic intellectual disability with severe microcephaly and epilepsy. J Med Genet 49, 731-736.

Cramer, N.P., Xu, X., T, F.H., and Galdzicki, Z. (2015). Altered intrinsic and network properties of neocortical neurons in the Ts65Dn mouse model of Down syndrome. Physiol Rep 3.

Crawford, A.H., Tripathi, R.B., Richardson, W.D., and Franklin, R.J.M. (2016). Developmental Origin of Oligodendrocyte Lineage Cells Determines Response to Demyelination and Susceptibility to Age-Associated Functional Decline. Cell Rep 15, 761-773.

da Costa Martins, P.A., Salic, K., Gladka, M.M., Armand, A.S., Leptidis, S., el Azzouzi, H., Hansen, A., Coenen-de Roo, C.J., Bierhuizen, M.F., van der Nagel, R., et al. (2010). MicroRNA-199b targets the nuclear kinase Dyrk1a in an auto-amplification loop promoting calcineurin/NFAT signalling. Nat Cell Biol 12, 1220-1227.

Dai, Z.M., Sun, S., Wang, C., Huang, H., Hu, X., Zhang, Z., Lu, Q.R., and Qiu, M. (2014). Stage-specific regulation of oligodendrocyte development by Wnt/beta-catenin signaling. J Neurosci 34, 8467-8473.

Dang, T., Duan, W.Y., Yu, B., Tong, D.L., Cheng, C., Zhang, Y.F., Wu, W., Ye, K., Zhang, W.X., Wu, M., et al. (2018). Autism-associated Dyrk1a truncation mutants impair neuronal dendritic and spine growth and interfere with postnatal cortical development. Mol Psychiatry 23, 747-758.

Davis, K.L., Stewart, D.G., Friedman, J.I., Buchsbaum, M., Harvey, P.D., Hof, P.R., Buxbaum, J., and Haroutunian, V. (2003). White matter changes in schizophrenia: evidence for myelin-related dysfunction. Arch Gen Psychiatry 60, 443-456.

Davis, T.H., Cuellar, T.L., Koch, S.M., Barker, A.J., Harfe, B.D., McManus, M.T., and Ullian, E.M. (2008). Conditional loss of Dicer disrupts cellular and tissue morphogenesis in the cortex and hippocampus. J Neurosci 28, 4322-4330.

Davisson, M.T., Schmidt, C., and Akeson, E.C. (1990). Segmental trisomy of murine chromosome 16: a new model system for studying Down syndrome. Prog Clin Biol Res 360, 263-280.

Dawson, M.R., Polito, A., Levine, J.M., and Reynolds, R. (2003). NG2-expressing glial progenitor cells: an abundant and widespread population of cycling cells in the adult rat CNS. Mol Cell Neurosci 24, 476-488.

De Graaf, K., Czajkowska, H., Rottmann, S., Packman, L.C., Lilischkis, R., Luscher, B., and Becker, W. (2006). The protein kinase DYRK1A phosphorylates the splicing factor SF3b1/SAP155 at Thr434, a novel in vivo phosphorylation site. BMC Biochem 7, 7.

De la Torre, R., De Sola, S., Hernandez, G., Farre, M., Pujol, J., Rodriguez, J., Espadaler, J.M., Langohr, K., Cuenca-Royo, A., Principe, A., et al. (2016). Safety and efficacy of cognitive training plus epigallocatechin-3-gallate in young adults with Down's syndrome (TESDAD): a double-blind, randomised, placebo-controlled, phase 2 trial. Lancet Neurol 15, 801-810.

De la Torre, R., De Sola, S., Pons, M., Duchon, A., de Lagran, M.M., Farre, M., Fito, M., Benejam, B., Langohr, K., Rodriguez, J., et al. (2014). Epigallocatechin-3-gallate, a DYRK1A inhibitor, rescues cognitive deficits in Down syndrome mouse models and in humans. Mol Nutr Food Res 58, 278-288.

De Pietri Tonelli, D., Pulvers, J.N., Haffner, C., Murchison, E.P., Hannon, G.J., and Huttner, W.B. (2008). miRNAs are essential for survival and differentiation of newborn neurons but not for expansion of neural progenitors during early neurogenesis in the mouse embryonic neocortex. Development 135, 3911-3921.

De Rubeis, S., He, X., Goldberg, A.P., Poultney, C.S., Samocha, K., Cicek, A.E., Kou, Y., Liu, L., Fromer, M., Walker, S., et al. (2014). Synaptic, transcriptional and chromatin genes disrupted in autism. Nature 515, 209-215.

Deciphering Developmental Disorders, S. (2015). Large-scale discovery of novel genetic causes of developmental disorders. Nature 519, 223-228.

Dehay, C., and Kennedy, H. (2007). Cell-cycle control and cortical development. Nat Rev Neurosci 8, 438-450.

Desai, A.R., and McConnell, S.K. (2000). Progressive restriction in fate potential by neural progenitors during cerebral cortical development. Development 127, 2863-2872.

Di Lullo, E., and Kriegstein, A.R. (2017). The use of brain organoids to investigate neural development and disease. Nat Rev Neurosci 18, 573-584.

Di Vona, C., Bezdan, D., Islam, A.B., Salichs, E., Lopez-Bigas, N., Ossowski, S., and de la Luna, S. (2015). Chromatin-wide profiling of DYRK1A reveals a role as a gene-specific RNA polymerase II CTD kinase. Mol Cell 57, 506-520.

Dillman, A.A., Hauser, D.N., Gibbs, J.R., Nalls, M.A., McCoy, M.K., Rudenko, I.N., Galter, D., and Cookson, M.R. (2013). mRNA expression, splicing and editing in the embryonic and adult mouse cerebral cortex. Nat Neurosci 16, 499-506.

Dimou, L., Simon, C., Kirchhoff, F., Takebayashi, H., and Gotz, M. (2008). Progeny of Olig2-expressing progenitors in the gray and white matter of the adult mouse cerebral cortex. J Neurosci 28, 10434-10442.

Dobrokhotov, O., Samsonov, M., Sokabe, M., and Hirata, H. (2018). Mechanoregulation and pathology of YAP/TAZ via Hippo and non-Hippo mechanisms. Clin Transl Med 7, 23.

Domingues, H.S., Portugal, C.C., Socodato, R., and Relvas, J.B. (2016). Oligodendrocyte, Astrocyte, and Microglia Crosstalk in Myelin Development, Damage, and Repair. Front Cell Dev Biol 4, 71.

Dong, Z., Yang, N., Yeo, S.Y., Chitnis, A., and Guo, S. (2012). Intralineage directional Notch signaling regulates self-renewal and differentiation of asymmetrically dividing radial glia. Neuron 74, 65-78.

Dow, D.J., Huxley-Jones, J., Hall, J.M., Francks, C., Maycox, P.R., Kew, J.N., Gloger, I.S., Mehta, N.A., Kelly, F.M., Muglia, P., et al. (2011). ADAMTSL3 as a candidate gene for schizophrenia: gene sequencing and ultra-high density association analysis by imputation. Schizophr Res 127, 28-34.

Dupont, S. (2016). Role of YAP/TAZ in cell-matrix adhesion-mediated signalling and mechanotransduction. Exp Cell Res 343, 42-53.

Durand, B., and Raff, M. (2000). A cell-intrinsic timer that operates during oligodendrocyte development. Bioessays 22, 64-71.

Duronio, R.J., and Xiong, Y. (2013). Signaling pathways that control cell proliferation. Cold Spring Harb Perspect Biol 5, a008904.

Dutta, D.J., Woo, D.H., Lee, P.R., Pajevic, S., Bukalo, O., Huffman, W.C., Wake, H., Basser, P.J., SheikhBahaei, S., Lazarevic, V., et al. (2018). Regulation of myelin structure and conduction velocity by perinodal astrocytes. Proc Natl Acad Sci U S A 115, 11832-11837.

Earl, R.K., Turner, T.N., Mefford, H.C., Hudac, C.M., Gerdts, J., Eichler, E.E., and Bernier, R.A. (2017). Clinical phenotype of ASD-associated DYRK1A haploinsufficiency. Mol Autism 8, 54.

Eckler, M.J., and Chen, B. (2014). Fez family transcription factors: controlling neurogenesis and cell fate in the developing mammalian nervous system. Bioessays 36, 788-797.

Eckler, M.J., Nguyen, T.D., McKenna, W.L., Fastow, B.L., Guo, C., Rubenstein, J.L.R., and Chen, B. (2015). Cux2-positive radial glial cells generate diverse subtypes of neocortical projection neurons and macroglia. Neuron 86, 1100-1108.

Eichhorn, S.W., Guo, H., McGeary, S.E., Rodriguez-Mias, R.A., Shin, C., Baek, D., Hsu, S.H., Ghoshal, K., Villen, J., and Bartel, D.P. (2014). mRNA destabilization is the dominant effect of mammalian microRNAs by the time substantial repression ensues. Mol Cell 56, 104-115.

Elosegui-Artola, A., Andreu, I., Beedle, A.E.M., Lezamiz, A., Uroz, M., Kosmalska, A.J., Oria, R., Kechagia, J.Z., Rico-Lastres, P., Le Roux, A.L., et al. (2017). Force Triggers YAP Nuclear Entry by Regulating Transport across Nuclear Pores. Cell 171, 1397-1410 e1314.

Elosegui-Artola, A., Oria, R., Chen, Y., Kosmalska, A., Perez-Gonzalez, C., Castro, N., Zhu, C., Trepat, X., and Roca-Cusachs, P. (2016). Mechanical regulation of a molecular clutch defines force transmission and transduction in response to matrix rigidity. Nat Cell Biol 18, 540-548.

Emery, B., and Lu, Q.R. (2015). Transcriptional and Epigenetic Regulation of Oligodendrocyte Development and Myelination in the Central Nervous System. Cold Spring Harb Perspect Biol 7, a020461.

Epplen, D.B., Prukop, T., Nientiedt, T., Albrecht, P., Arlt, F.A., Stassart, R.M., Kassmann, C.M., Methner, A., Nave, K.A., Werner, H.B., et al. (2015). Curcumin therapy in a Plp1 transgenic mouse model of Pelizaeus-Merzbacher disease. Ann Clin Transl Neurol 2, 787-796.

Eshed-Eisenbach, Y., and Peles, E. (2013). The making of a node: a co-production of neurons and glia. Curr Opin Neurobiol 23, 1049-1056.

Evers, J.M., Laskowski, R.A., Bertolli, M., Clayton-Smith, J., Deshpande, C., Eason, J., Elmslie, F., Flinter, F., Gardiner, C., Hurst, J.A., et al. (2017). Structural analysis of pathogenic mutations in the DYRK1A gene in patients with developmental disorders. Hum Mol Genet 26, 519-526.

Fagnani, M., Barash, Y., Ip, J.Y., Misquitta, C., Pan, Q., Saltzman, A.L., Shai, O., Lee, L., Rozenhek, A., Mohammad, N., et al. (2007). Functional coordination of alternative splicing in the mammalian central nervous system. Genome Biol 8, R108.

Faissner, A., and Reinhard, J. (2015). The extracellular matrix compartment of neural stem and glial progenitor cells. Glia 63, 1330-1349.

Fame, R.M., MacDonald, J.L., and Macklis, J.D. (2011). Development, specification, and diversity of callosal projection neurons. Trends Neurosci 34, 41-50.

Fan, G., Martinowich, K., Chin, M.H., He, F., Fouse, S.D., Hutnick, L., Hattori, D., Ge, W., Shen, Y., Wu, H., et al. (2005). DNA methylation controls the timing of astrogliogenesis through regulation of JAK-STAT signaling. Development 132, 3345-3356.

Fededa, J.P., Esk, C., Mierzwa, B., Stanyte, R., Yuan, S., Zheng, H., Ebnet, K., Yan, W., Knoblich, J.A., and Gerlich, D.W. (2016). MicroRNA-34/449 controls mitotic spindle orientation during mammalian cortex development. EMBO J 35, 2386-2398.

Fernandez-Martinez, J., Vela, E.M., Tora-Ponsioen, M., Ocana, O.H., Nieto, M.A., and Galceran, J. (2009). Attenuation of Notch signalling by the Down-syndrome-associated kinase DYRK1A. J Cell Sci 122, 1574-1583.

Fernandez, E., Cuenca, N., and De Juan, J. (1991). A useful programme in BASIC for axonal morphometry with introduction of new cytoskeletal parameters. J Neurosci Methods 39, 271-289.

Ferrer, I., Barrachina, M., Puig, B., Martinez de Lagran, M., Marti, E., Avila, J., and Dierssen, M. (2005). Constitutive Dyrk1A is abnormally expressed in Alzheimer disease, Down syndrome, Pick disease, and related transgenic models. Neurobiol Dis 20, 392-400.

Ferron, S.R., Pozo, N., Laguna, A., Aranda, S., Porlan, E., Moreno, M., Fillat, C., de la Luna, S., Sanchez, P., Arbones, M.L., et al. (2010). Regulated segregation of kinase Dyrk1A during asymmetric neural stem cell division is critical for EGFR-mediated biased signaling. Cell Stem Cell 7, 367-379.

Fields, R.D. (2008). White matter in learning, cognition and psychiatric disorders. Trends Neurosci 31, 361-370.

Fietz, S.A., Kelava, I., Vogt, J., Wilsch-Brauninger, M., Stenzel, D., Fish, J.L., Corbeil, D., Riehn, A., Distler, W., Nitsch, R., et al. (2010). OSVZ progenitors of human and ferret neocortex are epithelial-like and expand by integrin signaling. Nat Neurosci 13, 690-699.

Fietz, S.A., Lachmann, R., Brandl, H., Kircher, M., Samusik, N., Schroder, R., Lakshmanaperumal, N., Henry, I., Vogt, J., Riehn, A., et al. (2012). Transcriptomes of germinal zones of human and mouse fetal neocortex suggest a role of extracellular matrix in progenitor self-renewal. Proc Natl Acad Sci U S A 109, 11836-11841.

Florio, M., and Huttner, W.B. (2014). Neural progenitors, neurogenesis and the evolution of the neocortex. Development 141, 2182-2194.

Flynn, S.W., Lang, D.J., Mackay, A.L., Goghari, V., Vavasour, I.M., Whittall, K.P., Smith, G.N., Arango, V., Mann, J.J., Dwork, A.J., et al. (2003). Abnormalities of myelination in schizophrenia detected in vivo with MRI, and post-mortem with analysis of oligodendrocyte proteins. Mol Psychiatry 8, 811-820.

Fotaki, V., Dierssen, M., Alcantara, S., Martinez, S., Marti, E., Casas, C., Visa, J., Soriano, E., Estivill, X., and Arbones, M.L. (2002). Dyrk1A haploinsufficiency affects viability and causes developmental delay and abnormal brain morphology in mice. Mol Cell Biol 22, 6636-6647.

Fotaki, V., Martinez De Lagran, M., Estivill, X., Arbones, M., and Dierssen, M. (2004). Haploinsufficiency of Dyrk1A in mice leads to specific alterations in the development and regulation of motor activity. Behav Neurosci 118, 815-821.

Franceschini, A., Szklarczyk, D., Frankild, S., Kuhn, M., Simonovic, M., Roth, A., Lin, J., Minguez, P., Bork, P., von Mering, C., et al. (2013). STRING v9.1: protein-protein interaction networks, with increased coverage and integration. Nucleic Acids Res 41, D808-815.

Franco, S.J., and Muller, U. (2013). Shaping our minds: stem and progenitor cell diversity in the mammalian neocortex. Neuron 77, 19-34.

Franco, S.J., Gil-Sanz, C., Martinez-Garay, I., Espinosa, A., Harkins-Perry, S.R., Ramos, C., and Muller, U. (2012). Fate-restricted neural progenitors in the mammalian cerebral cortex. Science 337, 746-749.

Franklin, K.B.J., and Paxinos, G. (2013). Paxinos and Franklin's The mouse brain in stereotaxic coordinates, Fourth edition. edn (Amsterdam: Academic Press, an imprint of Elsevier).

Franklin, R.J., and Goldman, S.A. (2015). Glia Disease and Repair-Remyelination. Cold Spring Harb Perspect Biol 7, a020594.

Frantz, G.D., and McConnell, S.K. (1996). Restriction of late cerebral cortical progenitors to an upper-layer fate. Neuron 17, 55-61.

Freeman, M.R., and Rowitch, D.H. (2013). Evolving concepts of gliogenesis: a look way back and ahead to the next 25 years. Neuron 80, 613-623.

Fruttiger, M., Karlsson, L., Hall, A.C., Abramsson, A., Calver, A.R., Bostrom, H., Willetts, K., Bertold, C.H., Heath, J.K., Betsholtz, C., et al. (1999). Defective oligodendrocyte development and severe hypomyelination in PDGF-A knockout mice. Development 126, 457-467.

Fuccillo, M., Rallu, M., McMahon, A.P., and Fishell, G. (2004). Temporal requirement for hedgehog signaling in ventral telencephalic patterning. Development 131, 5031-5040.

Fukuda, S., Abematsu, M., Mori, H., Yanagisawa, M., Kagawa, T., Nakashima, K., Yoshimura, A., and Taga, T. (2007). Potentiation of astrogliogenesis by STAT3-mediated activation of bone morphogenetic protein-Smad signaling in neural stem cells. Mol Cell Biol 27, 4931-4937.

Furusho, M., Kaga, Y., Ishii, A., Hebert, J.M., and Bansal, R. (2011). Fibroblast growth factor signaling is required for the generation of oligodendrocyte progenitors from the embryonic forebrain. J Neurosci 31, 5055-5066.

Gadisseux, J.F., and Evrard, P. (1985). Glial-neuronal relationship in the developing central nervous system. A histochemical-electron microscope study of radial glial cell particulate glycogen in normal and reeler mice and the human fetus. Dev Neurosci 7, 12-32.

Gaiano, N., Nye, J.S., and Fishell, G. (2000). Radial glial identity is promoted by Notch1 signaling in the murine forebrain. Neuron 26, 395-404.

Gangaraju, V.K., and Lin, H. (2009). MicroRNAs: key regulators of stem cells. Nat Rev Mol Cell Biol 10, 116-125.

Gao, F.B., Durand, B., and Raff, M. (1997). Oligodendrocyte precursor cells count time but not cell divisions before differentiation. Curr Biol 7, 152-155.

Gao, P., Postiglione, M.P., Krieger, T.G., Hernandez, L., Wang, C., Han, Z., Streicher, C., Papusheva, E., Insolera, R., Chugh, K., et al. (2014). Deterministic progenitor behavior and unitary production of neurons in the neocortex. Cell 159, 775-788.

Garbern, J.Y., Cambi, F., Lewis, R., Shy, M., Sima, A., Kraft, G., Vallat, J.M., Bosch, E.P., Hodes, M.E., Dlouhy, S., et al. (1999). Peripheral Neuropathy Caused by Proteolipid Protein Gene Mutations. Ann N Y Acad Sci 883, 351-365.

Garcia-Cerro, S., Martinez, P., Vidal, V., Corrales, A., Florez, J., Vidal, R., Rueda, N., Arbones, M.L., and Martinez-Cue, C. (2014). Overexpression of Dyrk1A is implicated in several cognitive, electrophysiological and neuromorphological alterations found in a mouse model of Down syndrome. PLoS One 9, e106572.

Garcia-Cerro, S., Rueda, N., Vidal, V., Lantigua, S., and Martinez-Cue, C. (2017). Normalizing the gene dosage of Dyrk1A in a mouse model of Down syndrome rescues several Alzheimer's disease phenotypes. Neurobiol Dis 106, 76-88.

Garcia-Marques, J., and Lopez-Mascaraque, L. (2013). Clonal identity determines astrocyte cortical heterogeneity. Cereb Cortex 23, 1463-1472.

Garcia, O., Torres, M., Helguera, P., Coskun, P., and Busciglio, J. (2010). A role for thrombospondin-1 deficits in astrocyte-mediated spine and synaptic pathology in Down's syndrome. PLoS One 5, e14200.

Garcia, O., Torres, M., Helguera, P., Coskun, P., and Busciglio, J. (2010). A role for thrombospondin-1 deficits in astrocyte-mediated spine and synaptic pathology in Down's syndrome. PLoS One 5, e14200.

Gauthier, A.S., Furstoss, O., Araki, T., Chan, R., Neel, B.G., Kaplan, D.R., and Miller, F.D. (2007). Control of CNS cell-fate decisions by SHP-2 and its dysregulation in Noonan syndrome. Neuron 54, 245-262.

Ge, W.P., and Jia, J.M. (2016). Local production of astrocytes in the cerebral cortex. Neuroscience 323, 3-9.

Ge, W.P., Miyawaki, A., Gage, F.H., Jan, Y.N., and Jan, L.Y. (2012). Local generation of glia is a major astrocyte source in postnatal cortex. Nature 484, 376-380.

Ge, Y., and Porse, B.T. (2014). The functional consequences of intron retention: alternative splicing coupled to NMD as a regulator of gene expression. Bioessays 36, 236-243.

Gibson, E.M., Purger, D., Mount, C.W., Goldstein, A.K., Lin, G.L., Wood, L.S., Inema, I., Miller, S.E., Bieri, G., Zuchero, J.B., et al. (2014). Neuronal activity promotes oligodendrogenesis and adaptive myelination in the mammalian brain. Science 344, 1252304.

Goebbels, S., Wieser, G.L., Pieper, A., Spitzer, S., Weege, B., Yan, K., Edgar, J.M., Yagensky, O., Wichert, S.P., Agarwal, A., et al. (2017). A neuronal PI(3,4,5)P3-dependent program of oligodendrocyte precursor recruitment and myelination. Nat Neurosci 20, 10-15.

Gomes, W.A., Mehler, M.F., and Kessler, J.A. (2003). Transgenic overexpression of BMP4 increases astroglial and decreases oligodendroglial lineage commitment. Dev Biol 255, 164-177.

Gotz, M., and Huttner, W.B. (2005). The cell biology of neurogenesis. Nat Rev Mol Cell Biol 6, 777-788.

Greig, L.C., Woodworth, M.B., Galazo, M.J., Padmanabhan, H., and Macklis, J.D. (2013). Molecular logic of neocortical projection neuron specification, development and diversity. Nat Rev Neurosci 14, 755-769.

Gressens, P., Richelme, C., Kadhim, H.J., Gadisseux, J.F., and Evrard, P. (1992). The germinative zone produces the most cortical astrocytes after neuronal migration in the developing mammalian brain. Biol Neonate 61, 4-24.

Groen, W.B., Buitelaar, J.K., van der Gaag, R.J., and Zwiers, M.P. (2011). Pervasive microstructural abnormalities in autism: a DTI study. J Psychiatry Neurosci 36, 32-40.

Gross, R.E., Mehler, M.F., Mabie, P.C., Zang, Z., Santschi, L., and Kessler, J.A. (1996). Bone morphogenetic proteins promote astroglial lineage commitment by mammalian subventricular zone progenitor cells. Neuron 17, 595-606.

Guan, R., El-Rass, S., Spillane, D., Lam, S., Wang, Y., Wu, J., Chen, Z., Wang, A., Jia, Z., Keating, A., et al. (2013). rbm47, a novel RNA binding protein, regulates zebrafish head development. Dev Dyn 242, 1395-1404.

Guard, S.E., Poss, Z.C., Ebmeier, C.C., Pagratis, M., Simpson, H., Taatjes, D.J., and Old, W.M. (2019). The nuclear interactome of DYRK1A reveals a functional role in DNA damage repair. Sci Rep 9, 6539.

Gudz, T.I., Komuro, H., and Macklin, W.B. (2006). Glutamate stimulates oligodendrocyte progenitor migration mediated via an alphav integrin/myelin proteolipid protein complex. J Neurosci 26, 2458-2466.

Guedj, F., Bianchi, D.W., and Delabar, J.M. (2014). Prenatal treatment of Down syndrome: a reality? Curr Opin Obstet Gynecol 26, 92-103.

Guedj, F., Pereira, P.L., Najas, S., Barallobre, M.J., Chabert, C., Souchet, B., Sebrie, C., Verney, C., Herault, Y., Arbones, M., et al. (2012). DYRK1A: a master regulatory protein controlling brain growth. Neurobiol Dis 46, 190-203.

Guilak, F., Cohen, D.M., Estes, B.T., Gimble, J.M., Liedtke, W., and Chen, C.S. (2009). Control of stem cell fate by physical interactions with the extracellular matrix. Cell Stem Cell 5, 17-26.

Guimera, J., Casas, C., Estivill, X., and Pritchard, M. (1999). Human minibrain homologue (MNBH/DYRK1): characterization, alternative splicing, differential tissue expression, and overexpression in Down syndrome. Genomics 57, 407-418.

Guimera, J., Pritchard, M., Nadal, M., and Estivill, X. (1997). Minibrain (MNBH) is a single copy gene mapping to human chromosome 21q22.2. Cytogenet Cell Genet 77, 182-184.

Guo, C., Eckler, M.J., McKenna, W.L., McKinsey, G.L., Rubenstein, J.L., and Chen, B. (2013). Fezf2 expression identifies a multipotent progenitor for neocortical projection neurons, astrocytes, and oligodendrocytes. Neuron 80, 1167-1174.

Guo, F., Ma, J., McCauley, E., Bannerman, P., and Pleasure, D. (2009). Early postnatal proteolipid promoter-expressing progenitors produce multilineage cells in vivo. J Neurosci 29, 7256-7270.

Guo, H., Ingolia, N.T., Weissman, J.S., and Bartel, D.P. (2010a). Mammalian microRNAs predominantly act to decrease target mRNA levels. Nature 466, 835-840.

Guo, X., Williams, J.G., Schug, T.T., and Li, X. (2010b). DYRK1A and DYRK3 promote cell survival through phosphorylation and activation of SIRT1. J Biol Chem 285, 13223-13232.

Ha, M., and Kim, V.N. (2014). Regulation of microRNA biogenesis. Nat Rev Mol Cell Biol 15, 509-524.

Hakak, Y., Walker, J.R., Li, C., Wong, W.H., Davis, K.L., Buxbaum, J.D., Haroutunian, V., and Fienberg, A.A. (2001). Genome-wide expression analysis reveals dysregulation of myelination-related genes in chronic schizophrenia. Proc Natl Acad Sci U S A 98, 4746-4751.

Hammerle, B., Elizalde, C., and Tejedor, F.J. (2008). The spatio-temporal and subcellular expression of the candidate Down syndrome gene Mnb/Dyrk1A in the developing mouse brain suggests distinct sequential roles in neuronal development. Eur J Neurosci 27, 1061-1074.

Hammerle, B., Ulin, E., Guimera, J., Becker, W., Guillemot, F., and Tejedor, F.J. (2011). Transient expression of Mnb/Dyrk1a couples cell cycle exit and differentiation of neuronal precursors by inducing p27KIP1 expression and suppressing NOTCH signaling. Development 138, 2543-2554.

Hammerle, B., Vera-Samper, E., Speicher, S., Arencibia, R., Martinez, S., and Tejedor, F.J. (2002). Mnb/Dyrk1A is transiently expressed and asymmetrically segregated in neural progenitor cells at the transition to neurogenic divisions. Dev Biol 246, 259-273.

Han, D., Byun, S.H., Park, S., Kim, J., Kim, I., Ha, S., Kwon, M., and Yoon, K. (2015). YAP/TAZ enhance mammalian embryonic neural stem cell characteristics in a Tead-dependent manner. Biochem Biophys Res Commun 458, 110-116.

Hansen, D.V., Lui, J.H., Parker, P.R., and Kriegstein, A.R. (2010). Neurogenic radial glia in the outer subventricular zone of human neocortex. Nature 464, 554-561.

Harrison-Uy, S.J., and Pleasure, S.J. (2012). Wnt signaling and forebrain development. Cold Spring Harb Perspect Biol 4, a008094.

Hartline, D.K., and Colman, D.R. (2007). Rapid conduction and the evolution of giant axons and myelinated fibers. Curr Biol 17, R29-35.

Hatakeyama, J., Bessho, Y., Katoh, K., Ookawara, S., Fujioka, M., Guillemot, F., and Kageyama, R. (2004). Hes genes regulate size, shape and histogenesis of the nervous system by control of the timing of neural stem cell differentiation. Development 131, 5539-5550.

Haubensak, W., Attardo, A., Denk, W., and Huttner, W.B. (2004). Neurons arise in the basal neuroepithelium of the early mammalian telencephalon: a major site of neurogenesis. Proc Natl Acad Sci U S A 101, 3196-3201.

Hayakawa-Yano, Y., Suyama, S., Nogami, M., Yugami, M., Koya, I., Furukawa, T., Zhou, L., Abe, M., Sakimura, K., Takebayashi, H., et al. (2017). An RNA-binding protein, Qki5, regulates embryonic neural stem cells through pre-mRNA processing in cell adhesion signaling. Genes Dev 31, 1910-1925.

He, Y., Dupree, J., Wang, J., Sandoval, J., Li, J., Liu, H., Shi, Y., Nave, K.A., and Casaccia-Bonnefil, P. (2007). The transcription factor Yin Yang 1 is essential for oligodendrocyte progenitor differentiation. Neuron 55, 217-230.

Heallen, T., Zhang, M., Wang, J., Bonilla-Claudio, M., Klysik, E., Johnson, R.L., and Martin, J.F. (2011). Hippo pathway inhibits Wnt signaling to restrain cardiomyocyte proliferation and heart size. Science 332, 458-461.

Henderson, D.M., and Conner, S.D. (2007). A novel AAK1 splice variant functions at multiple steps of the endocytic pathway. Mol Biol Cell 18, 2698-2706.

Henneberger, C., Papouin, T., Oliet, S.H., and Rusakov, D.A. (2010). Long-term potentiation depends on release of D-serine from astrocytes. Nature 463, 232-236.

Hevner, R.F., Hodge, R.D., Daza, R.A., and Englund, C. (2006). Transcription factors in glutamatergic neurogenesis: conserved programs in neocortex, cerebellum, and adult hippocampus. Neurosci Res 55, 223-233.

Himpel, S., Panzer, P., Eirmbter, K., Czajkowska, H., Sayed, M., Packman, L.C., Blundell, T., Kentrup, H., Grotzinger, J., Joost, H.G., et al. (2001). Identification of the autophosphorylation sites and characterization of their effects in the protein kinase DYRK1A. Biochem J 359, 497-505.

Himpel, S., Tegge, W., Frank, R., Leder, S., Joost, H.G., and Becker, W. (2000). Specificity determinants of substrate recognition by the protein kinase DYRK1A. J Biol Chem 275, 2431-2438.

Hirabayashi, Y., Itoh, Y., Tabata, H., Nakajima, K., Akiyama, T., Masuyama, N., and Gotoh, Y. (2004). The Wnt/beta-catenin pathway directs neuronal differentiation of cortical neural precursor cells. Development 131, 2791-2801.

Hirabayashi, Y., Suzki, N., Tsuboi, M., Endo, T.A., Toyoda, T., Shinga, J., Koseki, H., Vidal, M., and Gotoh, Y. (2009). Polycomb limits the neurogenic competence of neural precursor cells to promote astrogenic fate transition. Neuron 63, 600-613.

Hoch, R.V., Rubenstein, J.L., and Pleasure, S. (2009). Genes and signaling events that establish regional patterning of the mammalian forebrain. Semin Cell Dev Biol 20, 378-386.

Holtzman, D.M., Santucci, D., Kilbridge, J., Chua-Couzens, J., Fontana, D.J., Daniels, S.E., Johnson, R.M., Chen, K., Sun, Y., Carlson, E., et al. (1996). Developmental abnormalities and age-related neurodegeneration in a mouse model of Down syndrome. Proc Natl Acad Sci U S A 93, 13333-13338.

Homem, C.C., and Knoblich, J.A. (2012). Drosophila neuroblasts: a model for stem cell biology. Development 139, 4297-4310.

Horn, D., Siebert, E., Seidel, U., Rost, I., Mayer, K., Abou Jamra, R., Mitter, D., and Kornak, U. (2017). Biallelic COL3A1 mutations result in a clinical spectrum of specific structural brain anomalies and connective tissue abnormalities. Am J Med Genet A 173, 2534-2538.

Hu, W.F., Chahrour, M.H., and Walsh, C.A. (2014). The diverse genetic landscape of neurodevelopmental disorders. Annu Rev Genomics Hum Genet 15, 195-213.

Huang, D.W., Sherman, B.T., Tan, Q., Collins, J.R., Alvord, W.G., Roayaei, J., Stephens, R., Baseler, M.W., Lane, H.C., and Lempicki, R.A. (2007). The DAVID Gene Functional Classification Tool: a novel biological module-centric algorithm to functionally analyze large gene lists. Genome Biol 8, R183.

Huang, H., Zhao, X.F., Zheng, K., and Qiu, M. (2013). Regulation of the timing of oligodendrocyte differentiation: mechanisms and perspectives. Neurosci Bull 29, 155-164.

Huang, W., Guo, Q., Bai, X., Scheller, A., and Kirchhoff, F. (2019). Early embryonic NG2 glia are exclusively gliogenic and do not generate neurons in the brain. Glia 67, 1094-1103.

Hulsen, T., de Vlieg, J., and Alkema, W. (2008). BioVenn - a web application for the comparison and visualization of biological lists using area-proportional Venn diagrams. BMC Genomics 9, 488.

Huttner, W.B., and Brand, M. (1997). Asymmetric division and polarity of neuroepithelial cells. Curr Opin Neurobiol 7, 29-39.

Huttner, W.B., and Kosodo, Y. (2005). Symmetric versus asymmetric cell division during neurogenesis in the developing vertebrate central nervous system. Curr Opin Cell Biol 17, 648-657.

Impey, S., McCorkle, S.R., Cha-Molstad, H., Dwyer, J.M., Yochum, G.S., Boss, J.M., McWeeney, S., Dunn, J.J., Mandel, G., and Goodman, R.H. (2004). Defining the CREB regulon: a genome-wide analysis of transcription factor regulatory regions. Cell 119, 1041-1054.

Inoue, Y., Kagawa, T., Matsumura, Y., Ikenaka, K., and Mikoshiba, K. (1996). Cell death of oligodendrocytes or demyelination induced by overexpression of proteolipid protein depending on expressed gene dosage. Neurosci Res 25, 161-172.

Inoue, Y., Nakamura, R., Mikoshiba, K., and Tsukada, Y. (1981). Fine structure of the central myelin sheath in the myelin deficient mutant Shiverer mouse, with special reference to the pattern of myelin formation by oligodendroglia. Brain Res 219, 85-94.

Iossifov, I., Ronemus, M., Levy, D., Wang, Z., Hakker, I., Rosenbaum, J., Yamrom, B., Lee, Y.H., Narzisi, G., Leotta, A., et al. (2012). De novo gene disruptions in children on the autistic spectrum. Neuron 74, 285-299.

Irimia, M., Weatheritt, R.J., Ellis, J.D., Parikshak, N.N., Gonatopoulos-Pournatzis, T., Babor, M., Quesnel-Vallieres, M., Tapial, J., Raj, B., O'Hanlon, D., et al. (2014). A highly conserved program of neuronal microexons is misregulated in autistic brains. Cell 159, 1511-1523.

Ishibashi, T., Dakin, K.A., Stevens, B., Lee, P.R., Kozlov, S.V., Stewart, C.L., and Fields, R.D. (2006). Astrocytes promote myelination in response to electrical impulses. Neuron 49, 823-832.

Iwamoto, K., Bundo, M., Yamada, K., Takao, H., Iwayama-Shigeno, Y., Yoshikawa, T., and Kato, T. (2005). DNA methylation status of SOX10 correlates with its downregulation and oligodendrocyte dysfunction in schizophrenia. J Neurosci 25, 5376-5381.

Iwashita, M., Ohta, H., Fujisawa, T., Cho, M., Ikeya, M., Kidoaki, S., and Kosodo, Y. (2019). Brain-stiffness-mimicking tilapia collagen gel promotes the induction of dorsal cortical neurons from human pluripotent stem cells. Sci Rep 9, 3068.

Jabaudon, D. (2017). Fate and freedom in developing neocortical circuits. Nat Commun 8, 16042.

Jacob, A.G., and Smith, C.W.J. (2017). Intron retention as a component of regulated gene expression programs. Hum Genet 136, 1043-1057.

Jacobs, S., and Doering, L.C. (2010). Astrocytes prevent abnormal neuronal development in the fragile x mouse. J Neurosci 30, 4508-4514.

Jacobs, S., Nathwani, M., and Doering, L.C. (2010). Fragile X astrocytes induce developmental delays in dendrite maturation and synaptic protein expression. BMC Neurosci 11, 132.

Jakovcevski, I., Filipovic, R., Mo, Z., Rakic, S., and Zecevic, N. (2009). Oligodendrocyte development and the onset of myelination in the human fetal brain. Front Neuroanat 3, 5.

Ji, J., Lee, H., Argiropoulos, B., Dorrani, N., Mann, J., Martinez-Agosto, J.A., Gomez-Ospina, N., Gallant, N., Bernstein, J.A., Hudgins, L., et al. (2015). DYRK1A haploinsufficiency causes a new recognizable syndrome with microcephaly, intellectual disability, speech impairment, and distinct facies. Eur J Hum Genet 23, 1473-1481.

Jiang, X., Liu, C., Yu, T., Zhang, L., Meng, K., Xing, Z., Belichenko, P.V., Kleschevnikov, A.M., Pao, A., Peresie, J., et al. (2015). Genetic dissection of the Down syndrome critical region. Hum Mol Genet 24, 6540-6551.

Jorgensen, A., Fagerheim, T., Rand-Hendriksen, S., Lunde, P.I., Vorren, T.O., Pepin, M.G., Leistritz, D.F., and Byers, P.H. (2015). Vascular Ehlers-Danlos Syndrome in siblings with biallelic COL3A1 sequence variants and marked clinical variability in the extended family. Eur J Hum Genet 23, 796-802.

Kaczmarski, W., Barua, M., Mazur-Kolecka, B., Frackowiak, J., Dowjat, W., Mehta, P., Bolton, D., Hwang, Y.W., Rabe, A., Albertini, G., et al. (2014). Intracellular distribution of differentially phosphorylated dual-specificity tyrosine phosphorylation-regulated kinase 1A (DYRK1A). J Neurosci Res 92, 162-173.

Kagawa, T., Ikenaka, K., Inoue, Y., Kuriyama, S., Tsujii, T., Nakao, J., Nakajima, K., Aruga, J., Okano, H., and Mikoshiba, K. (1994). Glial cell degeneration and hypomyelination caused by overexpression of myelin proteolipid protein gene. Neuron 13, 427-442.

Kamakura, S., Oishi, K., Yoshimatsu, T., Nakafuku, M., Masuyama, N., and Gotoh, Y. (2004). Hes binding to STAT3 mediates crosstalk between Notch and JAK-STAT signalling. Nat Cell Biol 6, 547-554.

Kawase-Koga, Y., Otaegi, G., and Sun, T. (2009). Different timings of Dicer deletion affect neurogenesis and gliogenesis in the developing mouse central nervous system. Dev Dyn 238, 2800-2812.

Kazanis, I., and ffrench-Constant, C. (2011). Extracellular matrix and the neural stem cell niche. Dev Neurobiol 71, 1006-1017.

Kessaris, N., Fogarty, M., Iannarelli, P., Grist, M., Wegner, M., and Richardson, W.D. (2006). Competing waves of oligodendrocytes in the forebrain and postnatal elimination of an embryonic lineage. Nat Neurosci 9, 173-179.

Kim, D., Pertea, G., Trapnell, C., Pimentel, H., Kelley, R., and Salzberg, S.L. (2013). TopHat2: accurate alignment of transcriptomes in the presence of insertions, deletions and gene fusions. Genome Biol 14, R36.

Kim, M.Y., Jeong, B.C., Lee, J.H., Kee, H.J., Kook, H., Kim, N.S., Kim, Y.H., Kim, J.K., Ahn, K.Y., and Kim, K.K. (2006). A repressor complex, AP4 transcription factor and geminin, negatively regulates expression of target genes in nonneuronal cells. Proc Natl Acad Sci U S A 103, 13074-13079.

Kim, O.H., Cho, H.J., Han, E., Hong, T.I., Ariyasiri, K., Choi, J.H., Hwang, K.S., Jeong, Y.M., Yang, S.Y., Yu, K., et al. (2017). Zebrafish knockout of Down syndrome gene, DYRK1A, shows social impairments relevant to autism. Mol Autism 8, 50.

Kim, W., and Jho, E.H. (2018). The history and regulatory mechanism of the Hippo pathway. BMB Rep 51, 106-118.

Kimura, R., Kamino, K., Yamamoto, M., Nuripa, A., Kida, T., Kazui, H., Hashimoto, R., Tanaka, T., Kudo, T., Yamagata, H., et al. (2007). The DYRK1A gene, encoded in chromosome 21 Down syndrome critical region, bridges between beta-amyloid production and tau phosphorylation in Alzheimer disease. Hum Mol Genet 16, 15-23.

Klingseisen, A., and Lyons, D.A. (2018). Axonal Regulation of Central Nervous System Myelination: Structure and Function. Neuroscientist 24, 7-21.

Konno, D., Shioi, G., Shitamukai, A., Mori, A., Kiyonari, H., Miyata, T., and Matsuzaki, F. (2008). Neuroepithelial progenitors undergo LGN-dependent planar divisions to maintain self-renewability during mammalian neurogenesis. Nat Cell Biol 10, 93-101.

Kosik, K.S., and Nowakowski, T. (2018). Evolution of New miRNAs and Cerebro-Cortical Development. Annu Rev Neurosci 41, 119-137.

Kosodo, Y., Toida, K., Dubreuil, V., Alexandre, P., Schenk, J., Kiyokage, E., Attardo, A., Mora-Bermudez, F., Arii, T., Clarke, J.D., et al. (2008). Cytokinesis of neuroepithelial cells can divide their basal process before anaphase. EMBO J 27, 3151-3163.

Krichevsky, A.M., King, K.S., Donahue, C.P., Khrapko, K., and Kosik, K.S. (2003). A microRNA array reveals extensive regulation of microRNAs during brain development. RNA 9, 1274-1281.

Kriegstein, A., and Alvarez-Buylla, A. (2009). The glial nature of embryonic and adult neural stem cells. Annu Rev Neurosci 32, 149-184.

Krumm, N., O'Roak, B.J., Shendure, J., and Eichler, E.E. (2014). A de novo convergence of autism genetics and molecular neuroscience. Trends Neurosci 37, 95-105.

Kucera, M., Isserlin, R., Arkhangorodsky, A., and Bader, G.D. (2016). AutoAnnotate: A Cytoscape app for summarizing networks with semantic annotations. F1000Res 5, 1717.

Kumamoto, T., Toma, K., Gunadi, McKenna, W.L., Kasukawa, T., Katzman, S., Chen, B., and Hanashima, C. (2013). Foxg1 coordinates the switch from nonradially to radially migrating glutamatergic subtypes in the neocortex through spatiotemporal repression. Cell Rep 3, 931-945.

Kurabayashi, N., Nguyen, M.D., and Sanada, K. (2015). DYRK1A overexpression enhances STAT activity and astrogliogenesis in a Down syndrome mouse model. EMBO Rep 16, 1548-1562.

Kuwahara, A., Hirabayashi, Y., Knoepfler, P.S., Taketo, M.M., Sakai, J., Kodama, T., and Gotoh, Y. (2010). Wnt signaling and its downstream target N-myc regulate basal progenitors in the developing neocortex. Development 137, 1035-1044.

Kwan, K.Y., Sestan, N., and Anton, E.S. (2012). Transcriptional co-regulation of neuronal migration and laminar identity in the neocortex. Development 139, 1535-1546.

Kwan, V., Unda, B.K., and Singh, K.K. (2016). Wnt signaling networks in autism spectrum disorder and intellectual disability. J Neurodev Disord 8, 45.

Laguna, A., Aranda, S., Barallobre, M.J., Barhoum, R., Fernandez, E., Fotaki, V., Delabar, J.M., de la Luna, S., de la Villa, P., and Arbones, M.L. (2008). The protein kinase DYRK1A regulates caspase-9-mediated apoptosis during retina development. Dev Cell 15, 841-853.

Lange, C., Huttner, W.B., and Calegari, F. (2009). Cdk4/cyclinD1 overexpression in neural stem cells shortens G1, delays neurogenesis, and promotes the generation and expansion of basal progenitors. Cell Stem Cell 5, 320-331.

Langmead, B., and Salzberg, S.L. (2012). Fast gapped-read alignment with Bowtie 2. Nat Methods 9, 357-359.

Langseth, A.J., Munji, R.N., Choe, Y., Huynh, T., Pozniak, C.D., and Pleasure, S.J. (2010). Wnts influence the timing and efficiency of oligodendrocyte precursor cell generation in the telencephalon. J Neurosci 30, 13367-13372.

Lathia, J.D., Patton, B., Eckley, D.M., Magnus, T., Mughal, M.R., Sasaki, T., Caldwell, M.A., Rao, M.S., Mattson, M.P., and ffrench-Constant, C. (2007). Patterns of laminins and integrins in the embryonic ventricular zone of the CNS. J Comp Neurol 505, 630-643.

Lau, N.C., Lim, L.P., Weinstein, E.G., and Bartel, D.P. (2001). An abundant class of tiny RNAs with probable regulatory roles in Caenorhabditis elegans. Science 294, 858-862.

Lavado, A., He, Y., Pare, J., Neale, G., Olson, E.N., Giovannini, M., and Cao, X. (2013). Tumor suppressor Nf2 limits expansion of the neural progenitor pool by inhibiting Yap/Taz transcriptional coactivators. Development 140, 3323-3334.

Lavado, A., Ware, M., Pare, J., and Cao, X. (2014). The tumor suppressor Nf2 regulates corpus callosum development by inhibiting the transcriptional coactivator Yap. Development 141, 4182-4193.

Lee, F.H.F., Lai, T.K.Y., Su, P., and Liu, F. (2019). Altered cortical Cytoarchitecture in the Fmr1 knockout mouse. Mol Brain 12, 56.

Lee, S., Leach, M.K., Redmond, S.A., Chong, S.Y., Mellon, S.H., Tuck, S.J., Feng, Z.Q., Corey, J.M., and Chan, J.R. (2012). A culture system to study oligodendrocyte myelination processes using engineered nanofibers. Nat Methods 9, 917-922.

Lee, X., Hu, Y., Zhang, Y., Yang, Z., Shao, Z., Qiu, M., Pepinsky, B., Miller, R.H., and Mi, S. (2011). Oligodendrocyte differentiation and myelination defects in OMgp null mice. Mol Cell Neurosci 46, 752-761.

Levelt, C.N., and Hubener, M. (2012). Critical-period plasticity in the visual cortex. Annu Rev Neurosci 35, 309-330.

Levy, D.E., and Darnell, J.E., Jr. (2002). Stats: transcriptional control and biological impact. Nat Rev Mol Cell Biol 3, 651-662.

Li, D., Jackson, R.A., Yusoff, P., and Guy, G.R. (2010). Direct association of Sprouty-related protein with an EVH1 domain (SPRED) 1 or SPRED2 with DYRK1A modifies substrate/kinase interactions. J Biol Chem 285, 35374-35385.

Li, H., de Faria, J.P., Andrew, P., Nitarska, J., and Richardson, W.D. (2011). Phosphorylation regulates OLIG2 cofactor choice and the motor neuron-oligodendrocyte fate switch. Neuron 69, 918-929.

Li, H., Radford, J.C., Ragusa, M.J., Shea, K.L., McKercher, S.R., Zaremba, J.D., Soussou, W., Nie, Z., Kang, Y.J., Nakanishi, N., et al. (2008). Transcription factor MEF2C influences neural stem/progenitor cell differentiation and maturation in vivo. Proc Natl Acad Sci U S A 105, 9397-9402.

Li, L., Tian, E., Chen, X., Chao, J., Klein, J., Qu, Q., Sun, G., Sun, G., Huang, Y., Warden, C.D., et al. (2018). GFAP Mutations in Astrocytes Impair Oligodendrocyte Progenitor Proliferation and Myelination in an hiPSC Model of Alexander Disease. Cell Stem Cell 23, 239-251 e236.

Li, Q., Zheng, S., Han, A., Lin, C.H., Stoilov, P., Fu, X.D., and Black, D.L. (2014). The splicing regulator PTBP2 controls a program of embryonic splicing required for neuronal maturation. Elife 3, e01201.

Li, Y.I., Sanchez-Pulido, L., Haerty, W., and Ponting, C.P. (2015). RBFOX and PTBP1 proteins regulate the alternative splicing of micro-exons in human brain transcripts. Genome Res 25, 1-13.

Licatalosi, D.D., and Darnell, R.B. (2010). RNA processing and its regulation: global insights into biological networks. Nat Rev Genet 11, 75-87.

Licatalosi, D.D., Yano, M., Fak, J.J., Mele, A., Grabinski, S.E., Zhang, C., and Darnell, R.B. (2012). Ptbp2 represses adult-specific splicing to regulate the generation of neuronal precursors in the embryonic brain. Genes Dev 26, 1626-1642.

Ligon, K.L., Kesari, S., Kitada, M., Sun, T., Arnett, H.A., Alberta, J.A., Anderson, D.J., Stiles, C.D., and Rowitch, D.H. (2006). Development of NG2 neural progenitor cells requires Olig gene function. Proc Natl Acad Sci U S A 103, 7853-7858.

Lim, L., Mi, D., Llorca, A., and Marin, O. (2018). Development and Functional Diversification of Cortical Interneurons. Neuron 100, 294-313.

Lioy, D.T., Garg, S.K., Monaghan, C.E., Raber, J., Foust, K.D., Kaspar, B.K., Hirrlinger, P.G., Kirchhoff, F., Bissonnette, J.M., Ballas, N., et al. (2011). A role for glia in the progression of Rett's syndrome. Nature 475, 497-500.

Liu, J., Geng, A., Wu, X., Lin, R.J., and Lu, Q. (2018). Alternative RNA Splicing Associated With Mammalian Neuronal Differentiation. Cereb Cortex 28, 2810-2816.

Liu, J., Luo, C., Yin, Z., Li, P., Wang, S., Chen, J., He, Q., and Zhou, J. (2016). Downregulation of let-7b promotes COL1A1 and COL1A2 expression in dermis and skin fibroblasts during heat wound repair. Mol Med Rep 13, 2683-2688.

Liu, R., Cai, J., Hu, X., Tan, M., Qi, Y., German, M., Rubenstein, J., Sander, M., and Qiu, M. (2003). Region-specific and stage-dependent regulation of Olig gene expression and oligodendrogenesis by Nkx6.1 homeodomain transcription factor. Development 130, 6221-6231.

Liu, W., Zhou, H., Liu, L., Zhao, C., Deng, Y., Chen, L., Wu, L., Mandrycky, N., McNabb, C.T., Peng, Y., et al. (2015). Disruption of neurogenesis and cortical development in transgenic mice misexpressing Olig2, a gene in the Down syndrome critical region. Neurobiol Dis 77, 106-116.

Lochhead, P.A., Sibbet, G., Morrice, N., and Cleghon, V. (2005). Activation-loop autophosphorylation is mediated by a novel transitional intermediate form of DYRKs. Cell 121, 925-936.

Lodato, S., and Arlotta, P. (2015). Generating neuronal diversity in the mammalian cerebral cortex. Annu Rev Cell Dev Biol 31, 699-720.

Long, K.R., and Huttner, W.B. (2019). How the extracellular matrix shapes neural development. Open Biol 9, 180216.

LoTurco, J.J., Owens, D.F., Heath, M.J., Davis, M.B., and Kriegstein, A.R. (1995). GABA and glutamate depolarize cortical progenitor cells and inhibit DNA synthesis. Neuron 15, 1287-1298.

Louvi, A., and Artavanis-Tsakonas, S. (2006). Notch signalling in vertebrate neural development. Nat Rev Neurosci 7, 93-102.

Love, M.I., Huber, W., and Anders, S. (2014). Moderated estimation of fold change and dispersion for RNA-seq data with DESeq2. Genome Biol 15, 550.

Lu, M., Zheng, L., Han, B., Wang, L., Wang, P., Liu, H., and Sun, X. (2011a). REST regulates DYRK1A transcription in a negative feedback loop. J Biol Chem 286, 10755-10763.

Lu, P., Takai, K., Weaver, V.M., and Werb, Z. (2011b). Extracellular matrix degradation and remodeling in development and disease. Cold Spring Harb Perspect Biol 3.

Lu, Q.R., Sun, T., Zhu, Z., Ma, N., Garcia, M., Stiles, C.D., and Rowitch, D.H. (2002). Common developmental requirement for Olig function indicates a motor neuron/oligodendrocyte connection. Cell 109, 75-86.

Luco, S.M., Pohl, D., Sell, E., Wagner, J.D., Dyment, D.A., and Daoud, H. (2016). Case report of novel DYRK1A mutations in 2 individuals with syndromic intellectual disability and a review of the literature. BMC Med Genet 17, 15.

Luders, K.A., Nessler, S., Kusch, K., Patzig, J., Jung, R.B., Mobius, W., Nave, K.A., and Werner, H.B. (2019). Maintenance of high proteolipid protein level in adult central nervous system myelin is required to preserve the integrity of myelin and axons. Glia 67, 634-649.

Luo, R., Jeong, S.J., Jin, Z., Strokes, N., Li, S., and Piao, X. (2011). G protein-coupled receptor 56 and collagen III, a receptor-ligand pair, regulates cortical development and lamination. Proc Natl Acad Sci U S A 108, 12925-12930.

Luskin, M.B., and Shatz, C.J. (1985). Studies of the earliest generated cells of the cat's visual cortex: cogeneration of subplate and marginal zones. J Neurosci 5, 1062-1075.

Lutolf, S., Radtke, F., Aguet, M., Suter, U., and Taylor, V. (2002). Notch1 is required for neuronal and glial differentiation in the cerebellum. Development 129, 373-385.

Ma, W., and Barker, J.L. (1995). Complementary expressions of transcripts encoding GAD67 and GABAA receptor alpha 4, beta 1, and gamma 1 subunits in the proliferative zone of the embryonic rat central nervous system. J Neurosci 15, 2547-2560.

Machon, O., van den Bout, C.J., Backman, M., Kemler, R., and Krauss, S. (2003). Role of beta-catenin in the developing cortical and hippocampal neuroepithelium. Neuroscience 122, 129-143.

Maenz, B., Hekerman, P., Vela, E.M., Galceran, J., and Becker, W. (2008). Characterization of the human DYRK1A promoter and its regulation by the transcription factor E2F1. BMC Mol Biol 9, 30.

Magavi, S., Friedmann, D., Banks, G., Stolfi, A., and Lois, C. (2012). Coincident generation of pyramidal neurons and protoplasmic astrocytes in neocortical columns. J Neurosci 32, 4762-4772.

Mahmoud, S., Gharagozloo, M., Simard, C., and Gris, D. (2019). Astrocytes Maintain Glutamate Homeostasis in the CNS by Controlling the Balance between Glutamate Uptake and Release. Cells 8.

Makeyev, E.V., Zhang, J., Carrasco, M.A., and Maniatis, T. (2007). The MicroRNA miR-124 promotes neuronal differentiation by triggering brain-specific alternative pre-mRNA splicing. Mol Cell 27, 435-448.

Makino, K., Jinnin, M., Hirano, A., Yamane, K., Eto, M., Kusano, T., Honda, N., Kajihara, I., Makino, T., Sakai, K., et al. (2013). The downregulation of microRNA let-7a contributes to the excessive expression of type I collagen in systemic and localized scleroderma. J Immunol 190, 3905-3915.

Makinson, C.D., Tanaka, B.S., Sorokin, J.M., Wong, J.C., Christian, C.A., Goldin, A.L., Escayg, A., and Huguenard, J.R. (2017). Regulation of Thalamic and Cortical Network Synchrony by Scn8a. Neuron 93, 1165-1179 e1166.

Malatesta, P., Hartfuss, E., and Gotz, M. (2000). Isolation of radial glial cells by fluorescent-activated cell sorting reveals a neuronal lineage. Development 127, 5253-5263.

Manuel, M.N., Mi, D., Mason, J.O., and Price, D.J. (2015). Regulation of cerebral cortical neurogenesis by the Pax6 transcription factor. Front Cell Neurosci 9, 70.

Mao, J., Maye, P., Kogerman, P., Tejedor, F.J., Toftgard, R., Xie, W., Wu, G., and Wu, D. (2002). Regulation of Gli1 transcriptional activity in the nucleus by Dyrk1. J Biol Chem 277, 35156-35161.

Marie, C., Clavairoly, A., Frah, M., Hmidan, H., Yan, J., Zhao, C., Van Steenwinckel, J., Daveau, R., Zalc, B., Hassan, B., et al. (2018). Oligodendrocyte precursor survival and differentiation requires chromatin remodeling by Chd7 and Chd8. Proc Natl Acad Sci U S A 115, E8246-E8255.

Marin-Padilla, M. (1995). Prenatal development of fibrous (white matter), protoplasmic (gray matter), and layer I astrocytes in the human cerebral cortex: a Golgi study. J Comp Neurol 357, 554-572.

Marin, O., and Rubenstein, J.L. (2003). Cell migration in the forebrain. Annu Rev Neurosci 26, 441-483.

Marques, S., van Bruggen, D., Vanichkina, D.P., Floriddia, E.M., Munguba, H., Varemo, L., Giacomello, S., Falcao, A.M., Meijer, M., Bjorklund, A.K., et al. (2018). Transcriptional Convergence of Oligodendrocyte Lineage Progenitors during Development. Dev Cell 46, 504-517 e507.

Marques, S., Zeisel, A., Codeluppi, S., van Bruggen, D., Mendanha Falcao, A., Xiao, L., Li, H., Haring, M., Hochgerner, H., Romanov, R.A., et al. (2016). Oligodendrocyte heterogeneity in the mouse juvenile and adult central nervous system. Science 352, 1326-1329.

Marshall, C.A., and Goldman, J.E. (2002). Subpallial dlx2-expressing cells give rise to astrocytes and oligodendrocytes in the cerebral cortex and white matter. J Neurosci 22, 9821-9830.

Marti, E., Altafaj, X., Dierssen, M., de la Luna, S., Fotaki, V., Alvarez, M., Perez-Riba, M., Ferrer, I., and Estivill, X. (2003). Dyrk1A expression pattern supports specific roles of this kinase in the adult central nervous system. Brain Res 964, 250-263.

Martin-Lopez, E., Garcia-Marques, J., Nunez-Llaves, R., and Lopez-Mascaraque, L. (2013). Clonal astrocytic response to cortical injury. PLoS One 8, e74039.

Martin, M. (2011). Cutadapt removes adapter sequences from high-throughput sequencing reads. EMBnet.journal 17, 10-12.

Martinez de Lagran, M., Benavides-Piccione, R., Ballesteros-Yanez, I., Calvo, M., Morales, M., Fillat, C., Defelipe, J., Ramakers, G.J., and Dierssen, M. (2012). Dyrk1A influences neuronal morphogenesis through regulation of cytoskeletal dynamics in mammalian cortical neurons. Cereb Cortex 22, 2867-2877.

Martinez de Lagran, M., Bortolozzi, A., Millan, O., Gispert, J.D., Gonzalez, J.R., Arbones, M.L., Artigas, F., and Dierssen, M. (2007). Dopaminergic deficiency in mice with reduced levels of the dual-specificity tyrosine-phosphorylated and regulated kinase 1A, Dyrk1A(+/-). Genes Brain Behav 6, 569-578.

Martynoga, B., Drechsel, D., and Guillemot, F. (2012). Molecular control of neurogenesis: a view from the mammalian cerebral cortex. Cold Spring Harb Perspect Biol 4.

Mason, H.A., Rakowiecki, S.M., Gridley, T., and Fishell, G. (2006). Loss of notch activity in the developing central nervous system leads to increased cell death. Dev Neurosci 28, 49-57.

Matsui, A., Yoshida, A.C., Kubota, M., Ogawa, M., and Shimogori, T. (2011). Mouse in utero electroporation: controlled spatiotemporal gene transfection. J Vis Exp.

Matsumoto, N., Ohashi, H., Tsukahara, M., Kim, K.C., Soeda, E., and Niikawa, N. (1997). Possible narrowed assignment of the loci of monosomy 21-associated microcephaly and intrauterine growth retardation to a 1.2-Mb segment at 21q22.2. Am J Hum Genet 60, 997-999.

Matsuo, R., Ochiai, W., Nakashima, K., and Taga, T. (2001). A new expression cloning strategy for isolation of substrate-specific kinases by using phosphorylation site-specific antibody. J Immunol Methods 247, 141-151.

Mauger, O., Lemoine, F., and Scheiffele, P. (2016). Targeted Intron Retention and Excision for Rapid Gene Regulation in Response to Neuronal Activity. Neuron 92, 1266-1278.

McConnell, S.K. (1995). Constructing the cerebral cortex: neurogenesis and fate determination. Neuron 15, 761-768.

McKenna, W.L., Betancourt, J., Larkin, K.A., Abrams, B., Guo, C., Rubenstein, J.L., and Chen, B. (2011). Tbr1 and Fezf2 regulate alternate corticofugal neuronal identities during neocortical development. J Neurosci 31, 549-564.

McKinnon, P.J. (2013). Maintaining genome stability in the nervous system. Nat Neurosci 16, 1523-1529.

Mekki-Dauriac, S., Agius, E., Kan, P., and Cochard, P. (2002). Bone morphogenetic proteins negatively control oligodendrocyte precursor specification in the chick spinal cord. Development 129, 5117-5130.

Meng, Z., Moroishi, T., and Guan, K.L. (2016). Mechanisms of Hippo pathway regulation. Genes Dev 30, 1-17.

Menn, B., Garcia-Verdugo, J.M., Yaschine, C., Gonzalez-Perez, O., Rowitch, D., and Alvarez-Buylla, A. (2006). Origin of oligodendrocytes in the subventricular zone of the adult brain. J Neurosci 26, 7907-7918.

Merico, D., Isserlin, R., Stueker, O., Emili, A., and Bader, G.D. (2010). Enrichment map: a network-based method for gene-set enrichment visualization and interpretation. PLoS One 5, e13984.

Metsalu, T., and Vilo, J. (2015). ClustVis: a web tool for visualizing clustering of multivariate data using Principal Component Analysis and heatmap. Nucleic Acids Res 43, W566-570.

Mi, D., Carr, C.B., Georgala, P.A., Huang, Y.T., Manuel, M.N., Jeanes, E., Niisato, E., Sansom, S.N., Livesey, F.J., Theil, T., et al. (2013). Pax6 exerts regional control of cortical progenitor proliferation via direct repression of Cdk6 and hypophosphorylation of pRb. Neuron 78, 269-284.

Michailov, G.V., Sereda, M.W., Brinkmann, B.G., Fischer, T.M., Haug, B., Birchmeier, C., Role, L., Lai, C., Schwab, M.H., and Nave, K.A. (2004). Axonal neuregulin-1 regulates myelin sheath thickness. Science 304, 700-703.

Miller, D.J., Duka, T., Stimpson, C.D., Schapiro, S.J., Baze, W.B., McArthur, M.J., Fobbs, A.J., Sousa, A.M., Sestan, N., Wildman, D.E., et al. (2012). Prolonged myelination in human neocortical evolution. Proc Natl Acad Sci U S A 109, 16480-16485.

Miller, R.H., and Raff, M.C. (1984). Fibrous and protoplasmic astrocytes are biochemically and developmentally distinct. J Neurosci 4, 585-592.

Mitew, S., Gobius, I., Fenlon, L.R., McDougall, S.J., Hawkes, D., Xing, Y.L., Bujalka, H., Gundlach, A.L., Richards, L.J., Kilpatrick, T.J., et al. (2018). Pharmacogenetic stimulation of neuronal activity increases myelination in an axon-specific manner. Nat Commun 9, 306.

Mito, T., and Becker, L.E. (1993). Developmental changes of S-100 protein and glial fibrillary acidic protein in the brain in Down syndrome. Exp Neurol 120, 170-176.

Miyata, T. (2008). Development of three-dimensional architecture of the neuroepithelium: role of pseudostratification and cellular 'community'. Dev Growth Differ 50 Suppl 1, S105-112.

Miyata, T., Kawaguchi, A., Saito, K., Kawano, M., Muto, T., and Ogawa, M. (2004). Asymmetric production of surface-dividing and non-surface-dividing cortical progenitor cells. Development 131, 3133-3145.

Moller, R.S., Kubart, S., Hoeltzenbein, M., Heye, B., Vogel, I., Hansen, C.P., Menzel, C., Ullmann, R., Tommerup, N., Ropers, H.H., et al. (2008). Truncation of the Down syndrome candidate gene DYRK1A in two unrelated patients with microcephaly. Am J Hum Genet 82, 1165-1170.

Molyneaux, B.J., Arlotta, P., Menezes, J.R., and Macklis, J.D. (2007). Neuronal subtype specification in the cerebral cortex. Nat Rev Neurosci 8, 427-437.

Molyneaux, B.J., Goff, L.A., Brettler, A.C., Chen, H.H., Hrvatin, S., Rinn, J.L., and Arlotta, P. (2015). DeCoN: genome-wide analysis of in vivo transcriptional dynamics during pyramidal neuron fate selection in neocortex. Neuron 85, 275-288.

Monteiro, P., and Feng, G. (2017). SHANK proteins: roles at the synapse and in autism spectrum disorder. Nat Rev Neurosci 18, 147-157.

Moon, B.S., Bai, J., Cai, M., Liu, C., Shi, J., and Lu, W. (2018). Kruppel-like factor 4-dependent Staufen1-mediated mRNA decay regulates cortical neurogenesis. Nat Commun 9, 401.

Mount, C.W., and Monje, M. (2017). Wrapped to Adapt: Experience-Dependent Myelination. Neuron 95, 743-756.

Mountcastle, V.B. (1997). The columnar organization of the neocortex. Brain 120 ( Pt 4), 701-722.

MuhChyi, C., Juliandi, B., Matsuda, T., and Nakashima, K. (2013). Epigenetic regulation of neural stem cell fate during corticogenesis. Int J Dev Neurosci 31, 424-433.

Munji, R.N., Choe, Y., Li, G., Siegenthaler, J.A., and Pleasure, S.J. (2011). Wnt signaling regulates neuronal differentiation of cortical intermediate progenitors. J Neurosci 31, 1676-1687.

Musah, S., Wrighton, P.J., Zaltsman, Y., Zhong, X., Zorn, S., Parlato, M.B., Hsiao, C., Palecek, S.P., Chang, Q., Murphy, W.L., et al. (2014). Substratum-induced differentiation of human pluripotent stem cells reveals the coactivator YAP is a potent regulator of neuronal specification. Proc Natl Acad Sci U S A 111, 13805-13810.

Nagy, K., Sung, H.K., Zhang, P., Laflamme, S., Vincent, P., Agha-Mohammadi, S., Woltjen, K., Monetti, C., Michael, I.P., Smith, L.C., et al. (2011). Induced pluripotent stem cell lines derived from equine fibroblasts. Stem Cell Rev 7, 693-702.

Nait-Oumesmar, B., Decker, L., Lachapelle, F., Avellana-Adalid, V., Bachelin, C., and Baron-Van Evercooren, A. (1999). Progenitor cells of the adult mouse subventricular zone proliferate, migrate and differentiate into oligodendrocytes after demyelination. Eur J Neurosci 11, 4357-4366.

Najas, S. (2014). Role of DYRK1A in the development of the cerebral cortex. Implication in Down Syndrome. In Departament de Ciències Experimentals i de la Salut (Universitat Pompeu Fabra), p. 256.

Najas, S., Arranz, J., Lochhead, P.A., Ashford, A.L., Oxley, D., Delabar, J.M., Cook, S.J., Barallobre, M.J., and Arbones, M.L. (2015). DYRK1A-mediated Cyclin D1 Degradation in Neural Stem Cells Contributes to the Neurogenic Cortical Defects in Down Syndrome. EBioMedicine 2, 120-134.

Nakashima, K., Yanagisawa, M., Arakawa, H., Kimura, N., Hisatsune, T., Kawabata, M., Miyazono, K., and Taga, T. (1999). Synergistic signaling in fetal brain by STAT3-Smad1 complex bridged by p300. Science 284, 479-482.

Namihira, M., Kohyama, J., Semi, K., Sanosaka, T., Deneen, B., Taga, T., and Nakashima, K. (2009). Committed neuronal precursors confer astrocytic potential on residual neural precursor cells. Dev Cell 16, 245-255.

Nave, K.A. (2010). Myelination and support of axonal integrity by glia. Nature 468, 244-252.

Nave, K.A., Lai, C., Bloom, F.E., and Milner, R.J. (1987). Splice site selection in the proteolipid protein (PLP) gene transcript and primary structure of the DM-20 protein of central nervous system myelin. Proc Natl Acad Sci U S A 84, 5665-5669.

Nazeri, A., Chakravarty, M.M., Felsky, D., Lobaugh, N.J., Rajji, T.K., Mulsant, B.H., and Voineskos, A.N. (2013). Alterations of superficial white matter in schizophrenia and relationship to cognitive performance. Neuropsychopharmacology 38, 1954-1962.

Nery, S., Wichterle, H., and Fishell, G. (2001). Sonic hedgehog contributes to oligodendrocyte specification in the mammalian forebrain. Development 128, 527-540.

Newman, M.A., Thomson, J.M., and Hammond, S.M. (2008). Lin-28 interaction with the Let-7 precursor loop mediates regulated microRNA processing. RNA 14, 1539-1549.

Ni, N., Zhang, D., Xie, Q., Chen, J., Wang, Z., Deng, Y., Wen, X., Zhu, M., Ji, J., Fan, X., et al. (2014). Effects of let-7b and TLX on the proliferation and differentiation of retinal progenitor cells in vitro. Sci Rep 4, 6671.

Niehrs, C., and Acebron, S.P. (2012). Mitotic and mitogenic Wnt signalling. EMBO J 31, 2705-2713.

Nieto, M., Schuurmans, C., Britz, O., and Guillemot, F. (2001). Neural bHLH genes control the neuronal versus glial fate decision in cortical progenitors. Neuron 29, 401-413.

Nigg, E.A., and Holland, A.J. (2018). Once and only once: mechanisms of centriole duplication and their deregulation in disease. Nat Rev Mol Cell Biol 19, 297-312.

Nishino, J., Kim, I., Chada, K., and Morrison, S.J. (2008). Hmga2 promotes neural stem cell self-renewal in young but not old mice by reducing p16Ink4a and p19Arf Expression. Cell 135, 227-239.

Noble, M., Murray, K., Stroobant, P., Waterfield, M.D., and Riddle, P. (1988). Platelet-derived growth factor promotes division and motility and inhibits premature differentiation of the oligodendrocyte/type-2 astrocyte progenitor cell. Nature 333, 560-562.

Nobs, L., Baranek, C., Nestel, S., Kulik, A., Kapfhammer, J., Nitsch, C., and Atanasoski, S. (2014). Stage-specific requirement for cyclin D1 in glial progenitor cells of the cerebral cortex. Glia 62, 829-839.

Noctor, S.C., Flint, A.C., Weissman, T.A., Dammerman, R.S., and Kriegstein, A.R. (2001). Neurons derived from radial glial cells establish radial units in neocortex. Nature 409, 714-720.

Noctor, S.C., Martinez-Cerdeno, V., Ivic, L., and Kriegstein, A.R. (2004). Cortical neurons arise in symmetric and asymmetric division zones and migrate through specific phases. Nat Neurosci 7, 136-144.

Nonaka-Kinoshita, M., Reillo, I., Artegiani, B., Martinez-Martinez, M.A., Nelson, M., Borrell, V., and Calegari, F. (2013). Regulation of cerebral cortex size and folding by expansion of basal progenitors. EMBO J 32, 1817-1828.

Nowakowski, T.J., Mysiak, K.S., O'Leary, T., Fotaki, V., Pratt, T., and Price, D.J. (2013). Loss of functional Dicer in mouse radial glia cell-autonomously prolongs cortical neurogenesis. Dev Biol 382, 530-537.

Nowakowski, T.J., Mysiak, K.S., Pratt, T., and Price, D.J. (2011). Functional dicer is necessary for appropriate specification of radial glia during early development of mouse telencephalon. PLoS One 6, e23013.

Nusse, R., and Clevers, H. (2017). Wnt/beta-Catenin Signaling, Disease, and Emerging Therapeutic Modalities. Cell 169, 985-999.

O'Brien, J.E., and Meisler, M.H. (2013). Sodium channel SCN8A (Nav1.6): properties and de novo mutations in epileptic encephalopathy and intellectual disability. Front Genet 4, 213.

O'Leary, D.D., Chou, S.J., and Sahara, S. (2007). Area patterning of the mammalian cortex. Neuron 56, 252-269.

O'Roak, B.J., Vives, L., Fu, W., Egertson, J.D., Stanaway, I.B., Phelps, I.G., Carvill, G., Kumar, A., Lee, C., Ankenman, K., et al. (2012). Multiplex targeted sequencing identifies recurrently mutated genes in autism spectrum disorders. Science 338, 1619-1622.

Oberheim, N.A., Goldman, S.A., and Nedergaard, M. (2012). Heterogeneity of astrocytic form and function. Methods Mol Biol 814, 23-45.

Oberheim, N.A., Takano, T., Han, X., He, W., Lin, J.H., Wang, F., Xu, Q., Wyatt, J.D., Pilcher, W., Ojemann, J.G., et al. (2009). Uniquely hominid features of adult human astrocytes. J Neurosci 29, 3276-3287.

Oberheim, N.A., Wang, X., Goldman, S., and Nedergaard, M. (2006). Astrocytic complexity distinguishes the human brain. Trends Neurosci 29, 547-553.

Oberst, P., Fièvre, S., Baumann, N., Concetti, C., and Jabaudon, D. (2018). Apical progenitors remain multipotent throughout cortical neurogenesis. bioRxiv, 478891.

Ochiai, W., Nakatani, S., Takahara, T., Kainuma, M., Masaoka, M., Minobe, S., Namihira, M., Nakashima, K., Sakakibara, A., Ogawa, M., et al. (2009). Periventricular notch activation and asymmetric Ngn2 and Tbr2 expression in pair-generated neocortical daughter cells. Mol Cell Neurosci 40, 225-233.

Oegema, R., de Klein, A., Verkerk, A.J., Schot, R., Dumee, B., Douben, H., Eussen, B., Dubbel, L., Poddighe, P.J., van der Laar, I., et al. (2010). Distinctive Phenotypic Abnormalities Associated with Submicroscopic 21q22 Deletion Including DYRK1A. Mol Syndromol 1, 113-120.

Okabe, Y., Takahashi, T., Mitsumasu, C., Kosai, K., Tanaka, E., and Matsuishi, T. (2012). Alterations of gene expression and glutamate clearance in astrocytes derived from an MeCP2-null mouse model of Rett syndrome. PLoS One 7, e35354.

Okui, M., Ide, T., Morita, K., Funakoshi, E., Ito, F., Ogita, K., Yoneda, Y., Kudoh, J., and Shimizu, N. (1999). High-level expression of the Mnb/Dyrk1A gene in brain and heart during rat early development. Genomics 62, 165-171.

Olmos-Serrano, J.L., Kang, H.J., Tyler, W.A., Silbereis, J.C., Cheng, F., Zhu, Y., Pletikos, M., Jankovic-Rapan, L., Cramer, N.P., Galdzicki, Z., et al. (2016). Down Syndrome Developmental Brain Transcriptome Reveals Defective Oligodendrocyte Differentiation and Myelination. Neuron 89, 1208-1222.

Ortega, M.C., Bribian, A., Peregrin, S., Gil, M.T., Marin, O., and de Castro, F. (2012). Neuregulin-1/ErbB4 signaling controls the migration of oligodendrocyte precursor cells during development. Exp Neurol 235, 610-620.

Ortiz, R., Georgieva, M.V., Gutierrez, S., Pedraza, N., Fernandez-Moya, S.M., and Gallego, C. (2017). Recruitment of Staufen2 Enhances Dendritic Localization of an Intron-Containing CaMKIIalpha mRNA. Cell Rep 20, 13-20.

Osorio, M.J., and Goldman, S.A. (2018). Neurogenetics of Pelizaeus-Merzbacher disease. Handb Clin Neurol 148, 701-722.

Osumi, N., Shinohara, H., Numayama-Tsuruta, K., and Maekawa, M. (2008). Concise review: Pax6 transcription factor contributes to both embryonic and adult neurogenesis as a multifunctional regulator. Stem Cells 26, 1663-1672.

Pan, Q., Shai, O., Lee, L.J., Frey, B.J., and Blencowe, B.J. (2008). Deep surveying of alternative splicing complexity in the human transcriptome by high-throughput sequencing. Nat Genet 40, 1413-1415.

Pan, Q., Shai, O., Misquitta, C., Zhang, W., Saltzman, A.L., Mohammad, N., Babak, T., Siu, H., Hughes, T.R., Morris, Q.D., et al. (2004). Revealing global regulatory features of mammalian alternative splicing using a quantitative microarray platform. Mol Cell 16, 929-941.

Pan, S., and Chan, J.R. (2017). Regulation and dysregulation of axon infrastructure by myelinating glia. J Cell Biol 216, 3903-3916.

Paquin, A., Hordo, C., Kaplan, D.R., and Miller, F.D. (2009). Costello syndrome H-Ras alleles regulate cortical development. Dev Biol 330, 440-451.

Paridaen, J.T., and Huttner, W.B. (2014). Neurogenesis during development of the vertebrate central nervous system. EMBO Rep 15, 351-364.

Paridaen, J.T., Wilsch-Brauninger, M., and Huttner, W.B. (2013). Asymmetric inheritance of centrosome-associated primary cilium membrane directs ciliogenesis after cell division. Cell 155, 333-344.

Parikshak, N.N., Luo, R., Zhang, A., Won, H., Lowe, J.K., Chandran, V., Horvath, S., and Geschwind, D.H. (2013). Integrative functional genomic analyses implicate specific molecular pathways and circuits in autism. Cell 155, 1008-1021.

Parnavelas, J.G. (2000). The origin and migration of cortical neurones: new vistas. Trends Neurosci 23, 126-131.

Parras, A., Anta, H., Santos-Galindo, M., Swarup, V., Elorza, A., Nieto-Gonzalez, J.L., Pico, S., Hernandez, I.H., Diaz-Hernandez, J.I., Belloc, E., et al. (2018). Autism-like phenotype and risk gene mRNA deadenylation by CPEB4 mis-splicing. Nature 560, 441-446.

Pehar, M., Ko, M.H., Li, M., Scrable, H., and Puglielli, L. (2014). P44, the 'longevity-assurance' isoform of P53, regulates tau phosphorylation and is activated in an age-dependent fashion. Aging Cell 13, 449-456.

Pereira, A., Jr., and Furlan, F.A. (2010). Astrocytes and human cognition: modeling information integration and modulation of neuronal activity. Prog Neurobiol 92, 405-420.

Petryniak, M.A., Potter, G.B., Rowitch, D.H., and Rubenstein, J.L. (2007). Dlx1 and Dlx2 control neuronal versus oligodendroglial cell fate acquisition in the developing forebrain. Neuron 55, 417-433.

Pilaz, L.J., Patti, D., Marcy, G., Ollier, E., Pfister, S., Douglas, R.J., Betizeau, M., Gautier, E., Cortay, V., Doerflinger, N., et al. (2009). Forced G1-phase reduction alters mode of division, neuron number, and laminar phenotype in the cerebral cortex. Proc Natl Acad Sci U S A 106, 21924-21929.

Price, J., and Thurlow, L. (1988). Cell lineage in the rat cerebral cortex: a study using retroviral-mediated gene transfer. Development 104, 473-482.

Qi, Y., Tan, M., Hui, C.C., and Qiu, M. (2003). Gli2 is required for normal Shh signaling and oligodendrocyte development in the spinal cord. Mol Cell Neurosci 23, 440-450.

Quesnel-Vallieres, M., Irimia, M., Cordes, S.P., and Blencowe, B.J. (2015). Essential roles for the splicing regulator nSR100/SRRM4 during nervous system development. Genes Dev 29, 746-759.

Raff, M.C., Lillien, L.E., Richardson, W.D., Burne, J.F., and Noble, M.D. (1988). Platelet-derived growth factor from astrocytes drives the clock that times oligodendrocyte development in culture. Nature 333, 562-565.

Raff, M.C., Miller, R.H., and Noble, M. (1983). A glial progenitor cell that develops in vitro into an astrocyte or an oligodendrocyte depending on culture medium. Nature 303, 390-396.

Raj, B., and Blencowe, B.J. (2015). Alternative Splicing in the Mammalian Nervous System: Recent Insights into Mechanisms and Functional Roles. Neuron 87, 14-27.

Raj, B., O'Hanlon, D., Vessey, J.P., Pan, Q., Ray, D., Buckley, N.J., Miller, F.D., and Blencowe, B.J. (2011). Cross-regulation between an alternative splicing activator and a transcription repressor controls neurogenesis. Mol Cell 43, 843-850.

Rakic, P. (1995). A small step for the cell, a giant leap for mankind: a hypothesis of neocortical expansion during evolution. Trends Neurosci 18, 383-388.

Rakic, P. (2000). Radial unit hypothesis of neocortical expansion. Novartis Found Symp 228, 30-42; discussion 42-52.

Ramón y Cajal, S. (1899). Textura del Sistema Nervioso del Hombre y los Vertebrados, Vol 3 (Madrid: Imprenta y Librería de Nicolás Moya).

Rasband, M.N., and Peles, E. (2015). The Nodes of Ranvier: Molecular Assembly and Maintenance. Cold Spring Harb Perspect Biol 8, a020495.

Rash, B.G., Lim, H.D., Breunig, J.J., and Vaccarino, F.M. (2011). FGF signaling expands embryonic cortical surface area by regulating Notch-dependent neurogenesis. J Neurosci 31, 15604-15617.

Rash, J.E., Yasumura, T., Hudson, C.S., Agre, P., and Nielsen, S. (1998). Direct immunogold labeling of aquaporin-4 in square arrays of astrocyte and ependymocyte plasma membranes in rat brain and spinal cord. Proc Natl Acad Sci U S A 95, 11981-11986.

Raveau, M., Shimohata, A., Amano, K., Miyamoto, H., and Yamakawa, K. (2018). DYRK1A-haploinsufficiency in mice causes autistic-like features and febrile seizures. Neurobiol Dis 110, 180-191.

Readhead, C., Schneider, A., Griffiths, I., and Nave, K.A. (1994). Premature arrest of myelin formation in transgenic mice with increased proteolipid protein gene dosage. Neuron 12, 583-595.

Reeves, R.H., Irving, N.G., Moran, T.H., Wohn, A., Kitt, C., Sisodia, S.S., Schmidt, C., Bronson, R.T., and Davisson, M.T. (1995). A mouse model for Down syndrome exhibits learning and behaviour deficits. Nat Genet 11, 177-184.

Regis, S., Grossi, S., Corsolini, F., Biancheri, R., and Filocamo, M. (2009). PLP1 gene duplication causes overexpression and alteration of the PLP/DM20 splicing balance in fibroblasts from Pelizaeus-Merzbacher disease patients. Biochim Biophys Acta 1792, 548-554.

Rehfeld, F., Rohde, A.M., Nguyen, D.T., and Wulczyn, F.G. (2015). Lin28 and let-7: ancient milestones on the road from pluripotency to neurogenesis. Cell Tissue Res 359, 145-160.

Reichenbach, A., Derouiche, A., and Kirchhoff, F. (2010). Morphology and dynamics of perisynaptic glia. Brain Res Rev 63, 11-25.

Reillo, I., de Juan Romero, C., Garcia-Cabezas, M.A., and Borrell, V. (2011). A role for intermediate radial glia in the tangential expansion of the mammalian cerebral cortex. Cereb Cortex 21, 1674-1694.

Reinhart, B.J., Slack, F.J., Basson, M., Pasquinelli, A.E., Bettinger, J.C., Rougvie, A.E., Horvitz, H.R., and Ruvkun, G. (2000). The 21-nucleotide let-7 RNA regulates developmental timing in Caenorhabditis elegans. Nature 403, 901-906.

Reinholdt, L.G., Ding, Y., Gilbert, G.J., Czechanski, A., Solzak, J.P., Roper, R.J., Johnson, M.T., Donahue, L.R., Lutz, C., and Davisson, M.T. (2011). Molecular characterization of the translocation breakpoints in the Down syndrome mouse model Ts65Dn. Mamm Genome 22, 685-691.

Ricard-Blum, S. (2011). The collagen family. Cold Spring Harb Perspect Biol 3, a004978.

Richardson, W.D., Kessaris, N., and Pringle, N. (2006). Oligodendrocyte wars. Nat Rev Neurosci 7, 11-18.

Richetto, J., Chesters, R., Cattaneo, A., Labouesse, M.A., Gutierrez, A.M.C., Wood, T.C., Luoni, A., Meyer, U., Vernon, A., and Riva, M.A. (2017). Genome-Wide Transcriptional Profiling and Structural Magnetic Resonance Imaging in the Maternal Immune Activation Model of Neurodevelopmental Disorders. Cereb Cortex 27, 3397-3413.

Rios, J.C., Melendez-Vasquez, C.V., Einheber, S., Lustig, M., Grumet, M., Hemperly, J., Peles, E., and Salzer, J.L. (2000). Contactin-associated protein (Caspr) and contactin form a complex that is targeted to the paranodal junctions during myelination. J Neurosci 20, 8354-8364.

Ritter, J., Schmitz, T., Chew, L.J., Buhrer, C., Mobius, W., Zonouzi, M., and Gallo, V. (2013). Neonatal hyperoxia exposure disrupts axon-oligodendrocyte integrity in the subcortical white matter. J Neurosci 33, 8990-9002.

Roach, A., Boylan, K., Horvath, S., Prusiner, S.B., and Hood, L.E. (1983). Characterization of cloned cDNA representing rat myelin basic protein: absence of expression in brain of shiverer mutant mice. Cell 34, 799-806.

Robaglia-Schlupp, A., Pizant, J., Norreel, J.C., Passage, E., Saberan-Djoneidi, D., Ansaldi, J.L., Vinay, L., Figarella-Branger, D., Levy, N., Clarac, F., et al. (2002). PMP22 overexpression causes dysmyelination in mice. Brain 125, 2213-2221.

Roewenstrunk, J., Di Vona, C., Chen, J., Borras, E., Dong, C., Arato, K., Sabido, E., Huen, M.S.Y., and de la Luna, S. (2019). A comprehensive proteomics-based interaction screen that links DYRK1A to RNF169 and to the DNA damage response. Sci Rep 9, 6014.

Rosenberg, S.S., Kelland, E.E., Tokar, E., De la Torre, A.R., and Chan, J.R. (2008). The geometric and spatial constraints of the microenvironment induce oligodendrocyte differentiation. Proc Natl Acad Sci U S A 105, 14662-14667.

Rowitch, D.H., and Kriegstein, A.R. (2010). Developmental genetics of vertebrate glial-cell specification. Nature 468, 214-222.

Ruaud, L., Mignot, C., Guet, A., Ohl, C., Nava, C., Heron, D., Keren, B., Depienne, C., Benoit, V., Maystadt, I., et al. (2015). DYRK1A mutations in two unrelated patients. Eur J Med Genet 58, 168-174.

Rubenstein, J.L. (2010). Three hypotheses for developmental defects that may underlie some forms of autism spectrum disorder. Curr Opin Neurol 23, 118-123.

Rybak, A., Fuchs, H., Smirnova, L., Brandt, C., Pohl, E.E., Nitsch, R., and Wulczyn, F.G. (2008). A feedback loop comprising lin-28 and let-7 controls pre-let-7 maturation during neural stem-cell commitment. Nat Cell Biol 10, 987-993.

Saade, M., Gonzalez-Gobartt, E., Escalona, R., Usieto, S., and Marti, E. (2017). Shh-mediated centrosomal recruitment of PKA promotes symmetric proliferative neuroepithelial cell division. Nat Cell Biol 19, 493-503.

Sabatier, C., Plump, A.S., Le, M., Brose, K., Tamada, A., Murakami, F., Lee, E.Y., and Tessier-Lavigne, M. (2004). The divergent Robo family protein rig-1/Robo3 is a negative regulator of slit responsiveness required for midline crossing by commissural axons. Cell 117, 157-169.

Sachs, H.G., Stambrook, P.J., and Ebert, J.D. (1974). Changes in membrane potential during the cell cycle. Exp Cell Res 83, 362-366.

Sadasivam, S., and DeCaprio, J.A. (2013). The DREAM complex: master coordinator of cell cycle-dependent gene expression. Nat Rev Cancer 13, 585-595.

Saher, G., Rudolphi, F., Corthals, K., Ruhwedel, T., Schmidt, K.F., Lowel, S., Dibaj, P., Barrette, B., Mobius, W., and Nave, K.A. (2012). Therapy of Pelizaeus-Merzbacher disease in mice by feeding a cholesterol-enriched diet. Nat Med 18, 1130-1135.

Saito, T., and Nakatsuji, N. (2001). Efficient gene transfer into the embryonic mouse brain using in vivo electroporation. Dev Biol 240, 237-246.

Salomoni, P., and Calegari, F. (2010). Cell cycle control of mammalian neural stem cells: putting a speed limit on G1. Trends Cell Biol 20, 233-243.

Samanta, J., and Kessler, J.A. (2004). Interactions between ID and OLIG proteins mediate the inhibitory effects of BMP4 on oligodendroglial differentiation. Development 131, 4131-4142.

Sanchez, M.A., and Armstrong, R.C. (2018). Postnatal Sonic hedgehog (Shh) responsive cells give rise to oligodendrocyte lineage cells during myelination and in adulthood contribute to remyelination. Exp Neurol 299, 122-136.

Sansom, S.N., Griffiths, D.S., Faedo, A., Kleinjan, D.J., Ruan, Y., Smith, J., van Heyningen, V., Rubenstein, J.L., and Livesey, F.J. (2009). The level of the transcription factor Pax6 is essential for controlling the balance between neural stem cell self-renewal and neurogenesis. PLoS Genet 5, e1000511.

Sanz-Rodriguez, M., Gruart, A., Escudero-Ramirez, J., de Castro, F., Delgado-Garcia, J.M., Wandosell, F., and Cubelos, B. (2018). R-Ras1 and R-Ras2 Are Essential for Oligodendrocyte Differentiation and Survival for Correct Myelination in the Central Nervous System. J Neurosci 38, 5096-5110.

Sauer, F.C. (1935). Mitosis in the neural tube and The cellular structure of the neural tube (Philadelphia,).

Scardigli, R., Baumer, N., Gruss, P., Guillemot, F., and Le Roux, I. (2003). Direct and concentration-dependent regulation of the proneural gene Neurogenin2 by Pax6. Development 130, 3269-3281.

Schindelin, J., Arganda-Carreras, I., Frise, E., Kaynig, V., Longair, M., Pietzsch, T., Preibisch, S., Rueden, C., Saalfeld, S., Schmid, B., et al. (2012). Fiji: an open-source platform for biological-image analysis. Nat Methods 9, 676-682.

Schmechel, D.E., and Rakic, P. (1979). A Golgi study of radial glial cells in developing monkey telencephalon: morphogenesis and transformation into astrocytes. Anat Embryol (Berl) 156, 115-152.

Schneider, P., Bayo-Fina, J.M., Singh, R., Kumar Dhanyamraju, P., Holz, P., Baier, A., Fendrich, V., Ramaswamy, A., Baumeister, S., Martinez, E.D., et al. (2015). Identification of a novel actin-dependent signal transducing module allows for the targeted degradation of GLI1. Nat Commun 6, 8023.

Schoenemann, P.T., Sheehan, M.J., and Glotzer, L.D. (2005). Prefrontal white matter volume is disproportionately larger in humans than in other primates. Nat Neurosci 8, 242-252.

Schulz, K., Vulpe, C.D., Harris, L.Z., and David, S. (2011). Iron efflux from oligodendrocytes is differentially regulated in gray and white matter. J Neurosci 31, 13301-13311.

Schuurmans, C., Armant, O., Nieto, M., Stenman, J.M., Britz, O., Klenin, N., Brown, C., Langevin, L.M., Seibt, J., Tang, H., et al. (2004). Sequential phases of cortical specification involve Neurogenin-dependent and -independent pathways. EMBO J 23, 2892-2902.

Scotti, M.M., and Swanson, M.S. (2016). RNA mis-splicing in disease. Nat Rev Genet 17, 19-32.

Sempere, L.F., Freemantle, S., Pitha-Rowe, I., Moss, E., Dmitrovsky, E., and Ambros, V. (2004). Expression profiling of mammalian microRNAs uncovers a subset of brain-expressed microRNAs with possible roles in murine and human neuronal differentiation. Genome Biol 5, R13.

Sessa, A., Mao, C.A., Hadjantonakis, A.K., Klein, W.H., and Broccoli, V. (2008). Tbr2 directs conversion of radial glia into basal precursors and guides neuronal amplification by indirect neurogenesis in the developing neocortex. Neuron 60, 56-69.

Shalgi, R., Hurt, J.A., Lindquist, S., and Burge, C.B. (2014). Widespread inhibition of posttranscriptional splicing shapes the cellular transcriptome following heat shock. Cell Rep 7, 1362-1370.

Shannon, P., Markiel, A., Ozier, O., Baliga, N.S., Wang, J.T., Ramage, D., Amin, N., Schwikowski, B., and Ideker, T. (2003). Cytoscape: a software environment for integrated models of biomolecular interaction networks. Genome Res 13, 2498-2504.

Shaw, P., Kabani, N.J., Lerch, J.P., Eckstrand, K., Lenroot, R., Gogtay, N., Greenstein, D., Clasen, L., Evans, A., Rapoport, J.L., et al. (2008). Neurodevelopmental trajectories of the human cerebral cortex. J Neurosci 28, 3586-3594.

Shen, H.Y., Huang, N., Reemmer, J., and Xiao, L. (2018). Adenosine Actions on Oligodendroglia and Myelination in Autism Spectrum Disorder. Front Cell Neurosci 12, 482.

Shen, S., Li, J., and Casaccia-Bonnefil, P. (2005). Histone modifications affect timing of oligodendrocyte progenitor differentiation in the developing rat brain. J Cell Biol 169, 577-589.

Shibasaki, T., Tokunaga, A., Sakamoto, R., Sagara, H., Noguchi, S., Sasaoka, T., and Yoshida, N. (2013). PTB deficiency causes the loss of adherens junctions in the dorsal telencephalon and leads to lethal hydrocephalus. Cereb Cortex 23, 1824-1835.

Shibata, M., Nakao, H., Kiyonari, H., Abe, T., and Aizawa, S. (2011). MicroRNA-9 regulates neurogenesis in mouse telencephalon by targeting multiple transcription factors. J Neurosci 31, 3407-3422.

Shikata, Y., Okada, T., Hashimoto, M., Ellis, T., Matsumaru, D., Shiroishi, T., Ogawa, M., Wainwright, B., and Motoyama, J. (2011). Ptch1-mediated dosage-dependent action of Shh signaling regulates neural progenitor development at late gestational stages. Dev Biol 349, 147-159.

Shim, J., and Nam, J.W. (2016). The expression and functional roles of microRNAs in stem cell differentiation. BMB Rep 49, 3-10.

Shimamura, K., and Rubenstein, J.L. (1997). Inductive interactions direct early regionalization of the mouse forebrain. Development 124, 2709-2718.

Shimojo, H., Ohtsuka, T., and Kageyama, R. (2008). Oscillations in notch signaling regulate maintenance of neural progenitors. Neuron 58, 52-64.

Shitamukai, A., Konno, D., and Matsuzaki, F. (2011). Oblique radial glial divisions in the developing mouse neocortex induce self-renewing progenitors outside the germinal zone that resemble primate outer subventricular zone progenitors. J Neurosci 31, 3683-3695.

Siarey, R.J., Carlson, E.J., Epstein, C.J., Balbo, A., Rapoport, S.I., and Galdzicki, Z. (1999). Increased synaptic depression in the Ts65Dn mouse, a model for mental retardation in Down syndrome. Neuropharmacology 38, 1917-1920.

Siegenthaler, J.A., and Pleasure, S.J. (2011). We have got you 'covered': how the meninges control brain development. Curr Opin Genet Dev 21, 249-255.

Siegenthaler, J.A., Ashique, A.M., Zarbalis, K., Patterson, K.P., Hecht, J.H., Kane, M.A., Folias, A.E., Choe, Y., May, S.R., Kume, T., et al. (2009). Retinoic acid from the meninges regulates cortical neuron generation. Cell 139, 597-609.

Sloan, S.A., and Barres, B.A. (2014). Mechanisms of astrocyte development and their contributions to neurodevelopmental disorders. Curr Opin Neurobiol 27, 75-81.

Smart, I.H., Dehay, C., Giroud, P., Berland, M., and Kennedy, H. (2002). Unique morphological features of the proliferative zones and postmitotic compartments of the neural epithelium giving rise to striate and extrastriate cortex in the monkey. Cereb Cortex 12, 37-53.

Snaidero, N., Mobius, W., Czopka, T., Hekking, L.H., Mathisen, C., Verkleij, D., Goebbels, S., Edgar, J., Merkler, D., Lyons, D.A., et al. (2014). Myelin membrane wrapping of CNS axons by PI(3,4,5)P3-dependent polarized growth at the inner tongue. Cell 156, 277-290.

Sofroniew, M.V. (2009). Molecular dissection of reactive astrogliosis and glial scar formation. Trends Neurosci 32, 638-647.

Sofroniew, M.V., and Vinters, H.V. (2010). Astrocytes: biology and pathology. Acta Neuropathol 119, 7-35.

Song, W.J., Sternberg, L.R., Kasten-Sportes, C., Keuren, M.L., Chung, S.H., Slack, A.C., Miller, D.E., Glover, T.W., Chiang, P.W., Lou, L., et al. (1996). Isolation of human and murine homologues of the Drosophila minibrain gene: human homologue maps to 21q22.2 in the Down syndrome "critical region". Genomics 38, 331-339.

Soppa, U., Schumacher, J., Florencio Ortiz, V., Pasqualon, T., Tejedor, F.J., and Becker, W. (2014). The Down syndrome-related protein kinase DYRK1A phosphorylates p27(Kip1) and Cyclin D1 and induces cell cycle exit and neuronal differentiation. Cell Cycle 13, 2084-2100.

Souchet, B., Guedj, F., Sahun, I., Duchon, A., Daubigney, F., Badel, A., Yanagawa, Y., Barallobre, M.J., Dierssen, M., Yu, E., et al. (2014). Excitation/inhibition balance and learning are modified by Dyrk1a gene dosage. Neurobiol Dis 69, 65-75.

Soundararajan, M., Roos, A.K., Savitsky, P., Filippakopoulos, P., Kettenbach, A.N., Olsen, J.V., Gerber, S.A., Eswaran, J., Knapp, S., and Elkins, J.M. (2013). Structures of Down syndrome kinases, DYRKs, reveal mechanisms of kinase activation and substrate recognition. Structure 21, 986-996.

Sparmann, A., Xie, Y., Verhoeven, E., Vermeulen, M., Lancini, C., Gargiulo, G., Hulsman, D., Mann, M., Knoblich, J.A., and van Lohuizen, M. (2013). The chromodomain helicase Chd4 is required for Polycomb-mediated inhibition of astroglial differentiation. EMBO J 32, 1598-1612.

Spitzer, N.C. (2006). Electrical activity in early neuronal development. Nature 444, 707-712.

Stahl, R., Walcher, T., De Juan Romero, C., Pilz, G.A., Cappello, S., Irmler, M., Sanz-Aquela, J.M., Beckers, J., Blum, R., Borrell, V., et al. (2013). Trnp1 regulates expansion and folding of the mammalian cerebral cortex by control of radial glial fate. Cell 153, 535-549.

Stein, B.E., Perrault, T.J., Jr., Stanford, T.R., and Rowland, B.A. (2009). Postnatal experiences influence how the brain integrates information from different senses. Front Integr Neurosci 3, 21.

Stenzel, D., Wilsch-Brauninger, M., Wong, F.K., Heuer, H., and Huttner, W.B. (2014). Integrin alphavbeta3 and thyroid hormones promote expansion of progenitors in embryonic neocortex. Development 141, 795-806.

Stessman, H.A., Xiong, B., Coe, B.P., Wang, T., Hoekzema, K., Fenckova, M., Kvarnung, M., Gerdts, J., Trinh, S., Cosemans, N., et al. (2017). Targeted sequencing identifies 91 neurodevelopmental-disorder risk genes with autism and developmental-disability biases. Nat Genet 49, 515-526.

Stolt, C.C., Lommes, P., Sock, E., Chaboissier, M.C., Schedl, A., and Wegner, M. (2003). The Sox9 transcription factor determines glial fate choice in the developing spinal cord. Genes Dev 17, 1677-1689.

Sturrock, R.R. (1980). Myelination of the mouse corpus callosum. Neuropathol Appl Neurobiol 6, 415-420.

Su, B., Zhao, W., Shi, B., Zhang, Z., Yu, X., Xie, F., Guo, Z., Zhang, X., Liu, J., Shen, Q., et al. (2014). Let-7d suppresses growth, metastasis, and tumor macrophage infiltration in renal cell carcinoma by targeting COL3A1 and CCL7. Mol Cancer 13, 206.

Sun, W., Cornwell, A., Li, J., Peng, S., Osorio, M.J., Aalling, N., Wang, S., Benraiss, A., Lou, N., Goldman, S.A., et al. (2017). SOX9 Is an Astrocyte-Specific Nuclear Marker in the Adult Brain Outside the Neurogenic Regions. J Neurosci 37, 4493-4507.

Sun, Y., Nadal-Vicens, M., Misono, S., Lin, M.Z., Zubiaga, A., Hua, X., Fan, G., and Greenberg, M.E. (2001). Neurogenin promotes neurogenesis and inhibits glial differentiation by independent mechanisms. Cell 104, 365-376.

Tabata, H. (2015). Diverse subtypes of astrocytes and their development during corticogenesis. Front Neurosci 9, 114.

Tabuchi, K., and Sudhof, T.C. (2002). Structure and evolution of neurexin genes: insight into the mechanism of alternative splicing. Genomics 79, 849-859.

Takahashi, K., Foster, J.B., and Lin, C.L. (2015). Glutamate transporter EAAT2: regulation, function, and potential as a therapeutic target for neurological and psychiatric disease. Cell Mol Life Sci 72, 3489-3506.

Takahashi, T., Nowakowski, R.S., and Caviness, V.S., Jr. (1995). The cell cycle of the pseudostratified ventricular epithelium of the embryonic murine cerebral wall. J Neurosci 15, 6046-6057.

Takizawa, T., Nakashima, K., Namihira, M., Ochiai, W., Uemura, A., Yanagisawa, M., Fujita, N., Nakao, M., and Taga, T. (2001). DNA methylation is a critical cell-intrinsic determinant of astrocyte differentiation in the fetal brain. Dev Cell 1, 749-758.

Tanaka, H., Ikenaka, K., and Isa, T. (2006). Electrophysiological abnormalities precede apparent histological demyelination in the central nervous system of mice overexpressing proteolipid protein. J Neurosci Res 84, 1206-1216.

Tanaka, H., Ma, J., Tanaka, K.F., Takao, K., Komada, M., Tanda, K., Suzuki, A., Ishibashi, T., Baba, H., Isa, T., et al. (2009). Mice with altered myelin proteolipid protein gene expression display cognitive deficits accompanied by abnormal neuron-glia interactions and decreased conduction velocities. J Neurosci 29, 8363-8371.

Tang, B.L. (2009). REST regulation of neural development: From outside-in? Cell Adh Migr 3, 1-2.

Tapial, J., Ha, K.C.H., Sterne-Weiler, T., Gohr, A., Braunschweig, U., Hermoso-Pulido, A., Quesnel-Vallieres, M., Permanyer, J., Sodaei, R., Marquez, Y., et al. (2017). An atlas of alternative splicing profiles and functional associations reveals new regulatory programs and genes that simultaneously express multiple major isoforms. Genome Res 27, 1759-1768.

Taverna, E., and Huttner, W.B. (2010). Neural progenitor nuclei IN motion. Neuron 67, 906-914.

Team, R.C. (2013). R: A language and environment for statistical computing. R.F.f.S. Computing, ed. (Vienna, Austria).

Tejedor, F., Zhu, X.R., Kaltenbach, E., Ackermann, A., Baumann, A., Canal, I., Heisenberg, M., Fischbach, K.F., and Pongs, O. (1995). minibrain: a new protein kinase family involved in postembryonic neurogenesis in Drosophila. Neuron 14, 287-301.

Tejedor, F.J. (2018). Dual Specificity Tyrosine-Phosphorylation Regulated Kinase 1A. In Encyclopedia of Signaling Molecules, S. Choi, ed. (Cham: Springer International Publishing), pp. 1438-1438.

Tejedor, F.J., and Hammerle, B. (2011). MNB/DYRK1A as a multiple regulator of neuronal development. FEBS J 278, 223-235.

Tekki-Kessaris, N., Woodruff, R., Hall, A.C., Gaffield, W., Kimura, S., Stiles, C.D., Rowitch, D.H., and Richardson, W.D. (2001). Hedgehog-dependent oligodendrocyte lineage specification in the telencephalon. Development 128, 2545-2554.

Telley, L., Govindan, S., Prados, J., Stevant, I., Nef, S., Dermitzakis, E., Dayer, A., and Jabaudon, D. (2016). Sequential transcriptional waves direct the differentiation of newborn neurons in the mouse neocortex. Science 351, 1443-1446.

Thompson, B.J., Bhansali, R., Diebold, L., Cook, D.E., Stolzenburg, L., Casagrande, A.S., Besson, T., Leblond, B., Desire, L., Malinge, S., et al. (2015). DYRK1A controls the transition from proliferation to quiescence during lymphoid development by destabilizing Cyclin D3. J Exp Med 212, 953-970.

Toma, K., and Hanashima, C. (2015). Switching modes in corticogenesis: mechanisms of neuronal subtype transitions and integration in the cerebral cortex. Front Neurosci 9, 274.

Tomassy, G.S., Dershowitz, L.B., and Arlotta, P. (2016). Diversity Matters: A Revised Guide to Myelination. Trends Cell Biol 26, 135-147.

Tong, C.K., Fuentealba, L.C., Shah, J.K., Lindquist, R.A., Ihrie, R.A., Guinto, C.D., Rodas-Rodriguez, J.L., and Alvarez-Buylla, A. (2015). A Dorsal SHH-Dependent Domain in the V-SVZ Produces Large Numbers of Oligodendroglial Lineage Cells in the Postnatal Brain. Stem Cell Reports 5, 461-470.

Totaro, A., Panciera, T., and Piccolo, S. (2018). YAP/TAZ upstream signals and downstream responses. Nat Cell Biol 20, 888-899.

Toth, A.B., Shum, A.K., and Prakriya, M. (2016). Regulation of neurogenesis by calcium signaling. Cell Calcium 59, 124-134.

Tripathi, R.B., Clarke, L.E., Burzomato, V., Kessaris, N., Anderson, P.N., Attwell, D., and Richardson, W.D. (2011). Dorsally and ventrally derived oligodendrocytes have similar electrical properties but myelinate preferred tracts. J Neurosci 31, 6809-6819.

Tsai, H.H., Li, H., Fuentealba, L.C., Molofsky, A.V., Taveira-Marques, R., Zhuang, H., Tenney, A., Murnen, A.T., Fancy, S.P., Merkle, F., et al. (2012). Regional astrocyte allocation regulates CNS synaptogenesis and repair. Science 337, 358-362.

Tsai, H.H., Niu, J., Munji, R., Davalos, D., Chang, J., Zhang, H., Tien, A.C., Kuo, C.J., Chan, J.R., Daneman, R., et al. (2016). Oligodendrocyte precursors migrate along vasculature in the developing nervous system. Science 351, 379-384.

Tschop, K., Conery, A.R., Litovchick, L., Decaprio, J.A., Settleman, J., Harlow, E., and Dyson, N. (2011). A kinase shRNA screen links LATS2 and the pRB tumor suppressor. Genes Dev 25, 814-830.

Tyas, D.A., Simpson, T.I., Carr, C.B., Kleinjan, D.A., van Heyningen, V., Mason, J.O., and Price, D.J. (2006). Functional conservation of Pax6 regulatory elements in humans and mice demonstrated with a novel transgenic reporter mouse. BMC Dev Biol 6, 21.

Ulzheimer, J.C., Peles, E., Levinson, S.R., and Martini, R. (2004). Altered expression of ion channel isoforms at the node of Ranvier in P0-deficient myelin mutants. Mol Cell Neurosci 25, 83-94.

Uranova, N.A., Vostrikov, V.M., Vikhreva, O.V., Zimina, I.S., Kolomeets, N.S., and Orlovskaya, D.D. (2007). The role of oligodendrocyte pathology in schizophrenia. Int J Neuropsychopharmacol 10, 537-545.

Urrego, D., Tomczak, A.P., Zahed, F., Stuhmer, W., and Pardo, L.A. (2014). Potassium channels in cell cycle and cell proliferation. Philos Trans R Soc Lond B Biol Sci 369, 20130094.

Uwechue, N.M., Marx, M.C., Chevy, Q., and Billups, B. (2012). Activation of glutamate transport evokes rapid glutamine release from perisynaptic astrocytes. J Physiol 590, 2317-2331.

van Bon, B.W., Balciuniene, J., Fruhman, G., Nagamani, S.C., Broome, D.L., Cameron, E., Martinet, D., Roulet, E., Jacquemont, S., Beckmann, J.S., et al. (2011). The phenotype of recurrent 10q22q23 deletions and duplications. Eur J Hum Genet 19, 400-408.

van Bon, B.W., Coe, B.P., Bernier, R., Green, C., Gerdts, J., Witherspoon, K., Kleefstra, T., Willemsen, M.H., Kumar, R., Bosco, P., et al. (2016). Disruptive de novo mutations of DYRK1A lead to a syndromic form of autism and ID. Mol Psychiatry 21, 126-132.

van Bon, B.W., Coe, B.P., de Vries, B.B., and al., e. (2015). DYRK1A-Related Intellectual Disability Syndrome (Seattle (WA).

van Tilborg, E., de Theije, C.G.M., van Hal, M., Wagenaar, N., de Vries, L.S., Benders, M.J., Rowitch, D.H., and Nijboer, C.H. (2018). Origin and dynamics of oligodendrocytes in the developing brain: Implications for perinatal white matter injury. Glia 66, 221-238.

Varelas, X. (2014). The Hippo pathway effectors TAZ and YAP in development, homeostasis and disease. Development 141, 1614-1626.

Vassilev, A., Kaneko, K.J., Shu, H., Zhao, Y., and DePamphilis, M.L. (2001). TEAD/TEF transcription factors utilize the activation domain of YAP65, a Src/Yes-associated protein localized in the cytoplasm. Genes Dev 15, 1229-1241.

Vidaki, M., Drees, F., Saxena, T., Lanslots, E., Taliaferro, M.J., Tatarakis, A., Burge, C.B., Wang, E.T., and Gertler, F.B. (2017). A Requirement for Mena, an Actin Regulator, in Local mRNA Translation in Developing Neurons. Neuron 95, 608-622 e605.

Vitali, I., Fievre, S., Telley, L., Oberst, P., Bariselli, S., Frangeul, L., Baumann, N., McMahon, J.J., Klingler, E., Bocchi, R., et al. (2018). Progenitor Hyperpolarization Regulates the Sequential Generation of Neuronal Subtypes in the Developing Neocortex. Cell 174, 1264-1276 e1215.

Voigt, T. (1989). Development of glial cells in the cerebral wall of ferrets: direct tracing of their transformation from radial glia into astrocytes. J Comp Neurol 289, 74-88.

Volfovsky, N., Haas, B.J., and Salzberg, S.L. (2003). Computational discovery of internal micro-exons. Genome Res 13, 1216-1221.

von Groote-Bidlingmaier, F., Schmoll, D., Orth, H.M., Joost, H.G., Becker, W., and Barthel, A. (2003). DYRK1 is a co-activator of FKHR (FOXO1a)-dependent glucose-6-phosphatase gene expression. Biochem Biophys Res Commun 300, 764-769.

Voronova, A., Yuzwa, S.A., Wang, B.S., Zahr, S., Syal, C., Wang, J., Kaplan, D.R., and Miller, F.D. (2017). Migrating Interneurons Secrete Fractalkine to Promote Oligodendrocyte Formation in the Developing Mammalian Brain. Neuron 94, 500-516 e509.

Vuong, C.K., Black, D.L., and Zheng, S. (2016). The neurogenetics of alternative splicing. Nat Rev Neurosci 17, 265-281.

Wake, H., Ortiz, F.C., Woo, D.H., Lee, P.R., Angulo, M.C., and Fields, R.D. (2015). Nonsynaptic junctions on myelinating glia promote preferential myelination of electrically active axons. Nat Commun 6, 7844.

Walcher, T., Xie, Q., Sun, J., Irmler, M., Beckers, J., Ozturk, T., Niessing, D., Stoykova, A., Cvekl, A., Ninkovic, J., et al. (2013). Functional dissection of the paired domain of Pax6 reveals molecular mechanisms of coordinating neurogenesis and proliferation. Development 140, 1123-1136.

Wallingford, J., Scott, A.L., Rodrigues, K., and Doering, L.C. (2017). Altered Developmental Expression of the Astrocyte-Secreted Factors Hevin and SPARC in the Fragile X Mouse Model. Front Mol Neurosci 10, 268.

Wan, C., Yang, Y., Feng, G., Gu, N., Liu, H., Zhu, S., He, L., and Wang, L. (2005). Polymorphisms of myelin-associated glycoprotein gene are associated with schizophrenia in the Chinese Han population. Neurosci Lett 388, 126-131.

Wang, E.T., Sandberg, R., Luo, S., Khrebtukova, I., Zhang, L., Mayr, C., Kingsmore, S.F., Schroth, G.P., and Burge, C.B. (2008a). Alternative isoform regulation in human tissue transcriptomes. Nature 456, 470-476.

Wang, H., Ge, G., Uchida, Y., Luu, B., and Ahn, S. (2011a). Gli3 is required for maintenance and fate specification of cortical progenitors. J Neurosci 31, 6440-6448.

Wang, P., Wang, L., Chen, L., and Sun, X. (2017). Dual-specificity tyrosine-phosphorylation regulated kinase 1A Gene Transcription is regulated by Myocyte Enhancer Factor 2D. Sci Rep 7, 7240.

Wang, W., Lin, C., Lu, D., Ning, Z., Cox, T., Melvin, D., Wang, X., Bradley, A., and Liu, P. (2008b). Chromosomal transposition of PiggyBac in mouse embryonic stem cells. Proc Natl Acad Sci U S A 105, 9290-9295.

Wang, X., Tsai, J.W., Imai, J.H., Lian, W.N., Vallee, R.B., and Shi, S.H. (2009). Asymmetric centrosome inheritance maintains neural progenitors in the neocortex. Nature 461, 947-955.

Wang, X., Tsai, J.W., LaMonica, B., and Kriegstein, A.R. (2011b). A new subtype of progenitor cell in the mouse embryonic neocortex. Nat Neurosci 14, 555-561.

Wang, Y., and Blelloch, R. (2011). Cell cycle regulation by microRNAs in stem cells. Results Probl Cell Differ 53, 459-472.

Wang, Y., Luo, J., Zhang, H., and Lu, J. (2016). microRNAs in the Same Clusters Evolve to Coordinately Regulate Functionally Related Genes. Mol Biol Evol 33, 2232-2247.

Wang, Y., Melton, C., Li, Y.P., Shenoy, A., Zhang, X.X., Subramanyam, D., and Blelloch, R. (2013). miR-294/miR-302 promotes proliferation, suppresses G1-S restriction point, and inhibits ESC differentiation through separable mechanisms. Cell Rep 4, 99-109.

Watt, F., and Molloy, P.L. (1988). Cytosine methylation prevents binding to DNA of a HeLa cell transcription factor required for optimal expression of the adenovirus major late promoter. Genes Dev 2, 1136-1143.

Wegiel, J., Dowjat, K., Kaczmarski, W., Kuchna, I., Nowicki, K., Frackowiak, J., Mazur Kolecka, B., Wegiel, J., Silverman, W.P., Reisberg, B., et al. (2008). The role of overexpressed DYRK1A protein in the early onset of neurofibrillary degeneration in Down syndrome. Acta Neuropathol 116, 391-407.

Wegiel, J., Kuchna, I., Nowicki, K., Frackowiak, J., Dowjat, K., Silverman, W.P., Reisberg, B., DeLeon, M., Wisniewski, T., Adayev, T., et al. (2004). Cell type- and brain structure-specific patterns of distribution of minibrain kinase in human brain. Brain Res 1010, 69-80.

Weigmann, A., Corbeil, D., Hellwig, A., and Huttner, W.B. (1997). Prominin, a novel microvilli-specific polytopic membrane protein of the apical surface of epithelial cells, is targeted to plasmalemmal protrusions of non-epithelial cells. Proc Natl Acad Sci U S A 94, 12425-12430.

Weissman, T.A., Riquelme, P.A., Ivic, L., Flint, A.C., and Kriegstein, A.R. (2004). Calcium waves propagate through radial glial cells and modulate proliferation in the developing neocortex. Neuron 43, 647-661.

Weyn-Vanhentenryck, S.M., Feng, H., Ustianenko, D., Duffie, R., Yan, Q., Jacko, M., Martinez, J.C., Goodwin, M., Zhang, X., Hengst, U., et al. (2018). Precise temporal regulation of alternative splicing during neural development. Nat Commun 9, 2189.

Weyn-Vanhentenryck, S.M., Mele, A., Yan, Q., Sun, S., Farny, N., Zhang, Z., Xue, C., Herre, M., Silver, P.A., Zhang, M.Q., et al. (2014). HITS-CLIP and integrative modeling define the Rbfox splicing-regulatory network linked to brain development and autism. Cell Rep 6, 1139-1152.

Widowati, E.W., Ernst, S., Hausmann, R., Muller-Newen, G., and Becker, W. (2018). Functional characterization of DYRK1A missense variants associated with a syndromic form of intellectual deficiency and autism. Biol Open 7.

Wiesel, T.N., and Hubel, D.H. (1963a). Effects of Visual Deprivation on Morphology and Physiology of Cells in the Cats Lateral Geniculate Body. J Neurophysiol 26, 978-993.

Wiesel, T.N., and Hubel, D.H. (1963b). Single-Cell Responses in Striate Cortex of Kittens Deprived of Vision in One Eye. J Neurophysiol 26, 1003-1017.

Willaredt, M.A., Tasouri, E., and Tucker, K.L. (2013). Primary cilia and forebrain development. Mech Dev 130, 373-380.

Williams, E.C., Zhong, X., Mohamed, A., Li, R., Liu, Y., Dong, Q., Ananiev, G.E., Mok, J.C., Lin, B.R., Lu, J., et al. (2014). Mutant astrocytes differentiated from Rett syndrome patients-specific iPSCs have adverse effects on wild-type neurons. Hum Mol Genet 23, 2968-2980.

Wilsch-Brauninger, M., Peters, J., Paridaen, J.T., and Huttner, W.B. (2012). Basolateral rather than apical primary cilia on neuroepithelial cells committed to delamination. Development 139, 95-105.

Winkler, C.C., Yabut, O.R., Fregoso, S.P., Gomez, H.G., Dwyer, B.E., Pleasure, S.J., and Franco, S.J. (2018). The Dorsal Wave of Neocortical Oligodendrogenesis Begins Embryonically and Requires Multiple Sources of Sonic Hedgehog. J Neurosci 38, 5237-5250.

Winter, J., Jung, S., Keller, S., Gregory, R.I., and Diederichs, S. (2009). Many roads to maturity: microRNA biogenesis pathways and their regulation. Nat Cell Biol 11, 228-234.

Witman, N., Heigwer, J., Thaler, B., Lui, W.O., and Morrison, J.I. (2013). miR-128 regulates non-myocyte hyperplasia, deposition of extracellular matrix and Islet1 expression during newt cardiac regeneration. Dev Biol 383, 253-263.

Witte, H., Schreiner, D., and Scheiffele, P. (2018). A Sam68-dependent alternative splicing program shapes postsynaptic protein complexes. Eur J Neurosci.

Wonders, C.P., and Anderson, S.A. (2006). The origin and specification of cortical interneurons. Nat Rev Neurosci 7, 687-696.

Woodhead, G.J., Mutch, C.A., Olson, E.C., and Chenn, A. (2006). Cell-autonomous beta-catenin signaling regulates cortical precursor proliferation. J Neurosci 26, 12620-12630.

Wrobel, C.N., Mutch, C.A., Swaminathan, S., Taketo, M.M., and Chenn, A. (2007). Persistent expression of stabilized beta-catenin delays maturation of radial glial cells into intermediate progenitors. Dev Biol 309, 285-297.

Wulczyn, F.G., Smirnova, L., Rybak, A., Brandt, C., Kwidzinski, E., Ninnemann, O., Strehle, M., Seiler, A., Schumacher, S., and Nitsch, R. (2007). Post-transcriptional regulation of the let-7 microRNA during neural cell specification. FASEB J 21, 415-426.

Xia, X., and Ahmad, I. (2016). let-7 microRNA regulates neurogliogenesis in the mammalian retina through Hmga2. Dev Biol 410, 70-85.

Yan, Q., Weyn-Vanhentenryck, S.M., Wu, J., Sloan, S.A., Zhang, Y., Chen, K., Wu, J.Q., Barres, B.A., and Zhang, C. (2015). Systematic discovery of regulated and conserved alternative exons in the mammalian brain reveals NMD modulating chromatin regulators. Proc Natl Acad Sci U S A 112, 3445-3450.

Yang, E.J., Ahn, Y.S., and Chung, K.C. (2001). Protein kinase Dyrk1 activates cAMP response element-binding protein during neuronal differentiation in hippocampal progenitor cells. J Biol Chem 276, 39819-39824.

Yang, S.L., Yang, M., Herrlinger, S., Liang, C., Lai, F., and Chen, J.F. (2015). MiR-302/367 regulate neural progenitor proliferation, differentiation timing, and survival in neurulation. Dev Biol 408, 140-150.

Yang, Y., Lewis, R., and Miller, R.H. (2011). Interactions between oligodendrocyte precursors control the onset of CNS myelination. Dev Biol 350, 127-138.

Ye, F., Chen, Y., Hoang, T., Montgomery, R.L., Zhao, X.H., Bu, H., Hu, T., Taketo, M.M., van Es, J.H., Clevers, H., et al. (2009). HDAC1 and HDAC2 regulate oligodendrocyte differentiation by disrupting the beta-catenin-TCF interaction. Nat Neurosci 12, 829-838.

Ye, J., Coulouris, G., Zaretskaya, I., Cutcutache, I., Rozen, S., and Madden, T.L. (2012). Primer-BLAST: a tool to design target-specific primers for polymerase chain reaction. BMC Bioinformatics 13, 134.

Yin, X., Jin, N., Gu, J., Shi, J., Zhou, J., Gong, C.X., Iqbal, K., Grundke-Iqbal, I., and Liu, F. (2012). Dual-specificity tyrosine phosphorylation-regulated kinase 1A (Dyrk1A) modulates serine/arginine-rich protein 55 (SRp55)-promoted Tau exon 10 inclusion. J Biol Chem 287, 30497-30506.

Yoon, K.J., Ringeling, F.R., Vissers, C., Jacob, F., Pokrass, M., Jimenez-Cyrus, D., Su, Y., Kim, N.S., Zhu, Y., Zheng, L., et al. (2017). Temporal Control of Mammalian Cortical Neurogenesis by m(6)A Methylation. Cell 171, 877-889 e817.

Yu, F.X., Zhao, B., Panupinthu, N., Jewell, J.L., Lian, I., Wang, L.H., Zhao, J., Yuan, H., Tumaneng, K., Li, H., et al. (2012). Regulation of the Hippo-YAP pathway by G-protein-coupled receptor signaling. Cell 150, 780-791.

Yu, J., Vodyanik, M.A., Smuga-Otto, K., Antosiewicz-Bourget, J., Frane, J.L., Tian, S., Nie, J., Jonsdottir, G.A., Ruotti, V., Stewart, R., et al. (2007). Induced pluripotent stem cell lines derived from human somatic cells. Science 318, 1917-1920.

Yu, Y., Chen, Y., Kim, B., Wang, H., Zhao, C., He, X., Liu, L., Liu, W., Wu, L.M., Mao, M., et al. (2013). Olig2 targets chromatin remodelers to enhancers to initiate oligodendrocyte differentiation. Cell 152, 248-261.

Zahr, S.K., Yang, G., Kazan, H., Borrett, M.J., Yuzwa, S.A., Voronova, A., Kaplan, D.R., and Miller, F.D. (2018). A Translational Repression Complex in Developing Mammalian Neural Stem Cells that Regulates Neuronal Specification. Neuron 97, 520-537 e526.

Zai, G., King, N., Wigg, K., Couto, J., Wong, G.W., Honer, W.G., Barr, C.L., and Kennedy, J.L. (2005). Genetic study of the myelin oligodendrocyte glycoprotein (MOG) gene in schizophrenia. Genes Brain Behav 4, 2-9.

Zecevic, N., Chen, Y., and Filipovic, R. (2005). Contributions of cortical subventricular zone to the development of the human cerebral cortex. J Comp Neurol 491, 109-122.

Zhang, C., Frias, M.A., Mele, A., Ruggiu, M., Eom, T., Marney, C.B., Wang, H., Licatalosi, D.D., Fak, J.J., and Darnell, R.B. (2010). Integrative modeling defines the Nova splicing-regulatory network and its combinatorial controls. Science 329, 439-443.

Zhang, H., and Miller, R.H. (1996). Density-dependent feedback inhibition of oligodendrocyte precursor expansion. J Neurosci 16, 6886-6895.

Zhang, X., Chen, M.H., Wu, X., Kodani, A., Fan, J., Doan, R., Ozawa, M., Ma, J., Yoshida, N., Reiter, J.F., et al. (2016a). Cell-Type-Specific Alternative Splicing Governs Cell Fate in the Developing Cerebral Cortex. Cell 166, 1147-1162 e1115.

Zhang, Y., Chen, K., Sloan, S.A., Bennett, M.L., Scholze, A.R., O'Keeffe, S., Phatnani, H.P., Guarnieri, P., Caneda, C., Ruderisch, N., et al. (2014). An RNA-sequencing transcriptome and splicing database of glia, neurons, and vascular cells of the cerebral cortex. J Neurosci 34, 11929-11947.

Zhang, Y., Liao, J.M., Zeng, S.X., and Lu, H. (2011). p53 downregulates Down syndrome-associated DYRK1A through miR-1246. EMBO Rep 12, 811-817.

Zhang, Y., Sloan, S.A., Clarke, L.E., Caneda, C., Plaza, C.A., Blumenthal, P.D., Vogel, H., Steinberg, G.K., Edwards, M.S., Li, G., et al. (2016b). Purification and Characterization of Progenitor and Mature Human Astrocytes Reveals Transcriptional and Functional Differences with Mouse. Neuron 89, 37-53.

Zhao, B., Ye, X., Yu, J., Li, L., Li, W., Li, S., Yu, J., Lin, J.D., Wang, C.Y., Chinnaiyan, A.M., et al. (2008). TEAD mediates YAP-dependent gene induction and growth control. Genes Dev 22, 1962-1971.

Zhao, C., Sun, G., Li, S., Lang, M.F., Yang, S., Li, W., and Shi, Y. (2010). MicroRNA let-7b regulates neural stem cell proliferation and differentiation by targeting nuclear receptor TLX signaling. Proc Natl Acad Sci U S A 107, 1876-1881.

Zhao, C., Sun, G., Ye, P., Li, S., and Shi, Y. (2013). MicroRNA let-7d regulates the TLX/microRNA-9 cascade to control neural cell fate and neurogenesis. Sci Rep 3, 1329.

Zhou, C.J., Borello, U., Rubenstein, J.L., and Pleasure, S.J. (2006). Neuronal production and precursor proliferation defects in the neocortex of mice with loss of function in the canonical Wnt signaling pathway. Neuroscience 142, 1119-1131.

Zhu, X., Bergles, D.E., and Nishiyama, A. (2008). NG2 cells generate both oligodendrocytes and gray matter astrocytes. Development 135, 145-157.